ON-LINE APPENDICES TO

Thermal Radiation: An Introduction

John R. Howell, M. Pinar Mengüç,
and Kyle Daun

CRC/Taylor and Francis, 2022

Contents*

***Click on Title to go to desired Appendix**

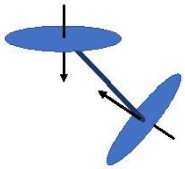

A: GRAPHS FOR CO_2, H_2O AND CO EMITTANCE

Alberti et al. (2018) use HITEMP 2010 line-by-line data to compose accurate emittance charts for CO_2, water vapor and CO, along with pressure and overlap corrections for mixtures of these absorbing/emitting gases mixed with nonparticipating N_2. Aside from the addition of CO to the original Hottel charts (Hottel 1954), the new charts are extended to higher pressures and temperatures. The authors have also constructed curve fits of the new data to allow accurate interpolation and made available an EXCEL worksheet using these interpolations to allow convenient calculation of the emittance of mixtures of CO_2, H_2O, CO and N_2 at temperatures and pressures within the range of the computed emittance values ($300 < T < 3000$ K and $0.1 < P < 100$ atm). The worksheet is available at ***https://doi.org/10.1016/j.jqsrt.2018.08.008.***

Prof. Alberti has kindly provided the charts for inclusion here, and they are reproduced below.

For a gas mixture, the total emittance is found from

$$\varepsilon_{tot} = \varepsilon_{H2O} + \varepsilon_{CO2} + \varepsilon_{CO} - \Delta\varepsilon_{CO2}^{H2O} - \Delta\varepsilon_{CO}^{H2O} - \Delta\varepsilon_{CO}^{CO2} + \Delta\varepsilon \qquad \text{(A.1)}$$

In Eq. (A.1), the first three terms are the emittances of the individual gases at their respective pressure-path lengths (bar-cm) and at the mixture temperature, found from Figures A.1 – A.3. These are based on an equivalent pressure, P_E, given by

$$\begin{aligned} P_E^{H2O} &= P_{tot}\left(1 + 5.00 x_{H2O}\right) \\ P_E^{CO2} &= P_{tot}\left(1 + 0.28 x_{CO2}\right) \\ P_E^{CO} &= P_{tot}\left(1 + 0.00 x_{CO}\right) \end{aligned} \qquad \text{(A.2)}$$

where the x_i values are the mole fractions of each component in the mixture with N_2. The next three terms are the binary overlap corrections from Figs. A.4 - A.6, and the final term in Eq. (A.1) is the ternary overlap correction, needed only if more than two gases are present in the mixture. This final term is given by

$$\Delta\varepsilon = \max(\Delta\varepsilon_{CO}^{H2O} + \Delta\varepsilon_{CO}^{CO2} - \varepsilon^{CO} : \varepsilon^{H2O}\varepsilon^{CO2}\varepsilon^{CO}) \qquad \text{(A.3)}$$

Some assumptions are built into the relations for pressure and overlap corrections, but comparisons between emittance values computed from the charts or worksheet and line-by-line calculations have shown that the graphical and worksheet results are within better than 1 percent of the exact LBL values. Alberti et al. (2018) give worked examples to illustrate use of the charts and worksheet.

Tam and Yuen (2019) provide an open-source tool for emittance and absorptance of CO_2-H_2O-N_2-O_2-soot mixtures for combustion calculations. Alberti et al. (2020) provide an updated method for computing the absorptance of CO_2, H_2O, CO, N_2 mixtures exposed to blackbody radiation at an arbitrary source temperature.

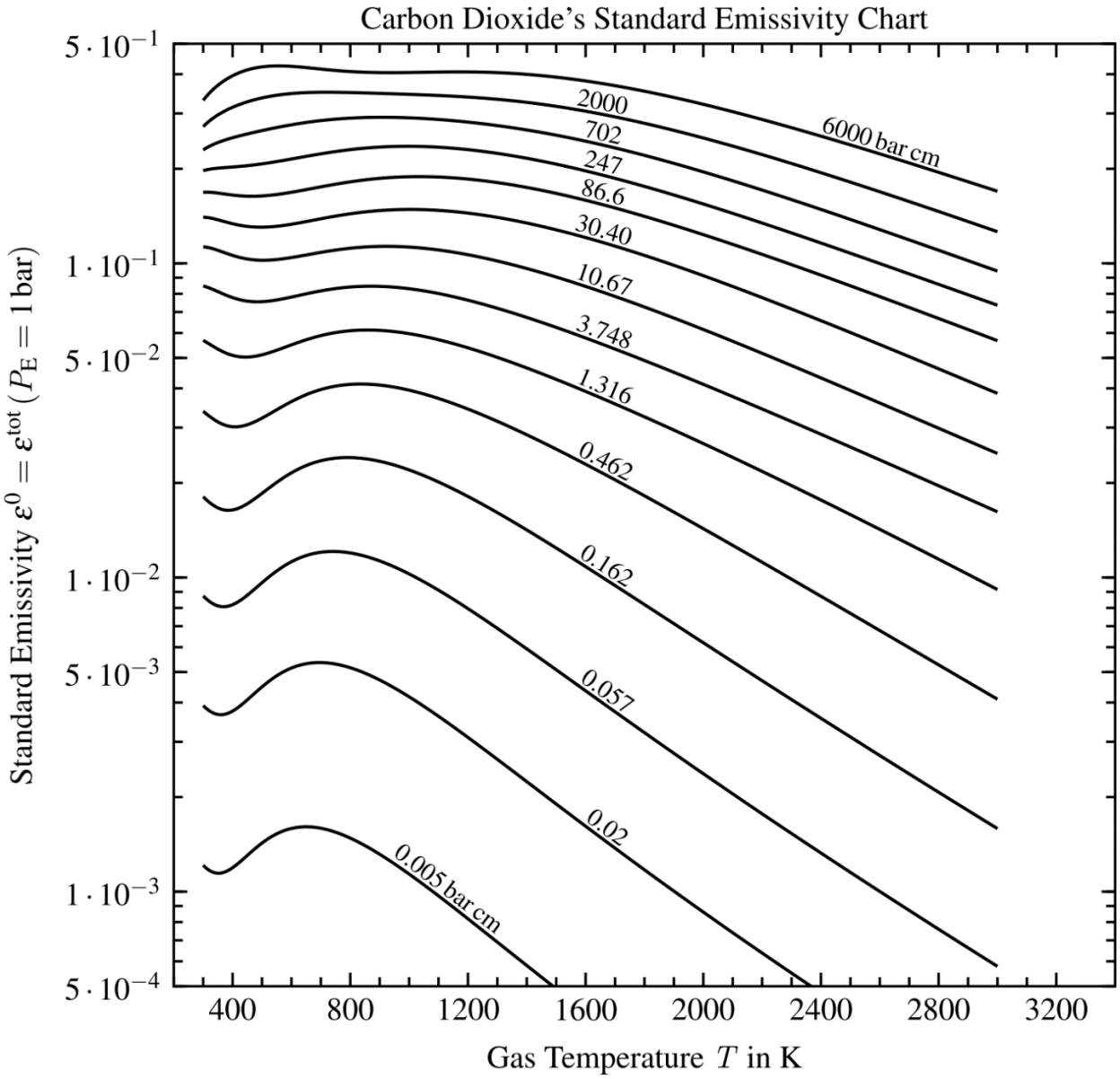

A.1 Emittance of Carbon Dioxide

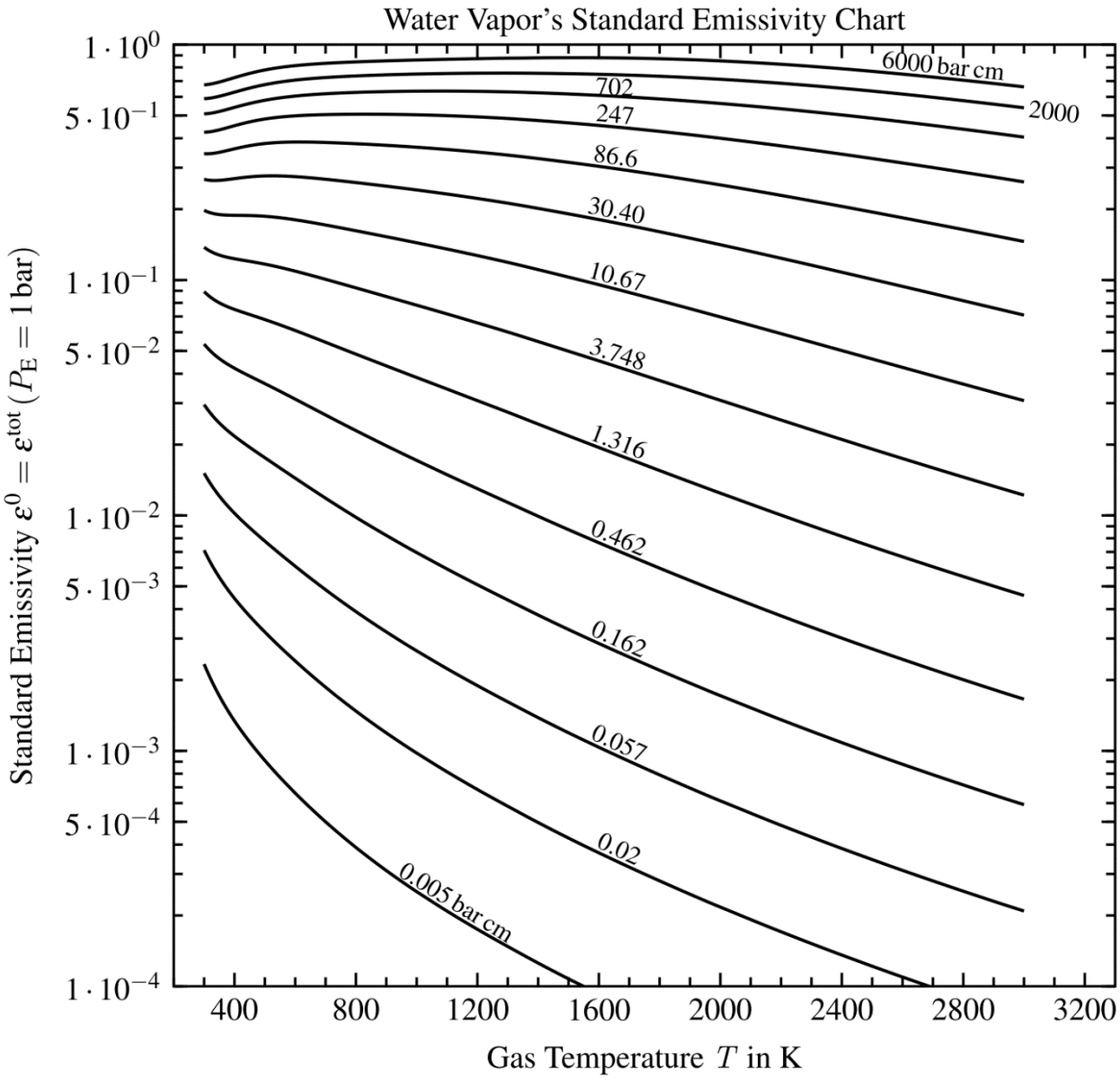

A.2 Emittance of Water Vapor

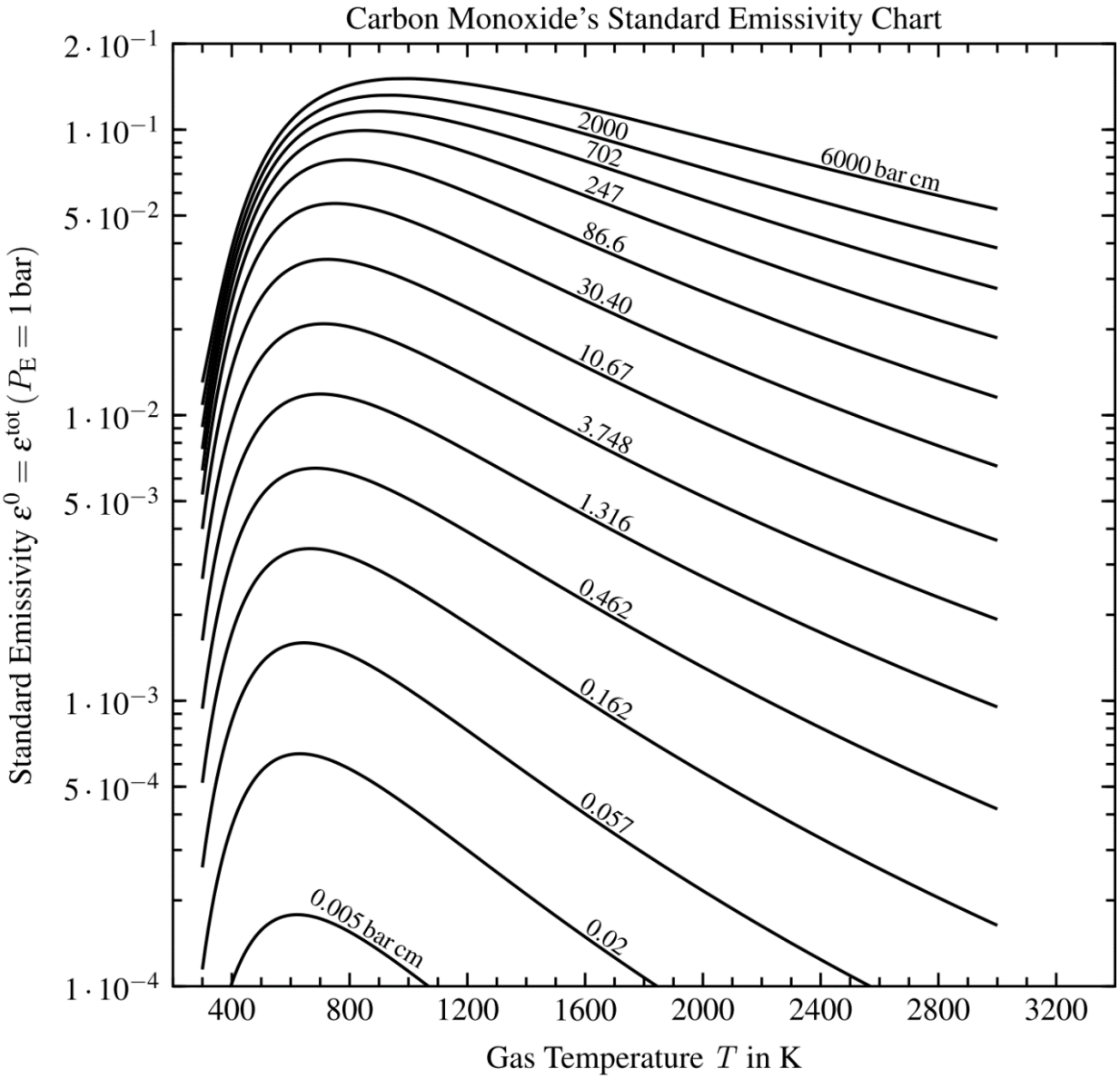

A.3 Emittance of Carbon Dioxide

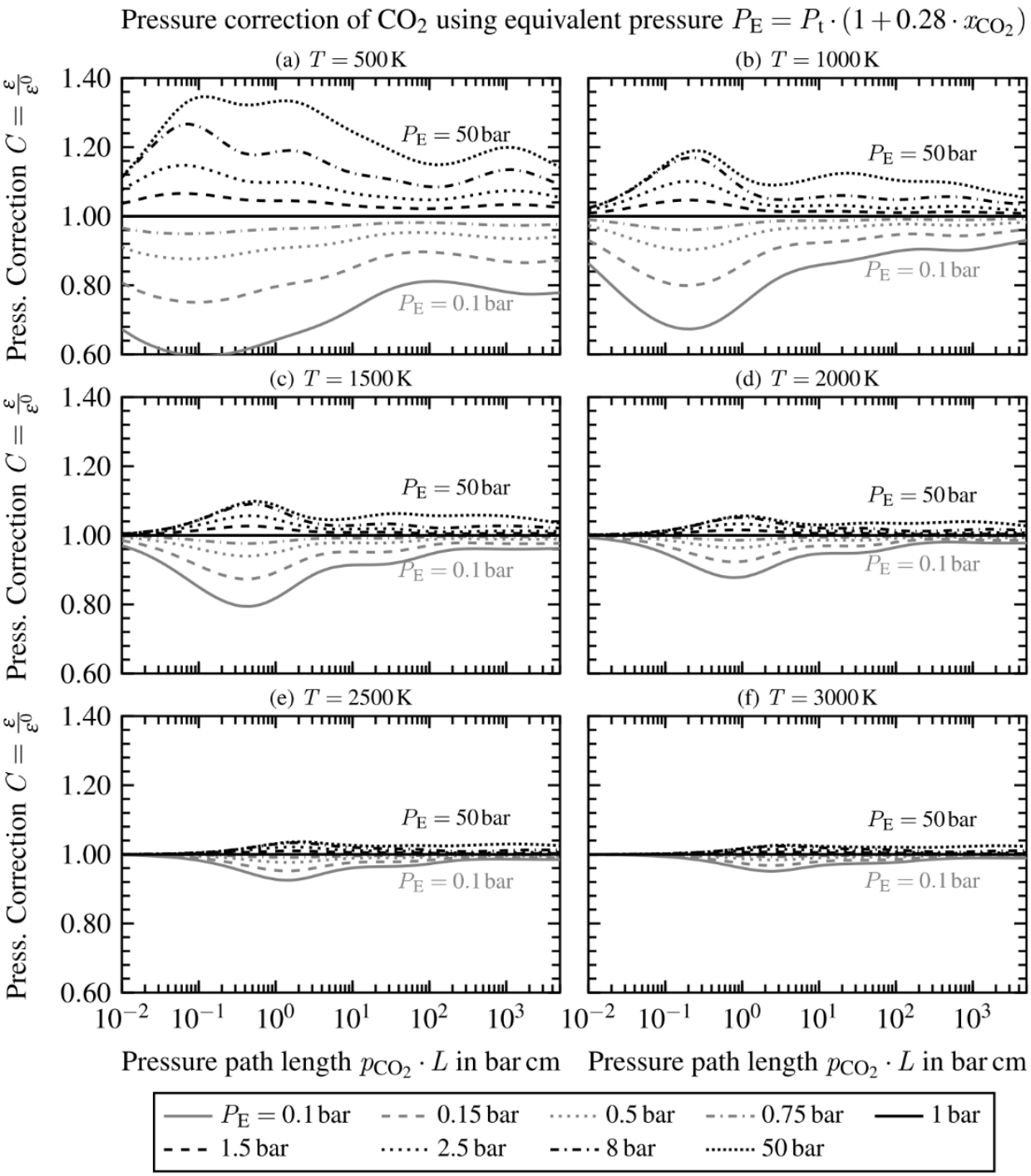

A.4 Pressure Correction for Carbon Dioxide

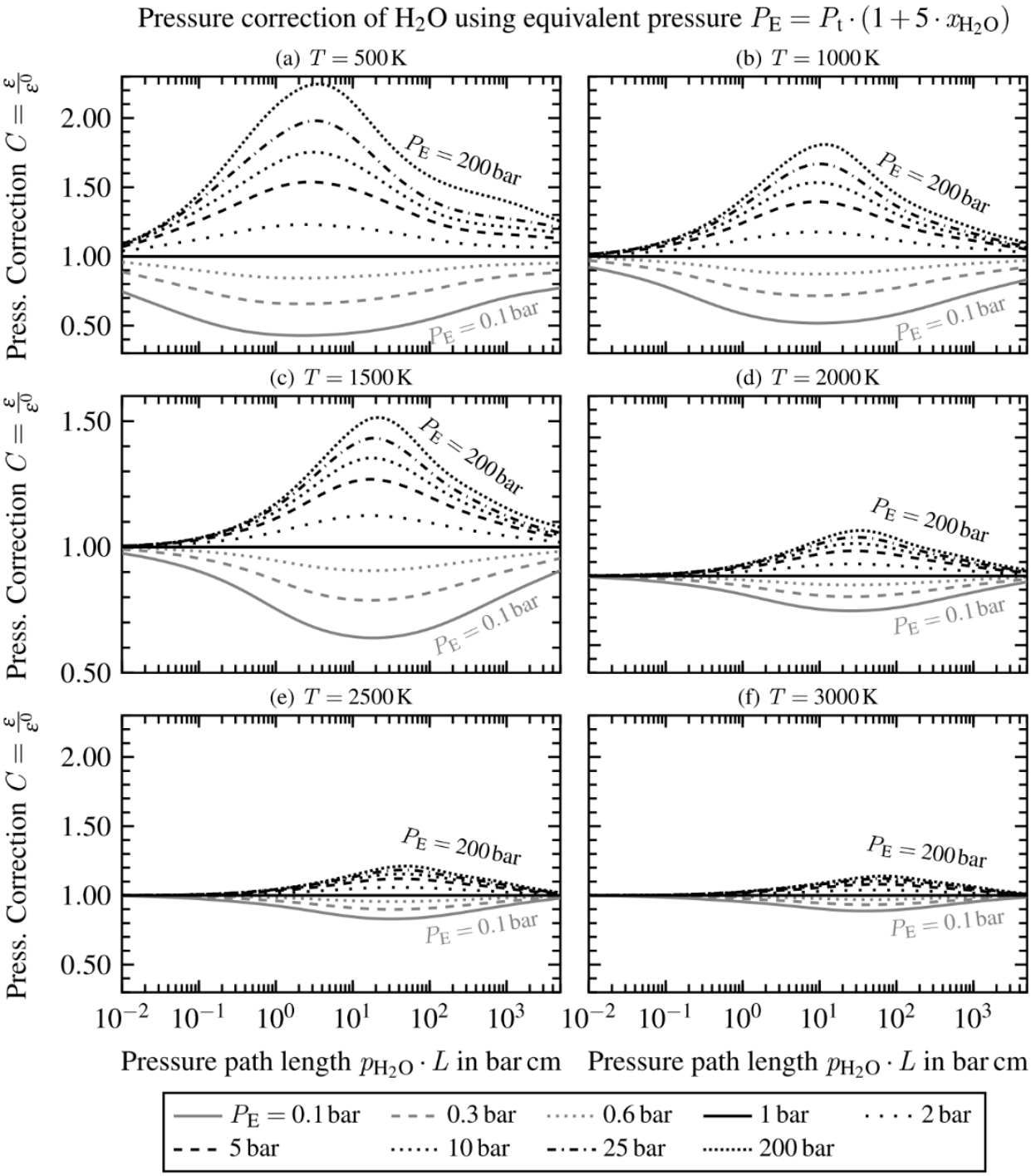

A.5 Pressure Correction for Water Vapor

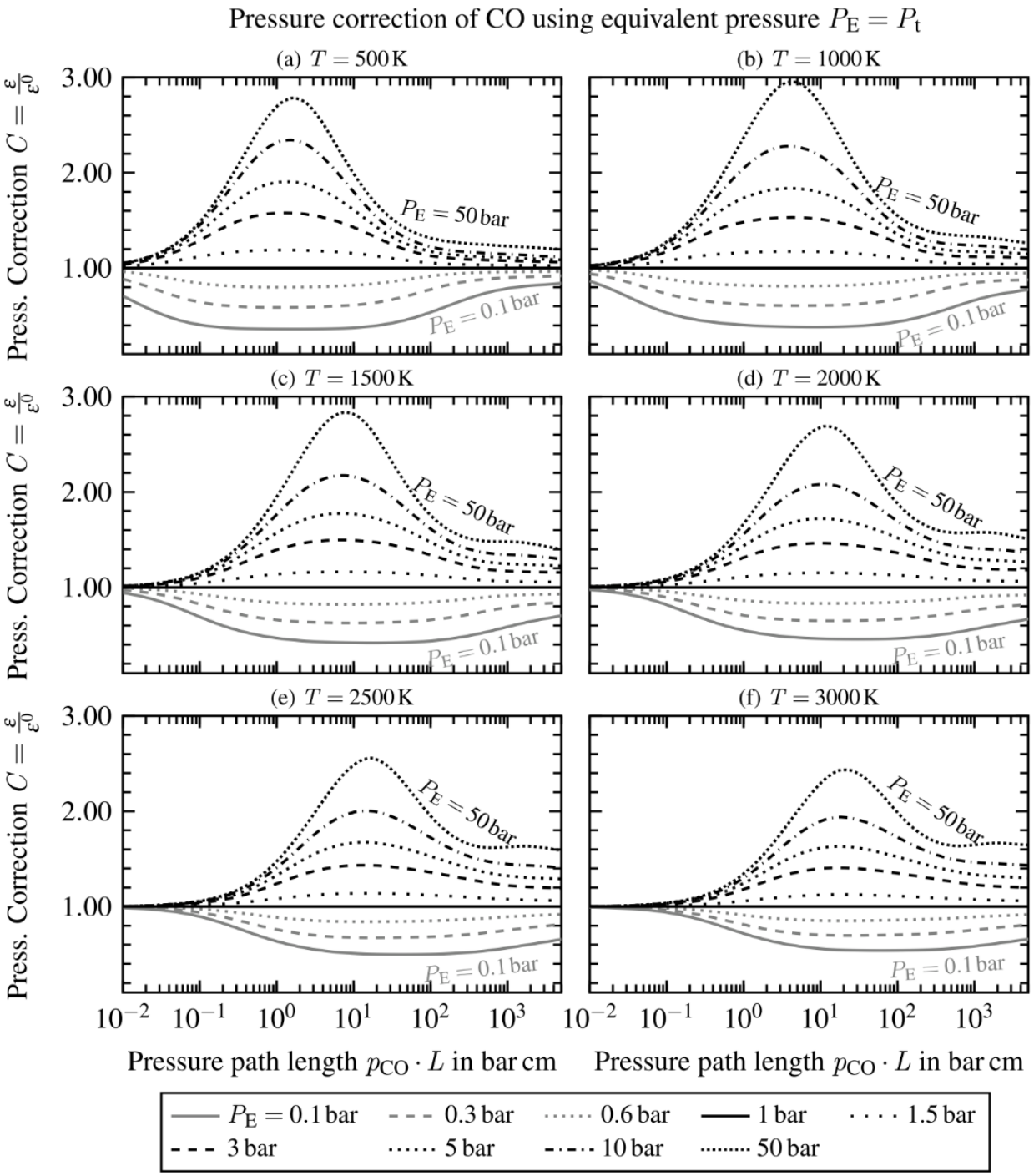

A.6 Pressure Correction for Carbon Monoxide

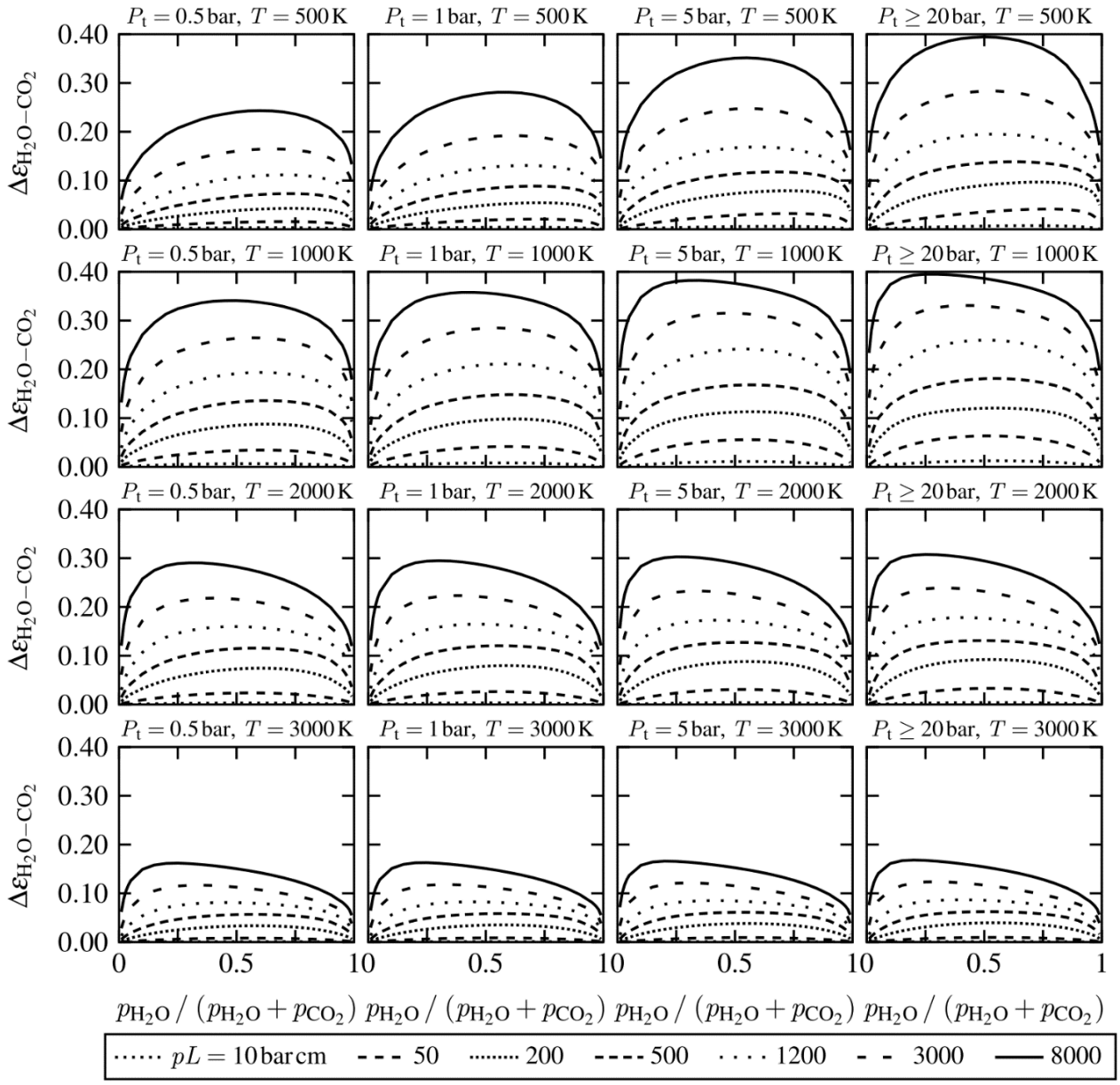

A.7 Overlap Correction for Water Vapor-Carbon Dioxide Mixtures

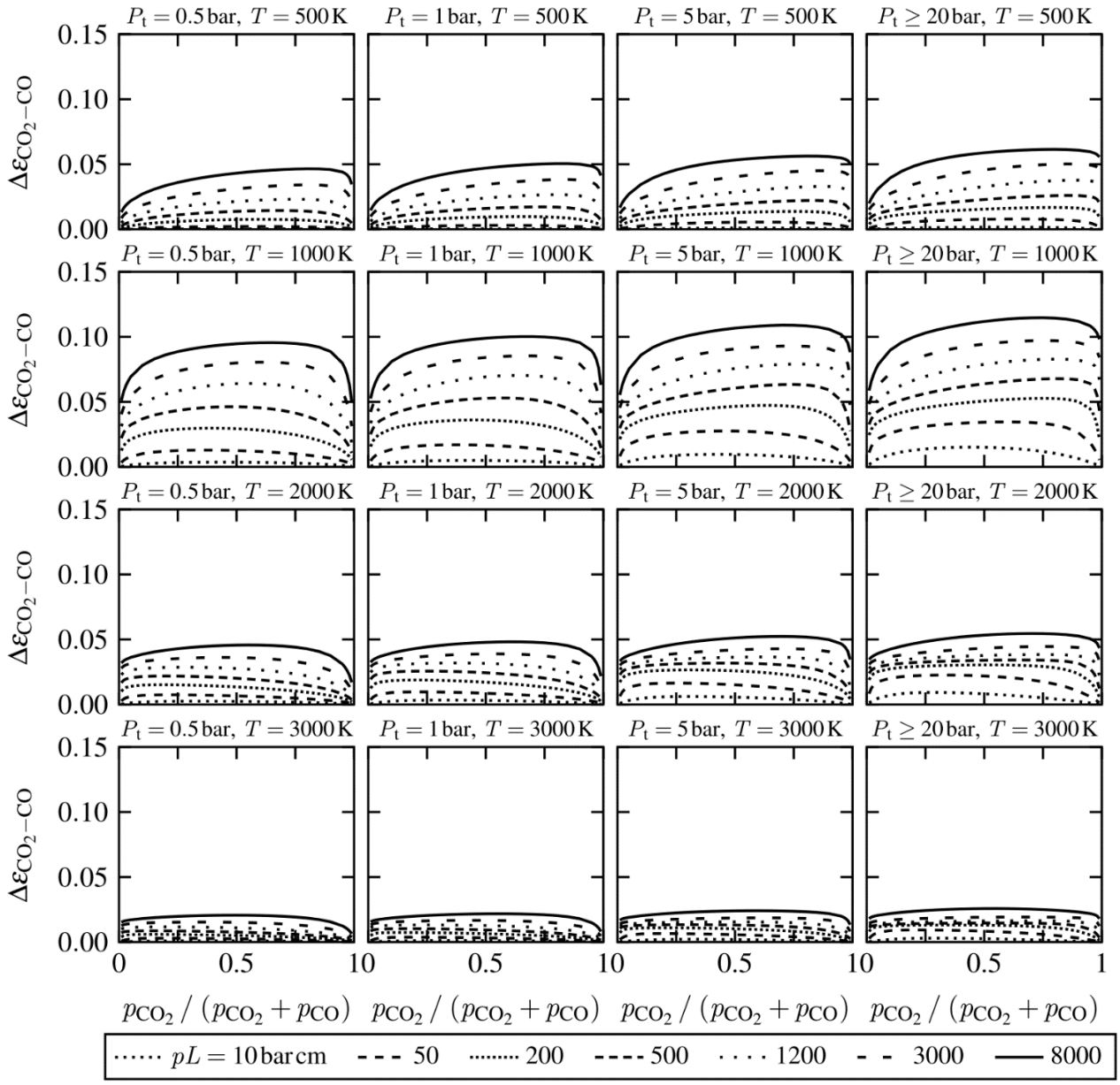

A.8 Overlap Correction for Carbon Dioxide-Carbon Monoxide Mixtures

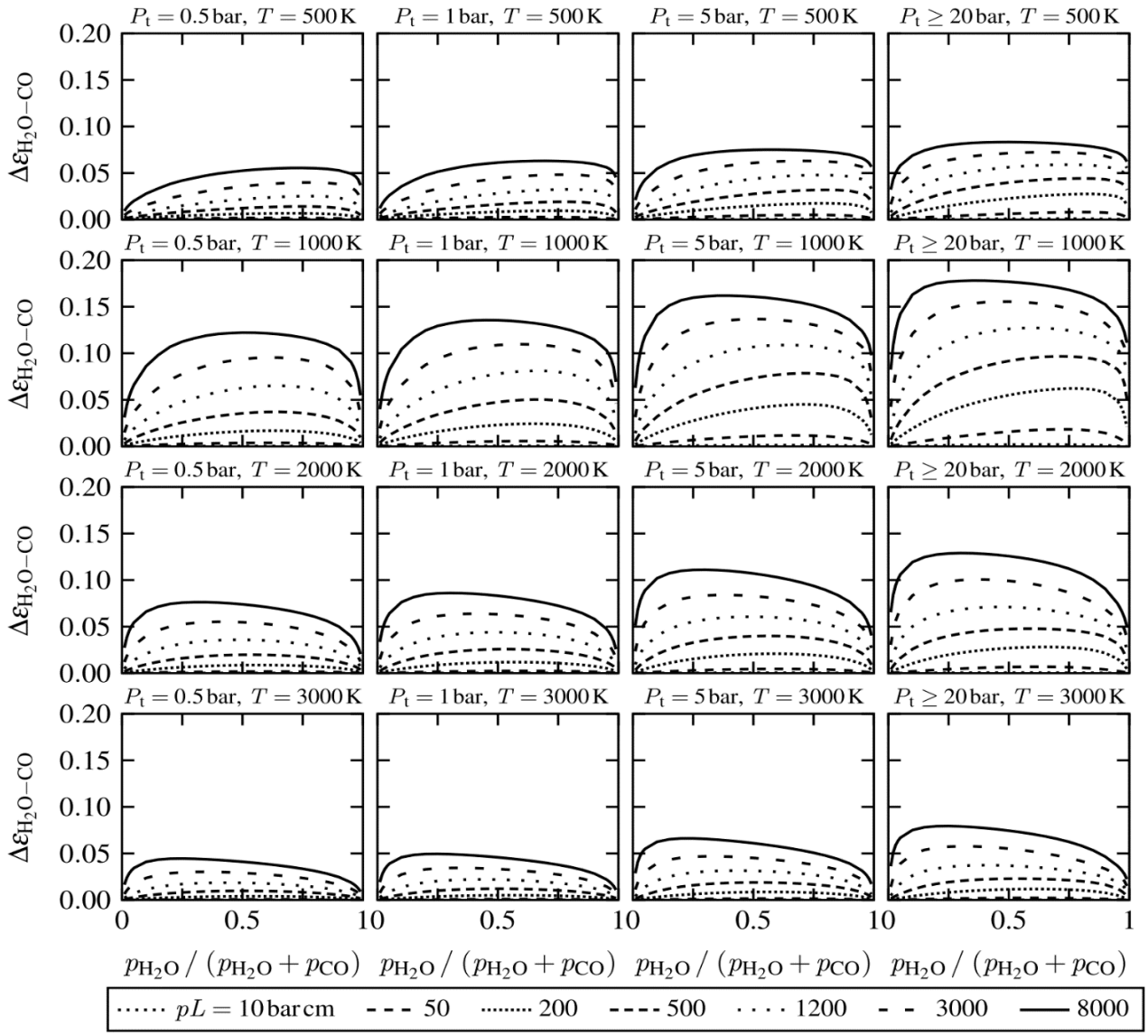

A.9 Overlap Correction for Water Vapor-Carbon Monoxide Mixtures

THE ORIGINAL HOTTEL CHARTS

Hottel's original graphs of the total emittance $\varepsilon(pL_e,T)$ for CO_2 and H_2O (Hottel, 1954; Hottel and Sarofim, 1967) have been widely used after they were published for radiative energy transfer calculations in combustion chambers. They were based on experimental data with extrapolations to high temperatures and large L_e-partial pressure regions based on theory and were a significant advance in providing data for engineering design.

Leckner (1972) gives empirical correlations for the total emittance derived from calculations summing narrow band behavior over the spectrum for both water vapor and CO_2. The most accurate expressions from Leckner agree within 5% to values calculated from spectral data for $T > 400$ K and are in close agreement with Hottel charts for ranges where Hottel based his charts on experimental data. Docherty (1982) compares Leckner's predictions with those of Hottel as well as with more recent experimental data and concludes that Leckner's predictions are more

accurate than Hottel's charts in the regions where Hottel extrapolated outside the range of experimental data available to him.

Leckner's correlations and equations are functions of p in bar and L_e in cm. The correlation equation is

$$\varepsilon(T, pL_e) = \exp\left\{a_0 + \sum_{j=1}^{M} a_j \left[\log(pL_e)\right]^j\right\} \tag{A.4}$$

where $a_j = c_{0j} + \sum_{i=1}^{N} c_{ij} \left(T/1000\right)^i$ and the values of c_{ij} are in Table A.1 for water vapor and for CO_2.

TABLE A.1
Coefficients c_{ij} for Equation A.4 to Calculate Water Vapor and CO_2 Emittance

j	c_{0j}	c_{1j}	c_{2j}	c_{3j}	c_{4j}
Water vapor, $T > 400$ K, $M = 2$, $N = 2$					
0	−2.2118	−1.1987	0.035596		
1	0.85667	0.93048	−0.14391		
2	−0.10838	−0.17156	0.045915		
Carbon dioxide, $T > 400$ K, $M = 3$, $N = 4$					
0	−3.9781	2.7353	−1.9822	0.31054	0.015719
1	1.9326	−3.5932	3.7247	−1.4535	0.20132
2	−0.35366	0.61766	−0.84207	0.39859	−0.063356
3	−0.080181	0.31466	−0.19973	0.046532	−0.0033086

For water vapor, the pressure correction from Leckner is

$$C_{H_2O} = 1 + (\Lambda_{H_2O} - 1)\Xi_{H_2O} \tag{A.5}$$

where $\Lambda_{H_2O} = \dfrac{\left[1.888 - 2.053\log_{10}(T/1000)\right]P_{E,\,H_2O} + 1.10(T/1000)^{-1.4}}{P_{E,\,H_2O} + \left[1.888 - 2.053\log_{10}(T/1000)\right] + 1.10(T/1000)^{-1.4} - 1}$

and $\Xi_{H_2O} = \exp\left(-\dfrac{\left\{\log_{10}[13.2(T/1000)^2] - \log_{10}(p_{H_2O}L_e)\right\}}{2}\right)$.

The effective pressure is given by $P_{E,\,H_2O} = P_t\left[1 + 4.9(p_{H_2O}/P_t)(273/T)^{1/2}\right]$ and P_t is the total pressure of the air–H_2O mixture. In the expression for Λ, the T in the expression in square brackets is replaced by 750 if $T < 750$ K.

The pressure correction for CO_2 from Leckner is given by

$$C_{CO_2} = 1 + (\Lambda_{CO_2} - 1)\Xi_{CO_2} \tag{A.6}$$

where $\Lambda_{CO_2} = \dfrac{\left[1.00 + 0.10(T/1000)^{-1.45}\right] P_{E,CO_2} + 0.23}{P_{E,CO_2} + \left[1.00 + 0.10(T/1000)^{-1.45}\right] - 0.77}$

and $\Xi_{CO_2} = \exp\left\{-1.47\left[\mu - \log_{10}(p_{CO_2} L_e)\right]\right\}$.

The effective pressure is given by $P_{E,CO_2} = P_t\left[1 + 0.28(p_{CO_2}/P_t)\right]$, where P_t is the total pressure of the air–CO_2 mixture. In the expression for Ξ, $\mu = \log_{10}[0.225(T/1000)^2]$ if $T > 700$ K, and $\mu = \log_{10}[0.054(T/1000)^{-2}]$ if $T < 700$ K.

An empirical expression for the band overlap correction that is in good agreement with the Hottel chart (Leckner 1972) valid for $1000 < T < 2200$ K and all pressures is

$$\Delta\varepsilon = \left(\frac{\zeta}{10.7 + 101\zeta} - 0.0089\zeta^{10.4}\right)\left[\log_{10}(pL_e)\right]^{2.76} \tag{A.7}$$

where $\zeta = p_{H_2O}/\left(p_{H_2O} + p_{CO_2}\right)$, $p = \left(p_{H_2O} + p_{CO_2}\right)$ is in bars, and L_e is in cm.

The emergence of the accurate line-by-line data bases (used in generating the charts and spread sheet by Alberti et al. 2018) has largely superseded the pioneering work of Hottel.

Example A.1

A container with effective radiation thickness of L_e = 2.4 m contains a mixture of 15 volume percent of CO_2, 20% H_2O vapor, and the remainder air. The total pressure of the gas mixture is 1 atm, and the gas temperature is 1200 K. What is the emittance of the gas?

The partial pressures of the gases are equal to the mole fraction of each times the total pressure. The mole fraction in an ideal gas mixture is equal to the volume fraction, so the partial pressures are $p_{CO_2} = 0.15$, $p_{H_2O} = 0.20$, and p_{air} = 0.65 atm. For water vapor, the a_j values are $a_j = c_{0j} + \sum_{i=1}^{N} c_{ij}\left(T/1000\right)^i$, giving $a_1 = -3.599$, $a_2 = 1.766$, and $a_3 = -0.248$. Using Equation A.4 (remembering to convert the pressures to bars), $\varepsilon_{H_2O}(T, pL_e) = \exp\left\{a_0 + \sum_{j=1}^{M} a_j\left[\log(pL_e)\right]^j\right\} = 0.313$.

A similar calculation for CO_2 gives $\varepsilon(CO_2)$ = 0.155. No pressure correction is necessary because the total pressure is 1 atm. The overlap correction is calculated using

$$\zeta = \frac{p_{H_2O}}{p_{H_2O} + p_{CO_2}} = \frac{0.20}{0.15 + 0.20} = 0.571$$

and

$$\left(p_{H_2O} + p_{CO_2}\right)L_e = (0.15 + 0.20)\,(\text{atm}) \times 1.01325\,(\text{bar/atm}) \times 240\,(\text{cm})$$
$$= 85.1(\text{bar} \times \text{cm}).$$

Substituting results in

$$\Delta\varepsilon = \left(\frac{\zeta}{10.7 + 101\zeta} - 0.0089\zeta^{10.4}\right)\left[\log_{10}(pL_e)\right]^{2.76} = 0.051$$

The total emittance of the gas mixture is then

$$\varepsilon_{mixture} = \varepsilon_{H_2O} + \varepsilon_{CO_2} - \Delta\varepsilon = 0.313 + 0.155 - 0.051 = 0.417$$

Using the data in the spreadsheet for the Alberti correlations gives a value of $\varepsilon_{Alberti} = 0.401$

REFERENCES:

Alberti, M., Weber, R., and Mancini, M.: Gray gas emissivities for H_2O-CO_2-CO-N_2 mixtures, *JQSRT*, 219, 274-291, Nov. 2018.

Alberti, M., Weber, R., and Mancini, M.: New formulae for gray gas absorptivities of H_2O, CO_2, and CO, *JQSRT*, 255, 107277, 2020.

Docherty, P.: Prediction of gas emissivity for a wide range of process conditions, Paper R5, *Proc. Seventh Intl. Heat Transfer Conf.*, vol. 2, pp. 481–485, Munich, Germany, 1982.

Hottel, H. C.: Radiant heat transmission, Chapter 4, in W. H. McAdams (ed.), *Heat Transmission*, 3rd edn., McGraw-Hill, New York, 1954.

Hottel, H. C. and Sarofim, A. F.: *Radiative Transfer*, McGraw–Hill, New York, 1967.

Leckner, B.: Spectral and total emissivity of water vapor and carbon dioxide, *Combust. Flame*, 19, 33–48, 1972.

Tam, W.C. and Yuen, W. W.: OpenSC – an Open-source Calculation Tool for Combustion Mixture Emissivity/Absorptivity, NIST Technical Note 2064, *National Inst. Standards and Technology*, Sept. 2019.

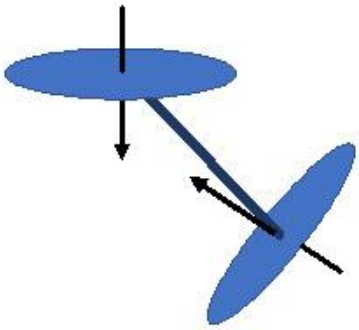

B: DIRECTIONAL/SPECULAR SURFACE ENCLOSURES

B.1 INTRODUCTION

Many radiation analyses assume diffuse emitting and reflecting surfaces, and some treatments include the effect of specular reflections with diffuse emission (Section 6.6). Diffuse or specular surface conditions are the most convenient to treat analytically, and in many instances the detailed consideration of directional emission and reflection effects is unwarranted. However, certain materials and special situations require the examination of directional effects.

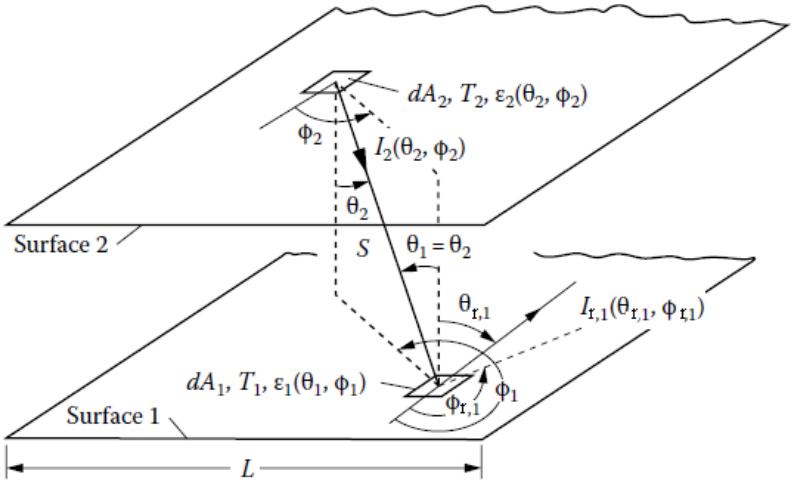

Figure B.1 Radiant interchange between parallel directional surfaces of finite width L that are infinitely long in the direction normal to the plane of the drawing.

The difficulty in treating the general case of directionally dependent properties is illustrated by performing an energy balance in a simple geometry: the radiative exchange between two infinitely long parallel nondiffuse gray surfaces of finite width L (Figure B.1). The radiation intensity leaving element dA_1 in direction $(\theta_{r,1},\phi_{r,1})$ is composed of emitted and reflected intensities:

$$I_1(\theta_{r,1},\phi_{r,1}) = I_{e,1}(\theta_{r,1},\phi_{r,1}) + I_{r,1}(\theta_{r,1},\phi_{r,1}) \tag{B.1}$$

These two components are given by modifications of Equations 3.4 and 3.41 to convert Equation B.1 to the form

$$I_1(\theta_{r,1},\phi_{r,1}) = \varepsilon_1(\theta_{r,1},\phi_{r,1}) I_{b,1}(T_1) + \int_{A_2} \rho_1(\theta_{r,1},\phi_{r,1},\theta_1,\phi_1) I_2(\theta_2,\phi_2) \frac{\cos^2\theta_2}{S^2} dA_2 \tag{B.2}$$

In the second term on the right of Equation B.2, the energy incident on dA_1 from each element dA_2 is multiplied by the bidirectional total reflectivity to give the contribution to the intensity reflected from dA_1 into direction $(\theta_{r,1},\phi_{r,1})$. This is then integrated over A_2 to include all energy incident on dA_1 from A_2.

A similar equation is written for an arbitrary element dA_2 on surface 2. The result is a pair of coupled integral equations to be solved for $I(\theta, \phi)$ at each position and for each direction on the two surfaces. Detailed property data for $\varepsilon(\theta, \phi)$ and $\rho(\theta_r, \phi_r, \theta_i, \phi_i)$ are often not available. For the case when T_1 and T_2 are not known and the temperature dependence of the properties is considerable, the solution for the entire energy-exchange distribution becomes very tedious. Approximations can be made, such as analytically simulating the real properties with simple functions, omitting certain portions of energy deemed negligible, or ignoring directional effects except those expected to provide significant changes from diffuse or specular analyses.

The effect of polarization has been neglected in this treatment. It can be quite important when multiple specular reflections are present, as one polarized component may be quickly attenuated after multiple reflections while the other may not. Using an average reflectivity will not capture that effect. This is especially the case for long channels such as light pipes and fiber optics.

An example is now given illustrating the effect of a directional-gray surface on radiative exchange.

Example B.1

Two parallel isothermal plates of infinite length and finite width L are arranged as in Figure B.2a. The upper plate is black, while the lower is a highly reflective gray material with parallel deep grooves of open angle 1° in its surface extending along the infinite direction. Such a surface might be constructed by stacking polished razor blades. The surroundings are at zero temperature. Compute the net energy gain by the directional surface if $T_2 > T_1$ and compare the result to the net energy gain if the directional-gray surface is replaced by a diffuse-gray surface with an emissivity equivalent to the hemispherical emissivity of the directional surface.

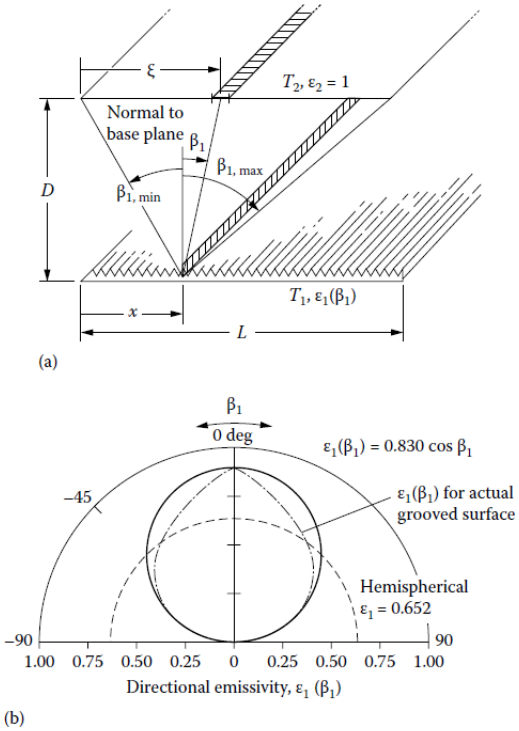

Figure B.2 Interchange between grooved directional-gray surface and black surface: (a) geometry of problem (environment at zero temperature); (b) emissivity of directional surface.

In Howell and Perlmutter (1963), the directional emissivity is calculated at the opening of an infinitely long groove with specularly reflecting walls of surface emissivity 0.01. This is given by the dot-dashed line in Figure B.2b. The angle β_1 is measured

from the normal of the opening plane of the grooved surface and is in the cross-sectional plane perpendicular to the length of the groove as in Figure B.2a. The $\varepsilon_1(\beta_1)$ has already been averaged over all circumferential angles for a fixed β_1. Thus, it is an effective emissivity for radiation from a strip on the grooved surface to a parallel infinitely long strip element on an imaginary semicylinder over the groove and with its axis parallel to the grooves. The angle β_1 is different from the usual cone angle θ_1. The actual emissivity $\varepsilon_1(\beta_1)$ of Figure B.2b is approximated for convenience by the analytical expression $\varepsilon_1(\beta_1) \approx 0.830 \cos\beta_1$. Using cylindrical coordinates to integrate over all β_1, the hemispherical emissivity of this surface is

$$\varepsilon_1 = \frac{\int_{-\pi/2}^{\pi/2} \varepsilon_1(\beta_1)\cos\beta_1 d\beta_1}{\int_{-\pi/2}^{\pi/2} \cos\beta_1 d\beta_1} = 0.830 \int_0^{\pi/2} \cos^2\beta_1 d\beta_1 = 0.652$$

and this is the dashed line in Figure B.2b.

The energy gained by surface 1 will first be determined when surface 2 is black and surface 1 is diffuse with $\varepsilon_1 = 0.652$. The energy emitted by the diffuse surface 1 per unit of the infinite length and per unit time is $Q_{e,1} = 0.652\,\sigma T_1^4 L$. Because surface 2 is black, none of this energy is reflected to surface 1. The energy per unit length and time emitted by black surface 2 that is absorbed by surface 1 is

$$Q_{a,1} = \alpha_1 \sigma T_2^4 \int_{A_2}\int_{A_1} dF_{d2-d1} dA_2 = \varepsilon_1 \sigma T_2^4 \int_{A_1}\int_{A_2} dF_{d1-d2} dA_1$$

The configuration factor between infinite parallel strips, from Example 5.2, is $dF_{d1-d2} = d(\sin\beta_1)/2$ so that

$$\int_{A_1}\left(\int_{A_2} dF_{d1-d2}\right) dA_1 = \frac{1}{2}\int_{x=0}^{L} (\sin\beta_{1,max} - \sin\beta_{1,min})\, dx$$

From Figure B.2a, $\sin\beta_1 = (\xi - x)\Big/\left[(\xi - x)^2 + D^2\right]^{1/2}$, which gives

$$Q_{a,1} = \varepsilon_1 \sigma T_2^4 \frac{1}{2}\int_{x=0}^{L}\left[\frac{L-x}{\left(x^2 - 2xL + L^2 + D^2\right)^{1/2}} + \frac{x}{\left(x^2 + D^2\right)^{1/2}}\right] dx$$

$$= 0.652\sigma T_2^4\left[\left(L^2 + D^2\right)^{1/2} - D\right]$$

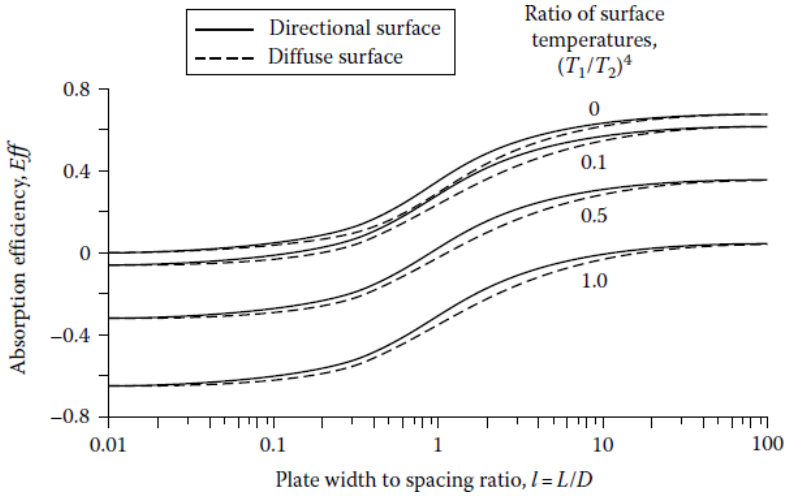

Figure B.3 Effect of directional emissivity on absorption efficiency of surface.

The net energy gained by surface 1, $Q_{a,1} - Q_{e,1}$, divided by the energy emitted by surface 2, is a measure of the efficiency of the surface as a directional absorber. For surface 1, being diffuse, this ratio is ($l = L/D$).

$$\mathrm{Eff}_{\mathrm{diffuse}} = \frac{Q_{a,1} - Q_{e,1}}{\sigma T_2^4 L} = \frac{0.652}{l}\left[\left(1+l^2\right)^{1/2} - 1 - \frac{T_1^4}{T_2^4} l\right]$$

When surface 1 is a directional (grooved) surface, the amount of energy emitted from surface 1 is the same as for a diffuse surface (although it has a different directional distribution) since both have the same hemispherical emissivity. The energy absorbed by the grooved surface is, by using $\alpha_1(\beta_1) = \varepsilon_1(\beta_1)$ for a gray surface,

$$\begin{aligned} Q_{a,1} &= \sigma T_2^4 \int_{A_2}\int_{A_1} \alpha_1(\beta_1) dF_{d2-d1} dA_2 = \frac{0.830\sigma T_2^4}{2} \int_{x=0}^{L}\int_{\beta_{1,\min}}^{\beta_{1,\max}} \cos^2\beta_1 d\beta_1 dx \\ &= \frac{0.830\sigma T_2^4}{4} \int_{x=0}^{L} \left[\frac{D(L-x)}{x^2 - 2xL + L^2 + D^2} + \tan^{-1}\left(\frac{L-x}{D}\right) + \frac{xD}{x^2 + D^2} + \tan^{-1}\frac{x}{D}\right] dx \\ &= \frac{0.830\sigma T_2^4}{2} \tan^{-1}\frac{L}{D} \end{aligned}$$

The absorption efficiency of the directional surface is then

$$\mathrm{Eff}_{\mathrm{directional}} = \frac{Q_{a,1} - Q_{e,2}}{\sigma T_2^4 L} = \frac{0.830}{2}\tan^{-1} l - 0.652\left(\frac{T_1}{T_2}\right)^4$$

The absorption efficiencies of the directional-gray and diffuse-gray surfaces are in Figure B.3 as a function of l with $(T_1/T_2)^4$ as a parameter. The *Eff* for the directional surface is higher than that for the diffuse surface for all values of l. As l approaches zero, the configuration approaches that of infinite elemental strips, and emission from surface 1 becomes much larger than absorption from surface 2. Thus, $Eff_{directional}$ and $Eff_{diffuse}$ are nearly equal since the surfaces always emit the same amount. As l approaches infinity, the directional effects are lost. At intermediate l a 10% difference in absorption efficiency is attainable.

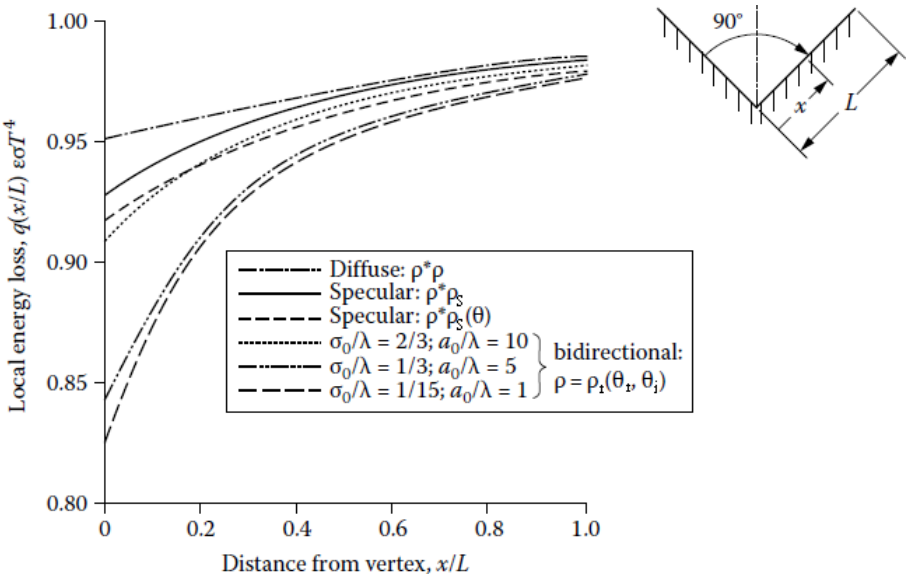

Figure B.4 Local radiative energy loss from surface of isothermal groove cavity. Hemispherical emissivity of surface is assumed with $\varepsilon = 0.1$.

The effects of directional properties on the local energy loss can be considerable for some geometries. In Figure B.4 some directional distributions of reflectivity are examined for their influence on local energy loss from the walls of an infinitely long groove. The results are from Viskanta et al. (1967), where for comparison the curves were gathered from original work and

various sources. The walls of the groove are at 90°, and the surface emissivity distributions are all normalized to give a hemispherical emissivity of 0.1. Curves are presented for diffuse reflectivity ρ, specular reflectivity assumed independent of incident angle ρ_s, specular reflectivity dependent on incident angle $\rho_s(\theta_i)$ based on electromagnetic theory, and three distributions of bidirectional reflectivity $\rho(\theta_r, \theta_i)$. The bidirectional distributions are based on Beckmann and Spizzichino (1963) for rough surfaces having various combinations of the ratio of rms optical-surface roughness amplitude to radiation wavelength, σ_0/λ, and the ratio of roughness autocorrelation distance to radiation wavelength, a_0/λ. Note that the results in Figure B.4 for the specular and diffuse models do *not* provide upper and lower limits to all the solutions, as is sometimes claimed. Additional information on surface roughness as it affects the directional properties of surfaces is in Section 4.2. Energy transfer was studied in a groove with two rough sides, each at uniform temperature. The roughness has a greater influence on the radiation exchange between the two sides than on the net radiation from the groove.

B.2 SURFACES WITH DIRECTIONALLY AND SPECTRALLY DEPENDENT PROPERTIES

The general case of radiative transfer in enclosures where surface properties depend on both direction and wavelength, and where properties can be temperature dependent, is complex to treat fully. When those dependencies must be included, numerical techniques are necessary. Toor (1967) used the Monte Carlo method to study radiation interchange for various simply arranged surfaces with directional properties. Zhang et al. (1997) derived the directional-spectral relation for radiative transfer between parallel plates. That is a generalization (with properties independent of angle ϕ) of Equation (6.5.3) in Example 6.5:

$$q = 2\int_{\theta=0}^{\pi/2}\int_{\lambda=0}^{\infty} \frac{E_{\lambda b,1}(T_1) - E_{\lambda b,2}(T_1)}{\dfrac{1}{\varepsilon_{\lambda,1}(\theta_1, T_1)} + \dfrac{1}{\varepsilon_{\lambda,2}(\theta_2, T_2)} - 1} d\lambda \sin\theta\cos\theta d\theta \tag{B.3}$$

A difficulty for such an evaluation is in finding the detailed radiative properties to sufficient accuracy. The technology of interest was for evaluating the insulating performance of a double glass window with a vacuum between the two panes. The glass surfaces are opaque in the infrared region

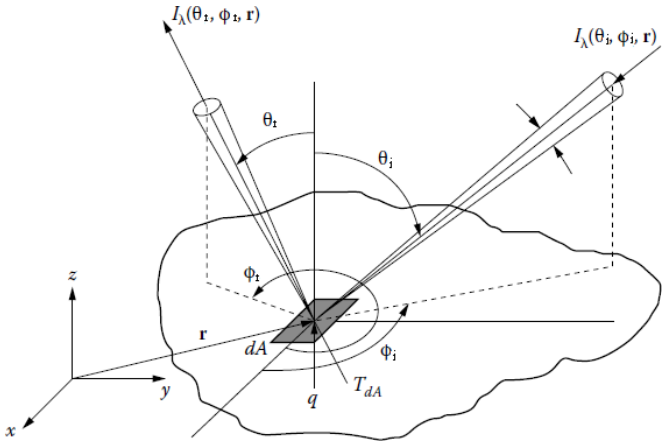

Figure B.5 Geometry for incoming and outgoing intensities at a differential surface area.

so that, for the temperatures involved, Equation (B.3) could be used for transfer across the vacuum space. Comparisons were made with experiments.

In this section, the general integral equations are formulated for radiation in such systems, and a considerably simplified example problem is solved. The procedure is a combination of the previous diffuse-spectral and directional-gray analyses. The equations are formulated at one wavelength as in Section 6.7 and in terms of intensities for each direction as in Section 6.8; this accounts for both spectral and directional effects. The interaction between two plane surfaces is developed first; this can be generalized to a multisurface enclosure as for gray surfaces in Section 6.3.

The energy balance is now developed for an area element dA at location r in an x, y, z coordinate system as in Figure B.5. The $I_{\lambda o}(\theta_r, \phi_r, \mathbf{r})$ is the outgoing spectral intensity from dA in the direction θ_r, ϕ_r as the result of both emission and reflection. The spectral intensity emitted by dA in this direction is

$$I_{\lambda e}(\theta_r, \phi_r, \mathbf{r}) = \varepsilon_\lambda(\theta_r, \phi_r, \mathbf{r}) I_{\lambda b}(\mathbf{r}) \tag{B.4}$$

These quantities also depend on T_{dA}, but this functional designation is omitted to simplify the notation. The intensity reflected from dA into the θ_r, ϕ_r direction results from the incident intensity from all directions of a hemisphere above dA. If the spectral intensity incident on dA within $d\Omega_i$ is $I_{\lambda i}(\theta_i, \phi_i, \mathbf{r})$, the intensity reflected from dA into direction θ_r, ϕ_r is

$$I_{\lambda,r}(\theta_r, \phi_r, \mathbf{r}) = \int_{\Omega_i=0}^{2\pi} \rho_\lambda(\theta_r, \phi_r, \theta_i, \phi_i, \mathbf{r}) I_{\lambda,i}(\theta_i, \phi_i, \mathbf{r}) \cos\theta_i \, d\Omega_i \tag{B.5}$$

The net energy flux supplied to dA for steady state is the difference between the outgoing and incoming radiative fluxes:

$$q(\mathbf{r}) = \int_{\lambda=0}^{\infty} J_\lambda(\mathbf{r})\,d\lambda - \int_{\lambda=0}^{\infty} G_\lambda(\mathbf{r})\,d\lambda \tag{B.6}$$

The $J\lambda(\mathbf{r})d\lambda$ is the angular integration of the emitted and reflected spectral fluxes over all outgoing directions:

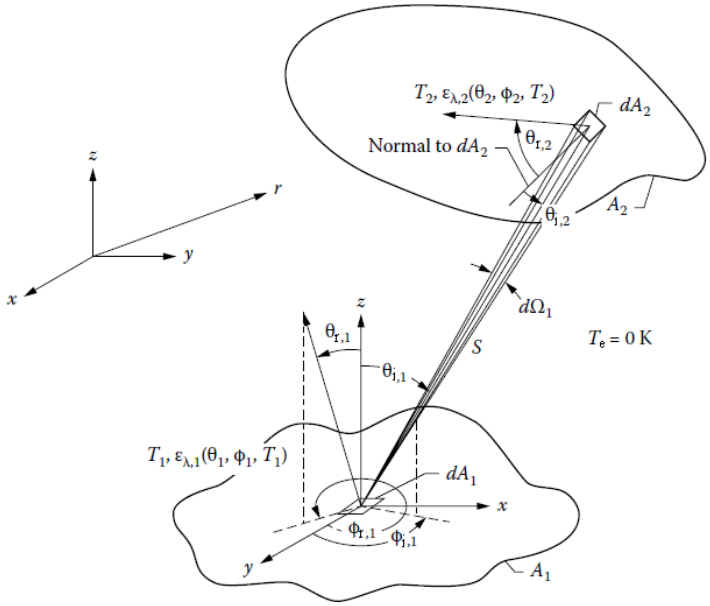

Figure B.6 The interchange between surfaces having directional spectral properties (environment at ~0 K).

$$\begin{aligned} J_\lambda(\mathbf{r})\,d\lambda = I_{\lambda b}(\mathbf{r})\,d\lambda \int_{\phi_r=0}^{2\pi}\int_{\theta_r=0}^{\pi/2} \varepsilon_\lambda(\theta_r, \phi_r, \mathbf{r}) \sin\theta_r \cos\theta_r d\theta_r d\phi_r \\ + \int_{\phi_r=0}^{2\pi}\int_{\theta_r=0}^{\pi/2} I_{\lambda,r}(\theta_r, \phi_r, \mathbf{r})\,d\lambda \sin\theta_r \cos\theta_r d\theta_r d\phi_r \end{aligned} \tag{B.7}$$

The $G_\lambda(\mathbf{r})d\lambda$ is the result of spectral fluxes incident from all $d\Omega_i$ directions:

$$G_\lambda(\mathbf{r})\,d\lambda = \int_{\phi_i=0}^{2\pi}\int_{\theta_i=0}^{\pi/2} I_{\lambda,i}(\theta_i, \phi_i, \mathbf{r})\,d\lambda \sin\theta_i \cos\theta_i d\theta_i d\phi_i \tag{B.8}$$

Equations (B.4) through (B.8) provide an exact formulation to obtain the energy flux $q(\mathbf{r})$ that must be supplied by other means to area dA to maintain its temperature at T_{dA} in the presence of incident and emitted radiation.

To develop an enclosure theory, various degrees of approximation can be made. If the enclosure is very simple, such as having only two infinite plane surfaces, it may be feasible to include variations of properties and surface temperature across each surface. To develop the required

integral equations, consider the two surfaces in Figure B.6 and let the surrounding environment be at low temperature so that it does not contribute incident radiation. The spectral energy leaving dA_2 at $\mathbf{r}_2$ that reaches dA_1 at $\mathbf{r}_1$ is $I_{\lambda o,2}(\theta_2,\phi_2,\mathbf{r}_2)d\lambda dA_2\cos\theta_2(dA_1\cos\theta_1/S^2)$. In terms of the incident intensity, the incident spectral intensity in $d\Omega_1$ is $I_{\lambda i,1}(\theta_1,\phi_1,\mathbf{r}_1)d\lambda dA_1\cos\theta_1 d\Omega_1$, where $d\Omega_1 = (dA_2\cos\theta_2)/S^2$. Thus, $I_{\lambda i,1}(\theta_1,\phi_1,\mathbf{r}_1) = I_{\lambda o,2}(\theta_2,\phi_2,\mathbf{r}_2)$ and, by using Equations (B.4) and (B.5),

$$I_{\lambda o,1}\left(\theta_{r,1},\phi_{r,1},\mathbf{r}_1\right) = \varepsilon_{\lambda,1}\left(\theta_{r,1},\phi_{r,1},\mathbf{r}_1\right) I_{\lambda b,1}\left(\mathbf{r}_1\right) + \int_{A_2} \rho_{\lambda,1}\left(\theta_{r,1},\phi_{r,1},\theta_{i,1},\phi_{i,1},\mathbf{r}_1\right) I_{\lambda o,2}\left(\theta_2,\phi_2,\mathbf{r}_2\right) \frac{\cos\theta_1\cos\theta_2}{\left|\mathbf{r}_2-\mathbf{r}_1\right|^2} dA_2 \tag{B.9}$$

Similarly, for surface 2, the outgoing intensity is

$$I_{\lambda o,2}\left(\theta_{r,2},\phi_{r,2},\mathbf{r}_2\right) = \varepsilon_{\lambda,2}\left(\theta_{r,2},\phi_{r,2},\mathbf{r}_2\right) I_{\lambda b,2}\left(\mathbf{r}_2\right) + \int_{A_1} \rho_{\lambda,1}\left(\theta_{r,2},\phi_{r,2},\theta_{i,2},\phi_{i,2},\mathbf{r}_2\right) I_{\lambda o,1}\left(\theta_1,\phi_1,\mathbf{r}_1\right) \frac{\cos\theta_2\cos\theta_1}{\left|\mathbf{r}_1-\mathbf{r}_2\right|^2} dA_1 \tag{B.10}$$

Equations (B.9) and (B.10) are both in terms of outgoing intensities, and they provide a set of simultaneous integral equations for $I_{\lambda o,1}$ and $I_{\lambda o,2}$, where the subscript o denotes the outgoing direction. An iterative numerical solution is required that can be quite complex as both unknowns are functions of position and angle. After $I_{\lambda o,1}(\theta_1, \phi_1, \mathbf{r}_1)$ and $I_{\lambda o,2}$ $(\theta_2, \phi_2, \mathbf{r}_2)$ are obtained, the total energy can be determined that must be supplied to each surface element to maintain the specified local surface temperature. The total energy supplied is the difference between the total emitted and absorbed energies:

$$\frac{dQ_1}{dA_1} = \int_{\lambda=0}^{\infty}\int_{\cap} \varepsilon_{\lambda,1}\left(\theta_{r,1},\phi_{r,1},\mathbf{r}_1\right) I_{\lambda b,1}\left(\mathbf{r}_1\right)\cos\theta_1 d\Omega_1 d\lambda - \int_{\lambda=0}^{\infty}\int_{A_2} \alpha_{\lambda,1}\left(\theta_{i,1},\phi_{i,1},\mathbf{r}_1\right) I_{\lambda o,2}\left(\theta_2,\phi_2,\mathbf{r}_2\right) \frac{\cos\theta_1\cos\theta_2}{\left|\mathbf{r}_2-\mathbf{r}_1\right|^2} dA_2 d\lambda \tag{B.11}$$

To develop an enclosure theory with more than a few surfaces, the $I_{\lambda o}$, temperature, and surface properties are usually assumed uniform over each enclosure surface. In addition, a finite number of angular intervals must be specified. If we let A_k and A_j be the kth and jth surfaces of an enclosure with N surfaces, then, by integrating Equation (B.9) over A_k and summing the contributions from all of the A_j surfaces,

$$I_{\lambda o,k}\left(\theta_{r,k},\phi_{r,k}\right) = \varepsilon_{\lambda,k}\left(\theta_{r,k},\phi_{r,k}\right) I_{\lambda b,k} + \frac{1}{A_k}\sum_{j=1}^{N}\int_{A_k}\int_{A_j} \rho_{\lambda,k}\left(\theta_{r,k},\phi_{r,k},\theta_{i,k},\phi_{i,k}\right) I_{\lambda o,j}\left(\theta_j,\phi_j\right) \frac{\cos\theta_k\cos\theta_j}{\left|\mathbf{r}_j-\mathbf{r}_k\right|^2} dA_j dA_k \tag{B.12}$$

When written out for each surface k and for a sufficient number of directions ($\theta_{r,k}$, $\phi_{r,k}$) to obtain acceptable accuracy in the angular integrations that follow, this yields a set of simultaneous equations for $I_{\lambda o,k}(\theta_{r,k},\phi_{r,k})$ for $k = 1,\ldots,N$.

With this degree of approximation, which is characteristic for enclosure analyses, consider the interaction of the two plane surfaces in Figure B.6. The surroundings are at low temperature relative to the surface temperature, so radiation from the surroundings is neglected; this provides a two-surface enclosure. Then, writing Equation (B.12) for $k = 1$ and 2,

$$I_{\lambda o,1}\left(\theta_{r,1},\phi_{r,1}\right) = \varepsilon_{\lambda,1}\left(\theta_{r,1},\phi_{r,1}\right) I_{\lambda b,1} + \frac{1}{A_1}\int_{A_1}\int_{A_2} \rho_{\lambda,1}\left(\theta_{r,1},\phi_{r,1},\theta_{i,1},\phi_{i,1}\right) I_{\lambda o,2}\left(\theta_2,\phi_2\right) \frac{\cos\theta_1 \cos\theta_2}{S^2}\, dA_j\, dA_k \tag{B.13}$$

$$I_{\lambda o,2}\left(\theta_{r,2},\phi_{r,2}\right) = \varepsilon_{\lambda,2}\left(\theta_{r,2},\phi_{r,2}\right) I_{\lambda b,2} + \frac{1}{A_2}\int_{A_2}\int_{A_1} \rho_{\lambda,2}\left(\theta_{r,2},\phi_{r,2},\theta_{i,2},\phi_{i,2}\right) I_{\lambda o,1}\left(\theta_1,\phi_1\right) \frac{\cos\theta_2 \cos\theta_1}{S^2}\, dA_1\, dA_2 \tag{B.14}$$

Equations (B.13) and (B.14) are in terms of outgoing intensities in each direction $\theta_{r,k}$, $\phi_{r,k}$; they are simultaneous integral equations for $I_{\lambda o,1}$ and $I_{\lambda o,2}$. A numerical solution can be obtained by writing these equations for many discrete angular intervals to develop a set of simultaneous equations.

After $I_{\lambda o,1}(\theta_{r,1},\phi_{r,1})$ and $I_{\lambda o,2}(\theta_{r,2},\phi_{r,2})$ are obtained for enough angular intervals to yield good accuracy, the total energy can be determined that must be supplied to each surface to maintain its specified temperature. This is the difference between energies carried away from and to the surface; for A_1 this gives

$$\frac{Q_1}{A_1} = \int_{\lambda=0}^{\infty}\int_{\cap} I_{\lambda o,1}\left(\theta_{r,1},\phi_{r,1}\right)\cos\theta_{r,1}\, d\Omega_{r,1}\, d\lambda - \frac{1}{A_1}\int_{\lambda=0}^{\infty}\int_{A_1}\int_{A_2} I_{\lambda o,2}\left(\theta_2,\phi_2\right)\frac{\cos\theta_1\cos\theta_2}{S^2}\, dA_2\, dA_1\, d\lambda \tag{B.15}$$

and similarly for A_2. For diffuse-gray surfaces, so that $I_{\lambda o,1}$ and $I_{\lambda o,2}$ are independent of λ, θ, and ϕ, this simplifies to $Q_1/A_1 = \pi I_{o,1} - \pi I_{o,2} F_{1-2} = J_1 - J_2 F_{1-2}$ as given by Equation (6.17).

If Q_1 rather than T_1 is specified, T_1 must be found and the solution becomes more difficult. A temperature is assumed for A_1, and the enclosure equations of the form Equations (B.13) and (B.14) are solved to find the $I_{\lambda o}$. The outgoing intensities are substituted into Equation (B.15), and the computed Q_1 is compared to the given value. The T_1 is then adjusted and the procedure repeated until agreement between given and computed Q_1 is attained. If Q is specified for more than one surface, the solution is even more difficult.

Example B.2

For an example that can be carried out in analytical form, a small area element dA_1 is considered on the axis of, and parallel to, a black circular disk as in Figure B.7. The element is at T_1, the disk at T_2, and the environment at $T_e \approx 0$ K. The dA_1 has a directional spectral emissivity independent of ϕ and approximated by

$$\varepsilon_{\lambda,1}(\theta_1, T_1) = 0.8\cos\theta_1(1 - e^{-C_2/\lambda T_1})$$

where C_2 is one of the constants in Planck's spectral distribution. As will be evident, this dependence on λ and T_1 was devised to simplify this illustrative example and obtain an analytical result. More generally, numerical integration can be used. Find the energy dQ_1 added to dA_1 to maintain T_1.

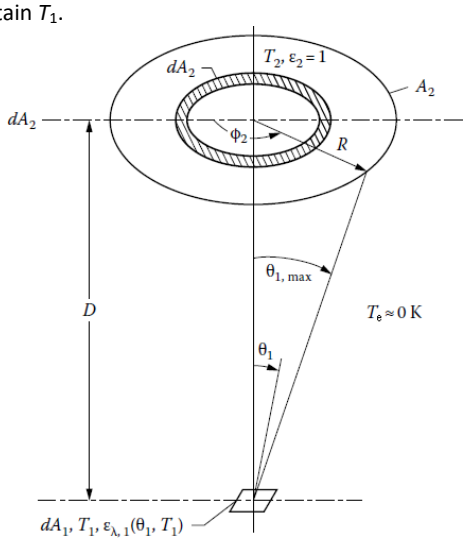

Figure B.7 Radiative energy exchange involving directional spectral surface element (cold environment at ~0 K).

The energy balance in Equation (B.11) is emitted energy minus absorbed incident energy. The energy emitted by dA_1 is

$$dQ_{e,1} = dA_1 \int_{\lambda=0}^{\infty} \int_{\cap} \varepsilon_{\lambda,1}(\theta_1) I_{\lambda b,1} \cos\theta_1 d\Omega_1 d\lambda$$

Insert the expressions for $\varepsilon_{\lambda,1} I_{\lambda b,1}$ (Equation (3.3)), and $d\Omega_1 = \sin\theta_1 d\phi_1$ to obtain

$$dQ_{e,1} = 0.8 dA_1 \int_{\lambda=0}^{\infty} \int_{\phi_1=0}^{2\pi} \int_{\theta_1=0}^{\pi/2} \cos^2\theta_1 (1 - e^{-C_2/\lambda T_1}) \frac{2C_1}{\lambda^5 (e^{C_2/\lambda T_1} - 1)} \sin\theta_1 d\theta_1 d\phi_1 d\lambda$$

Integrating over ϕ_1 and θ_1 gives

$$dQ_{e,1} = 0.8 dA_1 \frac{2\pi}{3} \int_0^{\infty} \frac{2C_1}{\lambda^5 e^{C_2/\lambda T_1}} d\lambda$$

Using the transformation $\zeta = C_2/\lambda T_1$, the relation $\int_0^{\infty} \zeta^3 e^{-\zeta} d\zeta = 3!$ from a table of definite integrals, and Stefan–Boltzmann constant σ from Equation (2.33) yields

$$dQ_{e,1} = \frac{48}{\pi^4} \sigma T_1^4 dA_1 = 0.493 \sigma T_1^4 dA_1$$

Thus, the total hemispherical emission is about half that of a blackbody.

The energy absorbed by dA_1 is

$$dQ_{a,1} = dA_1 \int_{\lambda=0}^{\infty} \int_{A_2} \alpha_{\lambda,1}(\theta_1, \phi_1) I_{\lambda o,2}(\theta_2, \phi_2) \frac{\cos\theta_1 \cos\theta_2}{S^2} dA_2 d\lambda$$

From Kirchhoff's law, the directional spectral absorptivity and emissivity are equal. For dA_2 taken as a ring element, the solid angle $\cos\theta_2 dA_2/S^2$ is written as $2\pi \sin\theta_1 d\theta_1$. This is used to write the absorbed energy as (where $I\lambda_{o,2} = I\lambda_{b,2}$ since A_2 is a black surface)

$$dQ_{a,1} = 2\pi(0.8)dA_1 \int_{\lambda=0}^{\infty} \int_{\theta_1=0}^{\theta_{1,\max}} (\cos^2\theta_1 \sin\theta_1 d\theta_1) I_{\lambda b,2}(1 - e^{-C_2/\lambda T_1}) d\lambda$$

$$= -1.6\pi dA_1 \frac{\cos^3\theta_1}{3}\bigg|_{\theta_1=0}^{\theta_{1,\max}} \int_0^{\infty} \frac{2C_1(1 - e^{-C_2/\lambda T_1})}{\lambda^5(e^{C_2/\lambda T_2} - 1)} d\lambda$$

$$= \frac{3.2\pi C_1 dA_1}{3}\left[1 - \frac{D^3}{(D^2 + R^2)^{3/2}}\right] \int_0^{\infty} \frac{1 - e^{-C_2/\lambda T_1}}{\lambda^5(e^{C_2/\lambda T_2} - 1)} d\lambda$$

Using the transformation $\zeta = C_2/\lambda T_1$, this is placed in the form

$$dQ_{a,1} = \frac{48}{\pi^4}\left[1 - \frac{1}{(1 + r^2)^{3/2}}\right] \sigma T_2^4 dA_1 G\left(\frac{T_2}{T_1}\right)$$

where $r = R/D$ and $G(T_2/T_1) = (1/6)\int_0^{\infty} \zeta^3 e^{-\zeta}(1 - e^{\zeta T_2/T_1})/(1 - e^{-\zeta}) d\zeta$. This integral was evaluated numerically, giving $G(1.0) = 1.000$, $G(1.5) = 1.045$, and $G(2.0) = 1.063$; hence, the effect of temperature ratio is small. Finally, the energy added to dA_1 to maintain it at T_1 is given by

$$dQ_1 = dQ_{e,1} - dQ_{a,1} = \frac{48\sigma}{\pi^4}\left\{T_1^4 - T_2^4\left[1 - \frac{1}{(1 + r^2)^{3/2}}\right] G\left(\frac{T_2}{T_1}\right)\right\} dA_1$$

As shown by Example B.2, it is difficult to devise an analytical function for $\varepsilon_\lambda(\theta, T)$ that can be integrated in closed form over both angle and wavelength. Numerical methods are required to solve problems of this type for $\varepsilon_\lambda(\theta, T)$ functions that represent experimental data.

The development in this section has shown that, although the formulation of radiation-exchange problems involving directional and/or spectral properties is not conceptually difficult, it is usually tedious to solve the resulting integral equations. To simplify the equations, it is usually necessary to make assumptions and approximations that can vary from case to case. Numerical techniques such as iteration are used for directional spectral formulations, since closed-form analytical solutions can rarely be obtained. An alternative numerical technique is the Monte Carlo method presented in Section 10.6. For complicated directional and spectral effects, this is often a better approach than using an integral equation formulation.

Some of the original research is now summarized. A surface with part specular and part diffuse reflectivity and a semigray analysis were used by Shimoji (1977) to find local temperatures in conical and V-groove cavities exposed to incident solar radiation parallel to the cone axis or V-groove bisector plane. Toor and Viskanta (1972) compared with experiment various analytical models using diffuse, specular, semigray, nongray, and combinations of these characteristics. They found, for the particular geometries and materials studied, that spectral effects were less important than directional effects and that the presence of one or more diffuse surfaces in an enclosure made the presence of specularly reflecting surfaces unimportant. If grooves on a surface have a size that is comparable to or smaller than the wavelength of the incident or emitted radiation, there can be

complex interactions of the electromagnetic waves within the grooves. This can produce unusual spectral and directional effects. The radiation behavior of materials with a grooved microstructure was studied by Hesheth et al. (1988), Glass et al. (1982), Wirgin and Maradudin (1985), Sentenac and Greffet (1994), Hajimirza et al. (2011, 2012) and Krishna and Lee (2018).

References

Beckmann, P. and Spizzichino, A.: *The Scattering of Electromagnetic Waves from Rough Surfaces*, Macmillan, New York, 1963.

Glass, N. E., Maradudin, A. A., and Celli, V.: Surface plasmons on a large-amplitude doubly periodically corrugated surface, *Phys. Rev. B*, 26(10), 5357–5365, 1982.

Hajimirza, S., El Hitti, G., Heltzel, A., and Howell, J.: Using inverse analysis to find optimum nanoscale radiative surface patterns to enhance solar cell performance, *Int. J. Thermal Sci*., 12, 93–102, 2011. doi: 10.1016/j.ijthermalsci.2011.12.011.

Hajimirza, S., El Hitti, G., Heltzel, A., and Howell, J.: Specification of micro-nanoscale radiative patterns using inverse analysis for increasing solar panel efficiency, *JHT*, 134, 102702-1–102702-8, October 2012.

Hesheth, P. J., Gebhart, B., and Zemel, J. N.: Measurements of the spectral and directional emission from microgrooved silicon surfaces, *JHT*, 110(3), 680–686, 1988.

Howell, J. R. and Perlmutter, M.: *Directional Behavior of Emitted and Reflected Radiant Energy from a Specular, Gray, Asymmetric Groove*, NASA TN D-1874, Washington, DC, 1963.

Krishna, A. and Lee, J.: Morphology-driven emissivity of microscale tree-like structures for radiative thermal management, *Nanoscale and Microscale Thermophysical Engineering*, 22(2), 124-136, 2018.

Sentenac, A. and Greffet, J.-J.: Design of surface microrelief with selective radiative properties, *IJHMT*, 37(4), 553–558, 1994.

Shimoji, S.: Local temperatures in semigray nondiffuse cones and V-grooves, *AIAA J*., 15(3), 289–290, 1977.

Toor, J. S.: *Radiant heat transfer analysis among surfaces having direction dependent properties by the Monte Carlo method*, MS thesis, Purdue University, Lafayette, IN, 1967.

Toor, J. S. and Viskanta, R.: A critical examination of the validity of simplified models for radiant heat transfer analysis, *IJHMT*, 15, 1553–1567, 1972.

Viskanta, R., Schornhorst, J. R., and Toor, J. S.: *Analysis and Experiment of Radiant Heat Exchange between Simply Arranged Surfaces*, AFFDL-TR-67-94, DDC No. AD-655335, Purdue University, Lafayette, IN, June 1967.

Wirgin, A. and Maradudin, A. A.: Resonant enhancement of the electric field in the grooves of bare metallic gratings exposed to s-polarized light, *Phys. Rev. B*, 31(8), 5573–5576, 1985.

Zhang, Q. C., Sinko, T. M., Dey, C. J., Collins, R. E., and Turner, G. M.: The measurement and calculation of radiative heat transfer between uncoated and doped tin oxide coated glass surfaces, *IJHMT*, 40(1), 61–71, 1997.

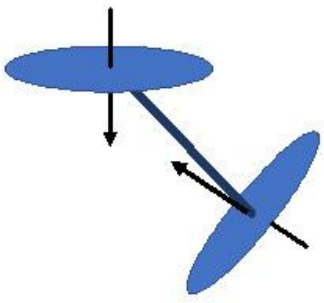

C: INTEGRATION METHODS

C.1: NUMERICAL INTEGRATION METHODS

Integration methods are discussed for use in numerical solutions of pure radiation or combined-mode problems. For radiative exchange, the integrals are often a function of two position variables, and integration is over one or both. For example, the configuration factor dF_{di-dj} from position $\mathbf{r}_i$ on surface i to position $\mathbf{r}_j$ on surface j appears in the integral over surface j to obtain F_{di-j} in the form [see Equation (5.12) in the text]

$$F_{di-j}(\mathrm{r}_i) = \int_{Aj} dF_{di-dj}(\mathrm{r}_i, \mathrm{r}_j) = \int_{Aj} K(\mathrm{r}_i, \mathrm{r}_j) dA_j \tag{C.1}$$

Many ways can be used to numerically approximate an integral. Because the integrands in radiative enclosure formulations are usually well behaved at the end points, *closed* numerical integration forms are often used that include the end points. *Open* methods do not include the end points and can be used when end-point values are indeterminate, such as for improper integrals that yield finite values when integrated. In analyses including convection and/or conduction, the numerical integration will usually use the grid spacing imposed by the differential terms. In some situations, it is enough to use numerical integration methods that have regular grid spacing. However, uneven spacings are often advantageous to place more points in regions where functions have large variations, or to adequately follow irregular boundaries. *Gaussian quadrature* can be used for variable grid spacing. Simpler schemes such as the *trapezoidal rule* or *Simpson's rule* may be adequate for some problems. These often employ uniform grid spacing and are closed, whereas Gaussian quadrature is open. The trapezoidal rule can readily be used with a nonuniform grid size. Textbooks on numerical methods provide detailed presentations of the many available integration methods and their relative accuracies, advantages, and disadvantages. Libraries of computer codes and computational software packages have many subroutines for single or multidimensional numerical integrations that can be applied directly.

C.1.1 TRAPEZOIDAL RULE

The *trapezoidal rule* is a closed numerical integration method that can easily employ a variable increment size. Consider the function in Figure C.1, where an equal grid spacing of Δz is shown for the integration range from z_0 to z_N. In the trapezoidal rule each pair of adjacent points, such as $f(x,z_j)$ and $f(x,z_{j+1})$, is connected by a straight line. Then the integral from z_j to z_{j+1} is approximated by

$$\int_{zj}^{z_{j+1}} f(x,z)dz \approx (z_{j+1} - z_j)\frac{f_j(x) + f_{j+1}(x)}{2}$$

This approximation can be made for each interval between grid points, so an irregular grid spacing can be used. For *equally sized increments*, the sum over all intervals gives the approximation

$$\int_{z_0}^{z_N} f(x,z)\,dz \approx \Delta z\left[\frac{1}{2} f_0(x) + \sum_{j=1}^{N-1} f_j(x) + \frac{1}{2} f_N(x)\right] \tag{C.2}$$

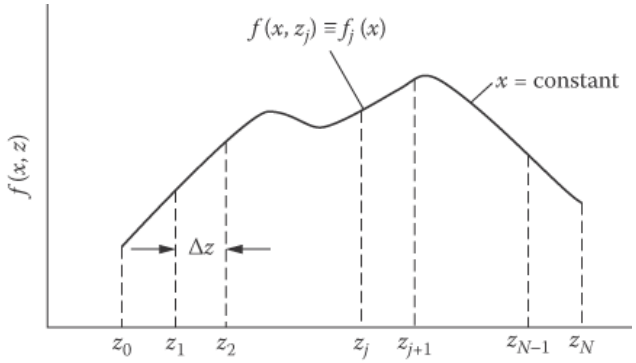

FIGURE C.1 Numerical integration of the function f(x, z) with respect to z for a fixed x.

EXAMPLE C.1

Using the ring-to-ring configuration factor, evaluate the configuration factor from a ring element on the interior of a right circular cylinder to the cylinder base for the geometry in Figure C.2 when $x = r$. Use the trapezoidal rule and compare the result with the analytical solution.

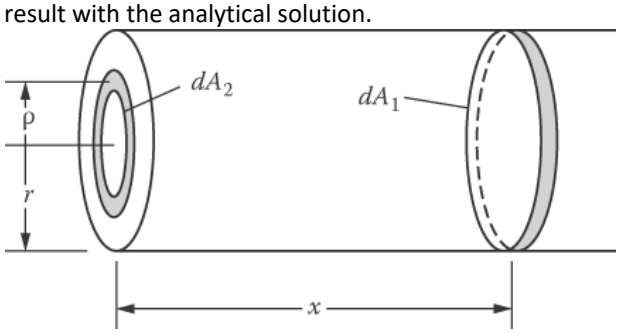

FIGURE C.2 Geometry for configuration factor from ring element on interior of cylinder to ring element on base.

The factor from dA_1 to a ring dA_2 on the base surface is

$$dF_{d1-d2}(X,R) = \frac{2XR(1+X^2-R^2)\,dR}{[(1+X^2+R^2)^2-4R^2]^{3/2}} \tag{C.3}$$

where $X = x/r$ and $R = \rho/r$. For this example, $X = 1$, so $f_j(X = 1, R_j)$ for Figure C.2 is given by

$$f_j(X=1,R_j) \equiv f_j(1) = \frac{2R_j(2-R_j^2)}{(4+R_j^4)^{3/2}}$$

where $R_j = j\Delta R$ and $\Delta R = 1/N$. Letting $f_j(X=1, j\Delta R) \equiv f_j(1)$,

$$f_0(1) = 0, \quad f_j(1) = \frac{2j\Delta R[2-(j\Delta R)^2]}{[4+(j\Delta R)^4]^{3/2}}, \quad f_N(1) = \frac{2}{5^{3/2}}$$

These terms are substituted into Equation (C.2), and for $N = 5$ yields

$$F_{d1-2}(X=1) = (1/5)[(1/2)\times 0 + 0.09794 + 0.18225 + 0.23451 + 0.23500 + (1/2)\times 0.17889] = 0.16783$$

The exact configuration factor is in Appendix C of the text as

$$F_{d1-2}(X=1) = \frac{X^{*^2}+\frac{1}{2}}{(X^{*^2}+1)^{1/2}} - X^*, \quad X^* = \frac{x}{2r} = \frac{X}{2} = \frac{1}{2}$$

which gives $F_{d1-2}(X=1) = F_{d1-2}(X^*=0.5) = 0.17082$. Larger numbers of increments improve the accuracy as follows:

N	$F_{d1-2}(X = 1)$	% Error
5	0.16783	−1.75
10	0.17007	−0.44
50	0.17079	−0.02
100	0.17081	−0.006
200	0.17082	0

C.1.2 SIMPSON'S RULE

The usual Simpson's rule is obtained by passing a parabola through three adjacent grid points. For equally spaced increments the integral from z_j to z_{j+2} is approximated by

$$\int_{z_j}^{z_{j+2}} f(z)dz \approx \frac{\Delta z}{3}(f_j + 4f_{j+1} + f_{j+2})$$

Because this uses two Δz increments, the repeated application for a range with many grid points requires an *even* number of increments (an odd number of points). For N equally spaced increments in Figure C.1, the result is

$$\int_{z_o}^{z_N} f(z)dz \approx \frac{\Delta z}{3}(f_0 + 4f_1 + 2f_2 + 4f_3 + \cdots + 4f_{N-1} + f_N) \qquad \text{(C.4)}$$

If an odd number of increments must be used, Simpson's rule can be applied over an even number of increments, and the trapezoidal rule used for the remaining increment.

If the curve in Figure C.1 goes through a sharp cusplike peak, it may not be accurate to apply Simpson's rule if the peak is at the central point of the three adjacent points; the cusplike behavior is not accurately approximated by a parabolic curve. Simpson's rule could be used for two increments on each side of the peak. Care should be used in selecting a suitable integration scheme for each application.

Higher-order approximations have been developed by passing a cubic curve through four adjacent points, a fourth-order curve through five adjacent points, etc. These yield the *Newton-Cotes closed integration formulas* of which the trapezoidal and Simpson's rules are the first two. Using a cubic curve through four adjacent points is called *Simpson's second rule*,

$$\int_{z_j}^{z_{j+3}} f(z)dz \approx \frac{3\Delta z}{8}(f_j + 3f_{j+1} + 3f_{j+2} + f_{j+3}) \qquad \text{(C.5)}$$

In most instances, the functions inside the integrals of the integral equations are complicated algebraic quantities. This is because they involve a configuration factor. There is usually little chance that an analytical solution can be found, so a numerical solution is used. Consider the simultaneous integral equations in Equations (6.13.1) and (6.13.2) of Example 6.13 in the text. With $T_1(x)$ and $T_2(y)$ specified, the right sides are known functions of x and y. Starting with Equation (6.13.1), a distribution for $q_2(y)$ is assumed as a first trial. Then the integration is carried out numerically for various x values to yield $q_1(x)$ at these x locations. This $q_1(x)$ distribution is inserted into Equation (6.13.2) and a $q_2(y)$ distribution is determined. This $q_2(y)$ is used to compute a new $q_1(x)$ from Equation (6.13.2) and the process is continued until $q_1(x)$ and $q_2(y)$ are no longer changing as the iterations proceed.

To perform the integrations in a computer solution, an accurate integration subroutine is required. Many subroutines are available, and they may require functions such as $q_1(x)$ and $q_2(y)$ evaluated at many evenly or unevenly spaced values of the x- and y-coordinates. The values can be obtained by curve fitting the $q_1(x)$ and $q_2(y)$ after each iteration with standard subroutines such as cubic splines. The $q_1(x)$ and $q_2(y)$ are then interpolated at the x and y values called for by the integration subroutine. A precaution should be noted. A quantity such as $J_j\ dF_{dk-dj}$ may go through rapid changes in magnitude because of the geometry involved in the configuration factor; for example, dF_{dk-dj} may

decrease rapidly as the distance increases between dA_k and dA_j For small separation distances, there can be a strong peak in the integration kernel. Care should be taken that the integration method is accurate for the functions involved. The integration should be done on each side of a sharp peak and not passed through it.

The Monte Carlo method of Chapter 10 in the text can be used for evaluating integrals, and some discussion of the methodology is given there.

Direct solvers for a set of simultaneous equations can also be used for integral equations. The integrals are expressed in finite-difference form to provide a set of simultaneous equations for the unknowns at each increment position as in Example C.2.

Example C.2

For integral Equation (6.14.1) of Example 6.14 of the text, derive a set of simultaneous algebraic equations to determine $J_2(\xi)$ for $I = 4$. For simplicity, divide the length into four equal increments ($\Delta\eta = 1$) and use the trapezoidal rule for integration.

When Equation (6.14.1) is applied at the end of the tube where $\xi = 0$, the relation is obtained:

$$J_2(0) - \left[\frac{1}{2}J_2(0)K(|0-0|) + J_2(1)K(|1-0|) + J_2(2)K(|2-0|) + J_2(3)K(|3-0|) + \frac{1}{2}J_2(4)K(|4-0|)\right](1) = q_2 \tag{C.6}$$

The quantity in brackets is the trapezoidal-rule approximation for the integral. The $K(|\eta-\xi|) = dF(|\eta-\xi|)/d\eta$ is the algebraic expression within the braces of Equation (6.14.2). The $J_2(0)$ terms in Equation C.6 are grouped together to provide the first of Equation C.7. The other four equations are the finite-difference equations at the other incremental positions along the enclosure:

$$\begin{aligned}
&J_2(0)\left[1-\frac{1}{2}K(0)\right] - J_2(1)K(1) - J_2(2)K(2) - J_2(3)K(3) - \frac{1}{2}J_2(4)K(4) = q_2\\
&-\frac{1}{2}J_2(0)K(1) + J_2(1)\left[1-K(0)\right] - J_2(2)K(1) - J_2(3)K(2) - \frac{1}{2}J_2(4)K(3) = q_2\\
&-\frac{1}{2}J_2(0)K(2) - J_2(1)K(1) + J_2(2)\left[1-K(0)\right] - J_2(3)K(1) - \frac{1}{2}J_2(4)K(2) = q_2\\
&-\frac{1}{2}J_2(0)K(3) - J_2(1)K(2) - J_2(2)K(1) + J_2(3)\left[1-K(0)\right] - \frac{1}{2}J_2(4)K(1) = q_2\\
&-\frac{1}{2}q_{o,2}(0)K(4) - q_{o,2}(1)K(3) - q_{o,2}(2)K(2) - q_{o,2}(3)K(1) + q_{o,2}(4)\left[1-\frac{1}{2}K(0)\right] = q_2
\end{aligned} \tag{C.7}$$

These equations are solved for J_2 at the five surface locations. From symmetry, and with q_2 uniform along the enclosure, it is possible to simplify the solution for this example by using $J_2(0) = J_2(4)$ and $J_2(1) = J_2(3)$.

Equations such as Equation (C.7) are first solved for a moderate number of increments along the surfaces. Then the increment size is reduced, and the solution is repeated. This is continued until sufficiently accurate $J(\xi)$ values are obtained. Equations (C.7) use the trapezoidal rule as a simple numerical approximation to the integrals. More accurate numerical integration schemes can be used, which may reduce the number of increments required for enough accuracy.

Example C.2 has only one integral equation. For the situation with two integral equations in Equations (6.13.1) and (6.13.2) of text Example 6.13, each surface can be divided into increments and equations written at each incremental location. This yields N simultaneous equations for the total of N positions on both plates that are solved simultaneously for the $T_1(r_1)$ and $q_2(r_2)$. This procedure is

an alternative to the iterative solution described previously. The solver for the system of simultaneous equations may work by iteration.

C.1.3 Other Numerical Integration Methods

Additional numerical integration techniques include Romberg integration, in which the trapezoidal rule is utilized. The integration is performed with a small number of increments and is then repeated for twice the number of increments by adding the contributions from the additional points, four times the number of increments, etc. The sequence of integration results is extrapolated to an improved result using Richardson extrapolation [see Press et al. (1992)]. The process is continued until desired convergence accuracy is achieved in the extrapolated result.

Gaussian integration is very useful; this is an open integration method using an array of unevenly spaced points. The uneven points can be positioned between a fixed grid of evenly or variably spaced points. This can be done by curve fitting, such as by cubic splines, for the individual portions of the curve between the fixed grid points. Values of the integrand at positions between the grid points for use in the Gaussian method are interpolated using the spline coefficients.

Many numerical integration subroutines have been written for computer use and the software can be readily applied. Curve-fitting software routines are available that can be used in conjunction with Gaussian or other techniques, requiring interpolation to obtain unevenly spaced values of the function being integrated. Some subroutines perform multidimensional integrations. Computational software packages for mathematics provide numerical integration using, for example, Romberg integration, Simpson's rule, and adaptive methods; singular and infinite end points are also treated.

Fan et al. (2019) examine fast algorithms for solving the steady state integral form of the RTE based on fast Fourier transforms for homogeneous media and a recursive skeletonization-factorization technique for inhomogeneous media. They show that a unique solution to the RTE exists and provide sample solutions for isotropic and anisotropic scattering in 2- and 3D. Zhou et al. (2020) propose methods to subtract singularities in integrated forms of the RTE for use in analytical and numerical solutions.

C.2: ANALYTICAL INTEGRATION METHODS FOR ENCLOSURES

The unknown wall energy fluxes or temperatures along the surfaces of an enclosure are found from solutions of single or simultaneous integral equations. The integral equations in the formulations up to now are linear; that is, the unknown q, J, or T^4 variables always appear to the first power (note that T^4 is the linear variable rather than T). For linear integral equations, there are various numerical and analytical solution methods; these are discussed in mathematics texts.

For some simple geometries and special conditions, the integral equations describing radiative transfer among surfaces may be solved analytically. Such solutions are usually limited to single-surface or two-surface enclosures, so are not described here in detail.

If the kernel of the integral equation is *separable*, that is, $K(\mathbf{r}_j,\mathbf{r}_k) = F_j(\mathbf{r}_j)F_k(\mathbf{r}_k)$, then $F_k(\mathbf{r}_k)$ may be removed from the integral over $\mathbf{r}_j$, possibly simplifying analytical or numerical integration. However, the kernel in radiation problems usually is *not* separable. The general theory of solution of integral equations using separable kernels is in Hildebrand (1992) and an application using a separable exponential approximation to the kernel (Usiskin and Siegel 1960), allowing reduction of the integral equation to a differential equation, is in Buckley (1927, 1928).

The *variational method* (Hildebrand 1992) may be applied if the kernel is *symmetric*, that is, $K(\xi,\eta) = K(\eta,\xi)$. This approach has been used for radiation in a cylindrical tube (Usiskin and Siegel 1960) and for radiative exchange between infinitely long parallel plates of finite width (Sparrow 1960).

An approximate solution may be obtained through a *Taylor series expansion* (Krishnan and Sundaram 1960, Perlmutter and Siegel 1963), which works well if the kernel $K\left(\left|\xi-\eta\right|\right)$ decays rapidly as $\xi - \eta$ increases as for the cylindrical geometry illustrated in Figure 6.14. The integrand of the integral equations then becomes a series that may be truncated after a few terms and then integrated term by term, reducing the integral equation to a differential equation. Applications are in Choi and Churchill (1985) and Qiao et al. (2000).

The *method of Ambartsumian* can be applied if the temperature or energy flux boundary conditions can be approximately described by an exponential variation or a sum of exponentials, allowing transformation of the integral equation into an initial value problem (Ambartsumian 1942, Kourganoff 1963, Crosbie and Sawheny 1974, 1975).

The problem of finding the intensity leaving a circular opening in a spherical cavity exposed to external uniform energy flux incident on element dA_2, $q_e(dA_2)$, and with a prescribed internal temperature distribution $T(dA_1)$ on the cavity surface has been solved analytically (Jakob 1957, Sparrow and Jonsson 1962). If the internal surface of the cavity has emissivity ε, then the intensity leaving an element dA_1* through the cavity opening in a direction is found to be

$$I\left(dA_1^*\right)=\frac{J_1(dA_1^*)}{\pi}=\frac{\varepsilon\sigma T_1^4\left(dA_1^*\right)}{\pi}+\frac{\frac{1}{\pi}\left(\frac{1-\varepsilon}{4\pi R^2}\right)\left[\int_{A_1}\varepsilon\sigma T_1^4(dA_1)dA_1+\int_{A_2}q_e(dA_2)dA_2\right]}{1-\left(1-\varepsilon\right)A_1/4\pi R^2} \tag{C.8}$$

All these analytical methods become intractable when multiple surfaces are present, and numerical solution techniques are almost always required for more realistic cases.

C.2.1 Exact Solution of Integral Equation for Radiation from a Spherical Cavity

Radiation from a spherical cavity as in Figure C.3a was analyzed by Jakob (1957) and Sparrow and Jonsson (1962). The spherical shape leads to a relatively simple integral-equation solution because there is an especially simple configuration factor between elements on the inside of a sphere. For the two differential elements dA_j and dA_k in Figure C.3b,

$$dF_{dj-dk}=\frac{\cos\theta_j\cos\theta_k}{\pi S^2}dA_k \tag{C.9}$$

Since the sphere radius is normal to both dA_j and dA_k, the distance between these elements is $S = 2R\cos\theta_j = 2R\cos\theta_k$. Then, Equation C.9 becomes

$$dF_{dj-dk}=\frac{dA_k}{4\pi R^2}=\frac{dA_k}{A_s} \tag{C.10}$$

Where A_s is the surface area of the entire sphere. If dA_j exchanges with the finite area, then Equation (C.10) becomes

$$F_{dj-k}=\frac{1}{4\pi R^2}\int_{A_k}dA_k=\frac{A_k}{4\pi R^2}=\frac{A_k}{A_s} \tag{C.11}$$

Equation (C.11) is *independent of* dA_j, so dA_j can be replaced by any finite area A_j to give

$$F_{j-k}=\frac{A_k}{4\pi R^2}=\frac{A_k}{A_s} \tag{C.12}$$

The configuration factor from any area to any area is simply the fraction of the total sphere area that the *receiving* area occupies.

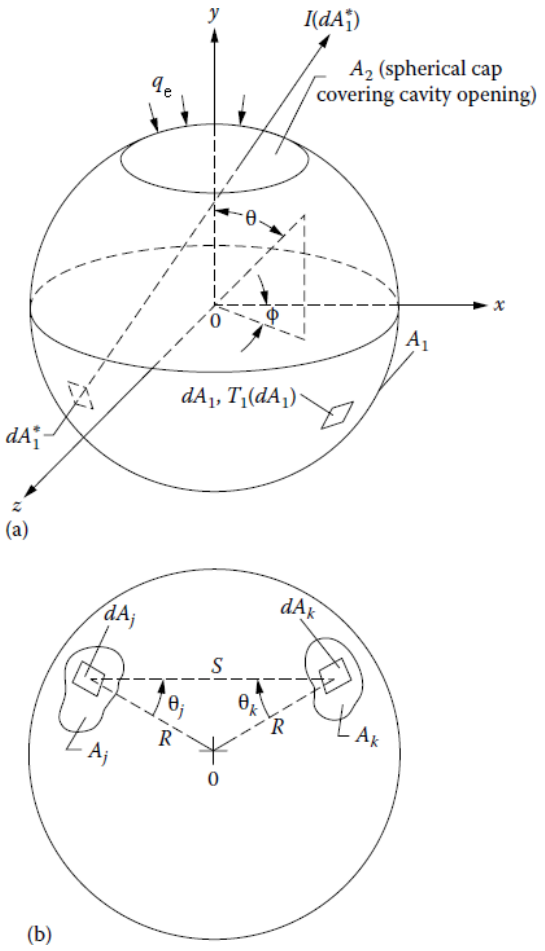

Figure C.3 Geometry for radiation within spherical cavity, (a) spherical cavity with diffuse entering radiation q_e and with surface at variable temperature T_1 and (b) area elements on spherical surface.

Consider the spherical cavity in Figure C.3a with a temperature distribution $T_1(dA_1)$ and a total surface area A_1. The spherical cap that would cover the cavity opening has area A_2. Assume there is diffuse radiative flux q_e (per unit area of A_2) entering through the cavity opening; the q_e can vary over A_2. It is desired to compute the radiation intensity $I(dA_1^*)$ leaving the cavity at a specified location and in a specified direction, as shown by the arrow in Figure C.3a. The desired intensity results from the diffuse flux leaving dA_1^* and equals $J_1(dA_1^*)/\pi$. The $J_1(dA_1^*)$ is found by applying Equation (6.38):

$$J_1\left(dA_1^*\right)-\left(1-\varepsilon_1\right)\int_{A_1} J_1\left(dA_1\right)dF_{d1^*-d1}-\left(1-\varepsilon_1\right)\int_{A_2} q_e\left(dA_2\right)dF_{d1^*-d2}=\varepsilon_1\sigma T_1^4\left(dA_1^*\right) \qquad \text{(C.13)}$$

and an exact solution will be found. The F factors from Equation (C.9) are substituted to give

$$J_1\left(dA_1^*\right)-\frac{1-\varepsilon_1}{4\pi R^2}\int_{A_1}J_1\left(dA_1\right)dA_1=\frac{1-\varepsilon_1}{4\pi R^2}\int_{A_2}q_e\left(dA_2\right)dA_2+\varepsilon_1\sigma T_1^4\left(dA_1^*\right) \tag{C.14}$$

To solve Equation (C.14), a trial solution $J_1\left(dA_1^*\right)=f\left(dA_1^*\right)+C$ is assumed, where $f(dA_1^*)$ is an unknown function of the location of dA_1^*, and *C* is a constant. Substituting into Equation (C.14) gives

$$f\left(dA_1^*\right)+C-\frac{1-\varepsilon_1}{4\pi R^2}\int_{A_1}f\left(dA_1\right)dA_1-\frac{1-\varepsilon_1}{4\pi R^2}CA_1=\frac{1-\varepsilon_1}{4\pi R^2}\int_{A_2}q_e\left(dA_2\right)dA_2+\varepsilon_1\sigma T_1^4\left(dA_1^*\right) \tag{C.15}$$

From the two terms that are functions of local position, $f\left(dA_1^*\right)=\varepsilon_1\sigma T_1^4\left(dA_1^*\right)$. The remaining terms are equated to determine *C*. This gives the desired result as an exact solution:

$$I\left(dA_1^*\right)=\frac{J_1\left(dA_1^*\right)}{\pi}=\frac{\varepsilon_1\sigma T_1^4\left(dA_1^*\right)}{\pi}+\frac{\frac{1}{\pi}\left[\frac{1-\varepsilon_1}{4\pi R^2}\right]\left[\int_{A_1}\varepsilon_1\sigma T_1^4\left(dA_1\right)dA_1+\int_{A_2}q_e\left(dA_2\right)dA_2\right]}{1-\left(1-\varepsilon_1\right)A_1/4\pi R^2} \tag{C.16}$$

C.3 NUMERICAL SOLUTION METHODS FOR NONLINEAR EQUATIONS

Most nonlinear equations for mixed-mode problems with radiation can be cast in the form

$$\left[\mathrm{A}_{ij}\right]\left[\vartheta_j\right]+\left[\mathrm{B}_{ij}\right]\left[\vartheta_j^4\right]=\left[\mathrm{C}_i\right] \tag{C.17}$$

It is important to examine the relative values of the elements A_{ij} and B_{ij}. If the A_{ij} are comparatively large, the problem can be treated as linear in ϑ_j; conversely, for large B_{ij}, the problem can be treated as linear in ϑ_j^4. When the coefficients *A* and *B* are approximately equal, other treatments are in order.

If we define $A_{ij}^*=A_{ij}+B_{ij}\vartheta_j^3$, Equation (C.17) becomes

$$\left[A_{ij}\right]\left[\vartheta_j\right]+\left[B_{ij}\right]\left[\vartheta_j^4\right]=\left[A_{ij}+B_{ij}\vartheta_j^3\right]\left[\vartheta_j\right]=\left[A_{ij}^*\right]\left[\vartheta_j\right]=\left[C_i\right] \tag{C.18}$$

This is a set of linear algebraic equations with coefficients A_{ij}^* that are variable and nonlinear. The equations cannot be solved by elimination or direct matrix inversion, because the A_{ij}^* are temperature dependent and thus are not known. Some numerical solution methods are now discussed.

C.3.1 SUCCESSIVE SUBSTITUTION METHODS

C.3.1.1 Simple Successive Substitution (SSS)

A simple solution method is to assume an initial set of temperatures $\vartheta_j^{(0)}$ and use them to compute $\left[A_{ij}^*\left(\vartheta_j^{(0)}\right)\right]$. This provides values for the elements in the matrix of coefficients, leaving the

temperature vector $[\vartheta_j]$ as the unknown. Equation (C.18) is then solved for a new set of temperatures $\left[\vartheta_j^{(n+1)}\right]$ from

$$\left[A_{ij}^{*}\left(\vartheta_j^{(n)}\right)\right]\left[\vartheta_j^{(n+1)}\right]=\left[C_i\right] \tag{C.19}$$

This process is continued until the difference between successive temperature sets is less than an acceptable error, indicating convergence. A difficulty is that this method depends on an accurate initial guess for $[\vartheta_j]$. An inaccurate guess can lead to unstable iterations that may diverge rapidly. For an extended discussion of some of the pitfalls of SSS, see Howell (2017).

C.3.1.2 Successive Underrelaxation

The simple successive substitution (SSS) method can be modified to obtain convergence in many cases if Equation (C.17) is written as

$$\left[A_{ij}^{*}\left(\vartheta_j^{*(n)}\right)\right]\left[\vartheta_j^{(n-1)}\right]=\left[C_i\right] \tag{C.20}$$

where the $A_{ij}^{*}\left(\vartheta_j^{*(n)}\right)$ are computed at each iteration by using a modified temperature

$$\vartheta_j^{*(n)}=\alpha\vartheta_j^{(n)}+(1-\alpha)\vartheta_j^{(n-1)} \tag{C.21}$$

The α is a weighting coefficient, or *relaxation parameter*, in the range $0 \le \alpha \le 1$. When $\alpha = 1$, the successive underrelaxation (SUR) method reduces to SSS; when $\alpha < 1$, the new guess is weighted toward the previous guess (i.e., underrelaxed), and oscillations between iterations are damped. If possible, the α should be chosen or found that provides optimized convergence. Decreasing α usually provides slower convergence, but greater assurance that convergence will occur. Sometimes decreasing α somewhat will increase convergence by reducing oscillatory behavior. Values of $\alpha \approx 0.3$ are reported by Cort et al. (1982) to often provide rapid convergence.

C.3.1.3 Regulated Successive Underrelaxation

Cort et al. (1982) proposed a method of regulated successive underrelaxation (RSUR) that allows the underrelaxation factor α to be chosen and modified for successive iterations. They recommend the following: (1) Initialize $\alpha = 1$; (2) solve Equation (C.21) for $\vartheta_j^{*(n)}$ (for the first iteration, an initial guess $\vartheta_j^{(0)}$ must be provided); (3) solve Equation (C.20) for ϑ_j^{n+1}; (4) calculate

$$\nu^{(n+1)}=\left[\sum_{j=1}^{N}\left(\vartheta_j^{(n+1)}-\vartheta_j^{(n)}\right)^2\right]^{1/2} \tag{C.22}$$

$$R^{(n+1)} = \left[\sum_{j=1}^{N} \left(\vartheta_j^{(n+1)} \right)^2 \right]^{1/2} \tag{C.23}$$

and if $v^{(n+1)} > v^{(n)}$ or if $v^{(n+1)} > (1/3)R^{(n+1)}$, reduce α by 0.1; and (5) repeat steps (2) through (4) until convergence.

Equation (C.22) checks for divergence of the solution between iterations, and Equation (C.23) is used to see whether the residual error after each iteration is smaller than a measure of the root-mean-square temperature over the region of the solution. The latter check eliminates slowly oscillating but converging solutions that pass the test of Equation (C.22) but converge very slowly.

Another approach is to rewrite Equation (C.17) in the form

$$A_{ii}\vartheta_i^{(n+1)} + B_{ii}\left(\vartheta_i^{(n+1)}\right)^4 = C_i - \sum_{j=1}^{N}(1-\delta_{ij})\left[A_{ij}\vartheta_j^{(n+1)} + B_{ij}\left(\vartheta_j^{(n+1)}\right)^4\right] \equiv D_i \tag{C.24}$$

where δ_{ij} is the Kronecker delta. An initial set of temperatures $\vartheta_j^{(0)}$ is guessed, and D_i is evaluated based on this set. Then the $\vartheta_j^{(1)}$ are found by iterative solution of Equation (C.24) and are used to evaluate the next set of D_i. This process is repeated to solve for $\vartheta_i^{(n)}$ until convergence. Tan (1989) points out that, for a given value of i, Equation (C.24) is a quartic equation with a single real positive root $\vartheta_i^{(n+1)}$ given by

$$\vartheta_i^{(n+1)} = \frac{y^{1/2}}{2}\frac{p-2}{(p-1)^{1/2}+1} \tag{C.25}$$

where $p = 2\left(1+\dfrac{4D_i}{B_{ii}y^2}\right)^{1/2}$, $y = \dfrac{2r}{(s+r)^{2/3}+(s-r)^{1/3}[(s+r)^{1/3}+(s-r)^{1/3}]}$

and $r = \dfrac{1}{2}\left(\dfrac{A_{ii}}{B_{ii}}\right)^2$, $s = \left[r^2 + \left(\dfrac{4D_i}{3B_{ii}}\right)^3\right]^{1/2}$.

Thus, for each set of D_i, the $\vartheta_i^{(n+1)}$ can be found directly from the nonlinear Equation (C.24) rather than by an inner iteration and then can be used to evaluate new D_i and continue to the next main iteration. This method is quite fast and can be combined with the SUR technique to determine succeeding approximations to provide a method that is *both* stable and fast.

C.3.2 Newton–Raphson-Based Methods for Nonlinear Problems

C.3.2.1 Modified Newton–Raphson

A modified Newton–Raphson (MNR) method is in Ness (1959) for the class of nonlinear problems encountered here. Starting from Equation (C.17),

$$\left[A_{ij}\right]\left[\vartheta_j\right] + \left[B_{ij}\right]\left[\vartheta_j^4\right] - \left[C_i\right] = 0 \tag{C.26}$$

an initial approximate temperature $\vartheta_j^{(0)}$ is guessed at each node. A correction factor δ_j is then computed so that $\vartheta_j = \vartheta_j^{(0)} + \delta_j$. This ϑ_j is used to compute a new δ_j, and this process is continued until δ_j becomes smaller than a specified value. The δ_j are found by solving the set of linear equations:

$$[f_{ij}][\delta_j] + [f_i] = 0 \tag{C.27}$$

where

$$f_i = \sum_{j=1}^{N} \left[A_{ij} \vartheta_j^{(0)} + B_{ij} \left(\vartheta_j^{(0)} \right)^4 \right] - C_i \tag{C.28}$$

and

$$f_{ij} = A_{ij} + 4B_{ij} \left(\vartheta_j^{(0)} \right)^3 \tag{C.29}$$

The MNR method may not converge if a poor initial temperature set is chosen.

7.5.3.2.2 Accelerated Newton–Raphson

Cort et al. (1982) proposed a method in which the amount of change in ϑ_i at each iteration is adjusted to accelerate convergence. They recommended that the f_{ij} in the MNR method be replaced by

$$f_{ij} = A_{ij} + \frac{4B_{ij}}{[1-(\beta/3)]} \left(\vartheta_j^{(0)} \right)^{(3-\beta)} \qquad \beta \geq 0 \tag{C.30}$$

This effectively modifies the slope of the changes in ϑ_j with respect to iteration number compared with that used in the MNR method. For $\beta = 0$, the accelerated Newton–Raphson (ANR) method reduces to MNR. If β is too large, oscillations and divergence between iterations may occur. For $\beta = 0.175$, the number of iterations to provide a given accuracy for a particular problem was reduced from 28 using MNR to 12 using ANR, and reductions in computer time of up to 80% were obtained. A starting value of $\beta = 0.15$ is recommended by Cort et al.

7.5.3.3 APPLICATIONS OF THE NUMERICAL METHODS

Results using the previous methods were compared in Cort et al. (1982) for some typical radiation–conduction problems with temperature-dependent properties and internal energy generation. Consideration was limited to surfaces with radiative exchanges to black surroundings at a single temperature, and the solutions were by finite elements. Because the example problems in this section showed that even complicated radiation–conduction–convection problems with multiple surfaces reduce to the same general form of Equations (C.17), the conclusions probably apply to a broader class of problems than was studied. In Costello and Shrenk (1966), a linearized solution is proposed that speeds convergence over the MNR method. For problems that are either conduction or radiation dominated or where both modes are important, the method performed well, providing a factor-of-ten improvement in solution speed. It was found that the SUR method gave convergence with the fewest

iterations and the least computer time; RSUR was useful to find the optimum value of the relaxation parameter α for use in the SUR method. For the Newton–Raphson method, ANR was always faster than MNR, but neither method was as fast as SUR.

In Howell (1992, 2017), the convergence ranges and behavior of equations of the form of Equations (C.17) are discussed, and the various solution methods of this chapter are examined. Nonlinear equations of this type can have behavior characterized by bifurcations and chaos of successive iterations so that steady solutions carried out by SSS, SUR, etc., may not converge. This is true whether the equations are cast as radiation-dominated or first-order temperature-dominated or the equations used are in mixed form such as Equation (C.18). Decreasing the relaxation factor extends the range of convergence, but often will not yield a solution for some ranges of parameters without unacceptable computer time. For conduction–radiation problems, bifurcation–chaos behavior results from the numerical method chosen and the equation form and does not imply that multiple physical solutions can exist. However, when there is coupling between radiation and the flow field, as in combined radiation and free convection, multiple physical steady-state solutions may exist. The particular flow configuration reached in a steady state analysis may depend on the initial conditions chosen and the set of velocity and temperature fields that are traversed in reaching steady state. In some cases, no steady solution is reached; it may be possible to solve for the steady-state solution by using a fully transient solution that proceeds to the final steady state from physically specified initial conditions.

Numerical solution techniques for steady-state and transient combined-mode problems with surface–surface radiative exchange are examined and discussed by Hogan and Gartling (2008). Three techniques that sequentially solve for radiative transfer followed by solution of the energy equation with a radiative source term are compared with a fully coupled solution. For the two example problems studied, the fully coupled method always produced the most accurate solution, although execution time made it unattractive for very large problems. A semi-implicit technique with a Newton type of update appeared to be the best choice for very large problems.

The finite-difference and finite-element numerical procedures that have been described used radiative enclosure theory with finite or infinitesimal areas to obtain a set of simultaneous equations with configuration factors for radiative exchange between surface areas. Convection was specified in terms of an energy transfer coefficient for each area; for example, for radiation exchange inside a tube with a flowing transparent gas, the energy transfer coefficient inside the tube is obtained from - available results from tube flow analyses or experimental correlations. For some situations, however, convection is quite dependent on the surface temperatures, such as for free convection, or the geometry is complex so that convective energy transfer correlations are not available with desired accuracy. In these cases, analyses have been made where convection is solved simultaneously with radiation as the flow and surface temperatures are strongly coupled; conduction may also be included, such as for free convection and radiation from a cooling fin as discussed in Section 7.4.3 of the book. To solve for the convection energy transfer, the methods of computational fluid mechanics are used.

Another consideration is that the analysis may not use configuration factors. The radiative exchange in an enclosure can be computed directly by a ray-tracing technique such as a Monte Carlo method (Section 10.5 of the book). This may be necessary if the surfaces are not diffuse so that configuration

factors do not apply. The discrete ordinates method, discussed in Section 10.3, was developed for enclosures filled with a medium that is not transparent, but rather absorbs, emits, and scatters radiation. If radiative participation by the medium is omitted, the method can be applied to enclosures containing a transparent medium such as a convecting transparent gas. In this method, the angular directions from each surface element are divided into a finite number, and radiation is followed along these discrete directions to evaluate the radiative exchange. In Tan et al. (1998), discrete ordinates are used in combination with the SIMPLE computer algorithms developed for computational fluid mechanics (Patankar 1980) to simultaneously solve the mass, momentum, and energy equations along with radiation transfer between surfaces.

For natural convection combined with radiation, many computational methods have been used for simultaneously solving the fluid flow and energy equations with radiative exchange. In Zhao et al. (1992), free convection and radiation were analyzed for heated cylinders in a rectangular enclosure. In Dehghan and Behnia (1996), net radiation enclosure analysis was used for the radiative transfer, and the flow and energy equations were placed in finite-difference form and solved with a pseudo transient method to analyze free convection in a cavity with a local heated area on one vertical wall. A vented cavity with a discrete energy source was analyzed by Yu and Joshi (1999) using the numerical methods from Patankar (1980); this study included combined radiation exchange, conduction, and natural convection, with the gas in the cavity being transparent. Free convection of transparent air in a heated vertical channel with one or more vents in one wall was analyzed by Moutsoglou et al. (1992). The flow and energy equations were solved by using finite-difference computational methods as developed by Patankar and Spalding (1972) and van Doormall and Raithby (1983).

REFERENCES:

Ambarzumian, V. A.: Diffusion of light by planetary atmospheres, *Astron. Zh.*, 19, 30–41, 1942.

Buckley, H.: On the radiation from the inside of a circular cylinder: Part I, *Philos. Mag.*, 4, 753–762, 1927; Part II, *Philos. Mag.*, 6, 447–457, 1928.

Choi, B. C. and Churchill, S. W.: A technique for obtaining approximate solutions for a class of integral equations arising in radiative heat transfer, *Int. J. Heat Fluid Flow*, 6(1), 42–48, 1985.

Cort, G. E., Graham, H. L., and Johnson, N. L.: Comparison of methods for solving non-linear finite element equations in heat transfer, ASME Paper 82-HT-40, *Proc. 21st National Heat Transfer Conf.*, Seattle, August 1982.

Costello, F. A. and Schrenk, G. L.: Numerical solution to the heat-transfer equations with combined conduction and radiation, *J. Comput. Phys.*, 1, 541–543, 1966.

Crosbie, A. L. and Sawheny, T. R.: Application of Ambarzumian's method to radiant interchange in a rectangular cavity, *JHT*, 96, 191–196, 1974.

Crosbie, A. L. and Sawheny, T. R.: Radiant interchange in a nonisothermal rectangular cavity, *AIAA J.*, 13(4), 425–431, 1975.

Dehghan, A. A. and Behnia, M.: Combined natural convection-conduction and radiation heat transfer in a discretely heated open cavity, *JHT*, 118(1), 56–64, 1996.

Fan, Y., An, J. and Yin, L.: Fast algorithms for integral formulations of steady-state radiative transfer equation, *J. Computational Physics*, 380(1), 191-211, Jan. 2018.

Hildebrand, F. B.: *Methods of Applied Mathematics*, 2nd edn., Dover, New York, 1992.

Hogan, R. E. and Gartling, D. K.: Solution strategies for coupled conduction/radiation problems, *Commun. Numer. Methods Eng.*, 24(6), 523–542, June 2008.

Howell, J. R.: Modern computational methods in radiative heat transfer, in K. T. Yang and W. Nakayama (eds.), *Computers and Computing in Heat Transfer Science and Engineering*, pp. 153–171, CRC Press, Boca Raton, FL, December 1992.

Howell, J. R.: The effect of bifurcation on numerical calculation of conjugate heat transfer with radiation, *JQSRT*, 196, 242-245, 2017.

Jakob, M.: *Heat Transfer*, vol. II, Wiley, New York, 1957.

Kourganoff, V.: *Basic Methods in Transfer Problems*, Dover, New York, 1963.

Krishnan, K. S. and Sundaram, R.: The distribution of temperature along electrically heated tubes and coils, I. Theoretical, *Proc. R. Soc. Lond., Ser. A*, 257(1290), 302–315, 1960.

Moutsoglou, A., Rhee, J. H., and Won, J. K.: Natural convection-radiation cooling of a vented channel, *IJHMT*, 35(11), 2855–2863, 1992.

Ness, A. J.: Solution of equations of a thermal network on a digital computer, *Solar Energy*, 3(2), p. 37, 1959.

Patankar, S. V.: *Numerical Heat Transfer and Fluid Flow*, Hemisphere, Washington, DC, 1980.

Patankar, S. V. and Spalding, D. B.: A calculation procedure for heat, mass, and momentum transfer in three-dimensional parabolic flows, *IJHMT*, 15, 1787–1806, 1972.

Perlmutter, M. and Siegel, R.: Effect of specularly reflecting gray surface on thermal radiation through a tube and from its heated wall, *JHT*, 85(1), 55–62, 1963.

Press, W. H., Flannery, B. P., Teukolsky, S. A., and Vetterling, W. T.: *Numerical Recipes in C: The Art of Scientific Computing*, 2d ed., Cambridge University Press, London, 1992.

Qiao, H., Ren, Y., and Zhang, B.: Approximate solution of a class of radiative heat transfer problems, *JHT*, 122(3), 606–612, 2000.

Sparrow, E. M.: Application of variational methods to radiation heat-transfer calculations, *JHT*, 82(4), 375–380, 1960.

Sparrow, E. M. and Jonsson, V. K.: *Absorption and Emission Characteristics of Diffuse Spherical Enclosures*, NASA TN D-1289, Washington, DC, 1962.

Tan, Z., Przekwas, A. J., Wang, D., Srinivasan, K., and Sun, R.: Numerical simulation of coupled radiation and convection for complex geometries, Paper AIAA-98-2677, *Seventh AIAA/ASME Joint Thermophysics and Heat Transfer Confeerence*, Albuquerque, NM, June 1998.

Usiskin, C. M. and Siegel, R.: Thermal radiation from a cylindrical enclosure with specified wall heat flux, *JHT*, 82(4), 369–374, 1960.

van Doormall, J. P. and Raithby, G. D.: Enhancements of the simple method for predicting incompressible fluid flows, *Numer. Heat Transfer*, 7, 147–163, 1983.

Yu, E. and Joshi, Y. K.: Heat transfer in discretely heated side-vented compact enclosures by combined conduction, natural convection, and radiation, *JHT*, 121(4), 1002–1010, 1999.

Zhou, R.-R., Li, B.-W., Wang, W.-K., and Sun, Y.-A.: Improved integration strategies for the singularity subtraction method to solve radiative integral transfer equations with specified temperature field, *IJTS*, 149, 106158, 2020.

Zhao, Z., Poulikakos, D., and Ren, Z.: Combined natural convection and radiation from heated cylinders inside a container, *JTHT*, 6(4), 713–720, 1992.

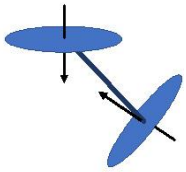

D: COMBINED MODE RADIATION TRANSFER

RADIATION COMBINED WITH CONDUCTION

First, consider the boundary conditions for the limiting situation of radiation being dominant so that conduction and convection effects are neglected. In this limit, a temperature discontinuity ("jump") occurs at a solid boundary (Section 10.2). When conduction and/or convection are present, the temperature is continuous at the boundaries, although the temperature gradient is generally not. For very small conduction and/or convection relative to radiation, the temperature gradients may be steep near a wall and the solution approaches the temperature jump condition. In this section, conduction is included with radiation. The addition of convection is in subsequent sections.

There are several cases where energy is transferred within a translucent medium by only radiation and conduction. These usually involve solid or highly viscous media, so convection in the medium is not important. Glass can absorb significant amounts of radiation in certain wavelength regions (see Figure 4.11 and Section 8.6). At elevated temperatures, there can be appreciable emission within glass. Glass is optically dense in the infrared region, and absorption and emission require consideration of radiative transport.

Radiation can be a significant part of the energy transfer in shields for atmospheric re-entry of spacecraft, fibrous insulation materials, foam insulations, high-temperature porous insulating materials, silica aerogels, gas-fluidized beds, and radiation-induced curing of thermoset filament-wound composites.

Throughout this section, the theory is for materials with $n \approx 1$, such as a radiating gas in a chamber or a gas containing suspended particles in a furnace or a hot exhaust plume. The effects of larger refractive index are considered in Chapter 11 for glass windows, translucent ceramic coatings, thin films, and other applications.

ENERGY BALANCE

For combined radiation and conduction in an absorbing–emitting and scattering medium, the energy Equation (9.2) is used. This is solved subject to the boundary conditions to obtain the temperature distribution in the medium; energy flows can then be found. Omitting convection, viscous dissipation, and volume expansion terms, Equation (9.2) becomes

$$\rho c \frac{\partial T}{\partial t} = \nabla \cdot (k \nabla T - \mathbf{q}_\mathrm{r}) + \dot{q} \tag{D.1}$$

If the $\nabla \cdot \mathbf{q}_r$ is substituted from Equation (9.3), the local energy balance is

$$\rho c \frac{\partial T}{\partial t} = \nabla \cdot \left(k \nabla T\right) + \dot{q} - 4\pi \int_{\lambda=0}^{\infty} \kappa_\lambda \left(T\right) I_{\lambda \mathrm{b}} \left(T\right) d\lambda + \int_{\lambda=0}^{\infty} \kappa_\lambda \left(T\right) \left[\int_{\Omega_{\mathrm{i}}=0}^{4\pi} I_\lambda \left(\Omega_\mathrm{i}\right) d\Omega_\mathrm{i} \right] d\lambda \tag{D.2}$$

The final radiation absorption term in Equation (D.2) depends on both the local temperature and on the surrounding radiation field.

PLANE LAYER WITH CONDUCTION AND RADIATION

Absorbing–Emitting Gray Medium without Scattering

A layer of translucent conducting–radiating medium is between parallel black walls at temperatures T_1 and T_2, as in Figure 10.3. The medium is gray and has a constant thermal conductivity k and a constant absorption coefficient κ. The steady energy transfer relations will be developed without scattering.

For 1D energy conduction and constant k, the $\nabla\cdot(k\nabla T)$ reduces to $k(d^2T/dx^2)$, and $\nabla\cdot\mathbf{q}_r$ becomes $dq_{r,x}/dx$. The temperature distribution is steady, $\partial T/\partial t = 0$, and there is no internal energy generation, $\dot{q} = 0$. Then, with $\tau = \kappa x$, Equation (D.2) reduces to

$$k\kappa \frac{d^2T}{d\tau^2} = \frac{dq_r(\tau)}{d\tau} \tag{D.3}$$

For a plane layer with diffuse–gray boundaries, $dq_r/d\tau$ is given by Equation (9.24). For black walls, the boundary fluxes are $J_1 = \sigma T_1^4/\pi$ and $J_2 = \sigma T_2^4/\pi$. For zero scattering in a gray medium, $\hat{I}(\tau) = \sigma T^4(\tau)/\pi$ from Equation (9.22). Then Equation (D.3) becomes, with $\tau_D = \kappa D$,

$$k\kappa \frac{d^2T}{d\tau^2} = -2\sigma T_1^4 E_2(\tau) - 2\sigma T_2^4 E_2(\tau_D - \tau) - 2\int_{\tau^*=0}^{\tau_D} \sigma T^4(\tau^*) E_1(|\tau - \tau^*|)\, d\tau^* + 4\sigma T^4(\tau) \tag{D.4}$$

The boundary conditions for T are $T(\tau=0) = T_1$ and $T(\tau=\kappa D = \tau_D) = T_2$. Define the dimensionless quantities $\vartheta = T/T_1$, $\vartheta_2 = T_2/T_1$, and $N_{CR} = k\kappa/4\sigma T_1^3$ to give

$$N_{CR} \frac{d^2\vartheta(\tau)}{d\tau^2} = \vartheta^4(\tau) - \frac{1}{2}\left[E_2(\tau) + \vartheta_2^4 E_2(\tau_D - \tau) + 2\int_{\tau^*=0}^{\tau_D} \vartheta^4(\tau^*) E_1(|\tau - \tau^*|)\, d\tau^* \right] \tag{D.5}$$

This is the energy equation for $\vartheta(\tau)$; the boundary conditions are $\vartheta(0) = 1$ and $\vartheta(\tau_D) = \vartheta_2$. The solution depends on the parameters N_{CR}, τ_D, and ϑ_2.

The *conduction–radiation parameter* (or *Stark number, sometimes also called the Stefan number*) $N_{CR} \equiv k\kappa/4\sigma T_j^3$ for a nonscattering medium is based on the jth temperature. The N_{CR} does *not* directly give the relative values of conduction to emission because the ratio of these values depends on both temperature difference and absolute temperature level. When scattering is included, the N_{CR} includes the scattering coefficient to become $N_{CR} \equiv k(\kappa + \sigma_s)/4\sigma T_j^3$ and the source term relation is modified.

The combined radiation and conduction energy transfer across the translucent layer can be obtained from the temperature distribution. From energy conservation, q is independent of location τ for the conditions considered where $\dot{q} = 0$, so the evaluation for q can be done at any τ location. Equation (9.24) gives the net radiative energy flux in terms of the temperature distribution across a gray gas between black walls. This radiative flux relation was obtained for convenience at $\tau = 0$. In addition,

at the same location, there is now a conduction flux $-k(dT/dx)|_{x=0} = -k\kappa(dT/d\tau)|_{\tau=0}$, so the energy flux relation becomes, in terms of the unknown temperature distribution,

$$q = -k\kappa \left.\frac{dT}{d\tau}\right|_{\tau=0} + \sigma T_1^4 - 2\sigma T_2^4 E_3(\tau_D) - 2\int_0^{\tau_D} \sigma T^4(\tau^*) E_2(\tau^*) d\tau^* \qquad \text{(D.6)}$$

On the right, the first term is the conduction away from wall 1 by the medium, the second is the radiation leaving black wall 1, the third is the radiation leaving wall 2 that is then attenuated by the translucent medium and reaches wall 1, and the last term is the radiation from the medium to wall 1. In dimensionless form,

$$\frac{q}{\sigma T_1^4} = -4N_{CR} \left.\frac{d\vartheta}{d\tau}\right|_{\tau=0} + 1 - 2\left[\vartheta_2^4 E_3(\tau_D) + \int_{\tau^*=0}^{\tau_D} \vartheta^4(\tau^*) E_2(\tau^*) d\tau^*\right] \qquad \text{(D.7)}$$

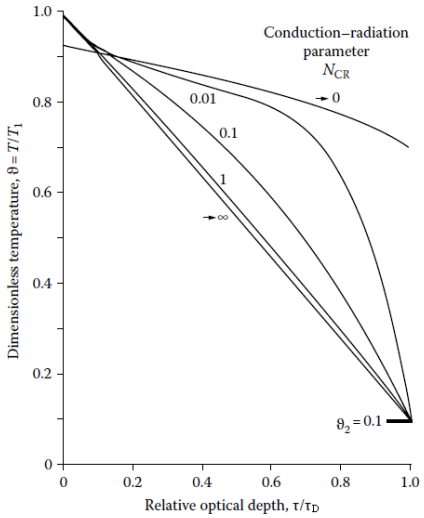

Figure D.1 Dimensionless temperature distribution in gray gas between infinite parallel black plates with conduction and radiation. Plate temperature ratio $\vartheta_2 = 0.1$; optical spacing $\tau_D = 1.0$. (From Viskanta, R. and Grosh, R.J., *J. Heat Trans.*, 84(1), 63, 1962b.)

Absorbing–Emitting Medium with Scattering

Scattering is now added to the absorbing and emitting plane layer with energy conduction. The medium is gray and scattering is isotropic. Scattering is conveniently included by using the radiative source function. For isotropic scattering the phase function $\Phi(\lambda, \Omega) = 1$, so for gray properties Equation (9.10) applies, and with $\tau = (\kappa + \sigma_s)x$ the energy Equation (D.1) becomes

$$k\beta \frac{d^2T}{d\tau^2} = 4\frac{(1-\omega)}{\omega}\left[\sigma T^4(\tau) - \pi\hat{I}(\tau)\right] \qquad \text{(D.8)}$$

The $\pi\hat{I}(\tau)$ is found by using the integral Equation (9.16) that gives, for a plane layer with black boundaries at uniform temperatures T_1 and T_2,

$$\pi\hat{I}(\tau)=(1-\omega)\sigma T^4(\tau)+\frac{\omega}{2}\left[\sigma T_1^4 E_2(\tau)+\sigma T_2^4 E_2(\tau_D-\tau)+\pi\int_{\tau^*=0}^{\tau_D}\hat{I}(\tau^*)E_1(|\tau^*-\tau|)d\tau^*\right] \quad (D.9)$$

Equations (D.4) and (D.6) are placed in dimensionless form by using the same quantities as in Equation (D.5) and by using $\pi\hat{I}/\sigma T_1^4$ as a dimensionless source function. The $N_{CR}=k(a+\sigma_s)/4\sigma T_1^3$ includes the scattering coefficient, and the scattering albedo ω is an additional parameter. The boundary conditions are the same as given after Equation (D.5). The solution is obtained by numerical integration and iteration, and results are in Viskanta (1965).

P_N METHOD FOR RADIATION COMBINED WITH CONDUCTION

The P_N method provides an expression for the local radiative source that is *differential i*n form and can be incorporated into the energy equation in differential form that includes convection and/or conduction. The P_N method thus can fit into whatever grid size is used for numerically solving the energy equation. The procedure for a combined radiation and conduction solution is in the following example.

Example 10.6

A plane layer of radiating and isotropically scattering medium with constant thermal conductivity *k*, constant radiative properties, optical thickness τ_D, and albedo ω is between infinite parallel diffuse–gray walls of emissivity ε_w at temperatures T_{w1} and T_{w2}. The medium has a uniform internal energy source $\dot{q}$. Derive the relations needed to obtain the energy flux to each bounding wall and the temperature distribution in the medium using the P_1 approximation.

With conduction, radiation, and internal energy generation, the energy Equation (10.2) is $\nabla\cdot(k\nabla T-q_r)+\dot{q}=0$ or, using a summation form for the radiation and conduction fluxes,

$$\sum_{i=1}^{3}\frac{\partial q_{r,i}}{\partial x_i}+\sum_{i=1}^{3}\frac{\partial q_{c,i}}{\partial x_i}=\dot{q} \quad (D.1.1)$$

For the present 1D problem, since $q_r = I^{(1)}$, where $I^{(1)}$ is the first moment of the intensity, the energy equation can be put in the dimensionless form

$$\frac{d\tilde{I}^{(1)}}{d\tau_1}=4N_{CR}\frac{d^2\vartheta}{d\tau_1^2}+\frac{\dot{S}}{\tau_D} \quad (D.1.2)$$

where $N_{CR}=\frac{k(\kappa+\sigma_s)}{4\sigma T_{w1}^3}$, $\dot{S}=\frac{\dot{q}D}{\sigma T_{w1}^4}$, $\tau_1=(\kappa+\sigma_s)x_1$, $\tau_D=(\kappa+\sigma_s)D$, $\tilde{I}^{(1)}=I^{(1)}/\sigma T_{w1}^4$, and $\vartheta=T/T_{w1}$.

This is the defining equation for the derivative of $\tilde{I}^{(1)}$. In the pure-radiation solution of Example 10.2 without internal energy sources, the derivative of the first moment in Equation (10.6.2) was set equal to zero, because for these conditions $\tilde{I}^{(1)}=q_r/\sigma T_{w1}^4$ is constant and $d\tilde{I}^{(1)}/d\tau_1=0$. This is not the case here with conduction and an internal energy source included. The presence of a second derivative of dimensionless temperature requires two boundary conditions for solving the energy equation: $\vartheta(\tau_1=0)=1$ and $\vartheta(\tau_1=\tau_D)=T_{w2}/T_{w1}$.

To proceed with the solution, two coupled second-order differential equations are derived for $\tilde{I}^{(0)}$ and $\tilde{I}^{(1)}$ (the nondimensional intensity integrated over all solid angles and the radiative flux). The first is obtained by equating Equation (10.6.1) and the first moment differential Equation (10.6.2) in the P_N method. For 1D, this gives

$$\frac{4N_{CR}}{1-\omega}\frac{d^2\vartheta}{d\tau_1^2}+\frac{\dot{S}}{\tau_D(1-\omega)}-4\vartheta^4=-\tilde{I}^{(0)} \quad (D.1.3)$$

where $\tilde{I}^{(0)} = I^{(0)}/\sigma T_{w1}^4$. The second equation is found by substituting the closure equation (Equation (10.44)) into the second-moment differential equation (Equation (10.46)) to obtain the relation between $\tilde{I}^{(0)}$ and $\tilde{I}^{(1)}$:

$$\frac{d\tilde{I}^{(11)}}{d\tau_1} = \frac{1}{3}\frac{d\tilde{I}^{(0)}}{d\tau_1} = -\tilde{I}^{(1)} \tag{D.1.4}$$

Now, Equation (D.1.4) is differentiated with respect to τ_1, and the result is substituted into Equation (D.1.2) to give

$$\frac{d^2\tilde{I}^{(0)}}{d\tau_1^2} + 12N_{CR}\frac{d^2\vartheta}{d\tau_1^2} + \frac{3\dot{S}}{\tau_D} = 0 \tag{D.1.5}$$

Equations (D.1.3) and (D.1.5) can be solved simultaneously for $\tilde{I}^{(0)}$ and θ. They can be combined into a single fourth-order equation in $\tilde{I}$ by differentiating Equation (D.1.3) twice with respect to τ_1 and the result is substituted into Equation (D.1.5) to eliminate the second derivative of $\tilde{I}^{(0)}$. The resulting fourth-order equation, or the two second-order equations, requires two boundary conditions in addition to the known boundary surface temperatures. These are generated from Equation (10.47) using Equation (10.2.9) to eliminate *J*, which results in

$$\begin{aligned}
&\frac{1}{4}\tilde{I}^{(0)}(\tau_1 = 0) = 1 - \left(\frac{1}{\varepsilon_w} - \frac{1}{2}\right)\tilde{I}^{(1)} \quad (\tau_1 = 0) \\
&\frac{1}{4}\tilde{I}^{(0)}(\tau_1 = \tau_D) = \vartheta_{w2}^4 + \left(\frac{1}{\varepsilon_w} - \frac{1}{2}\right)\tilde{I}^{(1)} \quad (\tau_1 = \tau_D)
\end{aligned} \tag{D.1.6}$$

or

$$\frac{1}{4}\tilde{I}_i^{(0)} = \vartheta_{wi}^4 \pm \left(\frac{1}{\varepsilon_w} - \frac{1}{2}\right)\tilde{I}_i^{(1)} \tag{D.1.7}$$

where the *i* subscript denotes walls 1 or 2 and the positive sign applies at wall *i* = 2. Inserting Equation (D.1.4) to eliminate $\tilde{I}^{(1)}$ results in the final boundary relations for $\tilde{I}^{(0)}$:

$$\pm\left(\frac{d\tilde{I}^{(0)}}{d\tau_1}\right)_i = -\frac{3}{4\left(\frac{1}{\varepsilon_w} - \frac{1}{2}\right)}\left[\tilde{I}_i^{(0)} - 4\vartheta_{wi}^4\right] \tag{D.1.8}$$

These can be directly applied as the boundary conditions for Equation (D.1.5). The problem is completely specified with two second-order differential Equations (D.1.3) and (D.1.5) and the four boundary conditions, the specified boundary temperatures for Equation (D.1.3), and the conditions (*i* = 1, 2) in Equation (D.1.8) for Equation (D.1.5). An iterative numerical solution can be used to obtain $\vartheta(\tau_1)$ and $\tilde{I}_i^{(0)}(\tau_1)$. Then $\tilde{I}_i^{(1)}$ at the boundaries (*i* = 1, 2) is found from Equations (D.1.6), which gives the desired radiative fluxes at the boundaries.

The total energy transfer also requires the amount of energy conduction. Since the temperature distribution has been determined, this can be found by evaluating $-k dT/dx$ at the boundaries.

Diffusion Method for Combined Radiation and Conduction

This approximate method solves the energy equation with the coupled energy transfers by conduction and radiation; radiative diffusion is included simultaneously with diffusion by energy conduction. As shown in the derivation in Section 10.2, the diffusion energy flux relation for radiative transfer has the same form as the Fourier conduction law. By using the Rosseland mean attenuation coefficient defined in Equation (10.27), the radiative flux vector for an absorbing, emitting, and isotropically scattering medium can be written from Equation (10.26) as

$$\mathbf{q}_{\mathrm{r}} = -\frac{4}{3\beta_{\mathrm{R}}}\nabla E_{\mathrm{b}} = -\frac{16\sigma T^3}{3\beta_{\mathrm{R}}}\nabla T \tag{D.10}$$

where β_R can be a function of position. Then, the local energy flux vector by combined radiation and conduction is

$$\mathbf{q} = \mathbf{q}_{\mathrm{r}} + \mathbf{q}_{\mathrm{c}} = -\left(\frac{16\sigma T^3}{3\beta_{\mathrm{R}}} + k\right)\nabla T \tag{D.11}$$

This can be used in energy Equation (9.1). For example, in 2D rectangular coordinates, with internal energy sources, the transient energy equation is

$$\rho c_{\mathrm{P}}\frac{\partial T}{\partial t} = \frac{\partial}{\partial x}\left[\left(\frac{16\sigma T^3}{3\beta_{\mathrm{R}}} + k\right)\frac{\partial T}{\partial x}\right] + \frac{\partial}{\partial y}\left[\left(\frac{16\sigma T^3}{3\beta_{\mathrm{R}}} + k\right)\frac{\partial T}{\partial y}\right] + \dot{q}(x, y) \tag{D.12}$$

The energy transfer is now analogous to energy conduction, with an effective thermal conductivity $\left(\frac{16\sigma T^3}{3\beta_{\mathrm{R}}} + k\right)$ that depends on temperature.

To obtain the temperature distribution in the medium, an equation such as Equation (D.12) is solved subject to the initial and boundary conditions. The boundary conditions would often be specified temperatures of the enclosure surfaces. However, as discussed earlier, near a boundary the diffusion approximation may not be accurate as the radiation is not near- isotropic.

For pure radiation, a temperature jump was introduced to join the diffusion solution in the medium to the wall temperature. For combined conduction–radiation, a similar concept was introduced by Goldstein and Howell (1968) and Howell and Goldstein (1969). By using asymptotic expansions to match linearized solutions for intensity, flux, and temperature near the wall with the diffusion solution for these quantities far from the wall, an effective jump condition was derived. As shown in Figure 10.18, the jump gives the boundary condition $T(x \to 0)$ that the diffusion solution must have if the diffusion solution is to extend to the wall. The jump is given in terms of the jump coefficient ψ, which is a function only of the conduction–radiation parameter $N_{\mathrm{CR}} = k\beta/4\sigma T_1^3$. In terms of quantities at wall 1, ψ_1 is given by

$$\psi_1 = \frac{\sigma\left[T_1^4 - T^4(x \to 0)\right]}{q_{\mathrm{r},1}} \tag{D.13}$$

where

$q_{r,1}$ is the radiative flux at the boundary as evaluated by the diffusion approximation

T_1 is the wall temperature

$T(x \to 0)$ is the extrapolated temperature *in the medium* at the wall, which is the effective jump temperature to be used in the diffusion solution

The ψ_1 is computed from the relations of Goldstein and Howell as

$$\psi_1 = \frac{3}{4\pi}\int_0^1 \tan^{-1}\frac{1}{\psi(\gamma)}\,d\gamma \quad \text{where } \psi(\gamma) = \frac{1}{\pi}\left(\frac{N_{CR}}{2\gamma^3} - \frac{2}{\gamma} - \ln\frac{1-\gamma}{1+\gamma}\right) \tag{D.14}$$

For large N_{CR}, the jump effect can be neglected, as energy conduction dominates over radiation effects near the wall.

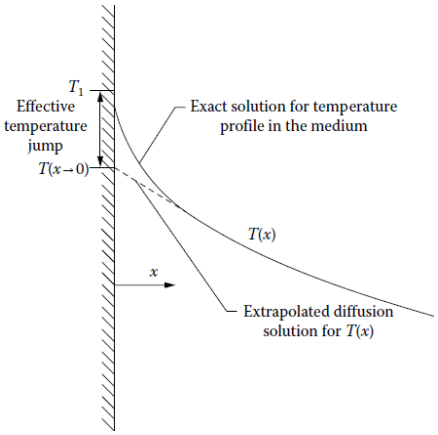

Figure D.2 Use of effective temperature jump as boundary condition for diffusion solution in combined conduction and radiation.

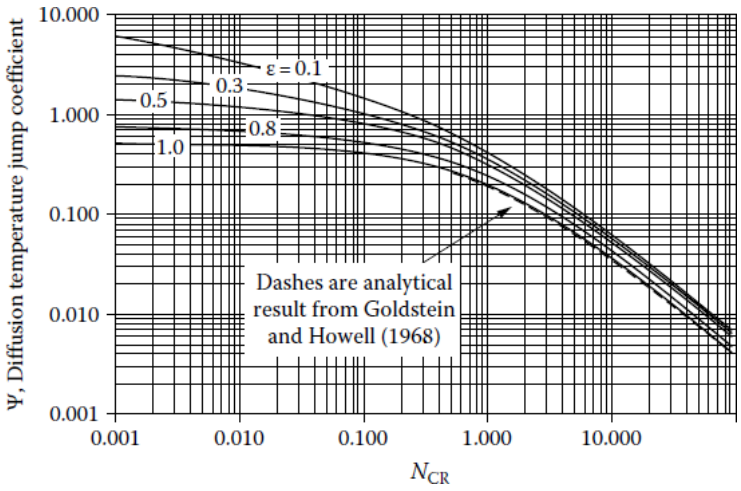

Figure D.3 Temperature jump coefficient for combined conduction–radiation solutions by the diffusion method. (From Goldstein, M.E. and Howell, J.R., Boundary conditions for the diffusion solution of coupled conduction-radiation problems, NASA TN D-4618, 1968 (for ε = 1); Larsen, M. E., Use of contact resistance algorithm to implement jump boundary conditions for the radiation diffusion approximation, *Proceedings of HT2005: 2005 ASME Summer Heat Trans Conference*, Paper HT2005–72561, San Francisco, CA, July, 2005 [for ε ≠ 1].)

Larsen (2005) extended the conduction/radiation slip condition to boundary conditions for gray opaque surfaces by numerically solving a range of conduction/radiation cases using the zone method (Section 10.4) and determining the slip condition that results. The numerical predictions for ε = 1 agree well with the analytical solution of Equation (D.14). The resulting slip coefficient Ψ versus N_1

from the analytical solution of Goldstein and Howell for black walls and for gray boundary emissivity from Larsen is shown in Figure D.3.

The combined-mode diffusion solution yields the temperature distribution in the medium. The result is

$$\frac{1-\vartheta^4(\tau)+3N_{CR}\left[1-\vartheta_2(\tau)\right]}{1-\vartheta_2^4+3N_{CR}\left(1-\vartheta_2\right)}=\frac{3\tau/4+\psi_1}{3\tau_D/4+\psi_1+\psi_2} \tag{D.15}$$

Temperature profiles are in Figure D.4. For $N_{CR} \to 0$ and $N_{CR} \to \infty$, the diffusion–jump method goes to the correct limiting solutions. The diffusion method provides accurate temperature distributions when the layer is optically thick and there is sufficient energy conduction to minimize temperature jump effects at the boundaries.

Within their limits of applicability, diffusion methods provide a useful interpretation of the conduction–radiation parameter. The ratio of molecular conductivity to radiative conductivity is $k/(16\sigma T^3/3\beta_R) = (3/4)(k\beta_R/4\sigma T^3) = (3/4)N_{CR}$. Therefore, in the diffusion limit, N_{CR} is a direct measure of the conduction/radiation conductivity ratio and consequently in this limit is also a direct measure of the ratio of the energy transferred by conduction and radiation.

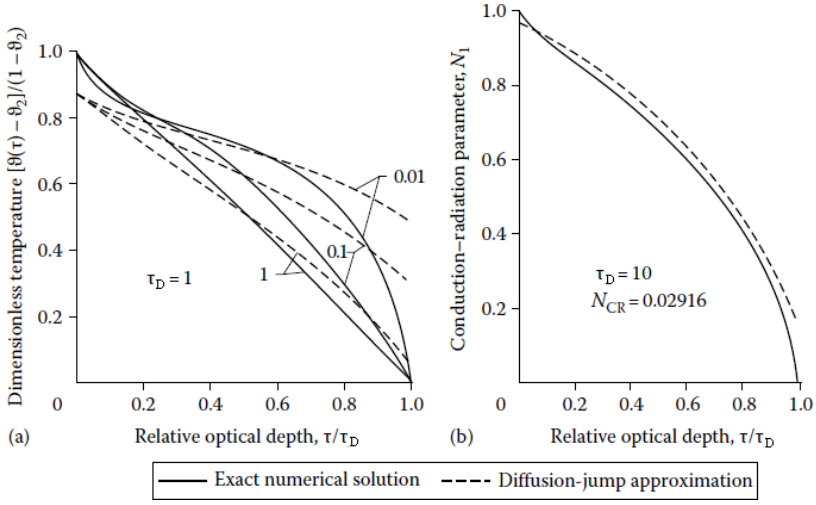

Figure D.4 Comparison of temperature profile by exact solution with diffusion-jump approximation. Wall temperature ratio $T_2/T_1 = 0.5$; wall emissivities $\varepsilon_1 = \varepsilon_2 = 1.0$. (a) Optical thickness $\tau_D = 1$; (b) optical thickness $\tau_D = 10$, conduction-radiation parameter $N_{CR} = 0.02916$. (From Viskanta, R. and Grosh, R.J., *Int. J. Heat Mass Trans*., 5, 729, 1962a.)

The Rosseland mean attenuation coefficient for the entire range of λ should not be used as the criterion for optical thickness. It may have a large value, but the spectral attenuation coefficient may be small in certain spectral regions that allow significant radiant transmission. The use of Rosseland mean coefficient may then lead to large errors. An approach for the optically thick regions is to define the wavelength bands in which the spectral attenuation coefficient is everywhere large and evaluate a Rosseland mean for each of these spectral regions.

COMBINED RADIATION, CONDUCTION, AND CONVECTION

The laminar boundary layer including radiative transfer using the optically thin and thick approximations is a good illustration (Figure D.5). The flowing medium absorbs and emits radiation, but scattering is not included; the wall at T_1 is black.

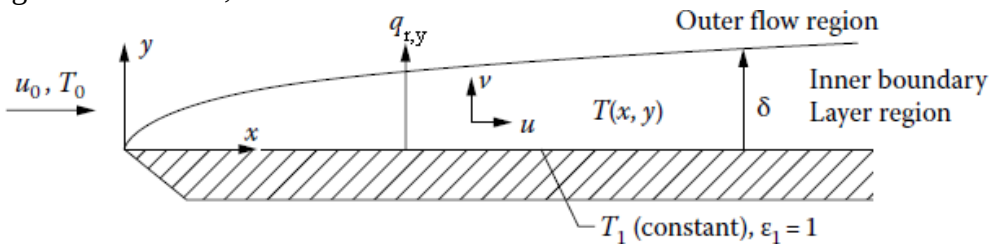

Figure D.5 Boundary layer flow over a flat plate, with free-stream velocity, u_0.

OPTICALLY THIN THERMAL BOUNDARY LAYER

To analyze laminar-flow energy transfer on a flat plate, an expression is needed for the radiative source term $-\partial q_{r,y}/\partial y$ in the energy equation. Within the boundary layer, it is assumed that the thermal conditions are changing slowly enough in the x direction, as compared with the y direction, so the conditions contributing to $q_{r,y}$ at a specific x, say x^+, are all at that x^+ and hence are at the temperature distribution $T(x^+, y)$. Then $\partial q_{r,y}/\partial y$ can be evaluated using 1D forms of relations such as Equations (D.2) and (D.3). For only one bounding wall in Equation (D.2), there is only a T_1 term, and the upper limit of the integral is extended to infinity. Also, the $T^4(\tau^*)$ is replaced by $T^4(x, \tau^*)$ to emphasize the approximation for the radiation term that the temperatures surrounding any position x^+ are all assumed at $T(x = x^+, y)$. Then, for flow over a black wall, the laminar boundary layer energy equation for $T(x, y)$ becomes, with the addition of the radiative energy terms,

$$\rho c_P \left(u\frac{\partial T}{\partial x} + v\frac{\partial T}{\partial y} \right) = k\frac{\partial^2 T}{\partial y^2} - 4\kappa\sigma T^4 + 2\kappa\sigma \left[T_1^4 E_2(\tau) + \int_{\tau^*=0}^{\infty} T^4(x,\tau^*) E_1\left(|\tau - \tau^*|\right) d\tau^* \right] \quad \text{(D.16)}$$

where $\tau = \kappa y$ and there is no scattering and c_P is the specific heat of the gas.

The temperature field is considered as composed of two regions. Near the wall in the usual thermal boundary layer of thickness δ that would be present in the absence of radiation, there are large temperature gradients, and energy conduction is important. This layer thickness is usually small; hence, for the formulation in this section, it is assumed optically thin so that radiation passes through it without attenuation. For larger y than in this layer, temperature gradients are small and energy conduction is neglected compared with radiative transfer.

In the outer region, the velocity in the x direction has the free-stream value u_0, and with the neglect of energy conduction in this region, the boundary layer energy equation reduces to

$$\rho c_P u_0 \frac{\partial T}{\partial x} = -4\kappa\sigma T^4 + 2\kappa\sigma \left[T_1^4 E_2(\tau) + \int_{\tau^*=0}^{\infty} T^4(x,\tau^*) E_1\left(|\tau - \tau^*|\right) d\tau^* \right] \quad \text{(D.17)}$$

To obtain an approximate solution by iteration, substitute the incoming free-stream temperature T_0 for the temperature on the right side as a first approximation and then carry out the integral to obtain a second approximation. For the outer region, to first-order terms,

$$T(x,y) = T_0 + \sigma\left(T_1^4 - T_0^4\right) E_2\left(\kappa y\right) \frac{2\kappa x}{\rho c_P u_0} + \cdots \tag{D.18}$$

where $T = T_0$ at $x = 0$.

At the edge of the thermal layer, $\kappa y = \kappa\delta$, which is small, so that $E_2(\kappa\delta) \approx E_2(0) = 1$. Hence, at $y = \delta$, Equation (D.18) becomes

$$T(x,\delta) = T_0 + \sigma\left(T_1^4 - T_0^4\right) \frac{2\kappa x}{\rho c_p u_0} + \cdots \tag{D.19}$$

Equation (D.19) is the edge boundary condition that the outer radiation layer imposes on the inner thermal layer. The $T(x, \delta)$ to this approximation is increasing linearly with x.

To solve the boundary layer equation in the inner thermal layer region, the last integral in Equation (D.17) is divided into two parts, from $\tau = 0$ to $\kappa\delta$ and from $\tau = \kappa\delta$ to ∞. The first portion is neglected as the thermal layer is optically thin, and the second is evaluated by using the outer solution Equation (D.18). By retaining only first-order terms, the boundary layer energy equation is reduced to

$$u\frac{\partial T}{\partial x} + v\frac{\partial T}{\partial y} = \alpha\frac{\partial^2 T}{\partial y^2} + \frac{2\kappa\sigma}{\rho c_p}\left(T_1^4 + T_0^4 - 2T^4\right) \tag{D.20}$$

The boundary conditions are given by Equation (D.18) at $y = \delta$, and the specified wall temperature $T = T_1$ at $y = 0$. The solution is not developed further here.

OPTICALLY THICK THERMAL BOUNDARY LAYER

At the opposite limit from the previous section, if the thermal layer has become very thick or the medium is highly attenuating, the boundary layer can be optically thick. The analysis is then simplified, as the diffusion approximation can be employed. From Equation (D.10), radiative diffusion adds a radiative conductivity to the ordinary thermal conductivity. Then, the laminar boundary layer energy equation becomes

$$\rho c_p\left(u\frac{\partial T}{\partial x} + v\frac{\partial T}{\partial y}\right) = \frac{\partial}{\partial y}\left[\left(\frac{16\sigma T^3}{3\beta} + k\right)\frac{\partial T}{\partial y}\right] \tag{D.21}$$

With the assumption of constant fluid properties, the momentum and continuity equations do not depend on temperature; consequently, the flow is unchanged by energy transfer. The velocity distribution is given by the Blasius solution in terms of a similarity variable $\eta = y\sqrt{u_0/\nu x}$. The ν under the square roots is the kinematic viscosity. The stream-function and velocity components are

$$\psi = \sqrt{\nu x u_0 f(\eta)}, \quad u = \frac{\partial \psi}{\partial y} = u_0 \frac{df}{d\eta}, \quad v = -\frac{\partial \psi}{\partial x} = \frac{1}{2}\sqrt{\frac{\nu u_0}{x}\left(\eta \frac{df}{d\eta} - f\right)} \tag{D.22}$$

where the function $f(\eta)$ is in Lee et al. (1990). These quantities are substituted into Equation (D.21), giving

$$-\frac{\Pr}{2} f \frac{d\vartheta}{d\eta} = \frac{d}{d\eta}\left[\left(\frac{4\vartheta^3}{3N_{CR}} + 1\right)\frac{d\vartheta}{d\eta}\right] \tag{D.23}$$

where $\vartheta = T/T_0$ and $N_{CR} = k\beta / 4\sigma T_0^3$; N_{CR} is the conduction–radiation parameter. The boundary conditions that were used in the numerical solution are $\vartheta = \vartheta_1 = T_1/T_0$ at $\eta = 0$, and $\vartheta = 1$ at $\eta = \infty$. To be more precise, a temperature jump condition from the use of radiative diffusion should be used at the wall.

NATURAL CONVECTION FLOW, RADIATIVE ENERGY TRANSFER, AND STABILITY

When natural convection is significant, buoyancy appears in the momentum equation while the continuity and energy equations are unchanged.

For fully developed flow in a tube, for example, the momentum equation is

$$\frac{dP}{dx} + \rho g = \mu_f \frac{1}{r}\frac{d}{dr}\left(r \frac{du}{dr}\right) \tag{D.24}$$

This must be solved in conjunction with the energy equation, as the buoyancy term ρg is temperature dependent

RADIATION INTERACTIONS WITH TURBULENCE

Radiation is coupled with turbulence in absorbing–emitting media. This was first recognized by Townsend (1958). The coupling is through the radiative flux divergence in the energy equation, which affects the local temperature and, importantly for combustion problems, the local species concentrations and reaction rates, which are quite temperature dependent. The turbulent fluctuations in these quantities also affect the local radiative properties. In addition, the fluctuation in local temperatures around the local mean can cause a very distorted distribution of local fourth-power temperatures, which in turn affects local emission of radiation and causes radiative emission to be greater than would be predicted using a local fourth-power temperature based solely on the local mean. Another factor to consider in mixed-mode problems!

REFERENCES

Goldstein, M. E. and Howell, J. R.: *Boundary Conditions for the Diffusion Solution of Coupled Conduction-Radiation Problems*, NASA TN D-4618, Washington, DC, 1968.

Howell, J. R. and Goldstein, M. E.: Effective slip coefficients for coupled conduction-radiation problems, *JHT*, 91(1), 165–166, 1969.

Larsen, M. E.: Use of contact resistance algorithm to implement jump boundary conditions for the radiation diffusion approximation, Paper HT2005-72561, *Proceedings 2005 ASME Summer Heat Transfer Conference*, San Francisco, CA, July 2005.

Lee, H. S., Menart, J. A., and Fakheri, A.: Multilayer radiation solution for boundary-layer flow of gray gases, *JTHT*, 4(2), 180–185, 1990.

Townsend, A. A., The effects of radiative transfer on turbulent flow of a stratified fluid, *J. Fluid Mech.* 4(4), 361–375, August 1958.

Viskanta, R.: Heat transfer by conduction and radiation in absorbing and scattering materials, *JHT*, 87(1), 143–150, 1965.

Viskanta, R. and Grosh, R. J.: Effect of surface emissivity on heat transfer by simultaneous conduction and radiation, *IJHMT*, 5, 729–734, 1962a.

Viskanta, R. and Grosh, R. J.: Heat transfer by simultaneous conduction and radiation in an absorbing medium, *JHT*, 84(1), 63–72, 1962b.

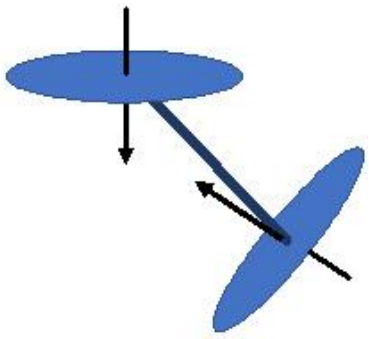

E: COMMERCIAL CODES FOR RADIATION

E.1 CODES FOR CONFIGURATION FACTORS

Many computer programs are available that use one or more of the methods outlined in Chapter 5 of the text for numerical calculation of configuration factors (see Section E.3 of this Appendix for web addresses.) Examples are FACET (Shapiro 1983), which uses area integration and contour integration; VIEW (Emery 1986), which can be used with the NASTRAN thermal analysis code; a program that relies on the computer-graphical analog to the unit-sphere method (Alciatore et al. 1989), and VIEW3D. The latter program provides factors between a differential element and an arbitrary 3D object. The program TSS (Thermal Simulation System, Chin et al. 1992), developed under NASA sponsorship, incorporates an advanced graphical user interface for displaying configurations. The CHAPARRAL program (Glass 1995) incorporates FACET for 2D factors and uses the hemicube method for computing 3D factors in very large surface element arrays. Many commercially available thermal analysis programs such as COMSOL, FLUENT, FIDAP, NEVADA, and the freeware program OpenFOAM also incorporate configuration factor computation using various methods, sometimes with choices among methods. The general code MATLAB has a plug-in module for configuration factors that uses contour integration to get factors between polygons in any configuration.

These and other computer codes provide a means to generate configuration factors for complex geometries and are invaluable for radiative analyses. Their accuracy can be assessed by comparison of computed results with the analytical expressions developed here for simpler geometries that can be used for test cases. Several different numerical methods for calculating configuration factors in complex configurations are compared by Emery et al. (1991) for computing speed, accuracy, and convenience. The geometries range from surfaces almost unobstructed in their view, to highly obstructed intersecting surfaces. The methods compared include double integration, Monte Carlo, contour integration, and projection techniques. If the view is not too complex, methods based on contour integration are found to be successful. The advent of massively parallel computers is making Monte Carlo methods (Section 10.5 of the text) particularly attractive for computing configuration factors. Walker et al. (2010, 2012) and Walker (2013) have examined the use of parallel Monte Carlo using either standard central processing units (CPUs) or graphical processing units (GPUs) and find good speed and accuracy in comparison with finite-element-based numerical integration for computing configuration factors for complex geometries. They employ superimposed primitives for fast rendering of many common objects.

E.2: CFD-BASED CODES

Most of the major commercially available computational fluid dynamics (CFD) codes employ one or more choices of methods for handling radiative transfer within a participating medium. For example, the ANSYS CFD code packages FLUENT and CFX between them provide choice from among surface–surface, diffusion, P_1, discrete transfer, discrete ordinates, and Monte Carlo solvers. The COMSOL built-in Heat Transfer module incorporates spectral surface properties for surface-surface exchange in simple geometries, and uses the Rosseland approximation, P_1 approximation or the discrete ordinate method (DOM) for radiation in participating media. OpenFOAM, a free online CFD code includes P1 and finite volume models, plus a configuration factor calculator for transparent medium problems.

Various models may be included for treating anisotropic scattering and spectral medium property variations, although these features are not available for all solvers. These and competing

codes continue to add features and capabilities, and careful comparison is warranted of the required capabilities for a problem or application.

E.3: AVAILABLE ON-LINE CODES AND DATABASES (Links checked as of 8/25/2019)

On-line resources are available for aid in computing many useful functions for radiation. These include:

CONFIGURATION FACTORS BETWEEN SURFACES:

FACET (Shapiro et al. 1983): **www.oecd-nea.org/tools/abstract/detail/nesc9578**

VIEW (Emery 1986): **https://bit.ly/2kOYJjO**

VIEW3D (Walton 1986): **www.View3d.sourceforge.net**

VIEW FACTORS (Lauzier): Plug in module to MATLAB:
https://www.mathworks.com/matlabcentral/fileexchange/5664-view-factors

Catalog (Howell, 1982 online: More than 350 factors, many with calculator):
www.ThermalRadiation.net/indexCat.html

LINE-BY-LINE SPECTRAL DATA

HITRAN 2016 (Gordon et al. 2017): **www.cfa.harvard.edu/hitran//**

HITEMP 2010 (Rothman et al. 2013): **https://hitran.org/hitemp/**

SPECAIR (Laux 2002) : **www.specair-radiation.net/**

GEISA (Jacquinet-Husson et al. 2017):
https://geisa.aeris-data.fr/line-transition-parameters-2019/

NIST Atomic Spectra (Kramida et al. 2012): **https://www.physics.nist.gov/asd**

GAS EMITTANCE FOR CO_2, H_2O, CO AND THEIR MIXTURES

Alberti et al. (2018), Spread sheet under "Supplementary Data" at:
doi.org/10.1016/j.jqsrt.2018.08.008

SCATTERING

References to scattering literature and codes: **https:www.scattport.org/index.php**

Mie scattering calculator (Prahl,2009) : **https://omlc.org/calc/mie_calc.html**

T-matrix for irregular particles (Mishchenko et al. 2013): at
https://www.giss.nasa.gov/staff/mmishchenko/t_matrix.html

OpenDDA: Discrete dipole approximation for Agglomerates, (McDonald et al. 2009):
www.opendda.org

ADDA: Discrete dipole code for agglomerates, (Yurkin and Hoekstra 2011):
https://github.com/adda-team/adda

Add-on package for MATLAB (Nieminen et al. 2007):
www.physics.uq.edu.au/people/nieminen/software.html

REFERENCES:

Agarwal, B. M. and Mengüç, M. P.: Single and multiple scattering of collimated radiation in an axisymmetric system, *IJHMT*, 34(3), 633–647, 1991.

Alberti, M., Weber, R., and Mancini, M.: Gray gas emissivities for H_2O-CO_2-CO-N_2 mixtures, *JQSRT*, 219, 274-291, Nov. 2018.

Alciatore, D., Lipp, S., and Janna, W. S.: Closed-form solution of the general three-dimensional radiation configuration factor problem with microcomputer solution, *Proceedings of the 26th National Heat Transfer Conference*, Philadelphia, PA, August 1989.

Chin, J. H., Panczak, T. D., and Fried, L.: Spacecraft thermal modeling, *Int. J. Numer. Methods Eng.*, 35, 641–653, 1992.

Datas, A., Hirashima, D., and Hanamura, K.: FTDT simulation of near-field radiative heat transfer between thin films supporting surface phonon polaritons: Lessons learned, *J. Thermal Sci. Technol*., 8(1), 91–105, 2013.

Didari, A. and Mengüç, M. P.: Analysis of near-field radiation transfer within nano-gaps using FDTD method, *JQSRT*, 146, 214–226, 2014.

Didari, A. and Mengüç, M. P.: Near-field thermal emission between corrugated surfaces separated by nano-gaps, *JQSRT*, 158, 43–51, 2015.

Emery, A. F.: VIEW—A radiation view factor program with interactive graphics for geometry definition (Version 5.5.3), 1986.

Emery, A. F., Johansson, O., Lobo, M., and Abrous, A.: A comparative study of methods for computing the diffuse radiation viewfactors for complex structures, *JHT*, 113(2), 413–422, 1991.

Glass, M. W.: *CHAPARRAL: A Library for Solving Large Enclosure Radiation Heat Transfer Problems*, Sandia National Laboratory Report SAND95-2049, Albuquerque, NM, August 1995.

Gordon, I. E., et al. (eds): The HITRAN 2016 molecular spectroscopic databas**e**, *JQSRT*, 203, 3-69, 2017.

Heltzel, A., Battula, A., Howell, J. R., and Chen, S.: Nanostructuring borosilicate glass with near-field enhanced energy using a femtosecond laser pulse, *J. Heat Transfer*, Special Issue on *Nanoscale Heat Transfer*, 129, 53–59, January 2007.

Heltzel, A., Chen, S., and Howell, J. R.: Surface plasmon-based nanopatterning assisted by gold nanospheres, *Nanotechnology*, 19(2), January 2008.

Heltzel, A., Theppakuttai, S., Howell, J. R., and Chen, S.: Analytical and experimental investigation of laser-microsphere interaction for nanoscale surface modification, *J. Heat Transfer*, 127(11), 1231–1235, 2005.

Howell, J. R.: ***Catalog of Radiation Configuration Factors,*** McGraw-Hill Book Company, New York, 1982; later eds. published in electronic form on-line.

Jacquinet-Husson, N. et al., The 2015 edition of the GEISA spectroscopic database, *J. Molecular Spectroscopy 327, 31-72, Sept. 2017.* (GEISA database updated in 2019)

Kramida, A., Ralchenko, Y., Reader, J. and NISTASDTeam: NIST Atomic Spectra Database (version 5.0), [Online]. National Institute of Standards and Technology, Gaithersburg, MD, 2012.

Laux, C. O.: Radiation and nonequilibrium collisional-radiative models, in D. Fletcher, J.-M. Charbonnier, G. S. R. Sarma, and T. Magin (eds.), *Physico-Chemical Modeling of High Enthalpy and Plasma Flows*, von Karman Institute Lecture Series 2002-07, Rhode-Saint-Genèse, Belgium, 2002.

Lauzier, N.: View Factors (https://www.mathworks.com/matlabcentral/fileexchange/5664-view-factors), MATLAB Central File Exchange. Retrieved August 7, 2021.

McDonald, J., Golden, A., and Jennings, G.: OpenDDA: A high-performance computational framework for the discrete dipole approximation, *Int. J. High Perf. Comp. Appl.* 23(1), 42–46, 2009

Mengüç, M. P., Manickavasagam, S., and D'sa, D. A.: Determination of radiative properties of pulverized coal particles from experiments, *FUEL*, 73(4), 613–625, 1994.

Mishchenko, M. I., Videen, G., Khlebtsov, N. G., and Wriedt, T.: Comprehensive T-matrix reference database: A 2012–2013 update, *JQSRT*, 123, 145–152, 2013.

Nieminen, T. A., Loke, V. L. Y., Stilgoe, A. B., Knöner, G., Branczyk, A. M., Heckenberg, N. R., and Rubinsztein-Dunlop, H.: Optical tweezers computational toolbox, *J. Opt. A*, 9, S196–S203, 2007.

Prahl, S.: Mie scattering calculator, http://omlc.ogi.edu/calc/mie_calc.html (accessed April 16, 2015). Oregon Medical Laser Center, Portland, OR, 2009.

Rothman, L. S., Gordon, I. E., Barbe, A. et al., The HITRAN 2012 molecular spectroscopic database, *JQSRT*, 130, 4–50, 2013.

Shapiro, A. B.: FACET—A computer view factor computer code for axisymmetric, 2d planar, and 3d geometries with shadowing, UCID-19887, University of California, Lawrence Livermore National Laboratory, Livermore, CA, August 1983

Shlager, K. L. and Schneider, J. B.: A Selective Survey of the Finite-Difference Time-Domain Literature, *IEEE Antennas Propag. Mag*., 37(4), 39-56, Aug. 1995.

Sun, W., Videen, G., Fu, Q., and Hu, Y.: Scattered-field FDTD and PSTD algorithms with CPML absorbing boundary conditions for light scattering by aerosols, *JQSRT*, 131, 166–174, 2013.

Taflove, A.: *Advances in FDTD Techniques and Applications in Photonics*, *Photonics North 2007*, Ottawa, Ontario, Canada, June 4, 2007.

Veselago, V., Braginsky, L., Shklover, V., and Hafner, C.: Negative refractive index materials, *J. Comput. Theoret. Nanosci.*, 3, 1–30, 2006.

Walker, T.: The use of primatives in the calculation of radiative view factors, PhD dissertation, School of Chemical and Biomolecular Engineering. University of Sydney, Sydney, New South Wales, Australia, December 2013.

Walker, T., Xue, S.-C., and Barton, G. W: Numerical determination of radiative view factors using ray tracing, *JHT*, 132(7), 072702-1–072702-6, 2010.

Walker, T., Xue, S.-C., and Barton, G. W: A robust Monte Carlo-Based ray-tracing approach for the calculation of view factors in arbitrary three- dimensional geometries, *Comput. Thermal Sci*., 4(5), 425–442, 2012.

Walton, G.N.: Algorithms for Calculating Radiation View Factors Between Plane Convex Polygons with Obstructions, National Bureau of Standards NBSIR 863463, Gaithersburg, MD, 1986.

Wriedt, T.: Light scattering theories and computer codes, *JQSRT*, 110, 833–843, 2009.

Yee, K. S.: Numerical solution of initial value problems involving Maxwell's equations in isotropic media, *IEEE Trans. Antennas Propag.*, 14, 302–307, 1966.

Yurkin, M. A. and Hoekstra, A. G.: The discrete-dipole-approximation code ADDA: Capabilities and known limitations, *JQSRT*, 112(13), 2234–2247, 2011.

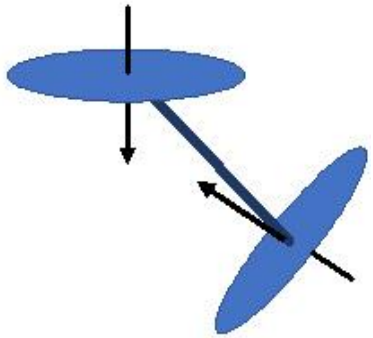

F. REFERENCES TO REVIEWS AND HISTORICAL PAPERS

F.1 GENERAL

Bone, W. A., and Townsend, D. T. A.: *Flame and Combustion in Gases*, Longmans, Green, London, 1927.

Born, M., Wolf, E., and Bhatia, A. B.: *Principles of Optics*, 7th expanded ed., Cambridge University Press, New York, 1999.

Breene, R. G.: *Theories of Spectral Line Shapes*, John Wiley and Sons, New York, 1981.

Carslaw, H. S., and Jaeger, J. C.: *Conduction of Heat in Solids*, 2d ed., Clarendon Press, Oxford, UK, 1959.

Coakley Jr, J. A. and Yang, P.: *Atmospheric Radiation: A Primer with Illustrative Solutions*, John Wiley & Sons, New York, 2014.

Garbuny, M.: *Optical Physics*, 2nd printing, Academic Press, New York, 1967.

Glassman, I., Yetter, R. A., and Glumac, N. G.: *Combustion*, 5th ed., Elsevier Science/Academic Press, Burlington, MA 2018.

Griem, H. R.: *Principles of Plasma Spectroscopy*, Cambridge University Press, 2005.

Hecht, E.: *Optics*. 4th ed., Pearson Education, Inc., Upper Saddle River, USA, 2002.

Herzberg, G.: *Molecular Spectra and Molecular Structure*, 2d ed., 3 vols., Krieger, Malabar, FL, 1992.

Howell, J. R.: The development of engineering radiative heat transfer, *IMECE2002-33131*, 73-78, IMECE, New Orleans, Nov. 2002.

Howell, J. R., Hall, M. J., and Ellzey, J. L.: Combustion of Hydrocarbon Fuels within Porous Inert Media, *Prog. Energy Comb. Science*, vol. 22, pp. 121–145, 1996.

Khalil, E. E.: *Modelling of Furnaces and Combustors*, Energy and Engineering Science Series, Gupta, A.K. and Lilley, D.G. (eds.), Abacus Press, Tunbridge Wells, U.K., 1982.

Kittel, C.: *Introduction to Solid State Physics*, John Wiley & Sons, Hoboken, 2005.

Kourganoff, V.: *Basic Methods in Transfer Problems*, Dover, New York, 1963.

Kuneš, J.: *Dimensionless Physical Quantities in Science and Engineering*, Elsevier, New York, 2012.

Kuo, K.: *Principles of Combustion*, 2nd ed., John Wiley & Sons, 2005.

Landau, L. D. and Lifshitz, E. M.: *Electrodynamics of Continuous Media*, Addison-Wesley, Reading, MA, 1960.

Law, C. K.: *Combustion Physics*, Cambridge University Press, 2006 (on-line, July 2010).

MacRobert, T. M.: *Spherical harmonics*, 3rd edn. Pergamon Press, New York, 1967.

Maier, S. A.: *Plasmonics: Fundamentals and Applications*, Springer, New York, 2007.

Majumdar, A.: Scanning Thermal Microscopy, *Ann. Rev. of Matls Sci.*, vol. 29, pp. 505–585, 1999.

Mandel, L. and Wolf, E.: *Optical Coherence and Quantum Optics*, Cambridge University Press, Cambridge, 1995.

Mandelbrot, B. B.: *Les Objets Fractals: Forme, Hasard et Dimension*, Flammarion, Paris, 1975.

Mandelbrot, B. B.: *The Fractal Geometry of Nature*, W. H. Freeman, San Francisco, CA, 1983.

Mark, J.C.: The spherical harmonics method. Part I. Atomic Energy Report No. MT 92, *National Research Council of Canada*, 1944.

Mohr, P. J., Newell, D. B., and Taylor, B. N.: CODATA recommended values of the fundamental physical constants: 2014, *Rev. Mod. Phys.*, 88, 035009, July-Sept. 2014.

Novotny, J. L., and Hecht, B.: *Principles of Nano-optics*, University Press, Cambridge, 2006.

Patankar, S. V.: *Numerical Heat Transfer and Fluid Flow*, Hemisphere, Washington, DC, 1980.

Penner, S. S.: *Quantitative Molecular Spectroscopy and Gas Emissivities*, Addison-Wesley, Reading, MA, 1959.

Shen, J., and Tang, T.S., *Spectral and High-Order Methods with Applications*, Science Press, Beijing, 2006.

Stone, J. M.: *Radiation and Optics*, McGraw–Hill, New York, 1963.

Tien, C. L., and Cunnington, G. R.: Cryogenic Insulation Heat Transfer, in T. F. Irvine, Jr., and J. P. Hartnett (eds.), *Advances in Heat Transfer*, 9, 349–417, Academic Press, New York, 1973.

Turns, S. R.: *An Introduction to Combustion; Concepts and Applications*, McGraw-Hill, New York, 2011.

Vincenti, W. G, and Kruger Jr., C. H.: *Introduction to Physical Gas Dynamics*, Corrected Ed., Krieger Publishing Company, Malabar, FL, 1986.

Williams, F. A.: *Combustion Theory*, 2nd ed., Taylor and Francis, New York, 1994.

Yeh, P.: *Optical Waves in Layered Media*, John Wiley & Sons, Hoboken, 2005.

Zel'dovich, Ya. B., and Raizer, Yu. P.: *Physics of Shock Waves and High-Temperature Hydrodynamic Phenomena*, vol. 1, pt. II, Academic Press, New York, 1966.

F.2 INVERSE METHODS

Alifanov, O. M.: *Inverse Heat Transfer Problems*, Springer, Berlin, 1994.

Alifanov, O. M., Artyukhin, E. A., and Rumyantsev, S. V.: *Extreme Methods for Solving Ill-Posed Problems with Applications to Inverse Heat Transfer Problems*, Begell House, New York, 1995.

Beck, J. V., Blackwell, B., and St. Clair, Jr., C. R.: *Inverse Heat Conduction: Ill-Posed Problems*, Wiley-Interscience, New York, 1995.

Beckman, F. S.: The Solution of Linear Equations by the Conjugate Gradient Method, in A. Ralston and H. S. Wilf (eds.), *Mathematical Methods for Digital Computers*, John Wiley and Sons, New York, 62–72, 1960.

Daun, K, Ertürk, H., and Howell, J. R.: Inverse Design Methods for High-Temperature Systems, *Arabian Journal of Science and Engineering*, 27(2C), pp. 3-48, 2003.

França, F. H. R., Howell, J. R., Ezekoye, O. A., and Morales, J. C.: Inverse design of thermal systems, in J. P. Hartnett and T. F. Irvine (eds.), *Advances in Heat Transfer*, vol. 36, 1, pp. 1–110, Academic Press, Waltham, MA, 2002.

Hansen, P. C., *Rank-Deficient and Discrete Ill-Posed Problems: Numerical Aspects of Linear Inversion*, SIAM, Philadelphia, 1998.

Kennedy, J. and Eberhart, R.: Particle swarm optimization, *Proc. ICNN'95 – Intl. Conf. on Neural Network*s, pp. 1942-1948, IEEE, Nov. 1995.

Kushner, H. J. and Clark, D. S.: *Stochastic Approximation Methods for Constrained and Unconstrained Systems*, Springer, New York, 1978.

Özişik, M. N., and Orlande, H. R. B.: *Inverse Heat Transfer: Fundamentals and Applications*, Taylor and Francis, New York, 2000.

Morozov, V. A.: *Methods for Solving Incorrectly Posed Problems*, Springer-Verlag, New York, 1984.

Tikhonov, A. N.: Solution of Incorrectly Formulated Problems and the Regularization Method, *Soviet Math. Dokl.*, 4, 1035–1038, 1963. [Engl. trans. *Dokl. Akad. Nauk. SSSR*, 151, 501–504, 1963.]

Vogel, C. R.: *Computational Methods for Inverse Problems*, SIAM, Philadelphia, PA, 2002.

Wing, G. W.: *A Primer on Integral Equations of the First Kind*, SIAM, Philadelphia, PA, 1991.

F.3 RADIATIVE TRANSFER

F.3.1 GENERAL

Amber, I. and O'Donovan, T. S.: Natural convection induced by the absorption of solar radiation: A review, *Renewable and Sustainable Energy Reviews*, 82, 3526–3545, 2018.

Cess, R. D.: The interaction of thermal radiation with conduction and convection heat transfer, in T. F. Irvine, Jr. and J. P. Hartnett (eds.), *Advances in Heat Transfer*, vol. 1, pp. 1–50, Academic Press, New York, 1964

Ficker, T.: General Model of Radiative and Convective Heat Transfer in Buildings: Part I: Algebraic Model of Radiative Heat Transfer, *Acta Polytechnica*, 59(3), 211-233, 2019.

Frank, M. and Klar, A.: Radiative heat transfer and applications for glass production processes, in A. Farina, A. Klar, R. M. M. Mattheijj, A. Mikelić, N. Siedow, and A. Fasano (eds.), *Mathematical Models in the Manufacturing of Glass*, *Proceedings of the C.I.M.E. Summer School*, pp. 57–134, Springer, Terme, Italy, 2008.

Hottel, H. C.: Radiant Heat Transmission, in W. H. McAdams (ed.), *Heat Transmission*, 3d ed., McGraw-Hill, New York, 1954.

Hottel, H. C, and Sarofim, A. F.: *Radiative Transfer*, McGraw–Hill, New York, 1967.

Hottel, H. C., Sarofim, A. F., Wankat, P. C., Noble, J. J., Silcox, G. D., and Knaebel, K. S.: Heat and Mass Transfer, in D. W. Green and R. H. Perry (eds.), *Perry's Chemical Engineer's Handbook*, 8th ed., Chap. 5, pp. 5-16–5-43, McGraw-Hill, 2008.

Howell, J. R., Menguc, M. P., Daun, K., and Siegel, R.: *Thermal Radiation Heat Transfer*, 7th ed., CRC/Taylor and Francis, Boca Raton, 2021.

Lee, S. -C, and Cunnington, G. R.: Theoretical Models for Radiative Transfer in Fibrous Media, in *Ann. Rev. Heat Transfer*, vol. IX, Chap. 3, pp. 159–218, Begell House, New York, 1998.

Modest, M. F. and Mazumder, S.: *Radiative Heat Transfer*, 4th ed., Academic Press, New York, 2021.

Özişik, M. N.: *Radiative Transfer, and Interactions with Conduction and Convection*, John Wiley & Sons, New York, 1973.

Sparrow, E. M.: On the Calculation of Radiant Interchange between Surfaces, in W. Ibele (ed.), *Modern Developments in Heat Transfer*, pp. 181–212, Academic Press, New York, 1963b.

Sparrow, E. M., and Cess, R. D.: *Radiation Heat Transfer*, augmented edition, Hemisphere, Washington, DC, 1978.

Stewart, S. M. and Johnson, R. B.: *Blackbody Radiation: A History of Thermal Radiation Computational Aids and Numerical Methods*, CRC Press, Boca Raton, 2016.

Tencer, J. and Howell, J.R.: Coupling Radiative Heat Transfer with Other Heat Transfer Modes, *J. Brazilian Society Engng Sci*, 38(5), 1473-1487, June 2016.

Timoshenko, V. P., and Trenev, M. G.: A Method for Evaluating Heat Transfer in Multilayered Semitransparent Materials, *Heat Transfer—Sov. Res*., vol. 18, no. 5, pp. 44–57, 1986.

Viskanta, R.: Radiation Transfer and Interaction of Convection with Radiation Heat Transfer, in Thomas F. Irvine, Jr., and James P. Hartnett (eds.), *Advances in Heat Transfer*, vol. 3, pp. 175–251, Academic Press, New York, 1966.

Viskanta, R., and Anderson, E. E.: Heat Transfer in Semi-transparent Solids, in J. P Hartnett and T. F. Irvine, Jr. (eds.), *Advances in Heat Transfer*, vol. 11, pp. 317–441, Academic Press, New York, 1975.

Viskanta, R., and Mengüç, M. P.: Radiation Heat Transfer in Combustion Systems, *Prog. Energy Combust. Sci.*, vol. 13, pp. 97–160, 1987.

Viskanta, R.: *Radiative Transfer in Combustion Systems: Fundamentals and Applications*, Begell House, New York, 2005.

F.3.2 ATMOSPHERIC RADIATION

Bohren, C.W. and Clothiaux, E.E.: *Fundamentals of Atmospheric Radiation*, John Wiley & Sons, New York, 2006.

Coakley Jr, J. A., and Yang, P.: *Atmospheric Radiation: A Primer with Illustrative Solutions*, John Wiley & Sons, New York, 2014.

Duffie, J. A., and Beckman, W. A.: *Solar Energy Thermal Processes*, 3d ed., Wiley, New York, 2006.

Goody, R. M., and Yung, Y. L.: *Atmospheric Radiation*, 2d ed., Oxford University Press, New York, 1989.

Kondratyev, Ya. K.: *Radiation in the Atmosphere*, Academic Press, New York, 1969.

Liou, K.-N.: *An Introduction to Atmospheric Radiation*, 2nd ed., Academic Press, 2002

Petty, G.W.: *A First Course in Atmospheric Radiation*, 2nd ed., Sundog Publishing, Madison, WI., 2006.

F.3.3 INVERSE SOLUTIONS IN RADIATION

Daun, K. J., Ertürk, H., and Howell, J. R.: Inverse Design Methods for High-Temperature Systems, *Arabian J. Sci. and Tech*, 27(2C), 3–48, 2003.

Daun, K. J., Ertürk, H., Howell, J. R., Gamba, M. and Hosseini Sarvari, M.: The Use of Inverse Methods for the Design and Control of Radiant Sources, *JSME International Journal*, ser. B, 46(4), 470–478, 2003.

França, F. H. R., Howell, J. R., Ezekoye, O. A., and Morales, J. C.: Inverse Design of Thermal Systems, in J. P. Hartnett and T. F. Irvine (eds.), *Advances in Heat Transfer*, 36(1), 1–110, Elsevier, 2002.

Rytov, S. M.: *A Theory of Electric Fluctuations and Thermal Radiation*, USSR Academy of Sciences, Moscow, 1953, republished Air Force Cambridge Research Center, Bedford, MA, 1959.

Rytov, S. M., Kravtsov, Y. A., and Tatarskii, V. I.: *Principles of Statistical Radiophysics 3: Elements of Random Fields*, Springer, Berlin, Heidelberg, New York, 1989.

F.3.4 k-DISTRIBUTION AND SLWSGG METHODS

André, F. and Vaillon, R.: Generalization of the *k*-moment Method Using the Maximum Entropy Principle; Application to the NBKM and Full Spectrum SLMB Gas Radiation Models, *JQSRT*, 113(12), 1508–1520, 2012.

André, F., Solovjov, V.P., Hou, L., Vaillon, R., and Lemonnier, D.: The Generalized k-Moment Method for the Modeling of Cumulative k-Distributions of H_2O at High Temperature, *JQSRT* 143, 92-99, 2014a.

André, F., Hou, L., Roger, M., and Vaillon, R.: The Multispectral Gas Radiation Modeling: A New Theoretical Framework Based on a Multidimensional Approach to *k*-Distribution Methods, *JQSRT*, vol. 147, pp. 178-195, 2014b.

Badger, J., Webb, B. W., and Solovjov, V. P.: An exploration of advanced SLW modeling approaches in comprehensive combustion predictions, *Combustion Sci. and Tech.*, pub. On line, 22 Oct. 2019.

Cai, J. and Modest, M. F.: Improved full-spectrum *k*-distribution implementation for inhomogeneous media using a narrow-band database, *JQSRT,* 141, 65-72, July 2014.

Guo, J., Li, X., Huang, X., Liu, Z., and Zheng, C.: A full spectrum k-distribution based weighted-sum-of gray-gases model for oxy-fuel combustion, *IJHMT*, 90, 218-226, Nov. 2015.

Denison, M. K. and Webb, B. W.: The spectral line weighted-sum-of-gray-gases model—A review, in M. P. Mengüç (ed.), *Radiative Transfer—I, Proceedings of the First International Symposium on Radiative Transfer*, pp. 193–208, Begell House, New York, 1996.

Howell, J. R.: Non-equilibrium Radiative Transfer Models: k-Distribution, *von Karman Institute Lecture Series STO-AVT-218-VKI, Radiation and Gas-Surface Interaction Phenomena in High-Speed Re-Entry*, University of Illinois at Urbana Champagne, April 2014.

Modest, M.F.: The Treatment of Nongray Properties in Radiative Heat Transfer: From Past to Present, *JHT*, 135(6) 061801-1 through 061801-12. doi:10.1115/1.40235, 2013.

Solovjov, V. P., Webb, B. W., and André, F.: Radiative Properties of Gases, in Kulacki, F. ed., *Handbook of Thermal Science and Engineering*, 1-74, Springer, 2017.

Wang, C., He, B., Modest, M. F., and Ren, T.: Efficient full-spectrum correlated-k-distribution look-up table, *JQSRT*, 219, 108–116, 2018.

F.3.5 MATHEMATICAL RESOURCES

Abramowitz, M. and Stegun, I. A.: *Handbook of Mathematical Functions*, Dover, New York, 1965.

Altaç, Z.: Integrals Involving Bickley and Bessel Functions in Radiative Transfer, and Generalized Exponential Integral Functions, *JHT*, vol. 118, no. 3, pp. 789–792, 1996.

Breig, W. F., and Crosbie, A. L.: Numerical Computation of a Generalized Exponential Integral Function, *Math. Comput.*, vol. 28, no. 126, pp. 575–579, 1974.

Chang, S. L., and Rhee, K. T.: Blackbody Radiation Functions, *Int. Comm. Heat Mass Transfer*, vol. 11, pp. 451–455, 1984.

Chung, T. J.: Integral and integrodifferential systems, in W. J. Minkowitz, E. M. Sparrow, G. E. Schneider, and R. H. Pletcher (eds.), *Handbook of Numerical Heat Transfer*, Chapter 14, Wiley, New York, 1988.

F.3.6 MICROSCALE-NANOSCALE

Basu, S., Chen, Y.B., and Zhang, Z.M.: Microscale Radiation in Thermophotovoltaic Devices- A Review, *Int. J. Energy Research*, vol. 31, no. 6-7, 689-716, 2007.

Boltasseva, A., and Shalaev, V.: Fabrication of Optical Negative-index Metamaterials: Recent Advances and Outlook, *Metamaterials*, vol. 2, pp. 1-17, 2008.

Cai, W. and Shalaev, V.: *Optical Metamaterials: Fundamentals and Applications*, Springer, New York, 2010.

Carey, V. P., Chen, G., Grigoropoulos, C., Kaviany, M., and Majumdar, A.: A Review of Heat Transfer Physics, *Nanosc. Microsc. Therm.*, vol. 12, pp. 1–60, 2008.

Chen, G.: *Nanoscale Energy Transport and Conversion*, Oxford University Press, New York, 2005.

Cahill, D.G., Ford, W.K., Goodson, K.E., Mahan, G.D., Majumdar, A., Maris, H.J., Merlin, R., and Phillpot, S.R.: Nanoscale thermal transport, *J. Appl. Phys*. vol. 93, pp. 793–818, 2003.

Cahill, D.G. et al.: Nanoscale thermal transport II. 2003–2012, *Appl. Phys. Revs*, vol. 1, 011305, 2014.

Corbitt, S., Francoeur, M., and Raeymaekers, B.: Implementation of Optical Dielectric Metamaterials: A Review," *JQSRT*, **158**, 3-16, 2015.

Family, R. and Mengüç, M.P.: Materials for radiative cooling: A review, *Procedia Environmental Sciences*, 38, 752 – 759, 2017.

Francoeur, M.: Thermal fundamentals, Chap. 4 in *Micro Energy Harvesting*, Briand, D., Yeatman, E. and Roundy, S. (eds.) Wiley-VCH, 2015.

Fu, C. J. and Zhang, Z. M.: Thermal radiative properties of metamaterials and other nanostructured materials: A review, *Frontiers of Energy and Power Engineering in China*, 3(1), 11-26, 2009.

Greffet, J. -J., Carminati, R., Joulain, K., Mulet, J. -P., Mainguy, S., and Chen, Y.: Coherent Emission of Light by Thermal Sources, *Nature*, vol. 416, pp. 61–64, March 7, 2002.

Liu, X., Wang, L., and Zhang, Z.M.: Near-Field Thermal Radiation: Recent Progress and Outlook, *Nanoscale and Microscale Thermophysical Engineering*, 19(2), 98-126, 2015

Narayanaswamy, A., and Chen, G.: Direct Computation of Thermal Emission from Nanostructures, *Ann. Rev. Heat Transfer*, vol. 14, pp. 169–195, 2005.

Otey, C. R., Zhu, L., Sandhu, S., and Fan, S.: Fluctuational electrodynamics calculations of near-field heat transfer in non-planar geometries: A brief overview, *JQSRT*, Special Issue on *Micro- and Nano-scale Radiative Transfer*, 132, 3–11, 2014.

Raether, H.: *Surface Plasmons on Smooth and Rough Surfaces and on Gratings*, Springer-Verlag, Berlin, 1988.

Shi, L., Dames, C., Lukes, J.R., Reddy, P., Duda, J., Cahill, D.G., Lee, J., Marconnet, A., Goodson, K.E., Bahk, J.-H., Shakouri, A., Prasher, R.S., Felts, J., King, W.P., Han, B., and Bischof, J.C.: Evaluating Broader Impacts of Nanoscale Thermal Transport Research, *Nanoscale and Microscale Thermophysical Engineering*, 19(2), 127-165, 2015

Taflove, A.: *Advances in FDTD Techniques and Applications in Photonics*, *Photonics North 2007*, Ottawa, Ontario, Canada, June 4, 2007.

Wong, B. T. and Mengüç, M. P.: *Thermal Transport for Applications in Micro- and Nanomachining*, Springer, Berlin, Germany, 2008.

Zhang, Z. M.: *Nano/Microscale Heat Transfer*, McGraw-Hill, New York, 2007.

F.3.7 PROPERTIES

Bernath, P. and Rothman, L.: HITRAN2016 Special Issue, *JQSRT*, 203, 1-582, Dec. 2017.

Fox, M: *Optical Properties of Solids*, Oxford University Press, Oxford, UK, 2001.

Fu, C. J. and Zhang, Z. M.: Thermal radiative properties of metamaterials and other nanostructured materials: A review, *Frontiers of Energy and Power Engineering in China*, 3(1), 11-26, 2009.

Gordon, I. E., et al. (eds): The HITRAN 2016 molecular spectroscopic database, *JQSRT*, 203, 3-69, 2017.

Kunitomo, T.: Present status of research on radiative properties of materials, *Int. J. Thermophys*., 5(1), 73–90, 1984.

Palik, E. D. (ed.): *Handbook of Optical Constants of Solids*, vols. I-IV, Elsevier, New York, 1998.

Reed, B., Biaglow, J., and Schneider, S.: *Advanced Materials for Radiation-Cooled Rockets*, vol. II, pp. 115–118, NASA Propulsion Engineering Research Center, Annual Report 199, NASA Lewis Research Center, N94-28052, Washington, DC, September 1993.

Rothman, L. S., Jacquemart, D., Barbe, A., et al.: The *HITRAN* 2004 Molecular Spectroscopic Database, *JQSRT*, vol. 96, pp. 139–204, 2005. For most recent version (2012) see http://www.cfa.harvard.edu/hitran//.

Rothman, L.S., Gordon, I.E., Barber, R.J., Dothe, H., Gamache, R.R., Goldman, A., Perevalov, V., Tashkun, S.A., and Tennyson, J.: "HITEMP, the High-temperature Molecular Spectroscopic Database," *JQSRT*, vol. 111, no. 15, 2139.2150 , 2010.

Rumble, J. R., (ed.): *Handbook of Chemistry and Physics*, 100th edn., CRC Press, Boca Raton, FL, 2018-2019.

Svet, D. I.: *Thermal Radiation; Metals, Semiconductors, Ceramics, Partly Transparent Bodies, and Films*, Consultants Bureau, Plenum Publishing, New York, 1965.

Tien, C. L.: Thermal Radiation Properties of Gases, in T. F. Irvine, Jr., and J. P. Hartnett (eds.), *Advances in Heat Transfer*, vol. 5, pp. 253–324, Academic Press, New York, 1968.

Touloukian, Y. S., and Ho, C. Y. (eds.): Thermophysical Properties of Matter, TRPC Data Services. Volume 7, *Thermal Radiative Properties: Metallic Elements and Alloys*, Touloukian, Y. S. and DeWitt, D. P. (1970); Volume 8, *Thermal Radiative Properties: Nonmetallic Solids*, Touloukian, Y. S. and DeWitt, D. P. (1972a); Volume 9, *Thermal Radiative Properties: Coatings*, Touloukian, Y. S., DeWitt, D. P., and Hernicz, R. S. (1972b), Plenum Press, New York.

Warren, S. G. and Brandt, R. E.: Optical constants of ice from the ultraviolet to the microwave: A revised compilation, *J. Geophys. Res.*, 113, D14220, 2008. (Tables of values available at *http://www.atmos.washington.edu/ice_optical_constants*)

Wood, W. D., Deem, H. W., and Lucks, C. F.: *Thermal Radiative Properties*, Plenum Press, New York, 1964.

F.3.8 RTE SOLUTION METHODS

Tencer, J. and Howell, J.R.: Coupling Radiative Heat Transfer with Other Heat Transfer Modes, *J. Brazilian Society Engng Sci*, 38(5), 1473-1487, June 2016.

F.3.8.1 FINITE ELEMENT

Nice, M. L.: Application of Finite Element Method to Heat Transfer in a Participating Medium, in T. M. Shih (ed.), *Numerical Properties and Methodologies in Heat Transfer*, pp. 497–514, Hemisphere, Washington, DC, 1983.

F.3.8.2 FINITE VOLUME

Chai, J. C., and Patankar, S. V.: Finite Volume Method for Radiation Heat Transfer, in W. Minkowycz and E. Sparrow (eds.), *Advances in Numerical Heat Transfer*, vol. 2, 109-141, Taylor and Francis, London, 2000.

Mathur, S. R., and Murthy, J. Y.: Unstructured Finite Volume Methods for Multi-mode Heat Transfer, in W. J. Minkowycz and E. M. Sparrow (eds.), *Advances in Numerical Heat Transfer*, vol. 2, pp. 37–70, Taylor and Francis, New York, 2000.

F.3.8.3 DISCRETE ORDINATES

Balsara, D.: Fast and accurate discrete ordinates methods for multidimensional radiative transfer. Part I, basic methods, *JQSRT*, 69, 671-707, 2001.

Carlson, B. G. and Lathrop, K. D.: Transport theory—The method of discrete ordinates, in H. Greenspan, C. N. Kelber, and D. Okrent (eds.), *Computing Methods in Reactor Physics*, Chapter 3, Gordon & Breach, New York, 1968.

Lathrop, K. D.: Use of discrete ordinate methods for solution of photon transport problems, *Nucl. Sci. Eng*., 24, 381–388, 1966.

F.3.8.4 MONTE CARLO

Barker, E., and Kelsey, J.: *Recommendation for Random Number Generation Using Deterministic Random Bit Generators*, NIST Special Publication 800-90A Revision 1, 109 pp., National Institute of Standards and Technology, Gaithersburg, MD, June 2015.

Burns, P. J. and Pryor, D. V.: Surface radiative transport at large scale via Monte Carlo, in C.-L. Tien (ed.), *Annual Review of Heat Transfer*, IX, Chapter 7, pp. 79–158, Begell House, New York, 1998.

Cashwell, E. D. and Everett, C. J.: *A Practical Manual on the Monte Carlo Method for Random Walk Problems*, Pergamon, New York, 1959.

Chen, G. and Boyd, I. D.: Statistical error analysis for the direct simulation Monte Carlo method. *J. Computational Physics*, 126, 434-448, 1996.

Dauchet, J., Bezian, J.-J., Blanco, S., Caliot, C., Charon, J., Coustet, C., El Hafi,, M., Eymet, V., Farges, O., Forest, V., Fournier, R., Galtier, M., Gautrais, J., Khuong, A.,Pelissier, L., Benjamin Piaud, B., Maxime Roger, M., Guillaume Terrée, G., and Sebastian Weitz, S.: Addressing nonlinearities in Monte Carlo, *Scientific Reports* 8, 13302, 2018.

Ertürk, H., and Howell, J. R.: Monte Carlo methods for radiative transfer, in: *Handbook of Thermal Science and Engineering*, F. Kulacki, ed., pp. 1-43, Springer, Cham, 2017.

Farmer, J. T., and Howell, J. R.: Monte Carlo Strategies for Radiative Transfer in Participating Media, in J. P. Hartnett and T. Irvine, (eds.), *Advances in Heat Transfer*, vol. 31, pp. 1–97, Acadamic Press, San Diego, 1998.

Fournier, R., Blanco, S., Eymet, V., El Hafi, M., and Spiesser, C.: Radiative, conductive and convective heat transfers in a single Monte Carlo algorithm, *J. Physics*: Conf. Series, 676(1), 012007, 2016.

Haji-Sheikh, A., and Sparrow, E. M.: Probability Distributions and Error Estimates for Monte Carlo Solutions of Radiation Problems, in T. F. Irvine, W. E. Ibele, J. P. Hartnett, and R. J. Goldstein (eds.), *Progress in Heat and Mass Transfer*, vol. 2, pp. 1–12, Pergamon, Oxford, 1969.

Haji-Sheikh, A.: Monte Carlo Methods, in W. J. Minkowycz, E. M. Sparrow, G. E. Schneider, and R. H. Pletcher (eds.), *Handbook of Numerical Heat Transfer*, Chap. 16, pp. 672–723, Wiley Interscience, New York, 1988

Haji-Sheikh, A., and Howell, J. R.: Monte Carlo Methods, in W. J. Minkowycz, E. M. Sparrow, and J. Y. Murthy (eds.), *Handbook of Numerical Heat Transfer*, 2d ed., Chap. 8, pp. 249–296, Wiley Interscience, New York, 2006.

Halton, J. H.: A Retrospective and Prospective Survey of the Monte Carlo Method, *SIAM Rev*., vol. 12, no. 1, pp. 1–63, 1970.

Hammersley, J. M., and Handscomb, D. C.: *Monte Carlo Methods*, Wiley, New York, 1964.

Howell, J. R.: The Monte Carlo method in radiative heat transfer, *JHT*, 120(3), 547–560, 1998.

Howell, J. R. and Perlmutter, M.: Monte Carlo solution of thermal transfer through radiant media between gray walls, *JHT***,** 86(1), 116-122, Feb. 1964.

Howell, J. R. and Perlmutter, M.: Monte Carlo solution of radiant heat transfer in nongrey nonisothermal gas with temperature dependent properties, *AICHE J***.,** 10(4), 562-567, July 1964.

Howell, J. R., and Daun, K.: The Past and Future of the Monte Carlo Method in Thermal Radiation Transfer, *JHT*, 143, 100801, Oct. 2021.

Mahan, J. R., *The Monte Carlo Ray-Trace Method in Radiation Heat Transfer and Applied Optics*. John Wiley & Sons, New York, 2018.

Metropolis, N., and Ulam, S.: The Monte Carlo Method, *J. Am. Stat. Assoc*., vol. 44, no. 247, pp. 335–341, 1949.
Perlmutter, M. and Howell, J. R.: Radiant transfer through a gray gas between concentric cylinders using Monte Carlo, *JHT*, 86(2), 169-179, May 1964.
Schreider, Yu. A. (ed.): *Method of Statistical Testing—Monte Carlo Method*, American Elsevier, New York, 1964.
Taussky, O. and Todd, J.: Generating and testing of pseudo-random numbers, in H. A. Meyer (ed.), *Symposium on Monte Carlo Methods*, pp. 15–28, Wiley, New York, 1956.
Walters, D. V., and Buckius, R. O.: Monte Carlo Methods for Radiative Heat Transfer in Scattering Media, in C. -L. Tien (ed.), *Annual Review of Heat Transfer*, vol. 5, Chap. 3, pp. 131–176, CRC Press, Boca Raton, 1994.
Wollaber, A. B.: *Advanced Monte Carlo Methods for Thermal Radiation Transport*, PhD dissertation, Univ. Michigan, 2008.
Yang, W.-J., Taniguchi, H., and Kudo, K.: Radiative Heat Transfer by the Monte Carlo Method, in J. P. Hartnett and T. F. Irvine (eds.), *Advances in Heat Transfer*, vol. 27, pp. 1–215, Academic Press, San Diego, 1995.
Yarbrough, D. W., and Lee, C. -L.: Monte Carlo Calculation of Radiation View Factors, in F. R. Payne et al. (eds.), *Integral Methods in Science and Engineering 85*, pp. 563–574, Hemisphere, Washington, DC, 1985.

F.3.8.5 LATTICE BOLTZMANN

Asinari, P., Mishra, S.C., and Borchiellini, R.: A lattice Boltzmann formulation for the analysis of radiative heat transfer problems in a participating medium, *Numerical Heat Transfer-A, Fundamentals*, 57(2), 126-146, March 2010.
Guo, Z. L. and Shu, C.: *Lattice Boltzmann Method and Its Applications in Engineering.* World Scientific Publishing, 2013.
Krüger, T., Kusumaatmaja, H., Kuzmin, A., Shardt, O., Silva, G., and Viggen, E. M.: *The Lattice Boltzmann Method: Principles and Practice.* Springer Verlag, 2017.
McHardy, C. B.: A lattice Boltzmann method for the simulation of light transfer in turbid media and its application in computational studies on microalgae growth kinetics, Dr. Eng. Dissertation, Technischen Universität Berlin, 2019.
McHardy, C., Horneber, T., and Rauh, C.: New lattice Boltzmann method for the simulation of three-dimensional radiation transfer in turbid media, *Optics Express*, 16999-17017, 24(15), 25 Jul 2016.
Succi, S.: *The Lattice Boltzmann Method for Fluid Dynamics and Beyond*, Oxford University Press, 2001.

F.3.9 SCATTERING

Baillis, D., and Sacadura, J.F., Thermal Radiation Properties of Dispersed Media: Theoretical Prediction and Experimental Characterization, *JQSRT* 67, 327-363, 2000.
Barber, P. W., and Hill, S. S.: *Light Scattering by Particles: Computational Methods*, World Scientific, Singapore, 1990.
Bayvel, L. P., and Jones, A. R.: *Electromagnetic Scattering and Its Applications*, Applied Science, London, pp. 5–6, 1981.
Beckmann, P., and Spizzichino, A.: *The Scattering of Electromagnetic Waves from Rough Surfaces*, Macmillan, New York, 1963.
Bohren, C., and Huffman, D.: *Absorption and Scattering of Light by Small Particles*, Wiley-Interscience, New York, 1983.
Charalampopoulos, T. T.: Morphology and dynamics of agglomerated particulates in combustion systems using light scattering techniques, *Prog. Energy Combust. Sci.*, 18, 13–45, 1992.
Doicu, A., Wriedt, T., and Eremin, Y. A.: *Light Scattering by Systems of Particles*, Springer, Heidelberg, 2006.
Dombrovsky, L. A. and Baillis, D.: *Thermal Radiation in Disperse Systems: An Engineering Approach*, Begell House, Redding, PA, 2010.
Frisad, J. R. and Kragh, H.: On Ludvig Lorenz and his 1890 treatise on light scattering by spheres, *Eur. Phys. J.- H,* 44(2), 137–160, Aug. 2019.
Henyey, L. G., and Greenstein, J. L.: Diffuse Radiation in the Galaxy, *Astrophys. J.*, vol. 88, pp. 70–83, 1940.
Kerker, M.: *The Scattering of Light and Other Electromagnetic Radiation*, Academic Press, New York, 1961.
Mie, G.: Beiträge zur Optik trüber Medien, speziell kolloidaler Metallösungen, *Ann. Phys.*, vol. 330, pp. 377–445, 1908.
Mie, G.: Optics of Turbid Media, *Ann. Phys*., vol. 25, no. 3, pp. 377–445, 1908.
Mishchenko, M. I., Hovenier, J. W., and Travis, L. D.: *Light Scattering by Nonspherical Particles*, Academic Press, New York, 2000.
Mishchenko, M. I., Travis, L. D., and Lacis, A. A.: *Scattering, Absorption, and Emission of Light by Small Particles*, Cambridge University Press, London, 2002.
Mishchenko, M. I., Travis, L. D., and Lacis, A. A.: *Multiple Scattering of Light by Particles: Radiative Transfer and Coherent Back Scattering*, Cambridge Press, New York, 2006.
Rayleigh, Lord: On scattering of light by small particles, *Philos. Mag.*, 41, 447–454, 1871.

Rayleigh, Lord: On the incidence of electric and aerial waves upon small obstacles in the form of ellipsoids or elliptic cylinders and on the passage of electric waves through a circular aperture in a conducting screen, *Phil. Mag.*, 44, 28–52, 1897.

Rother, T.: *Electromagnetic Wave Scattering on Nonspherical Particles, Basic Methodology and Simulations*, Springer Series Optical Sciences, 2009.

Schuerman, D. W. (ed.): *Light Scattering by Irregularly Shaped Particles*, Plenum Press, State University of New York at Albany, NY, 1979.

Stokes, G. G.: On the Composition and Resolution of Streams of Polarized Light from Different Sources, *Trans. Camb. Phil. Soc.*, vol. 9, pp. 399–424, 1852. (Reprinted in *Mathematical and Physical Papers*, vol. 3, Cambridge University Press, pp. 233–258, London, 1901.)

Tang, K., Yang, Y., and Buckius, R. O.: Theory and Experiments on Scattering from Rough Interfaces, in C. -L. Tien (ed.), *Annual Review of Heat Transfer*, vol. X, Chap. 3, pp. 101–140, Begell House, 1999b.

Tien, C. L., and Drolen, B. L.: Thermal Radiation in Particulate Media with Dependent and Independent Scattering, *Annual Review of Numerical Fluid Mechanics and Heat Transfer*, vol. 1, pp. 1–32, Hemisphere, Washington, DC, 1987.

Tsang, L., Kong, J. A., and Ding, K. H.: *Scattering of Electromagnetic Waves*, Wiley, New York, 2000.

Van de Hülst, H. C: *Light Scattering by Small Particles*, Wiley, New York, 1957; Dover Publications, New York, 1981.

Xu, R.: *Particle Characterization: Light Scattering Methods*, Springer, 2001.

F.4 POROUS MEDIA

Abdul, M., Abdullaha, M., and Abu Bakarb, M.: Combustion in porous media and its applications—A comprehensive survey. *J. Environmental Management*, 90:2287-2312, 2009.

Howell, J. R., Hall, M. J., and Ellzey, J. L.: Combustion of hydrocarbon fuels within porous inert media, *Prog. Energy Comb. Sci.*, 22(2), 121–145, 1996.

Kamal, M. M. and Mohamad, A. A.: Combustion in porous media, a review, *J. Power and Energy* 220(5), 487–508, 2006.

Lu, J. and Lu, W-q.: Review: Heat and mass transfer in porous medium, Mathematic/numerical models and research directions, *Int. J. Petrochemic. Sci. Eng.* 3(3), 97-100, 2018.

Mishra, N. K., Muthukumar, P., and Panigrahy, S**.**: A review on clean combustion within porous media, in *Air Pollution and Control*, N. Sharma et al. eds., pp. 209-224, Springer Link, 2018.

Mujeebu, M. A., Abdullah, M. Z., Abu Bakar, M. Z., Mohamad, A. A., Muhad, R. M. N., and Abdullah, M. K.: Combustion in porous media and its applications – A comprehensive survey, *J. Environmental Management*, 90, 2287-2312, 2009.

Mujeebu, M. A.: Combustion in porous media for porous burner application, in *Convective Heat Transfer in Porous Media*, Mahmoudi, Y., Hooman, K., and Vafai, K. (eds.), Taylor and Francis-CRC Press, 2020.

Tien, C. L. and Drolen, B. L.: Thermal radiation in particulate media with dependent and independent scattering, in *Annual Review of Numerical Fluid Mechanics and Heat Transfer*, vol. 1, pp. 1–32, Hemisphere, Washington, DC, 1987.

Xu, H. J., Xing, Z. B., Wang, F. Q., and Cheng, Z. M.: Review on heat conduction, heat convection, thermal radiation and phase change heat transfer of nanofluids in porous media: Fundamentals and applications, *Chem. Engng. Sci* 195, 462-483, 2019.

F.5 GLOBAL WARMING

Bodansky, D. and Parker, A.: Research on solar climate intervention is the best defense against moral hazard, *Issues in Sci. and Tech*., XXXVII(4), Summer, 2021.

Crutzen, P. J.: Albedo enhancement by stratospheric sulfur injections: A contribution to resolve a policy dilemma? *Clim. Change.* 77, 211–219, 2006.

Dombrovsky, L. A. and Kokhanovsky, A. A.: The influence of pollution on solar heating and melting of a snowpack, *JQSRT* 233, 42-51, Aug. 2019.

Incropera, F. P.: *Climate Change: A Wicked Problem*, Cambridge University Press, New York, 2016.

Maslowski, W., Kinney, J. C., Higgens, M., and Roberts, A.: The future of Arctic sea ice, *Ann. Rev. Earth Planet. Sci*., 40, 625–654, 2012.

Masson-Delmotte, V., Zhai, P., Pirani, A., Connors, S. L., Péan, C., Berger, S., Caud, N., Chen, Y., Goldfarb, L., Gomis, M. I., Huang, M., Leitzell, K., Lonnoy, E., Matthews, J. B. R., Maycock, T. K., Waterfield, T., Yelekçi, O., Yu, R., and Zhou, B. (eds.): UN International Panel on Climate Change, 2021: *Climate Change 2021: The Physical Science*

Basis. Contribution of Working Group I to the Sixth Assessment Report of the Intergovernmental Panel on Climate Change. Cambridge University Press. In Press. 2021.

Ocean Studies Board. *Climate intervention: Reflecting sunlight to cool the earth*, National Research Council, National Academies Press, 260 pp., Washington DC, 2015.

World Meteorological Organization, *State of the Global Climate in 2020*, WMO-No. 1264, April 2021.

F.6 AVAILABLE COMPUTER CODES

Alberti, M., Weber, R., and Mancini, M.: Gray gas emissivities for H_2O-CO_2-CO-N_2 mixtures, *JQSRT*, 219, 274-291, Nov. 2018. EXCEL spreadsheet for emissivity calculation under *Supplemental Materials* at *DOI: 10.1016/j.jqsrt.2018.08.008.*

Emery, A. F.: VIEW—A radiation view factor program with interactive graphics for geometry definition (Version 5.5.3), 1986, available at https://bit.ly/2kOYJjO (accessed 9/23/2019).

Flatau, P. J.: SCATTERLIB (http://atol.ucsd.edu/scatlib/scatterlib.htm, accessed May 26, 2015), 2009.

Kneizys, F. X., Shettle, E. P., Gallery, W. O., Chetwynd, J. H., Jr., Abreu, L. W., Selby, J. E. A., Fenn, R. W., and McClatchey, R. A.: Atmospheric transmittance/radiance: Computer code LOWTRAN 5, Paper 697, *Optical Physics Div., Air Force Geophysics Lab.*, Hanscom AFB, 21 Feb. 1980.

Laux, C.O., Radiation and nonequilibrium collisional-radiative models, von Karman Institute Lecture Series 2002-07, D. Fletcher, J.-M. Charbonnier, G.S.R. Sarma, and T. Magin (eds.), *Physico-Chemical Modeling of High Enthalpy and Plasma Flows*, Von Karman Institute for Fluid Dynamics, Rhode-Saint-Genèse, Belgium, 2002. SPECAIR program available at http://www.specair-radiation.net/.)

McDonald, J., Golden, A., and Jennings, G.: OpenDDA: A high-performance computational framework for the discrete dipole approximation, *Int. J. High Perf. Comp. Appl.* 23(1), 42–46, 2009. http://www.science.uva.nl/research/scs/Software/adda/.

Prahl, S.: Mie scattering calculator, http://omlc.ogi.edu/calc/mie_calc.html (accessed April 16, 2015). Oregon Medical Laser Center, Portland, OR, 2009.

Sandia National Laboratories: International workshop - measurements and computations of turbulent nonpremixed flames - CH4/H2/N2 jet flames, 2018. http://www.sandia.gov/TNF/DataArch/DLRflames.html

Shapiro, A. B.: FACET—A computer view factor computer code for axisymmetric, 2d planar, and 3d geometries with shadowing, UCID-19887, University of California, Lawrence Livermore National Laboratory, Livermore, CA, August 1983 (LLNL Methods Development Group, http://www.oecd-nea.org/tools/abstract/detail/nesc9578/, accessed 1/19/2019). (Check)

Wriedt, T.: Electromagnetic scattering programs, http://www.t-matrix.de/, accessed April 27, 2015, 2010.

F.7 HISTORICAL REFERENCES

Agassi, J.: The Kirchhoff-Planck Radiation Law, *Science*, 156, pp. 30-37, April 1967.

Ambarzumian, V. A.: Diffusion of light by planetary atmospheres, *Astron. Zh*., vol. 19, pp. 30–41, 1942.

Aschkinass, E.: Heat radiation of metals, *Ann. Phys*., 17, no. 5, pp. 960–976, 1905.

Barr, E. S.: Historical Survey of the Early Development of the Infrared Spectral Region, *Am. J. Phys*., 28, no. 1, pp. 42–54, 1960.

Beer, A.: Bestimmung der Absorption des rothen Lichts in farbigen Flüssigkeiten. (Determination of the absorption of red light in colored liquids). *Annalen der Physik und Chemie (in German).* 86(5): 78–88, 1852.

Boltzmann, L.: Ableitung des Stefan'schen Gesetzes, betreffend die Abhängigkeit der Wärmestrahlung von der Temperatur aus der electromagnetischen Lichttheorie, *Ann. Phys*., ser. 2, vol. 22, pp. 291–294, 1884.

Bouguer, Pierre: *Essai d'Optique, sur la gradation de la lumiere*, Claude Jombert, Paris, 16–22, 1729.

Chandrasekhar, S.: *Radiative Transfer*, Dover, New York, 1960.

Charle, M.: *Les Manuscripts de Léonard de Vinci, Manuscripts C, E, et K de la Bibliothèque de l'Institute Publiés en Facsimilés Phototypiques*, Ravisson-Mollien, Paris. 1888. (Referenced in Knowles Middleton, W. E.: Note on the Invention of Photometry, *Am. J. Phys*., vol. 31, no. 3, pp. 177–181, 1963.)

Crepeau, J.: A brief history of the T^4 law, *Proc. HT 2009; 2009 Summer Heat Transfer Conf*., Paper HT2009-88060, San Francisco, July 2009.

d'Aguillon, F., S. J.: *Opticorum Libri Sex*, Antwerp, 1613. (Referenced in Knowles Middleton, W. E.: Note on the Invention of Photometry, *Am. J. Phys*., 31(3), 177–181, 1963.

Davisson, C, and Weeks, J. R., Jr.: The relation between the total thermal emissive power of a metal and its electrical resistivity, *JOSA*, 8(5), 581–605, 1924.

Descartes, R.: Meditations on First Philosophy, Library of Liberal Arts, Prentice Hall, Englewood Cliffs (1951) [originally published 1641].

Draper, J. W.: On the production of light by heat, *Phil. Mag*., ser. 3, 30, 345–360, 1847.

Drude, P.: Zur Elektronentheorie der Metalle, *Annalen der Physik*, 306(3): 566–613., 1900a.

Drude, P.: Zur Elektronentheorie der Metalle; II Teil: Galvanomagnetische und Thermomagnetische Effecte, *Annalen der Physik*, 308(11): *369-402*, 1900b.

Eckert, E.: Das Strahlungsverhaltnis von Flachen mit Einbuchtungen und von zylindrischen Bohrungen, *Arch. Waermewirtsch*., vol. 16(5), 135–138, 1935.

Eckert, E.R.G.: Messung der Gesamtstrahlung von Wasserdampf und Kohlnesaure in Mischung mit nichtstrahlung Gasen bei temperaturen bis 1300ºC, *VDI Forshungshefte*, 387, 1-20, 1937.

Eddington, A. S.: *The Internal Constitution of the Stars*, Cambridge University Press, 1926.

Einstein, A.: Über einen die Erzeugung und Verwandlung des Lichtes betreffenden heuristischen Gesichtspunkt, *Annalen der Physik.* 17(6), 132–148, 1905.

Fabry, C. and Perot, A.: Theorie et applications d'une nouvelle methode de spectroscopie interferentielle, *Ann. Chim. Phys.* 16(7), *1899.*

Foote, E.: Circumstances affecting the heat in the Sun's rays, *Am. J. Sci. Art*., 22, 382-383, 1856.

Frisad, J. R. and Kragh, H.: On Ludvig Lorenz and his 1890 treatise on light scattering by spheres, *Eur. Phys. J.- H,* 44(2), 137–160, Aug. 2019.

Gardon, R.: A review of radiant heat transfer in glass, *J. Am. Ceram. Soc*., 44(7), pp. 305–312, 1961.

Hagen, E. and Rubens, H.: Metallic reflection, *Ann. Phys.*, 1(2), 352–375, 1900. (See also E. Hagen and H. Rubens: Emissivity and electrical conductivity of alloys, *Deutsch. Phys. Ges. Verhandl*., 6(4), 128–136, 1904.)

Hale, G. E.: Sir Arthur Schuster, *Astrophysical J.*, 81(2), March 1935.

Heaviside, O.: On the electromagnetic effects due to the motion of electrification through a dielectric, *Phil. Mag. S.5* 27: 324, 1889.

Heaviside, O.: On the forces, stresses, and fluxes of energy in the electromagnetic field, *Phil. Trans. Royal Soc. A* 183:423–80, 1892.

Herschel, William; Investigation of the Powers of the prismatic Colours to heat and illuminate Objects; with Remarks, that prove the different Refrangibility of Radiant Heat. To which is added, an Inquiry into the Method of viewing the Sun advantageously, with Telescopes of large Apertures and high magnifying Powers, *Trans. Roy. Soc. (London)*, 90, Pt. II, pp. 255-326 plus 16 plates, 1800.

Horvath, H.: Gustav Mie and the scattering and absorption of light by particles: Historic development and basics, *JQSRT*, 110, no. 11, pp. 787–799, July 2009.

Horvath, H., (ed.): Light Scattering: Mie and More–Commemorating 100 Years of Mie's 1908 Publication, *JQSRT Special Issue*, 110, no. 11, 2009b.

Huggins, W. and Miller, W. A., Notes on the lines in the spectra of some of the fixed stars, *Proc. Royal Society of London*, 12, 444-445, 1862 – 1863.

Huygens, C.: *Treatise on Light*. English Translation by Silvanus P. Thompson, 1667.

Jackson, R.: Eunice Foote, John Tyndall and a question of priority, Roy. J. History of Science, Feb. 2019.

Jeans, Sir J.: On the partition of energy between matter and the ether, *Phil. Mag*., vol. 10, pp. 91–97, 1905.

Kirchhoff, G.: Appendix, Über das Verhältniß zwischen dem Emissionsvermögen und dem Absorptionsvermögen der Körper für Wärme und Licht, in *Untersuchungen über das Sonnenspectrum und die Spectren der chemischen Elemente*, Ferd. Dümmler's Verlagsbuchhandlung, Berlin, pages 22-39, 1862.

Lambert, J. H.: *Photometrie: Photometria, sive de mensura et gradibus luminus, colorum et umbrae*, (1760) republished by Verlag von Wilhelm Engelmann, Leipzig, 1892.

Langley, S. P.: Experimental Determination of Wave-Lengths in the Invisible Prismatic Spectrum, *Mem. Natl. Acad. Sci*., 2, pp. 147–162, 1883.

Lebedev, P.: Untersuchungen über die Druckkräfte des Lichtes, *Annalen der Physik*, 4th Series, 6, 433-458, 1901.

Lewis, H. R.: Einstein's Derivation of Planck's Radiation Law, *Am. J. Phys*., 41(1), pp. 38–14, 1973.

Lilienfeld, P.: Gustav Mie: The Person, *Appl. Opt.*, 30, no. 33, pp. 4696–4698, 1991.

Lorenz, L., Über die Identität der Schwingungen des Lichtes mit den Elektrischen Strömen. *Ann. der Physik und Chemie*, 131, 243-263, 1867a.

Lorenz, L., On the identity of the vibrations of light with electrical currents. *Phil. Mag*., 34, 287-301, 1867b.

Lorenz, L.: Lysbevaegelsen i og uden for en af plane Lysbolger belyst Kugle, *Det Kongelige Danske Videnskabernes Selskabs Skrifter*, 6. Raekke, 6. Bind, 1890, 1, pp. 1–62. (see Classical Papers at http://www.t-matrix.de/)

Lorenz, L: Sur la lumière réfléchie et réfractée par une sphère (surface) transparente, in Oeuvres scientifiques de L. Lorenz." revues et annotées par H. Valentiner. Tome Premier, Libraire Lehmann & Stage, Copenhague, 1898, pp. 403–529. (see Classical Papers at http://www.t-matrix.de/)

Lorentz, H. A.: The motion of electrons in metallic bodies. I. *Proc. Koninklijke Akademie van Wetenschappen*, 7, 438-453, 1905a.

Lorentz, H. A.:The motion of electrons in metallic bodies. II. *Proc. Koninklijke Akademie van Wetenschappen*, 7, 585-593, 1905b.

Lorentz, H. A.:, The motion of electrons in metallic bodies. III. *Proc. Koninklijke Akademie van Wetenschappen.* 7, 684-691, 1905c.

Lorentz, H. A.: On the radiation of heat in a system of bodies having a uniform temperature, *Proc. Koninklijke Akademie van Wetenschappen.* 8: 401-421, 1905d.

Lorentz, H. A.: *The theory of electrons and its applications to the phenomena of light and radiant heat*, B. G. Teubner, Liepzig, 1st ed. 1909; 2nd ed. 1916.

Glummer, O. and Pringsheim, E., *Verhandl. Der Deutschen Physikal. Gesells*., 1, 23 and 215, 1899.

Lummer, O. and Pringsheim, E., *Verhandl. Der Deutschen Physikal. Gesells.*, 2, 163, 1900.

Maxwell, J. C.: A Dynamical Theory of the Electromagnetic Field, in W. D. Niven (ed.), *The Scientific Papers of James Clerk Maxwell*, vol. 1, Cambridge University Press, London, 1890.

McRea, W.H.: Obituary, Edward Arthur Milne, *The Observatory*, 70, 225-232, Dec. 1950.

Metropolis, N., and Ulam, S.: The Monte Carlo Method, *J. Am. Stat. Assoc*., 44, no. 247, pp. 335–341, 1949.

Mie, G.: Beiträge zur Optik trüber Medien, speziell kolloidaler Metallösungen, *Ann. Phys.*, 330, 377–445, 1908.

Mie, G.: Optics of Turbid Media, *Ann. Phys*., 25(3), 377–445, 1908.

Milne, F. A.: Thermodynamics of the Stars, in *Handbuch der Astrophysik*, 3, pp. 65–255, Springer-Verlag, OHG, Berlin, 1930.

Mott, N. F., and Zener, C.: The Optical Properties of Metals, *Cambridge Philos. Soc. Proc*., pt. 2, vol. 30, pp. 249–270, 1934.

Newton, I.: *Opticks: or, a Treatise of the Reflexions, Refractions, Inflexions and Colours of Light*, 1 edn, Sam. Smith, and Benj. Walford, London, 1704.

Nobili, L. and Melloni, M.: New Experiments in Caloric, performed by means of the Thermomultiplier, *Am. J. Sci. and Arts*, 1, pp. 185-180, 1833. (Trans. from *Annales de Chim. et de Phys.*, Oct. 1831.)

Nusselt, W.: Graphische Bestimmung des Winkelverhaltnisses bei der Wärmestrahlung, *VDI Z*., vol. 72, p. 673, 1928.

Park, D. and Epstein, H.T.: On the Planck Radiation Formula, *Am. J. Phys*., vol. 17, pp. 301-302, 1949.

Planck, M.: Distribution of Energy in the Spectrum, *Ann. Phys*., vol. 4, no. 3, pp. 553–563, 1901.

Planck, M.: *The Origin and Development of the Quantum Theory*, 1918 Nobel Prize Address delivered June, 2, 1920, Oxford at the Clarendon Press, 1922.

Planck, M.: *The Theory of Heat Radiation*, 2nd. ed. (trans. by M. Masius), Dover, New York, 1959.

Poljak, G.: Analysis of the Heat Exchange by Radiation Between Gray Surfaces by the Saldo Method, *Tech. Phys. USSR*, 1, no. 5/6, pp. 555-590, 1935.

Rayleigh, Lord: On Scattering of Light by Small Particles, *Philos. Mag.*, 41, pp. 447–454, 1871.

Rayleigh, Lord: The Law of Complete Radiation, *Phil. Mag*., 49, pp. 539–540, 1900.

Rosseland, S.: Zur Quantentheorie der radioaktiven Zerfallsvorgänge, Z. Physik 14, 173–181, 1923.

Rosseland, S.: *Theoretical Astrophysics: Atomic Theory and the Analysis of Stellar Atmospheres and Envelopes*, Clarendon Press, Oxford, 1936.

Rytov, S. M.: *A Theory of Electric Fluctuations and Thermal Radiation*, USSR Academy of Sciences, Moscow, 1953, republished Air Force Cambridge Research Center, Bedford, MA, 1959.

Schuster, A.: Radiation through a Foggy Atmosphere, *Astrophys. J*., 21, pp. 1–22, 1905.

Schwarzschild, K.: Equilibrium of the Sun's Atmosphere, *Ges. Wiss. Gottingen Nachr., Math-Phys. Klasse*, vol. 1, pp. 41–53, 1906.

Saunders, O. A.: Notes on Some Radiation Heat Transfer Formulae, *Proc. Phys. Soc. London*, 41, pp. 569–575, 1929.

Schmidt, E., and Eckert, E. R. G.: Über die Richtungsverteilung der Wärmestrahlung von Oberflächen, *Forsch. Geb. Ingenieurwes*., 6(4), pp. 175–183, 1935.

Stark, J.: Der Dopplereffekt bei den kanalstrahlen und die spektra der positiven atomionen, *Physikalische Zeitschrift*, 6, 892–897, 1905.

Stefan, J.: Über die beziehung zwischen der wärmestrahlung und der temperatur, *Sitzber. Akad. Wiss. Wien*, 79(2), 391–428, 1879.

Stokes, G. G.: On the Composition and Resolution of Streams of Polarized Light from Different Sources, *Trans. Camb. Phil. Soc.*, vol. 9, pp. 399–424, 1852. (Reprinted in *Mathematical and Physical Papers*, vol. 3, Cambridge University Press, pp. 233–258, London, 1901.)

Tikhonov, A. N.: On the stability of inverse problems, *Dokl. Akad. Nauk SSSR*, 39(5), 195–198, 1943.
Tikhonov, A. N.: Solution of incorrectly formulated problems and the regularization method, *Soviet Math. Dokl.*, 4, 1035–1038, 1963. [Engl. trans. *Dokl. Akad. Nauk. SSSR*, 151, 501–504, 1963.]
Townsend, A. A.: The Effects of Radiative Transfer on Turbulent Flow of a Stratified Fluid, *J. Fluid Mech.*, 4(4), pp. 361-375, Aug. 1958.
Tyndall, James: *Heat Considered as a Mode of Motion being a Course of Twelve Lectures*, D. Appleton and Company, New York,1865.
Tyndall, James: On the blue colour of the sky, the polarization of skylight, and on the polarization of light by cloudy matter generally, *Proc. Royal Soc. London*, 17, 223–233, 1869.
Wien, W.: Temperatur und Entropie der Strahlung, *Ann. Phys*., ser. 2, vol. 52, pp. 132–165, 1894.
Wien, W.: Über die Energievertheilung im Emissionsspectrum eines schwarzen Körpers, *Ann. Phys*., ser. 3, vol. 58, pp. 662–669, 1896.
Zerefos, C. S., Tetsis, P., Kazantzidis, A., Amiridis, V., Zerefos, S. C., Luterbacher, J., Eleftheratos, K., Gerasopoulos, E., Kazadzis, S., and Papayannis, A.: Further evidence of important environmental information content in red-to-green ratios as depicted in paintings by great masters, *Atmos. Chem. Phys*.14, 2987-3015, 2014.

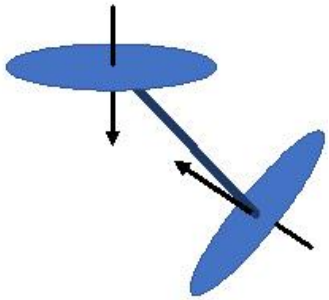

G: A HISTORY OF THERMAL RADIATION AND SHORT BIOGRAPHIES

G.1 HISTORY OF THERMAL RADIATION

The historical development of the blackbody relations differs from the sequence in which they are presented in *Thermal Radiation: An Introduction*. The derivation of the approximate spectral distributions of Wien and of Rayleigh and Jeans, the Stefan–Boltzmann law, and Wien's displacement law are all presented there as logical consequences of the fundamental spectral distribution of intensity derived by Max Planck. However, these relations were formulated *prior* to publication of Planck's work (1901) and were originally derived through complex thermodynamic arguments (see the Timeline following the biographies below.)

Joseph Stefan (1879) proposed, after study of some experimental results, that emissive power was related to the fourth power of the absolute temperature of a radiating body. His student, Ludwig Eduard Boltzmann (1884), was able to derive the same relation by analyzing a Carnot cycle in which radiation pressure was assumed to act as the pressure of the working fluid.

Wilhelm Carl Werner Otto Fritz Franz (Willy) Wien (1894, 1896) derived the displacement law by consideration of a piston moving within a mirrored cylinder. He found that the spectral energy density in an isothermal enclosure and the spectral emissive power of a blackbody are both directly proportional to the fifth power of the absolute temperature when "corresponding wavelengths" are chosen. He later derived his spectral distribution of intensity through thermodynamic argument plus assumptions concerning the absorption and emission processes (1896). Lord Rayleigh (1900) and Sir James Jeans (1905) based their spectral distribution on the assumption that the classical idea of equipartitioning of energy was valid.

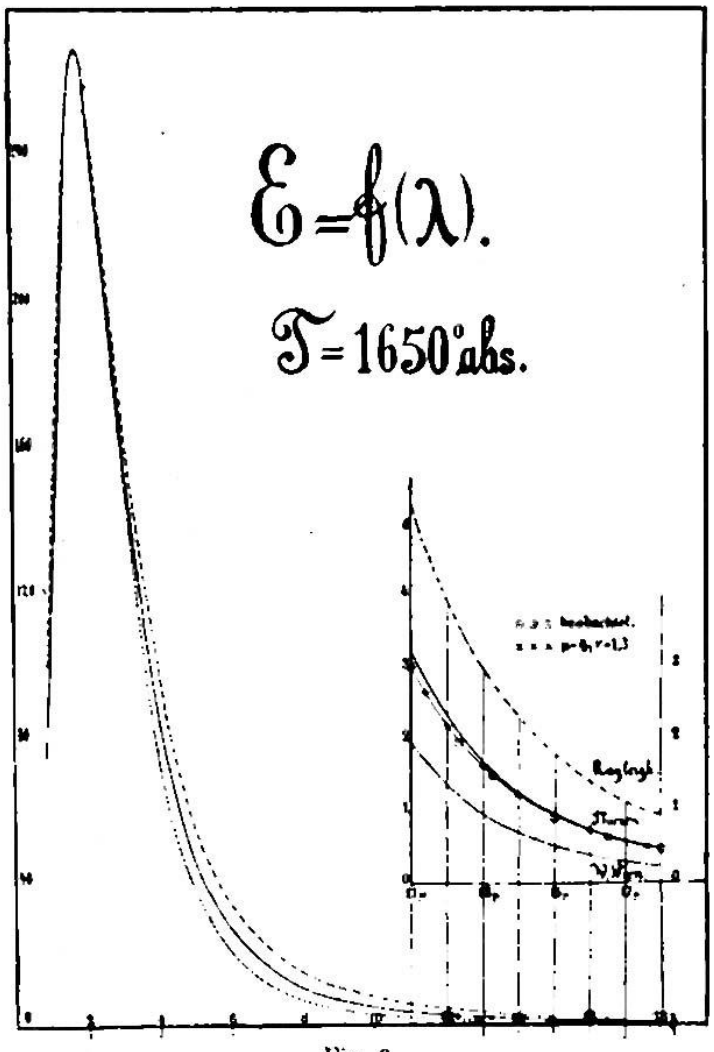

Fig. 3.

Careful measurements of the blackbody spectral distribution by Otto Lummer and Ernst Pringsheim (1900) (and some theoretical considerations) indicated that Wien's expression for the spectral distribution was invalid at high temperatures and/or large wavelengths. This led Planck to an investigation of harmonic oscillators that were assumed to be the emitters and absorbers of radiant energy. The figure (left) from Lummer and Pringsheim shows, at the lower right, the disagreement between the Rayleigh, Wien, and experimental data at large λT values. Various further assumptions about the

average energy of the oscillators led Planck to derive both the Wien and Rayleigh–Jeans distributions. Planck finally found an empirical equation that fit the measured energy distributions over the entire spectrum. In determining what modifications to the theory would allow derivation of this empirical equation, he was led to the make assumptions that form the basis of quantum theory. His equation leads directly to all the results derived previously by Wien, Stefan, Boltzmann, Rayleigh, and Jeans.

Gustav Mie used the EM theory to predict the scattering coefficient and phase function for radiation interacting with small spherical particles (1908a, b), and a historical overview of his contributions is in Horvath (2009a).

Short biographies of the major historical contributors to the theory and practice of thermal radiation energy transfer abridged from various sources are given below, along with a timeline that sets the sequence of their accomplishments. Barr (1960) gives an interesting and informative comprehensive review of the history of the field of thermal radiation. Howell (2002) gives a review of the development of radiation energy transfer. Lewis (1973) and Crepeau (2009) discuss the derivation of Planck's law, and Stewart and Johnson (2016) give a historical overview of Planck's Law and the computational methods historically invoked in computing it in various forms.

REFERENCES

Barr, E. S.: Historical survey of the early development of the infrared spectral region, *Am. J. Phys*., 28(1), 42–54, 1960.

Boltzmann, L.: Ableitung des Stefan'schen Gesetzes, betreffend die Abhängigkeit der Wärmestrahlung von der Temperatur aus der electromagnetischen Lichttheorie, *Ann. Phys*., *Ser. 2*, 22, 291–294, 1884.

Crepeau, J.: A brief history of the T^4 law, Paper HT2009-88060, *Proceedings of the HT 2009; 2009 Summer Heat Transfer Conference*, San Francisco, CA, July 2009.

Horvath, H. (ed.): Light scattering: Mie and more–commemorating 100 years of Mie's 1908 publication, *JQSRT*, 110(11), 783–786, 2009a.

Horvath, H.: Gustav Mie and the scattering and absorption of light by particles: Historic development and basics, *JQSRT*, 110(11), 787–799, July 2009b.

Howell, J. R.: The development of engineering radiative heat transfer, *IMECE2002-33131*, 73-78, IMECE, New Orleans, Nov. 2002.

Jeans, Sir. J.: On the partition of energy between matter and the ether, *Phil. Mag*., 10, 91–97, 1905.

Lewis, H. R.: Einstein's derivation of Planck's radiation law, *Am. J. Phys*., 41(1), 38–14, 1973.

Lummer, O. and Pringsheim, E.: Über die Strahlung des Schwarzen Körpers für Lange Wellen, *Verhandlungen der Deutschen Physikalischen Gesellschaft*. **2**, 163-180, 1900.

Mie, G.: Beiträge zur Optik trüber Medien, speziell kolloidaler Metallösungen, *Ann. Phys.*, 330, 377–445, 1908a.

Mie, G.: Optics of turbid media, *Ann. Phys*., 25(3), 377–445, 1908b.

Planck, M.: Distribution of energy in the spectrum, *Ann. Phys*., 4(3), 553–563, 1901.

Rayleigh, Lord: The law of complete radiation, *Phil. Mag*., 49, 539–540, 1900.

Stefan, J.: Über die beziehung zwischen der wärmestrahlung und der temperatur, *Sitzber. Akad. Wiss. Wien*, 79(2), 391–428, 1879.

Stewart, S. M. and Johnson, R. B.: *Blackbody Radiation: A History of Thermal Radiation Computational Aids and Numerical Methods*, CRC Press, Boca Raton, 2016.

Wien, W.: Temperatur und Entropie der Strahlung, *Ann. Phys*., *Ser. 2*, 52, 132–165, 1894.

Wien, W.: Über die Energievertheilung im Emissionsspectrum eines schwarzen Körpers, *Ann. Phys., Ser. 3*, 58, 662–669, 1896.

G.2: BIOGRAPHIES OF FIGURES IN THE DEVELOPMENT OF RADIATION THEORY

August Beer (1825-1863) was a German physicist. In 1852, he published a paper on the absorption of red light in colored aqueous solutions of various salts. He showed that the intensity of light transmitted through a solution at a given wavelength decays exponentially with increasing path length and the solute concentration.

Ludwig Eduard Boltzmann (1844-1906) made seminal contributions to the kinetic theory of gases and on energy transfer by radiation, but is probably best known for his invention, independently of J. Willard Gibbs, of statistical mechanics and the formulation of entropy on a microscopic basis. He derived Stefan's fourth power law for radiation emission by considering a heat engine with light as the working fluid. He committed suicide in 1906, probably because of depression (he was subject to what we now call bipolar disorder) brought on by broad criticism of his work. Boltzmann's epitaph in the Central Cemetery in Vienna reads

Ludwig Boltzmann
1844-1906
$S = k\,lnW$

Pierre Bouguer (1698-1758) first discovered the law in 1729 of exponential decay of light intensity through an absorbing medium (in his case, the atmosphere), now often called the Beer-Lambert Law. He was an accomplished naval architect (known as "the Father of Naval Architecture), beating out Euler for a prize by the French Academy of Sciences for a paper on the masting of ships. Craters on the Moon and Mars are named after him.

Robert Wilhelm Eberhard Bunsen (1811-1899) investigated spectra emitted by heated elements using a spectrometer designed with Gustav Kirchhoff. They discovered the elements cesium and rubidium using the device. Bunsen developed gas-analytical methods and was a pioneer in photochemistry. With his laboratory assistant, Peter Desaga, he developed the Bunsen burner. John Tyndall was one of his graduate students.

Nicolas Leonard Sadi Carnot (1796-1832) was the son of Napoleon's Minister of War ("the Great Carnot"), and was educated as a military engineer. In 1824, he published his only paper, "Reflexions on the Motive Power of Fire, and on Machines Fitted to Develop that Fire," which outlined one form of the Second Law as well as a reasoned form of the first law. His analysis of the most efficient possible cycle efficiency and a cycle that has this efficiency carry his name. This analysis was based on caloric theory, although unpublished notes indicate that he had begun to doubt that theory. He died of cholera at age 36, having provided probably the single most important contribution to classical thermodynamics.

Anders Celsius (1701-1744), although primarily an astronomer, introduced a thermometer scale with 0 at the boiling point of water, and 100 at the freezing point. The scale was reversed after his death to provide the present Celsius scale (formerly called the centigrade scale). Celsius showed that the boiling point of water varied with atmospheric pressure, and introduced corrections to the temperature scale to account for this.

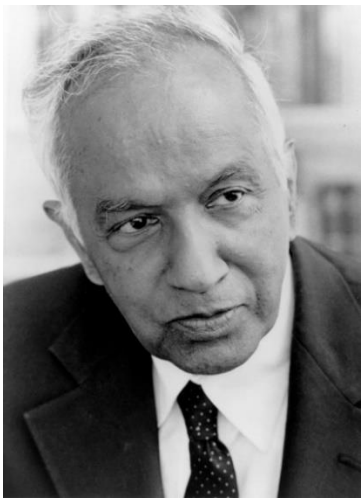

Subrahmanyan Chandrasekhar (1910-1995) won the Nobel Prize in 1938 for his work on the structure and evolution of stars, later showing star progression toward becoming a black hole. His uncle was Chandrasekhara Venkata Raman who won the 1930 Nobel Prize in Physics for his work on Raman scattering of photons. His book *Radiative Transfer* (1960) outlines the discrete ordinates method (DOM) now used extensively in thermal radiation transfer and introduces methods for treating scattering using Stoke's parameters.

Photo courtesy of University of Chicago Photographic Archive, [apf1-09456], Special Collections Research Center, University of Chicago Library.

Louis de Broglie (1892-1987) did not originally envisage a career in science. He entered the Sorbonne in Paris taking a course in history and graduated at 18 with an arts degree. He then became interested in mathematics and physics and chose to study for a degree in theoretical physics.

De Broglie was awarded his undergraduate degree in 1913 but his career was put on hold by World War I. His doctoral thesis put forward his theory of electron waves, based on the work of Einstein and Planck. It proposed the theory for which he is best known, the particle-wave duality theory that matter has the properties of both particles and waves. The wave nature of the electron was experimentally confirmed in 1927.

His was awarded the Nobel Prize in 1929 and continued to work on extensions of wave mechanics. He questioned whether the statistical nature of quantum physics reflects an ignorance of the underlying theory or whether statistics is all that can be known.

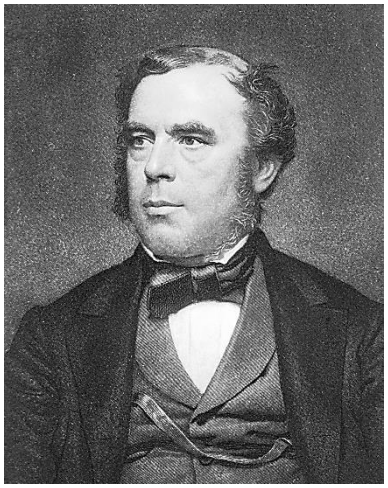

John William Draper (1811-1882) was an English-born American scientist. In 1847 he observed the *Draper point* of 798 K at which the emission from a heated object becomes visible to the human eye. In his 1847 paper he presented data on the emission vs. temperature from a heated object (replotted here on an absolute scale) but failed to recognize the fourth-power dependence, because an absolute temperature scale was not yet in use.

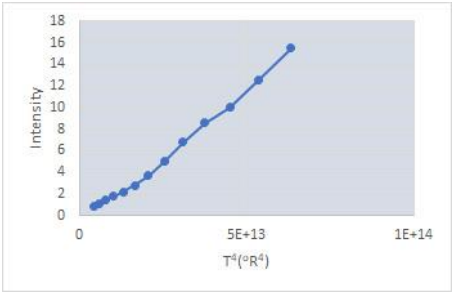

He is credited with taking the one of the first photographic portraits in 1839. An image of his sister from 1840 is considered the oldest surviving portrait photo. He also took the first detailed photograph of the moon in 1840.

Paul Karl Ludwig Drude (1863-1906) studied first mathematics and then physics at the University of Göttingen. His dissertation was on reflection and refraction in crystals. He performed pioneering work on the optics of absorbing media and connected the optical with the electrical and thermal properties of solids. In 1900 he developed a model to explain the relation among thermal, electrical, and optical properties of matter. He introduced the symbol *c* for the speed of light. The Drude model would be further advanced in 1933 by Arnold Sommerfeld and Hans Bethe, becoming the *Drude-Sommerfeld Model*. In 1906, at the height of his career, be became a member of the Prussian Academy of Sciences. A few days after his inauguration lecture, for inexplicable reasons, he committed suicide.

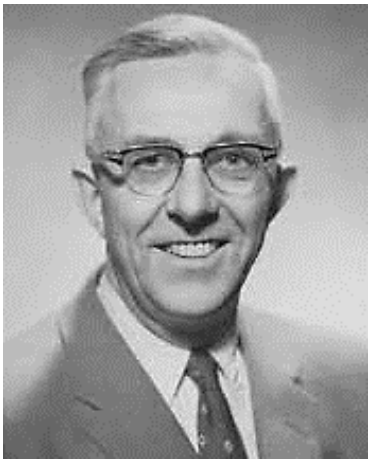

Ernst Rudolph George (ERG) Eckert (1904-2004) was born in Prague. After earning his Dr. Ing. in 1927, he moved to Danzig to work with Ernst Schmidt at the Engine Laboratory. He researched radiation from solids and gases, and published measurements of directional emissivity from various materials as well as directional reflectivity of blackbody radiation. He also developed optical methods for obtaining configuration factors. In 1937, he turned to measurement of the emissivity of CO_2-N_2 mixtures as well as water vapor at various temperatures and partial pressures. His later career was spent in investigating high-speed flows. He spent a long and productive career in Germany, Czechoslovakia, and the U.S. at NASA Lewis (now Glenn) Research Center and from 1951 at the University of Minnesota.

Albert Einstein (1879-1955) of course is best known for his theory of relativity and for promulgating the world's most famous equation, relating energy and mass through $E=mc^2$. His 1921 Nobel Prize in Physics, however, was "for his services to theoretical physics, and especially for his discovery of the law of the photoelectric effect." The latter effect, which experimentally showed the presence of quantum energy in incident radiation, was a major impetus to the acceptance of quantum theory and provided support for Planck's hypothesis of the existence of quantum energy states needed in his derivation of the blackbody distribution.

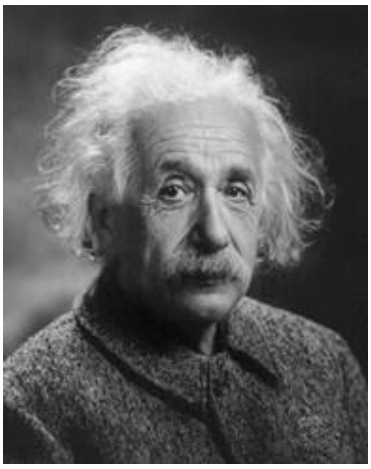

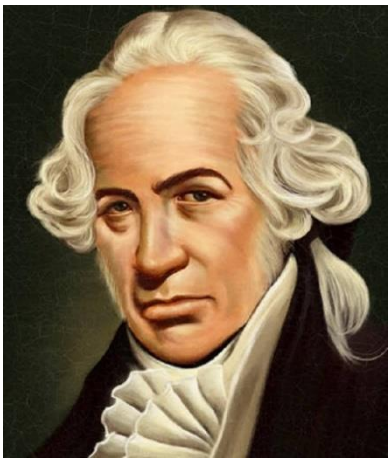

Gabriel Daniel Fahrenheit (1686-1736) developed both an alcohol and mercury thermometer, as well as the temperature scale that bears his name. He was the first to calibrate thermometers with a reproducible scale; previously, each thermometer had an arbitrary scale. His original scale for the alcohol thermometer used the zero point at the temperature of an equal mixture by weight of ice and salt, and 90 degrees as the temperature of the human body, resulting in 30 degrees for the freezing point of water. Later, the mercury thermometer allowed expansion of the scale to the boiling point of water at 212 degrees, and the rest of the scale was revised to 98.6 degrees for the body temperature and the freezing point of water to 32 degrees.

Maurice Paul Auguste Charles Fabry (1867-1945) received his doctorate from the University of Paris in 1892 for his work on interference fringes, which established him as an authority in the field of optics and spectroscopy. He explained the phenomenon of interference fringes and together with Alfred Pérot he invented the Fabry–Pérot interferometer in 1899, making possible the accurate measurement of wavelength and refractive index. In 1904, he was appointed Professor of Physics at the University of Marseille, where he spent 16 years. While studying the light spectra of the Sun and stars with the interferometer, Fabry and Henri Buisson demonstrated in 1913 that solar ultraviolet radiation is filtered out by an ozone layer in the upper atmosphere.

Eunice Newton Foote (1819-1888) was an amateur American scientist and women's rights activist who is believed to be the first person to observe through experiment the ability of CO_2 and water vapor to strongly absorb solar radiation and link this to the possibility of effects on climate. This predated John Tyndall's similar work and conclusions. Although she published her work in 1856, some four years before Tyndall, he is usually cited as the first person to note these effects. No photograph of Eunice Foote is known to exist; the one shown may be her or a relative.

Joseph Thomas Gier (1910-1961) received his undergraduate degree in Mechanical Engineering at UC Berkeley in 1933, followed by a Master of Engineering degree in 1940. He was initially employed as a laboratory technician under Llewellyn Boelter. After serving as a lecturer and researcher, Gier was promoted to Associate Professor of Electrical Engineering at UC Berkeley in 1951, becoming the first tenured African-American professor in the University of California system. He formed a fruitful partnership with Robert V. Dunkle, a Mechanical Engineering professor in 1943. Together they developed instrumentation to characterize the radiative properties of surfaces and conceived of spectral selectivity to improve the performance of solar collectors.

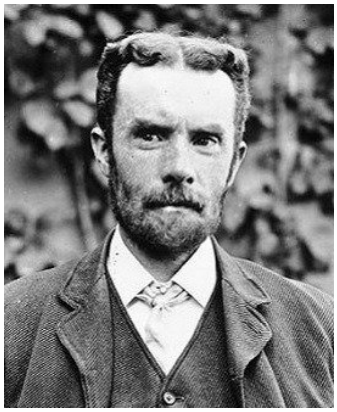

Oliver Heaviside (1850-1925) was a self-taught engineer/mathematician/physicist who invented methods for solving differential equations and made many contributions to vector calculus. In 1888/9, he reformulated Maxwell's twenty field equations into a more manageable and now generally used set of four equations in terms of four variables (Chapter 4 of the textbook). Heaviside was often at odds with his employer and the scientific community but made important contributions to physics, astronomy, and mathematics.

William Herschel (1738-1822) was a German-born British astronomer. He constructed his first large telescope in 1774 and spent nine years carrying out sky surveys to investigate double stars. In March 1781 he discovered the planet Uranus.

He pioneered the use of astronomical spectrophotometry, measuring stellar spectral distributions. In 1800, he discovered the presence of infrared radiation in sunlight by passing it through a prism and holding a thermometer just beyond the red end of the visible spectrum. It showed a higher temperature than the visible spectrum, implying energy in then unknown infrared portion of the spectrum. He improved the measurement of the rotation period of Mars, and determined that the Martian polar caps vary seasonally.

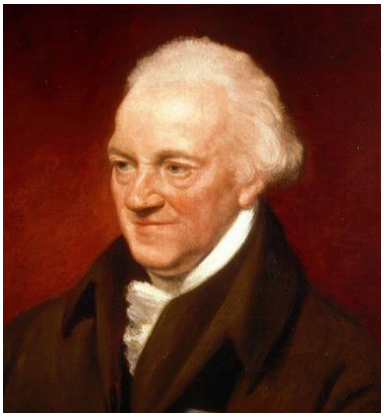

Hoyt Clarke Hottel (1903-1998) was a Professor at MIT from 1928 until his death and became an Emeritus Professor in 1968. He developed gas emissivity charts for the important combustion gases, the crossed-string method for determining configuration factors in 2D geometries, and in 1927 papers he established the engineering basis for treating radiation in furnaces, including the zone method. Hottel also contributed to the fields of combustion and solar energy.

Margaret Lindsay Huggins (1848-1915) was a pioneer in measuring stellar spectra. She, along with her husband William Huggins, was the first to show that the stars were indeed suns, based on the similarity of their emission spectra with that of the Sun (especially spectral lines of magnesium and calcium). Their instrumentation was based on a spectroscope model proposed by Bunsen and Kirchhoff. Observations of Sirius showed a slight Doppler shift in the measured spectra, which indicated that it was moving away from the Earth. This eventually led to the discovery of the expanding universe.

Christiaan Huygens (1629-1695) was born and died at The Hague. His father had studied natural philosophy and was a diplomat. Christiaan gained access through him to the top scientific circles of the times. He studied law and mathematics at the University of Leiden and the College of Orange at Breda.

In 1654 his attention was directed to the improvement of the telescope. In 1655, using one of his own lenses, he detected the first moon of Saturn. His astronomical observations required some exact means of measuring time, and this led him in 1656 to invent the pendulum clock. His reputation was now so great that in 1665, Louis XIV offered him a pension if he would live in Paris, which became his place of residence. In 1670 he had a serious illness which resulted in leaving Paris for Holland. By 1671 he returned to Paris. In 1672 Louis XIV invaded the Low Countries and Huygens found himself in the position of being in an important position in Paris at a time France was at war with his own country. Scientists of this era felt themselves above political wars and Huygens, with support from his friends, continued his work.

The first watch regulated by a balance spring was made under Huygens's directions and presented by him to Louis XIV. He returned to Holland in 1681 and devoted himself to the construction of lenses of enormous focal length, and he discovered the achromatic telescope eye piece which is known by his name.

In 1689 he came from Holland to England to make the acquaintance of Newton, whose *Principia* had been published in 1687. Huygens recognized the merits of the work but believed any theory incomplete which did not explain gravitation by mechanical means and so didn't accept Newton's theory of universal gravitation which "appears to me absurd." On his return in 1690 Huygens published his treatise on light in which the wave theory was expounded and explained. The immense reputation of Newton led to disbelief in any theory which he rejected, and to the general adoption of Newton's corpuscular theory over wave ideas.

In the final years of his life Huygens composed one of the earliest discussions of extraterrestrial life, published after his death as the *Cosmotheoros* (1698).

James Hopwood Jeans (1877-1946) was educated in London. Initially interested in the classics, he soon turned towards mathematics.

Jeans went to Trinity College Cambridge in 1896 on a mathematical scholarship. As an undergrad he gained experience in experimental physics in the Cavendish Laboratory during 1899-1900. During recovery from tuberculosis in 1902 and 1903 he worked on his first major text *The Dynamical Theory of Gases*. Planck had announced in 1900 his formula on black-body radiation, but Jeans was strongly opposed to Planck's results.

He held a series of positions between 1900 and 1906, and during this period he published his second major text *Theoretical Mechanics* (1906). He published *The Mathematical Theory of Electricity and Magnetism* in 1908 while in the United States. In 1909 he returned to England and held the post of Lecturer in Applied Mathematics at Cambridge until he retired in 1912. Jeans continued work and wrote *Radiation and Quantum Theory* in 1914. In this work he showed that he had come to accept Planck's black-body formula.

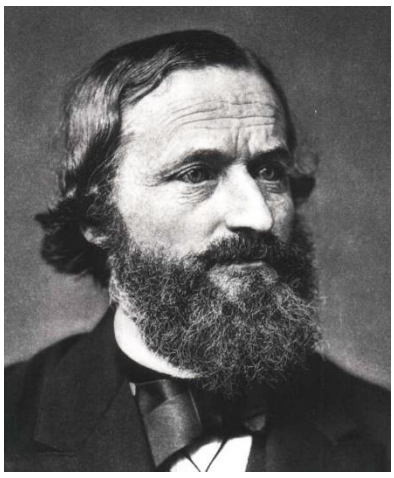

Gustav Robert Kirchhoff (1824 -1887) had a broad influence on physics and engineering. He proposed in 1859 and provided a proof in 1861 that, in simple terms, "For an arbitrary body emitting and absorbing thermal radiation in thermodynamic equilibrium, the emissivity is equal to the absorptivity." This was shown to apply for spectral, directional, and total properties. He first described the ideal radiation emitter in 1862 and called it the *schwarzer körper* (blackbody) because, as the perfect emitter, it must also be the perfect absorber and thus a zero reflector that would appear black to the eye.

He, along with Robert Bunsen used a prism to analyze the spectrum emitted by heated samples. Applying this new research tool, they discovered two new elements, cesium (1860) and rubidium (1861). He also promulgated the laws of electrical circuit analysis.

Johann Heinrich Lambert (1728-1777) was a self-taught mathematician, astronomer, logician, and philosopher. Aside from his work in radiation, he offered the first proof that π was an irrational number. In 1758, he published his first book, describing the exponential decay of light, followed in 1760 by his more complete book *Photometrie* that describes the exponential decay as well as the cosine dependence of the emission from a diffuse surface.

Pyotr Nikolaevich Lebedev (1866-1912) was the first to measure radiation pressure on a solid body (1899) at Moscow State University which he published in 1901. The measurements of the tiny force (Solar radiation exerts about 9 mPa at the Earth's orbit) were fairly inaccurate (off by about 20 percent) but provided the first experimental confirmation of Maxwell's theory of electromagnetism. He also performed important experiments on millimeter-wave radiation. He created the first school of science in Russia, now part of the Russian Academy of Science. A crater on the far side of the moon is named for him.

Gilbert Newton Lewis (1875- 1946) was a precocious child who learned to read at age three. At age 13 he entered the prep school of the University of Nebraska and continued to the University. After his second year, he transferred to Harvard, where he concentrated in chemistry, getting his B.A. in 1896 and Ph.D. in 1899.

After earning his Ph.D., he studied under Wilhelm Ostwald at Leipzig and Nernst at Göttingen. In 1905 MIT appointed him to the faculty. He became assistant professor in 1907, associate professor on 1908, and full professor in 1911. He left MIT to become dean of the College of Chemistry at UC Berkeley in 1912.

In 1908 he published the first of several papers on relativity, in which he derived the mass-energy relationship in a different way from Einstein's. In 1913, he was elected to the National Academy of Sciences, but in 1934 he resigned in a dispute over internal politics. In 1926, he coined the term "photon" for the smallest unit of radiant energy. He died at 70 of a heart attack while working in his laboratory.

Hendrik Antoon Lorentz (1853-1928) was a Dutch physicist who made significant contributions to Einstein's theory of special relativity. His 1875 dissertation at Leiden University was "On the theory of reflection and refraction of light", which refined Maxwell's EM theory. His 1892 electron theory proposed that in matter there are electrons that conduct electric currents and whose oscillations give rise to light. He shared the 1902 Nobel prize with Peter Zeeman for discovering and explaining the Zeeman effect which shows that a strong magnetic field can affect the wavelength of radiation emission.

Ludvig Valentin Lorenz (1829-1891) was a Danish chemical engineer who became interested in physics. Because he published in Danish, his work went unrecognized for many years. He published the relation between the density of a pure transparent material and light refraction in 1869. He also derived the correct velocity of light from electromagnetic theory. In 1890 he preceded Gustav Mie in proposing a theory of light scattering from spherical particles, sometimes now called the Lorenz-Mie theory.

Otto Richard Lummer (1860-1925) (left) **and Ernst Pringsheim (1859-1917)**(right). Lummer received the Ph.D. under Helmholtz in 1882 and joined the University of Berlin as lecturer in physics in 1886. He became professor in 1896 and in 1905 was appointed full professor of theoretical physics at the University of Breslau, where his close collaborator Ernst Pringsheim had preceded him by six months. In 1898, Lummer and Ferdinand Kurlbaum had published an account of their cavity radiation source (*hohlraum*), used largely unchanged for radiation measurements to the present. It was a hole in the wall of a platinum box, divided by diaphragms, with its interior blackened.

Pringsheim's doctoral dissertation of 1882 determined the direction of his research- heat and light radiation. Despite his appointment in theoretical physics at Breslau, Pringsheim's scientific production was largely experimental. At Berlin it was characterized first by a period of research done alone and then in

cooperation with Lummer after 1896. He developed the radiometer into a useful instrument for measuring infrared radiation.

In 1896, Lummer and Pringsheim turned to investigations of thermal radiation. Continuing Wien's work, Pringsheim assisted Lummer in implementing Kirchhoff's concept of the blackbody They verified the Stefan-Boltzmann law for the temperature dependence of total radiated energy. They then measured the spectral distribution of the radiation energy with the aid of a hohlraum.

In September 1900 they published a paper stating the "invalidity of the Wien-Planck spectral equation." Such negative statements were the main stimuli for Planck to seek a new radiation expression.

James Clerk Maxwell (1831-1879), along with his many extremely important contributions in electromagnetic theory and other fields of science, formulated the kinetic theory of gases. He is often considered the most influential physicist after Einstein and Newton.

He described the propagation of an electromagnetic wave using a system of 20 equations, and showed that the speed of electromagnetic wave propagation was equal to the speed of light, implying that light was itself an electromagnetic wave.

Working with Clausius, he used a statistical approach to find the velocity distribution in an assembly of gas molecules at a given temperature (later derived using the maximum entropy principle by Boltzmann, and now called the Maxwell-Boltzmann distribution). He also observed the relationships among thermodynamic properties embodied in Maxwell's Relations.

Gustav Adolf Feodor Wilhelm Ludwig Mie (1868-1957) was a professor of physics with a strong background in mathematics. He researched colloids at the University of Greifswald in North-Eastern Germany. One of his PhD students investigated the scattering and attenuation of light by gold colloids. Mie used his knowledge of the Maxwell equations and solutions of very similar problems in the literature to treat the theoretical problem of scattering and absorption of light by a small absorbing sphere. Since these calculations were done by hand, Mie had to limit his theoretical results to three terms in infinite expansions, and this limited treatment to particles smaller than 200 nm at visible wavelengths. Mie's paper was hardly noticed for the next 50 years. He developed the Mie system of units in 1910 with the basic units Volt, Ampere, Coulomb and Second (VACS-system).

Edward Arthur Milne (1896-1950) was an English astrophysicist who worked on radiation pressure and the generation of white dwarf stars. **Arthur Stanley Eddington (1882-1944),** also English, investigated the importance of nuclear reactions in stellar structure. The pair provided a second solution to the radiative transfer equation (after Schuster-Schwarzschild) based on a two-flux (rather than two intensity) model.

Michael I. Mishchenko (1959-2020) received Ph.D. in Physics (with honors) from the Ukrainian National Academy of Sciences, Kiev. He worked at the Main Astronomical Observatory in Kiev (1987-1992) and then joined the research staff of the NASA Goddard Institute for Space Studies in New York. He made many contributions to the theory and application of radiation scattering, including multiple scattering of polarized light in clouds composed of non-spherical particles, computing the bidirectional reflection function for flat snow and soil surfaces, interpreting quantitatively the photometric and polarization effects exhibited by Saturn's rings and outer-planet satellites, and the peculiar radar returns caused by ice-covered surfaces.

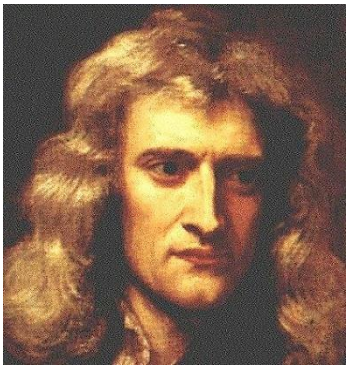

Isaac Newton (1643-1727) established the fundamentals of calculus, his laws of mechanics and gravitation, and fundamental studies of the behavior of light. His laws of mechanics form a major part of the understanding of mechanical work in classical thermodynamics. He built the first practical reflecting telescope, and developed a theory of color based on obervations of the prismatic visible spectrum. Newton argued that the geometric nature of reflection and refraction of light could only be explained if light was made of particles, referred to as corpuscles, because waves do not tend to travel in straight lines, and refraction was caused by accelerating of the corpuscles due to attraction by the denser medium. He explained why the particles were partially refracted and partially reflected at a glass (prism) surface by noting that the particles had “fits of attraction and fits of repulsion.” His theory was superseded by the wave theory of Huygens, which proved more successful in explaining many phenomena. Measurements of the speed of light in vacuum and then in media with nonunity refractive index showed that light speed is lower, not greater in such media, putting the final nail in the corpuscular theory. Alexander Pope wrote the famous epitaph:

Nature and nature's laws lay hid in night;
God said "Let Newton be" and all was light.

Leopoldo Nobili (1784-1835) (left) and **Macedonio Melloni (1798-1854)** (right) developed a thermopile-based radiometer read by a galvanometer, and investigated radiation from various sources. They showed (1831) that different surfaces emitted differing amounts of radiation at the same temperature, and that the radiometer reacted similarly to light sources and heated surfaces.

Max Planck (1858-1947) laid the basis for quantum mechanics and was the forerunner of modern physics based on that theory. He studied with Helmholtz, and was impressed with the powerful conclusions that could be drawn from the Second Law. He originally developed his blackbody spectral distribution based on the observation that the denominator in classically derived distributions such as that of Wien needed to be slightly smaller to fit the experimental data. His attempts to explain the theoretical basis of his proposed spectral energy equation led him to hypothesize the existance of quantized energy levels, a concept at odds with all of classical physics and thermodynamics. He was forced to accept Boltzmann's interpretation of the Second Law as a statistical rather than an absolute law.

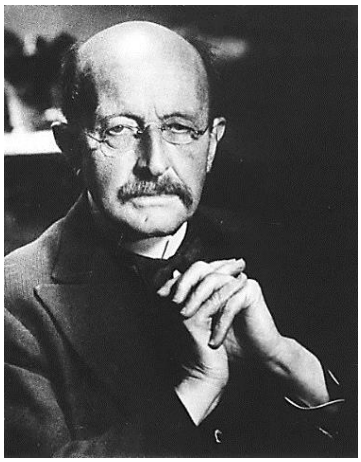

Pierre Prevost (1759-1839) was born in the Republic of Geneva, and skittered between the church, law, education, travel, and philosophy before concentrating on physical science after meeting Lagrange in Berlin. In 1791, he proposed that the radiation from a body is emitted regardless of the presence or absence of other bodies ("Prevost's Law"). He also commented on how radiative equilibrium between a body and its surroundings is obtained.

William John Macquorn Rankine (1820-1872) was born in Edinburgh, Scotland. He wrote practical treatises on thermodynamics, including the first systematic treatment of steam engine theory, and the exposition of what we now call the Rankine cycle. He proposed the Rankine absolute temperature scale in 1859. He was also a poet, writing *The Mathematician in Love*, and a song writer, composing such ballads as *They Never Shall Have Gibraltar*.

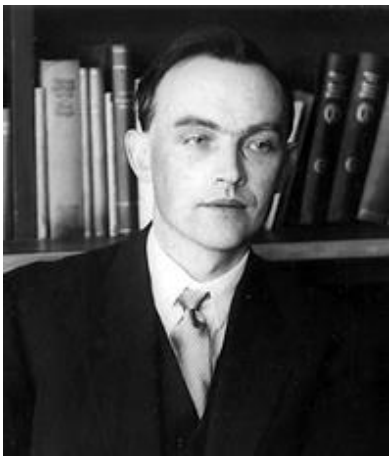

Svein Rosseland (1894-1985) was a theoretical astrophysicist who followed early education in Norway with a fellowship at the Institute of Physics in Copenhagen in 1920, where he met many pioneers in atomic physics, including Neils Bohr. In 1924, he published the paper describing the opacity coefficient of stellar matter, now known as the Rosseland coefficient. He made important contributions to theoretical astrophysics throughout his career. His 1936 text, *Theoretical Astrophysics*, may be his most important work. He left occupied Norway in 1941 to the US and then England, finally returning to Norway in 1946.

Photo courtesy of Creative Commons-Oslo Museum

Sergei Mikhailovich Rytov (1908-1996) contributed to the development of near-field radiation transfer concepts with his pioneering studies on fluctuational electrodynamics. Earlier in his career, he developed an approximate solution of Maxwell's equations to describe the propagation of an electromagnetic wave through a turbulent atmosphere, and was a pioneer in the field of radiophysics. This work has widely been used in inverse techniques for determining the phase function and scattering coefficient of scattering media from remote signals. Later, he developed the description of the effect of thermal fluctuations in electrodynamics and published some of the most cited papers and and a book on the subject.

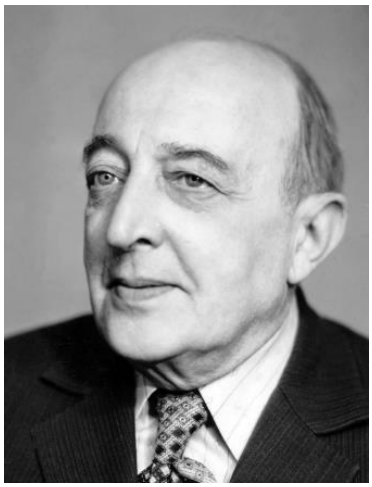

Erwin Rudolf Josef Alexander Schrödinger (1887-1961) was a Nobel Prize-winning (1933) Austrian physicist who developed fundamental results in quantum theory. The *Schrödinger equation* describes the wave function of a particle and how it changes dynamically in time. He did not like the consequences that flow from interpreting the equation, and said "I don't like it, and I'm sorry I had anything to do with it." He wrote in various fields of physics: statistical mechanics and thermodynamics, physics of dielectrics, color theory, electrodynamics, general relativity, and cosmology. He made several attempts to construct a unified field theory and is also known for his "Schrödinger's cat" thought-experiment.

Franz Arthur Friedrich Shuster (1851-1934) studied with Kirchhoff, Maxwell, Helmholtz and Rayleigh among others. He is credited with initial work on predicting antimatter and the eleven-year sunspot cycle. **Karl Schwarzschild (1873-1916)** worked on radiative pressure on small particles, atomic spectra, laid the foundation for the theory of black holes, and generalized the theory of the Stark effect. Schuster and Schwarzchild developed the two-stream model of radiative transfer in one-dimensional systems. The model is based on assuming a different uniform intensity in the forward and backward hemisphere of directions.

Robert Siegel (1927-2017) received his ScD in mechanical engineering from MIT in 1953. He joined NASA in 1955 and was a senior research scientist at the Lewis/Glenn Research Center for 44 years. He did seminal research on reduced gravity heat transfer. There was no text dedicated to radiative transfer during the late 1950s and radiation was an important component in NASA's spacecraft designs and propulsion systems. NASA management requested him to write basic manuals on radiation for use by NASA's engineers. The resulting three NASA Special Publications (SPs) on radiative properties, surface-surface radiation, and radiation in participating media became the basis for the graduate text *Thermal Radiation Heat Transfer* now in its seventh edition. Dr. Siegel made important contributions to transient radiation analysis, flow in radiating channels, barrier coating and variable refractive index systems, and radiation in droplet arrays.

He was inducted into the inaugural class of the NASA Glenn Research Center Hall of Fame in 2015 as one of the "Giants of Heat Transfer."

Ephraim M. Sparrow (1928–2019) received his PhD from Harvard in 1952. He was a prolific researcher across many fields of heat transfer while working at various posts including the NACA Lewis Research center (now NASA Glenn) and finally at the University of Minnesota where he was a working faculty member until he died. In the field of radiation, he applied contour integration to the calculation of configuration factors, introduced the use of variational methods in conjugate heat transfer systems, investigated the emittance of various cavity geometries, and studied radiation effects in fin configurations.

Johannes Stark (1874-1957) received the Nobel Prize in 1919 for his "discovery of the Doppler effect in canal rays and the splitting of spectral lines in electric fields", the latter effect on lines now called Stark broadening. His request in 1907 as a journal editor for a review article by the relatively (!!) unknown Albert Einstein led Einstein along a path to his General Theory of Relativity. Stark later became a strong advocate of Adolph Hitler and the Nazi party and was a main figure in the *Deutsch Physik* movement, seeking to remove Jewish scientists (including Einstein) and their contributions from German physics.

Following WW II, Stark was classified as a "major offender," and was given a four-year (suspended) sentence by a denazification court.

Josef Stefan (1835-1893) was born in Austria and attended elementary school in Klagenfurt, where he showed his talent. In 1845, he entered the Klagenfurt Lyceum and graduated top of his class. He left for Vienna in 1853 to study mathematics and physics and earned his qualification for university teaching in mathematical physics at the University of Vienna in 1858.

Stefan published nearly 80 scientific articles, mostly in the Bulletins of the Vienna Academy of Sciences. He is best known for originating Stefan's law in 1879, which states that the total radiation from a black body is proportional to the fourth power of its absolute thermodynamic temperature *T*. In 1884, the law was derived from a thermodynamic analysis by Stefan's student Ludwig Boltzmann and hence is known as Stefan–Boltzmann law. The law is now usually derived from Planck's law of black body radiation.

Using his law, Stefan determined the temperature of the Sun's surface to be 5,430 °C (9,810 °F), comparable to the presently accepted average value of 5780K. This was the first reasonable prediction of the apparent temperature of the Sun.

John William Strutt, Lord Rayleigh (1842-1919) was one of the very few members of higher nobility who won fame as an outstanding scientist. He entered Cambridge in 1861 where he read mathematics, and his exceptional abilities enabled him to overtake his better prepared competitors. From then on, he devoted his full time to science.

In 1859, John Tyndall had discovered that bright light scattering off nanoscopic particulates was faintly blue-tinted. He conjectured that a similar scattering of sunlight gave the sky its blue hue, but he could not explain the preference for blue light, nor could atmospheric dust explain the intensity of the sky's color. In 1871, Rayleigh published two papers on the color and polarization of skylight to quantify Tyndall's effect in water droplets in terms of the volumes and refractive indices of particulates. In 1881 with the benefit of James Clerk Maxwell's 1865 proof of the electromagnetic nature of light, he showed that his equations followed from electromagnetism. In 1899, he showed that they applied to individual molecules, with the terms containing particulate volumes and refractive indices replaced with terms for molecular polarizability.

In 1879 he was appointed to follow Maxwell as Professor of Experimental Physics and Head of the Cavendish Laboratory at Cambridge. He left Cambridge in 1884 to continue his experimental work and from 1887 to 1905 he was Tyndall's successor as Professor of Natural Philosophy in the Royal Institution of Great Britain.

His first research was mainly mathematical, concerning optics and vibrating systems, but his later work ranged over almost the whole field of physics, covering sound, wave theory, color vision, electrodynamics, electromagnetism, light scattering, flow of liquids, hydrodynamics, density of gases, viscosity, capillarity, elasticity, and photography. He was a Fellow of the Royal Society (1873) and won the Nobel Prize in 1904 for measuring gas densities and the discovery of Argon. He died on June 30, 1919.

William Thomson, Lord Kelvin (1824-1907) became Professor of Natural Philosophy in 1846 at the University of Glasgow at age 22, and remained there for 53 years. He established the first physics teaching laboratory, and was responsible for the quote "I often say that when you can measure what you are speaking about, and express it in numbers, you know something about it; but when you cannot measure it, when you cannot express it in numbers, your knowledge is of a meagre and unsatisfactory kind." Of course, he also said "Radio has no future," "X-rays are clearly a hoax," and "The aeroplane is scientifically impossible."

He suggested his eponymous absolute temperature scale in 1848 based on Carnot's work. While working on the laying of the Atlantic cable, he found time to publish work in 1849 (at age 25) that included the first use of the words *thermodynamic* and *mechanical energy*. By 1850 he had abandoned the caloric theory, and worked with Joule to extend Joule's earlier experiments to examine the expansion of gases, leading to the measurement and introduction of the Joule-Thomson coefficient.

His interest in thermal conduction and thermodynamics led him to an incorrect estimate of the age of the Earth as 20 to 400 million years (and not infinite). His estimate was incorrect because it neglected the effect of radioactive decay and the internal convection of the core, both unknown at the time. (The presently accepted value is $4.54\times10^9 \pm 1\%$ years.)

He was elevated to the House of Lords in 1892, the first scientist so honored.

Andrey Nikolayevich Tikhonov (1906-1993) was a Russian mathematician. He graduated from Moscow State University with a PhD in 1927. He immediately made important contributions to topology and mathematical physics and proved the fundamental uniqueness of the heat equation. Of most importance to this book is the method he developed for solving ill-posed inverse problems. He is credited with being the first to develop the method now known as *Tikhonov regularization* in 1963 although others (e.g., Phillips, 1962) developed very similar methods at nearly the same time.

John Tyndall (1820-1893) was chiefly an experimentalist. From 1853 to 1887 he was professor of physics at the Royal Institution of Great Britain in London. His experiments on radiation and the radiation absorption of gases were the basis for his 1872 book *Contributions to Molecular Physics in the Domain of Radiant Heat* and are also described in his 1863 text *Heat Considered as a Mode of Motion*. He proposed that differing types of molecules have differing absorptions of infrared radiation because their molecular structures give them differing oscillating resonances and that the absorption behavior of molecules is quite different from that of the atoms composing the molecules. For example, nitric oxide (NO) absorbed more than a thousand times more infrared radiation than either nitrogen (N_2) or oxygen (O_2). He also observed that – no matter whether a gas is a weak absorber of broad-spectrum radiant energy – any gas will strongly absorb the radiant energy coming from a separate body of the same type of gas, demonstrating a kinship between the molecular mechanisms of absorption and emission. He found that moist air was a much better radiation absorber than dry air and speculated on what this meant in terms of meteorology and climate. He was probably unaware of Foote's earlier work.

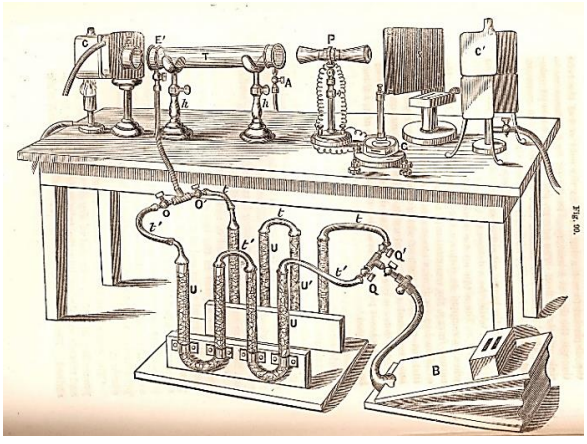

Tyndall's apparatus for measuring the difference in radiation absorptance of moist and dry air. The moist or dry air is pumped from a bag (B) into a cylinder (T) enclosed at each end with a rock salt window. C is a blackbody source; P is a radiometer connected to a galvanometer (G). A secondary high temperature source (burner heated) C' could also be viewed by the detector if the intervening screen was removed. (From Tyndall 1865).

Stanislaw Ulam (1909-1984) was a Polish-born scientist who worked at Los Alamos on the nuclear weapons Manhattan Project during WW II. Following recovery from serious brain surgery, in 1947 he brought forth the idea of implementing statistical techniques for modeling the individual histories of neutrons during their supercritical reactions, now known as the Monte Carlo method, as a substitute for solving the very complex equations otherwise required. He developed the idea along with John von Neumann, Enrico Fermi, Nicholas Metropolis and others. Metropolis and Ulam published the first paper in the open literature on the method in 1949.

Raymond Viskanta (1931-2021) was born in Lithuania, and with his family migrated to Germany in 1944 and on to the US in 1949. He received his PhD from Purdue University in 1960 and joined the Purdue faculty in 1962. He made wide ranging and significant contributions to engineering understanding and applications to highly nonlinear problems involving radiation coupled with conduction and/or convection, radiating systems with transients, radiation transfer in combustion systems and for glass manufacturing, and radiation effects on melting and solidification, porous media, and buoyancy driven systems. He was widely respected as a mentor and beloved by his many students.

Wilhelm Carl Werner Otto Fritz Franz (Willy) Wien (1864-1928) was born in East Prussia. He studied mathematics and physics at the Universities of Göttingen and Berlin. Between 1883 and 1885, he worked in Hermann von Helmholtz's laboratory and in 1886, he took a doctorate with a thesis on diffraction and on the influence of materials on the color of refracted light.

In 1893, he announced what would later be called the law of displacement: that the product of wavelength and absolute temperature for a blackbody is constant. In 1896, he proposed a formula which described the spectral composition of radiation from an ideal body, which he called a blackbody. This work impelled Max Planck to propose quantum effects to bring Wien's distribution into agreement with experimental measurements. His blackbody formula earned Wien the 1911 Nobel Prize in physics.

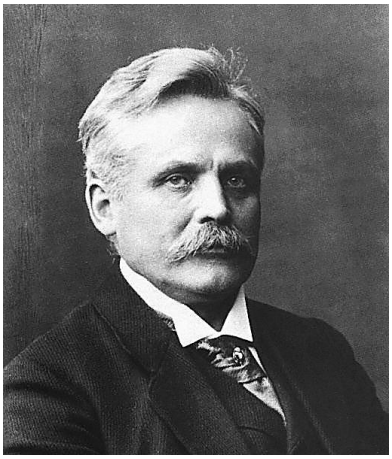

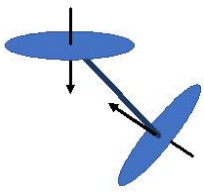

H: TIMELINE OF IMPORTANT EVENTS IN RADIATION

"Now, the Devil confound those Ancients, for they have stolen all my good thoughts from me!"
John Hope, c. 1780

1672 **Isaac Newton** publishes his corpuscular theory of light (based on ideas of "corpuscularism" originally set forth by **Rene Descartes** in 1637) positing that light is composed of individual corpuscles that travel in straight lines and have intrinsic characteristics such as color.

1690 **Christiaan Huygens** publishes a treatise on the wave theory of light, which can explain effects such as diffraction and slowly displaces Newton's theory.

~1700 **Gabriel Daniel Fahrenheit** proposes a reproducible temperature scale for alcohol and mercury thermometers.

1729 **Pierre Bouguer** establishes the exponential attenuation of light through the atmosphere.

1742 **Anders Celsius** proposes a temperature scale based on water's ice and boiling points.

1760 **Johann Lambert**'s book reaffirms Bouguer's exponential attenuation law and describes the cosine law dependence of radiation from a diffuse surface.

1791 **Pierre Prevost** postulates that all bodies radiate energy regardless of the presence of other bodies.

1800 **William Herschel** finds the presence of radiative energy in the previously unknown infrared portion of the spectrum.

1824 **Sadi Carnot** publishes analysis establishing the Second Law of Thermodynamics for ideal reversible heat engines, operating on a cycle now known as the Carnot Cycle.

1831 **Leopoldo Nobili** and **Macedonio Melloni** use the thermopile-based radiometer to demonstrate that light and radiant energy have similar characteristics.

1847 **John William Draper** observes the temperature at which a heated object becomes visible but misses the fourth power dependence of emission in his data, perhaps because the absolute temperature scale had yet to be established.

1848 **Lord Kelvin** proposes an absolute temperature scale based on Carnot's reversible cycle.

1852 **August Beer** shows that the exponential attenuation of light through a solution depends on the concentration of the absorbing solute. The exponential attenuation relation is often called the Beer-Lambert Law, although it was first proposed by Bouguer in 1729.

1856 **Eunice Newton Foote** publishes experimental results showing that CO_2 and water vapor are strong absorbers of solar radiation and speculates on the possible effects on climate.

1859 **W.J.M. Rankine** proposes an absolute temperature scale. **James Tyndall** observes that blue light is preferentially scattered by small particles. **Gustav Kirchhoff** shows that the emissivity and absorptivity of a body in radiative equilibrium must be equal, both on a spectral and total basis. **Kirchhoff** and **Robert Bunsen** show that emission spectra can be used to identify elements from their spectral patterns and develop a spectroscope to identify the presence of trace metals in flame tests. Method leads to discovery of cesium and rubidium as new elements in the following year.

1859-66 **James Clerk Maxwell** develops a heuristic theory of the distribution of velocities among a set of ideal gas particles.

1861 **Gustav Kirchhoff** coins the term *blackbody* for the ideal absorber and emitter of thermal radiation. **Margaret and William Huggins** use a spectroscope based on the Kirchhoff-Bunsen design to demonstrate that stars are far-away suns.

1863 **John Tyndall** makes measurements of total gas absorptance, noting that NO, H_2O, CO_2, CH_4 and others are strong absorbers compared with N_2 and O_2, and indicates that their presence in the atmosphere may well affect climate. He was unaware of earlier work by Foote.

1864 **Maxwell** publishes *A Dynamical Theory of the Electromagnetic Field*, mathematically describing the propagation of electromagnetic waves using twenty differential equations. He also performs a statistical derivation of the velocity distribution of gas molecules.

c.1870 **Ludwig Boltzmann** rederives Maxwell's velocity distribution based on the maximum entropy principle, placing it on a sound theoretical basis. It is now known as the Maxwell-Boltzmann distribution.

1871 **Lord Rayleigh** publishes his conclusions on scattering from small particles and shows that his ideas extend to scattering by molecules.

1879 **Josef Stefan** proposes empirically that emission from a blackbody is proportional to the fourth power of the absolute temperature.

1884 **Boltzmann** provides theoretical justification for Stefan's proposal.

1888/9 **Oliver Heaviside** reduces Maxwell's twenty electromagnetic wave equations to the set of four now used.

1892 **Hendrik Lorentz** proposes relation between electrical and radiative properties of conductors.

1894 **Willy Wien** proposes a thermodynamically based relation between the wavelength and temperature of one ideal blackbody and the "corresponding" wavelength and temperature of another (the "Displacement Law.")

1896 **Wien** proposes a thermodynamically based relation for the spectral distribution of radiation emission from an ideal blackbody.

1899 **Maurice Paul Auguste Charles Fabry** with Alfred Pérot invents the interferometer, allowing accurate measurements of wavelength and refractive index. **Pyotr Nikolaevich Lebedev** makes the first measurement of radiation pressure, providing experimental confirmation of Maxwell' electromagnetic theory.

1900 **Rayleigh** proposes a relation for the spectral distribution of the emission of radiation from an ideal blackbody. However, his relation approaches very large values at short wavelengths, in opposition to experimental data (the "ultraviolet catastrophe".) **Otto Lummer** and **Ernst Pringsheim** provide careful measurements of the spectral emission of radiation from an ideal blackbody and show that both the Wein and Rayleigh distributions lie outside the data error bounds at large or small λT values, respectively. **Paul Drude** extends relation between radiative and electrical properties of conductors.

1901 **Max Planck** proposes a relation for the spectral distribution of emission of radiation from an ideal blackbody that modifies the Wien distribution and agrees with the Lummer-Pringsheim data. The required assumption of quantized energy states necessary to derive his distribution leads to the beginning of quantum theory.

1905 **James Jeans** bolsters Rayleigh's idea of a spectral distribution by invoking the classical idea of the equipartition of energy. **Albert Einstein** shows that the photoelectric effect of electrons ejected from a surface exposed to light cannot be satisfactorily explained by wave theory, but that the incident radiation must have energy quantum characteristics. This gives credence to Planck's quantum energy state hypothesis.

1905-6 **Arthur Schuster** and **Karl Schwarzschild** develop a two-intensity stream model of radiative transfer, giving one of the first analytical solutions to radiative transfer in participating media.

1908 **Gustav Mie** establishes the radiation scattering characteristics of particles.

1909 **Johannes Stark** receives Nobel Prize for discovering the effect of electrical fields on spectral lines.

1921 **E. A. Milne** and **Arthur Eddington** provide a solution to the radiative transfer equation in participating media based on a modified two-stream model.

1923 **Luis de Broglie** hypothesizes that since electromagnetic radiation can be interpreted in terms of particles, then matter particles should also have the characteristics of waves (an extension of the idea of wave-particle duality).

1924 **Svein Rosseland** describes the opacity of stellar matter in terms of the now named Rosseland coefficient.

1926 **Erwin Schrödinger** publishes his wave equation, describing the wave characteristics of particles as predicted to exist by de Broglie, leading to rapid advances in quantum theory. **G.N. Lewis** coins the term *photon* for the particle/wave carrying radiant energy.

1927- **Hoyt Hottel** in a series of papers, chapters and texts provides the engineering basis and combustion gas property values for calculating radiation transfer in combustion furnaces.

1937 **E.R.G. Eckert** measures the emittance of CO_2-N_2 and H_2O-N_2 mixtures.

1947 **Stanislaw Ulam** proposes the Monte Carlo method for modeling neutron interactions, later extended to model thermal radiation.

1953 **Sergei Mikhailovich Rytov** publishes seminal work on the effect of electrical fluctuations on thermal radiation, or fluctuation electrodynamics,

1963 **Andrey Tikhonov** introduces regularization methods to treat ill-posed inverse problem.

1960- **Michael Mishchenko, Raymond Viskanta, Ephraim Sparrow, Robert Siegel** and others expand the engineering treatment of thermal radiation transfer by applying mathematical and physical principles.

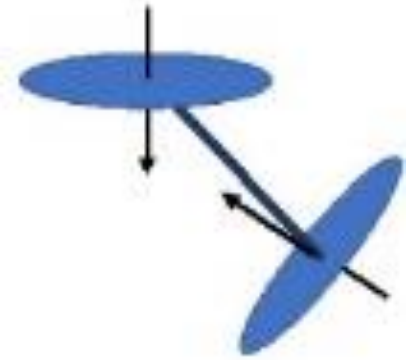

I: ADDITIONAL HOMEWORK

The homework in this Appendix is meant to provide instructors or students an additional range of problems from those in the text for extra assignment or home study. Solutions are in the Solution Manual, available from the publisher.

Chapter 2:

I.2.1 Radiant energy at a wavelength of 2.0 μm is traveling through a vacuum. It then enters a medium with a refractive index of 1.28.

(a) Find the following quantities for the radiation in the vacuum: speed, frequency, and wave number.

(b) Find the following quantities for the radiation in the medium: speed, frequency, wave number, and wavelength.

Answer: (a) 2.9979×10^8 m/s; 1.4990×10^{14} s^{-1}; 5×10^5 m^{-1}. (b) 2.342×10^8 m/s; 1.4990×10^{14} s^{-1}; 6.40×10^5 m^{-1}; 1.5625×10^{-6} m

I.2.2 What range of radiation wavelengths is present within a glass sheet that has a wavelength-independent refractive index of 1.29 when the sheet is exposed in vacuum to incident radiation in the visible range λ_0 = 0.4–0.7 μm?

Answer: 0.310–0.543 μm

I.2.3 Plot the hemispherical spectral emissive power $E_{\lambda b}$ for a blackbody in air [W/($m^2 \cdot$μm)] as a function of wavelength (μm) for surface temperatures of 2000 and 6250 K.

I.2.4 A blackbody at 1100 K is radiating in the vacuum of outer space.

(a) What is the ratio of the spectral intensity of the blackbody at λ = 1.0 μm to the spectral intensity at λ = 4.0 μm?

(b) What fraction of the blackbody emissive power lies between the wavelengths of λ = 1.0 μm and λ = 4.0 μm?

(c) At what wavelength does the peak energy in the radiated spectrum occur for this blackbody?

(d) How much energy is emitted by the blackbody in the range $1.0 \leq \lambda \leq 4.0$ μm?

Answer: (a) 0.0541; (b) 0.5488.; (c) 2.6344μm; (d) 45484 W/m^2

I.2.5 Solar radiation is emitted by a fairly thin layer of hot plasma near the sun's surface. This layer is cool compared with the interior of the sun, where nuclear reactions are occurring. Various methods can be used to estimate the resulting effective radiating temperature of the sun, such as determining the best fit of a blackbody spectrum to the observed solar spectrum. Use two other methods (as follows), and compare the results to the oft-quoted value of T_{solar} = 5780 K.

(a) Using Wien's law and taking the peak of the solar spectrum as 0.50 μm, estimate the solar radiating temperature.

(b) Given the measured solar constant in the Earth's orbit of 1368 W/m^2 and using the "inverse square law" for the reduction in energy flux with distance, estimate the solar temperature. The mean radius of the Earth's orbit around the sun is 149×10^6 km and the diameter of the sun is 1.392×10^6 km.

Answer: (a) 5796 K; (b) 5766 K

I.2.6 A blackbody radiates such that the wavelength at its maximum emissive power is 2.50 μm. What fraction of the total emissive power from this blackbody is in the range λ = 0.7 to λ = 6 μm?

Answer: 0.805

I.2.7 A radiometer is sensitive to radiation only in the interval $3.6 \leq \lambda \leq 8.5$ μm. The radiometer is used to calibrate a blackbody source at 1200 K. The radiometer records that the emitted energy is 5000 W/m^2. What percentage of the blackbody radiated energy in the prescribed wavelength range is the source actually emitting?

Answer: 11.2%

I.2.8 What temperature must a blackbody have for 25% of its emitted energy to be in the visible wavelength region?

Answer: 4,343 K, 12,460 K (Note: two solutions are possible!)

I.2.9 Show that the blackbody spectral intensity $I_{\lambda b}$ increases with T at any fixed value of λ.

I.2.10 A sheet of silica glass transmits 87% of the radiation that is incident in the wavelength range between 0.38 and 2.7 μm and is essentially opaque to radiation having longer and shorter wavelengths. Estimate the percent of solar radiation that the glass will transmit. (Consider the sun as a blackbody at 5780 K.)

If the garden in a greenhouse radiates as a black surface and is at 40°C, what percent of this radiation will be transmitted through the glass?

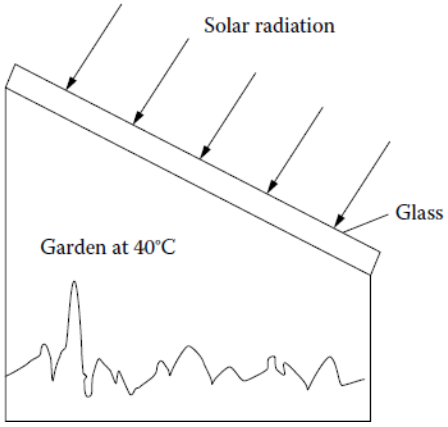

Answer: 75.6%; 0.003%

I.2.11 Derive Wien's displacement law in terms of wave number by differentiation of Planck's spectral distribution in terms of wave number, and show that $T/\eta_{max} = 5099.4$ μm·K.

I.2.12 A student notes that the peak emission of the sun according to Wien's displacement law is at a wavelength of about $\lambda_{max} = C_3/5780$ K = 2897.8/ 5780 = 0.501 μm. Using $\eta_{max} = 1/0.501$ μm, the student solves again for the solar temperature using the result derived in Homework Problem I.2.11. Does this computed temperature agree with the solar temperature? Why? (This is not trivial—put some thought into *why*.)

I.2.13 Derive the relation between the wave number and the wavelength at the peak of the blackbody emission spectrum. (You may use the result of Homework Problem I.2.11.)

Answer: η_{max} (cm^{-1}) = 5682.6/λ_{max} (μm)

I.2.14 A 6 by 10 cm black rectangular sheet of metal is heated uniformly with 2600 W by passing an electric current through it. One face of the rectangle is well insulated. The other face is exposed to vacuum and very cold surroundings. At thermal equilibrium, what fraction of the emitted energy is in the wave number range from 0.40 to 2 μm^{-1}?

Answer: 0.5086

I.2.15 Radiation from a blackbody source at 2,200 K is passing through a layer of air at 12,000 K and 1 atm. Considering only the transmitted radiation (i.e., not accounting for emission by the air), what path length is required to attenuate by 35% the energy at the wavelength corresponding to the maximum emission by the blackbody source? At this λ, take $\kappa_\lambda = 1.2 \times 10^{-1}$ cm^{-1} for air at 12,000 K and 1 atm.

Answer: 3.59 cm

I.2.16 A gas layer at constant pressure P has a linearly decreasing temperature across the layer and a constant mass absorption coefficient κ_m (no scattering). For radiation passing in a normal direction through the layer, what is the ratio I_2/I_1 as a function of T_1, T_2, and L? The temperature range T_2 to T_1 is low enough that emission from the gas can be neglected. The gas constant is R.

Chapter 3:

I.3.1 For a surface with hemispherical spectral emissivity ε_λ, does the maximum of the E_λ distribution occur at the same λ as the maximum of the $E_{\lambda b}$ distribution at the same temperature? (*Hint*: examine the behavior of $dE_\lambda/d\lambda$.) Plot the distributions of E_λ as a function of λ for the data of Figure 2.9 of the text at 600 K and for the property data at 700 K. At what λ is the maximum of E_λ? How does this compare with the maximum of $E_{\lambda b}$?

I.3.2 The surface temperature-independent hemispherical spectral absorptivity of a surface is measured when it is exposed to isotropic incident spectral intensity, and the results are approximated as shown in the following graph. What is the total hemispherical emissivity of this surface when it is at a temperature of 1200 K?

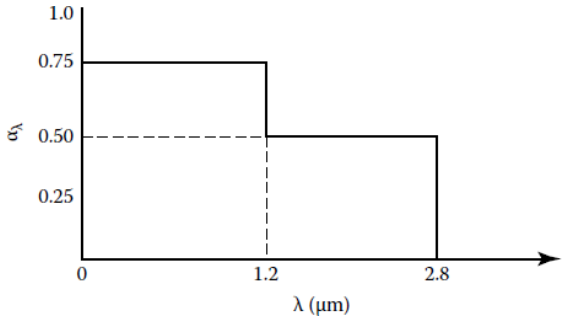

Answer: 0.179.

I.3.3 A white ceramic surface has a hemispherical spectral emissivity distribution at 1500 K as shown. What is the hemispherical total emissivity of the surface at this surface temperature?

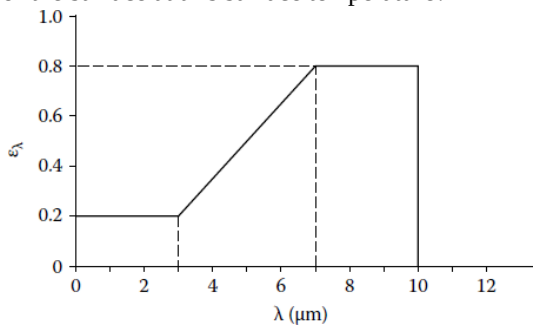

Answer: 0.292.

I.3.4 A surface has the following values of hemispherical spectral emissivity at a temperature of 900 K.

λ (μm)	ε_λ(900 K)
<1	0
1	0
1.5	0.2
2	0.4
2.5	0.6
3	0.8
3.5	0.8
4	0.8
4.5	0.7
5	0.6
6	0.4
7	0.2
8	0
>8	0

(a) What is the hemispherical total emissivity of the surface at 900 K?

(b) What is the hemispherical total absorptivity of the surface at 900 K if the incident radiation is from a gray source at 1800 K that has an emissivity of 0.815? The incident radiation is uniform over all incident angles.

Answer: (a) 0.476; (b) 0.427.

I.3.5 A diffuse surface at 1100 K has a hemispherical spectral emissivity that can be approximated by the solid line shown.

(a) What is the hemispherical-total emissive power of the surface? What is the total intensity emitted in a direction 60° from the normal to the surface?

(b) What percentage of the total emitted energy is in the wavelength range $5 < \lambda < 10$ μm? How does this compare with the percentage emitted in this wavelength range by a gray body at 1100 K with an emissivity $\varepsilon = 0.611$?

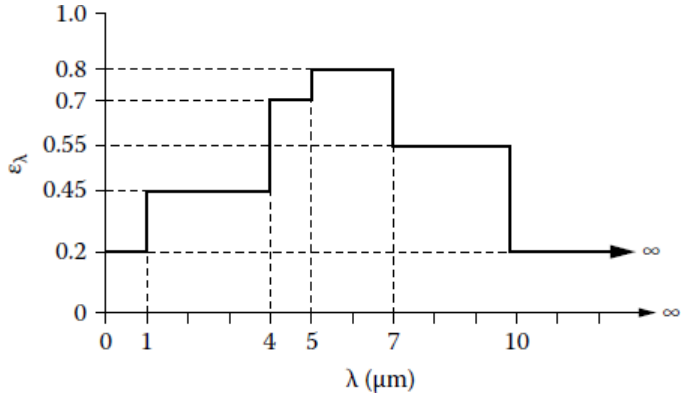

Answer: (a) 44,010 W/m^2; 14,009 W/m^2 · sr: (b) 36.7%; 24.0%.

I.3.6 The ε_λ for a metal at 1100 K is approximated as shown, and it does not vary significantly with the metal temperature. The surface is diffuse.

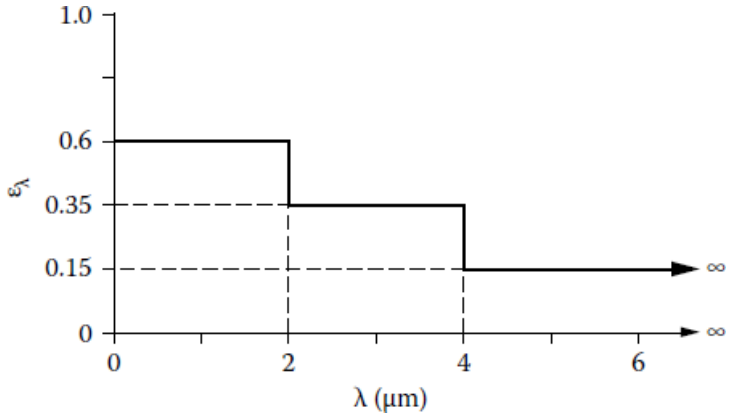

(a) What is α for incident radiation from a gray source at 1100 K with $\varepsilon_{source} = 0.822$?

(b) What is α for incident radiation from a source at 1100 K made from the same metal as the receiving plate?

Answer: (a) 0.285; (b) 0.356.

I.3.7 A flat metal plate 0.1 m wide by 1.0 m long has a temperature that varies only along the long direction. The temperature is 900 K at one end, and decreases linearly over the one meter length to 350 K. The hemispherical spectral emissivity of the plate does not change significantly with temperature but is a function of wavelength. The wavelength dependence is approximated by a linear function decreasing from $\epsilon_\lambda = 0.85$ at $\lambda = 0$ to $\epsilon_\lambda = 0.02$ at $\lambda = 10$ □m. What is the rate of radiative energy loss from one side of the plate? The surroundings are at a very low temperature.

Answer: 416.6 W.

Chapter 4:

I.4.1 A smooth hot ceramic dielectric sphere with an index of refraction $n = 1.40$ is photographed with an IR camera. Calculate how bright the image is at locations B and C relative to that at A. (Camera is distant from sphere.)

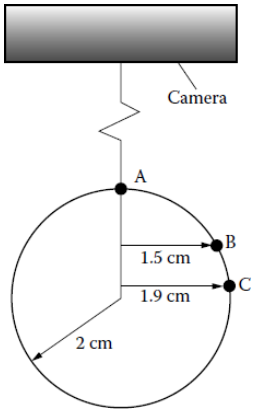

Answer: 0.987; 0.849.

I.4.2 A smooth dielectric material has a normal spectral emissivity of $\varepsilon_{\lambda,n} = 0.765$ at a wavelength in air of 6 μm. Find or estimate values for the perpendicular component of the directional-hemispherical-spectral reflectivity $\rho_{\lambda,\perp}(\theta)$ at the same wavelength and for incidence at $\theta = 40°$.

Answer: (a) 0.736; (b) 0.327.

I.4.3 A smooth ceramic dielectric has an index of refraction $n = 1.48$, which is independent of wavelength. If a flat ceramic disk is at 1100 K, how much emitted energy per unit time is received by the detector when it is placed at $\theta = 0°$ or at $\theta = 60°$? Use relations from the EM theory.

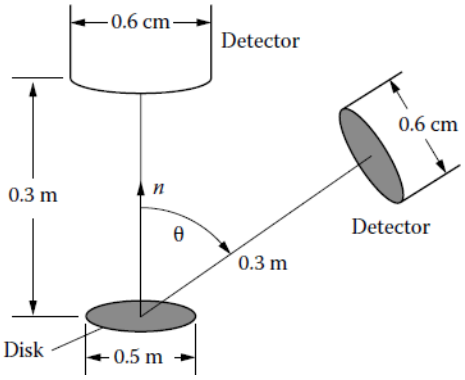

Answer: 15.69×10^{-5} W at $\theta = 0°$; 7.845×10^{-5} W at $\theta = 60°$.

I.4.4 A clean metal surface has a normal spectral emissivity of $\varepsilon_{\lambda,n} = 0.055$ at a wavelength of 12 μm. Find the value of the electrical resistivity of the metal.

Answer: 2.834×10^{-4} Ω-cm.

I.4.5 Evaluate the normal spectral reflectivity of clean aluminum at 400 K when $\lambda_0 = 6$, 12, and 24 μm. For aluminum, the temperature coefficient of resistivity is 0.0039.

Answer: 0.971; 0.980; 0.986.

I.4.6 Polished platinum at 300 K is irradiated normally by a gray-body source at 1200 K. Evaluate its normal total absorptivity α_n. (Use the method of Example 3.4 of the text.)

Answer: 0.0655.

I.4.7 The hemispherical total emissive power emitted by a polished metallic surface is 2500 W/m^2 at temperature T_A. What would you expect the emissive power to be if the temperature were doubled? What assumptions are involved in your answer?

Answer: 80,000 W/m^2.

I.4.8 The following figure gives some experimental data for the hemispherical-spectral reflectivity of polished aluminum at room temperature. Extrapolate the data to $\lambda = 10$ μm. Use whatever method you want, but list your assumptions. Discuss the probable accuracy of your extrapolation. (*Hint:* The electrical resistivity of pure

aluminum is about $r_e = 2.73 \times 10^{-6}$ Ohm-cm at 293 K. At 10 μm, take $\bar{n} = 33.6 - 76.4i$. You may use any, all, or none of these data as you wish.)

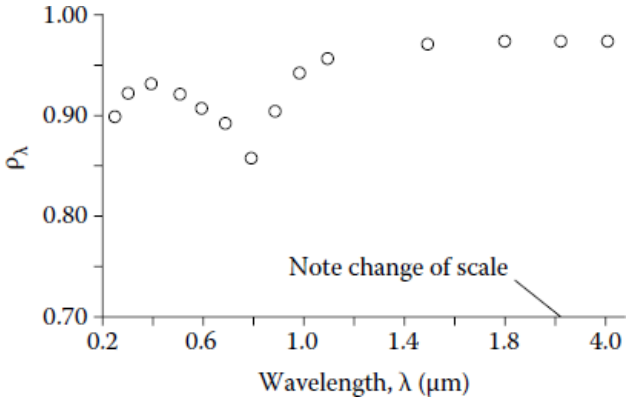

Answer: 0.975.

I.4.9 Using Hagen–Rubens emissivity relation, plot the normal spectral emissivity as a function of wavelength for a polished aluminum surface used in a cryogenic application at 50 K. What is the normal total emissivity? (*Note*: Do not use any relations valid only near room temperature.)

I.4.10 Metals cooled to very low temperatures approaching absolute zero become superconducting; that is, the value of $r_e(T \approx 0) \approx 0$. Based on EM theory predictions, what is your estimate of the values of the simple refractive index *n*, the absorption index *k*, and the normal spectral and normal total emissivities at such conditions? What assumptions are implicit in your estimates? What assumptions are implicit in your estimates? (The results predicted by the Hagen-Rubens relation, and other results from classical electromagnetic theory, become inaccurate at T < 100 K. Predictions of radiative properties at low absolute temperatures using more exact theoretical approaches are reviewed in Toscano, W. M. and Cravalho, E. G.: Thermal radiative properties of the noble metals at cryogenic temperatures, *JHT*, 98(3), 438–445, 1976.

I.4.11 The normal spectral absorptivity of a SiO–Al selective surface can be approximated as shown by the long-dashed line in Figure 4.20 of the text. The surface receives a flux *q* from the normal direction. The equilibrium temperature of the surface is 1200 K. Assume the hemispherical-spectral $\varepsilon_\lambda = \alpha_\lambda(\theta = 0)$. What is the value of *q* if it comes from a gray-body source at 4900 K?

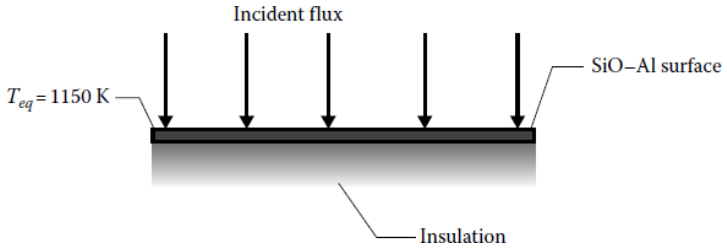

Answer: 12,640 W/m^2.

I.4.12 A directionally selective gray surface has properties as shown below. The $\alpha(\theta)$ is isotropic with respect to the azimuthal angle ϕ.

(a) What is the ratio $\alpha_n(\theta = 0)/\varepsilon$ (the normal directional absorptivity over the hemispherical emissivity) for this surface?

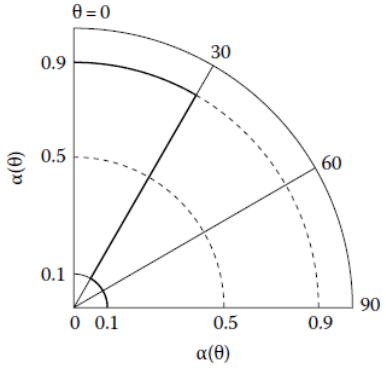

(b) If a thin plate with the aforementioned properties is in Earth orbit around the sun with incident solar flux of 1350 W/m^2, what equilibrium temperature will it reach? Assume that the plate is oriented normal to the sun's rays and is perfectly insulated on the side away from the sun.

(c) What is the equilibrium temperature if the plate is oriented at 40° to the sun's rays?

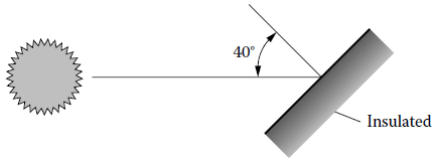

(d) What is the equilibrium temperature if the plate is normal to the sun's rays but is not insulated? Assume the plate is very thin and has the same directional radiation properties on both sides. Neglect radiation emitted by or reflected from the Earth.

Answer: (a) 3.0; (b) 517 K; (c) 297 K; (d) 435 K.

I.4.13 A flat plate in Earth orbit is insulated on one side, and the other side is facing normal to the solar intensity. The incident solar flux is 1350 W/m^2. A coating on the plate surface facing the sun has a total hemispherical emissivity of 0.250 over a broad range of plate temperatures. Surroundings above the plate are at a very low temperature. Telemetry signals to Earth indicate that the plate temperature is 730 K.

(a) What is the normal solar absorptivity α_{solar} of the plate surface facing the sun?

(b) If α_{solar} is independent of angle, what is the plate temperature if the plate is tilted so that its normal is 40° away from the solar direction?

Answer: (a) 2.982; (b) 683 K.

I.4.14 The spectral absorptivity of a SiO–Al selective surface can be approximated as shown below. The surface is in Earth orbit around the sun and has the solar flux 1353 W/m^2 incident on it in the normal direction. What is the equilibrium temperature of the surface if the surroundings are very cold?

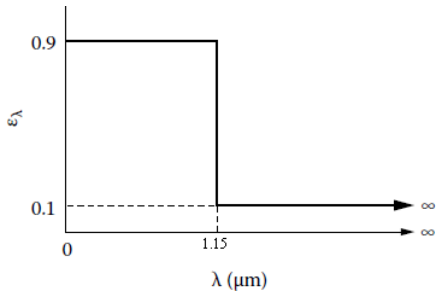

Answer: 672 K.

I.4.15 A thin plate has a directional-gray surface on one side with the directional emissivity shown below on the left. On the other side of the plate is a coating with diffuse-spectral emissivity shown below on the right. The surroundings are at very low temperature. Find the equilibrium temperature of the plate if it is exposed in vacuum to a normal solar flux of 1353 W/m^2 with a solar spectrum equivalent to that of a blackbody at 5780 K when

(a) The directional-gray side is facing normal to the sun.

(b) The diffuse-spectral side is facing normal to the sun.

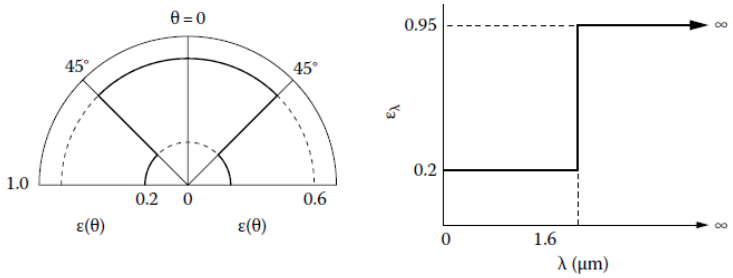

Answer: (a) 376 K; (b) 265 K.

I.4.16 A gray surface has a directional total absorptivity given by $\alpha(\theta) = 0.80 \cos^4 \theta$. This flat surface is exposed to normally incident sunlight of flux 1050 W/m^2. A fluid flows past the back of the thin radiation absorber plate at T_{fluid} = 325 K and with a velocity that gives an energy transfer coefficient of h = 64 W/m$^2 \cdot$ K. What is the equilibrium temperature of this flat-plate radiation collector?

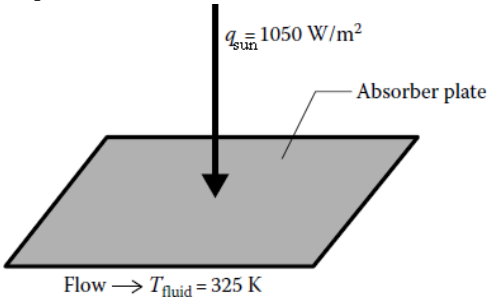

Answer: 335 K.

I.4.17 A plate is coated with a material combining directional and spectral selectivity so that the plate has a normal total solar absorptivity of 0.92 and an IR hemispherical emissivity of 0.040 at long wavelengths. When placed in sunlight normal to the sun's rays, what temperature will the plate reach (neglecting conduction and convection and with no energy losses from the unexposed side of the plate)? What assumptions did you make in reaching your answer? The incident solar flux ("insolation") is 1000 W/m^2.

Answer: 648 K.

I.4.18 A solar water heater consists of a sheet of glass 1 cm thick over a black surface that is assumed in perfect contact with the water below it. Estimate the water temperature for normally incident solar radiation. (Assume that Figure 8.10 of the text can be used for the glass properties and that the glass is perfectly transparent for wavelengths shorter than those shown. Take into account approximately the reflections at the glass surfaces; this is treated in more detail in Chapter 11.)

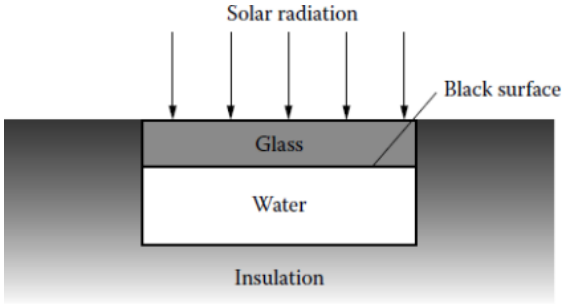

Answer: 389 K.

I.4.19 A gasoline storage tank is receiving sunlight on a somewhat cloudy day so that the incident radiation normal to the top of the tank is 900 W/m^2. The sides are not receiving solar radiation. The tank top and sides are painted with white paint having spectral reflectivity of $\rho_\lambda = 0.9$ for $\lambda < \lambda_{cutoff} = 2$ μm, and $r_l = 0.1$ for $\lambda > \lambda_{cutoff} = 2$ μm

(a) Estimate the average equilibrium temperature that the tank will achieve. (Neglect emitted and reflected radiation from the ground. Do not account for free or forced convection to the air, although this will be appreciable.) The ambient radiating temperature of the surroundings is T_e = 300 K.

(b) What is the average tank temperature if the top is painted white but the sides have a gray coating with an emissivity of 0.825?

(c) What is the temperature if the entire tank is painted with the gray coating?

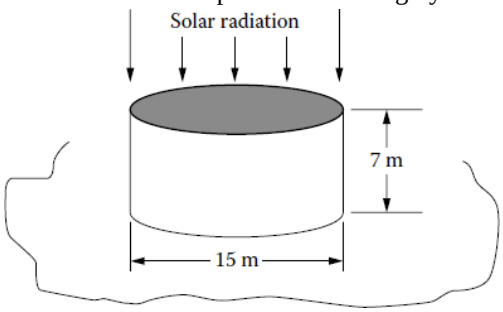

I.4.20 Consider the Earth as a spinning sphere exposed on one hemisphere to solar energy at the solar flux of 1353 W/m^2.

(a) If the average solar absorptivity of the Earth is taken as equal to its emissivity (a gray body), what is the estimated equilibrium temperature of the Earth?

(b) If the solar absorptivity and low-temperature emissivity are taken as the properties of fine snow (Tables B.1, B.2 of the text), what will be the Earth's equilibrium temperature?

(c) If the solar absorptivity and low-temperature emissivity are taken as the properties of plowed soil (Tables B.1, B.2 of the text), what will be the Earth's equilibrium temperature?

(d) Given the results of parts c and d, what do you see as the impact of the melting of polar ice and glaciers due to global warming? Is there a feedback mechanism that tends to increase or mitigate the effects of warming? (For more in-depth discussion, see Maslowski et al. 2012)

Answer: (a) 4.7°C; (b) −133.5°C; (c) 56.3°C.

I.4.21 A flat-plate radiator in space in Earth orbit is oriented normal to the solar radiation. It is receiving direct solar radiation of 1350 W/m^2, radiation emission from the Earth, and solar radiation reflected from the Earth. What must the radiator temperature be to dissipate a total of 3500 W of waste energy from both sides of each 1 m^2 of the radiator?

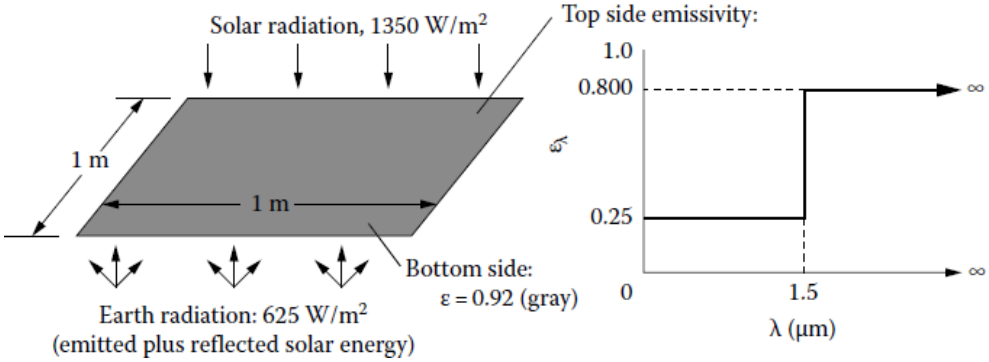

Answer: 450.1. K.

I.4.22 A light pipe (refractive index n_2 = 1.3950) of diameter 0.1 cm is placed with its flat end 1 cm from a heated semiconductor wafer. What diameter of the wafer surface is viewed by the light pipe?

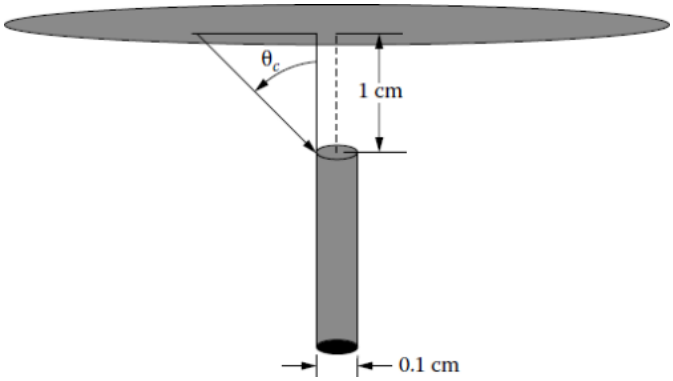

Answer: All values of $0 < \theta < \pi/2$.

Chapter 5:

I.5.1 Derive by any three methods, including use of the factors in Appendix C if you choose, the configuration factor F_{1-2} for the infinitely long geometry shown below in cross section.

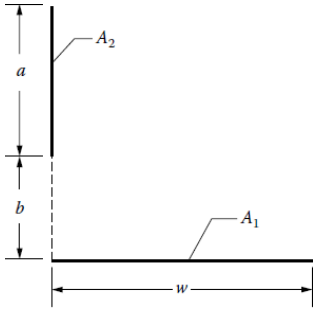

Answer: $F_{1-2} = \{A + (1 + B^2)^{1/2} - [(A + B)^2 + 1]^{1/2}\}/2$,
where $A = a/w$, $B = b/w$.

I.5.2 The configuration factor between two infinitely long directly opposed parallel plates of finite width L is F_{1-2}. The plates are separated by a distance D.

(a) Derive an expression for F_{1-2} by integration of the configuration factor between parallel differential strip elements.

(b) Derive an expression for F_{1-2} by the crossed-string method.

Answer: $\left[1+\left(\frac{D}{L}\right)^2\right]^{1/2} - \left(\frac{D}{L}\right)$.

I.5.3 The configuration factor between two infinitely long parallel plates of finite width L is F_{1-2} in the configuration shown below in cross section.

(a) Derive an expression for F_{1-2} by the crossed-string method.

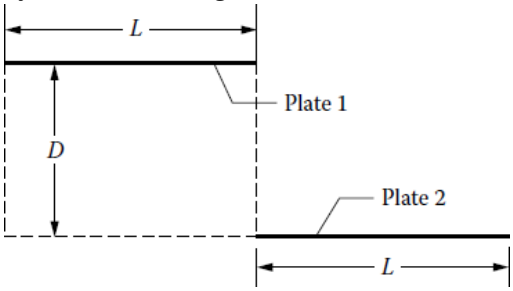

(b) Derive an expression for F_{1-2} by using the results of Homework Problem 4.6 and configuration factor algebra.

(c) Find the configuration factor F_{1-2} for the geometry of infinitely long plates shown below in cross section.

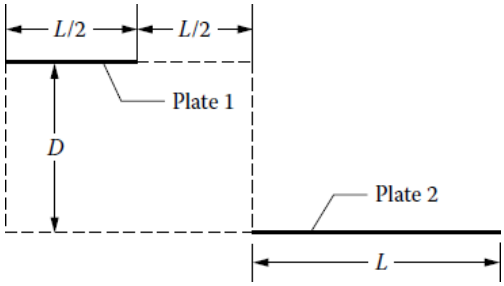

Answer: (a), (b) $\left[1+\left(\frac{D}{2L}\right)^2\right]^{1/2}+\frac{D}{2L}-\left[1+\left(\frac{D}{L}\right)^2\right]^{1/2}$;

(c) $F_{1-2}=2\left[1+\left(\frac{D}{2L}\right)^2\right]^{1/2}-\left[1+\left(\frac{D}{L}\right)^2\right]^{1/2}-\left[\left(\frac{D}{L}\right)^2+\left(\frac{3}{2}\right)^2\right]^{1/2}+\left[\left(\frac{D}{L}\right)^2+\left(\frac{1}{2}\right)^2\right]^{1/2}$.

I.5.4 (a) For the 2D geometry shown in cross section, derive a formula for F_{2-2} in terms of r_1 and r_2.

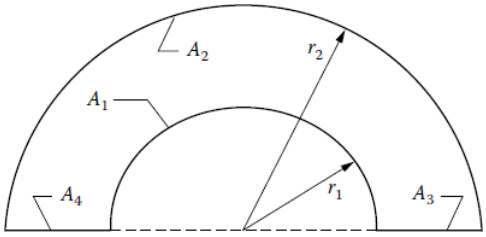

(b) Find F_{2-2} for the 2D geometry. A_1 is a square (A_1 refers to the total area of the four sides) and A_2 is part of a circle.

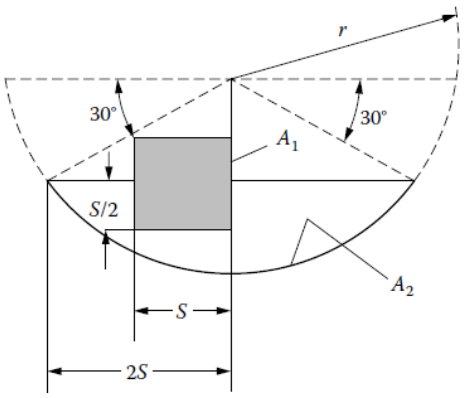

Answer:

(a) $F_{2-2}=1-\frac{2}{\pi}\left[1-\left(\frac{r_1}{r_2}\right)^2\right]^{1/2}-\frac{2}{\pi}\frac{r_1}{r_2}\sin^{-1}\left(\frac{r_1}{r_2}\right)$.

(b) F_{2-2} = 0.1359.

I.5.5 Compute the configuration factor F_{1-2} between faces A_1 and A_2 of the infinitely long parallel plates shown below in cross section when the angle β is equal to (a) 30° and (b) 75°.

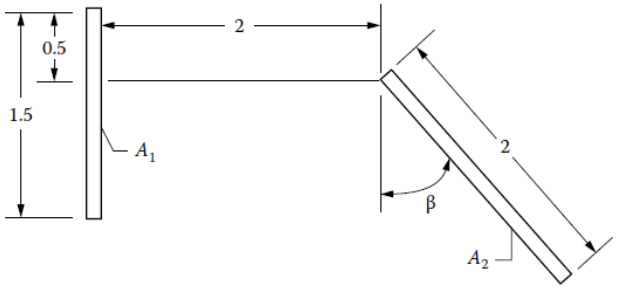

Answer: (a) 0.2752; (b) 0.0915.

I.5.6 A sphere of radius r is divided into two quarter spheres and one hemisphere. Obtain the configuration factors between all areas inside the sphere, F_{1-2}, F_{2-2}, F_{3-1}, F_{1-1}, etc. From these factors find F_{4-5}, where A_4 and A_5 are equal semicircles that are at right angles to each other.

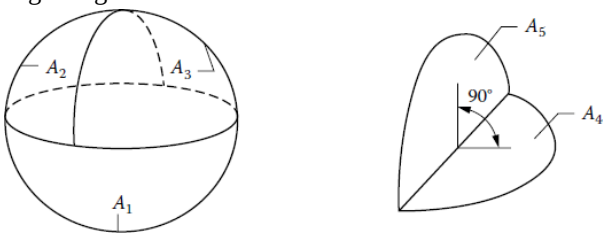

Answer: $F_{4-5} = 0.25$.

I.5.7 For the 2D geometry shown, the view between A_1 and A_2 is partially blocked by an intervening structure. Determine the configuration factor F_{1-2}.

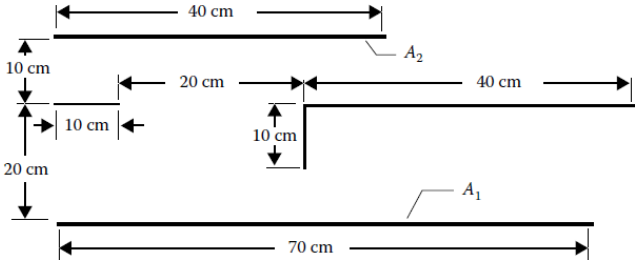

Answer: 0.1815.

I.5.8 The cylindrical geometry shown in cross section is very long in the direction normal to the plane of the drawing. The cross section consists of two concentric three-quarter circles and two straight lines. Obtain the value of the configuration factor F_{2-2}.

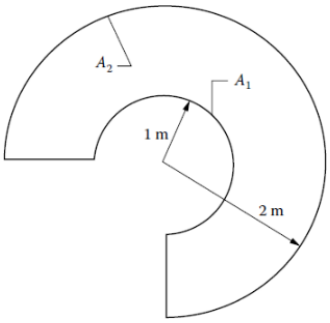

Answer: 0.3547.

I.5.9 Using the relation $F_{3-(1+2)} = F_{3-1} + F_{3-2}$, show whether the relation $F_{(1+2)-3} = F_{1-3} + F_{2-3}$ is also valid.

I.5.10 A plate A_1 in the configuration below is to be moved along positions from $S = 0$ cm to $S = 100$ cm. Plot the configuration factor F_{1-2} versus S for this configuration.

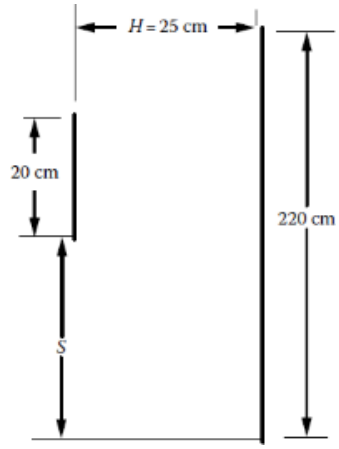

I.5.11 Derive the configuration factor F_{1-2} from a finite rectangle A_1 to an infinite plane A_2 where the rectangle is tilted at an angle η relative to the plane and one edge of the rectangle is in the infinite plane.

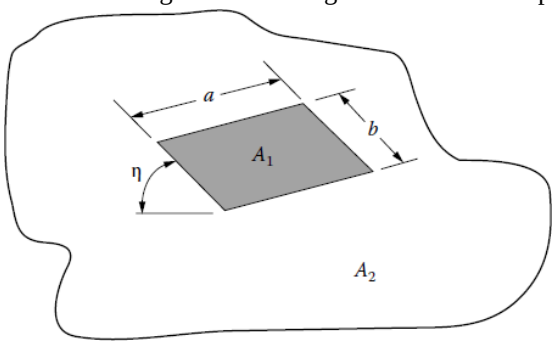

Answer: $F_{1-2} = (1/2)\,(1 - \cos\eta)$.

I.5.12 The four flat plates shown in cross section are very long in the direction normal to the plane of the cross section shown. Obtain the value of the configuration factor F_{1-2}. What are the values of F_{2-1} and F_{1-3}?

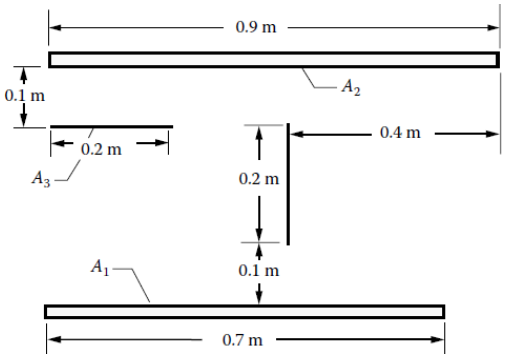

Answer: $F_{1-2} = 0.4260$; $F_{2-1} = 0.3314$; $F_{1-3} = 0.1704$.

I.5.13 A long tube in a tube bundle is surrounded by six other identical equally spaced tubes as shown in cross section below. What is the configuration factor from the central tube to each of the surrounding tubes?

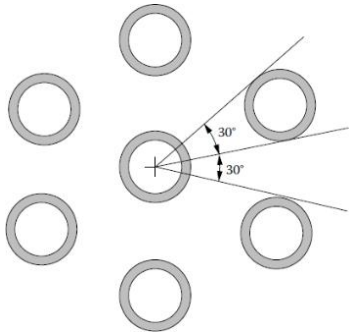

Answer: 0.0844 (>1/12).

I.5.14 Find F_{1-2} by any two methods for the 2D geometry shown in cross section.

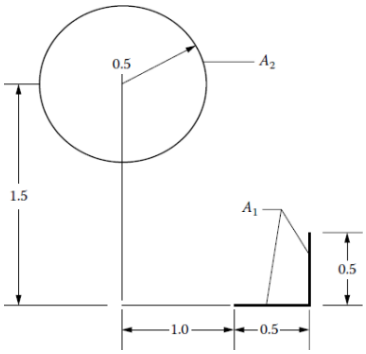

Answer: 0.1974.

I.5.15 Find the configuration factor F_{1-2} from the quarter disk to the parallel planar ring.

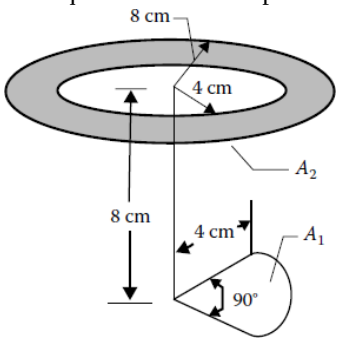

Answer: 0.2973.

I.5.16 Use the crossed-string method to derive the configuration factor between an infinitely long strip of differential width and a parallel infinitely long cylindrical surface.

Answer: $F_{d1-2} = (1/2)\ (\sin \beta_2 + \sin \beta_1)$.

I.5.17 Use the disk-to-disk configuration factor 10 of on-line Appendix C at *ThermalRadiation.net/text* to obtain the factor F_{d1-d2} between the interior surfaces of two differential rings on the interior of a right circular cone.

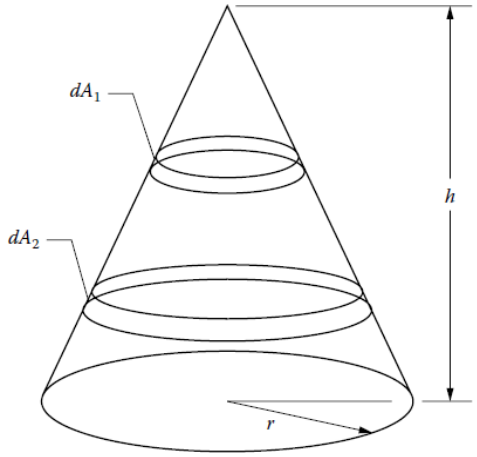

Answer:

$R \equiv r/h;\ \alpha \equiv (R^2+1);\ \beta \equiv (2R^4 - R^2 - 5)$

$$dF_{d1-d2} = -\frac{\cos\alpha}{2Rx^2}\left\{x - 2y\alpha + \frac{\alpha^{1/2}\left[\alpha x^4 + x^3 y\beta + 3x^2y^2(\beta+8) + xy^3\alpha(6R^2-7) + 2y^4Z^2\right]}{\left[\alpha(x+y)^2 - 4xy\right]^{3/2}}\right\}$$

I.5.18 In terms of disk-to-disk configuration factors, derive the factor between the finite ring A_1 and the finite area A_2 on the inside of a cone.

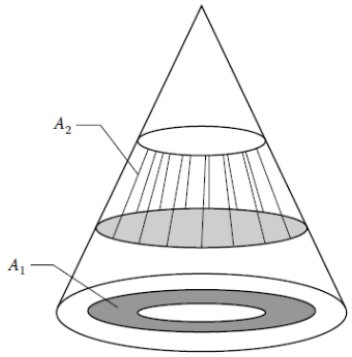

I.5.19 A closed right circular cylindrical shell with base diameter 1 m and height 1 m is located at the center of a spherical shell 1 m in radius.

(a) Determine the configuration factor between the inside of the sphere and itself.

(b) If the top of the cylindrical shell is removed, determine the configuration factor between the inside of the sphere and the inside of the bottom of the cylindrical shell.

Answer: (a) 0.6250; (b) 0.01072.

I.5.20 Show by an algebraic derivation whether the configuration factor from the interior curved surface of the frustum of a cone A_1 to its base A_2 as given in configuration factor C-111 of the configuration factor catalog at ***http://www.ThermalRadiation.net/ /indexCat.html*** is equivalent to that given in factor C-112.

I.5.21 Obtain the value of the configuration factor dF_{d1-2} for the geometry shown. The areas dA_1 and A_2 are parallel.

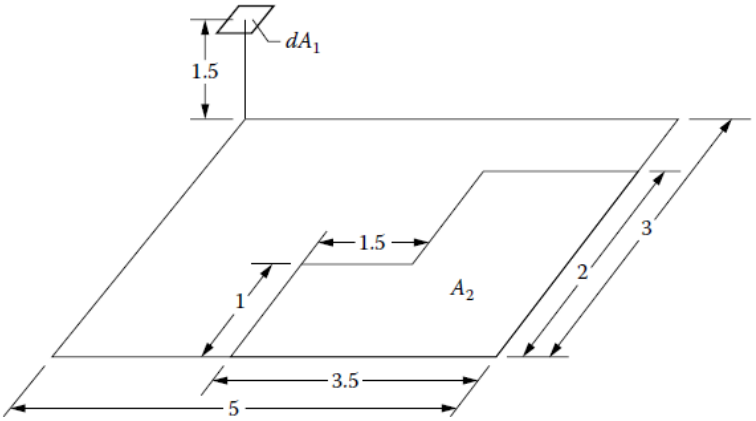

Answer: 0.01261.

I.5.22 For the geometry below and the special case of $l_1 = l_3$, derive algebraic expressions for the factors F_{1-2}, F_{1-3}, and F_{3-3}. Use relations from factors C-77 and C-97 from the online catalog at http://www.ThermalRadiation.net/indexCat.html.

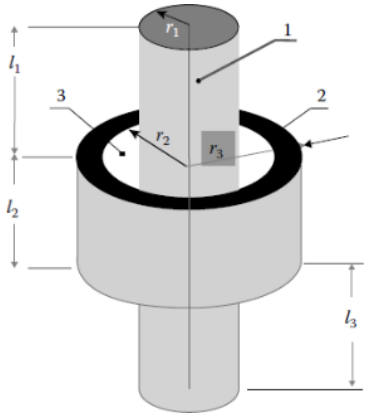

I.5.23 For the infinite parallel cylinders 1 and 2 with plate 3 forming a "deck" between them, find the factors F_{1-2}, F_{1-3}, and F_{2-2} in algebraic form.

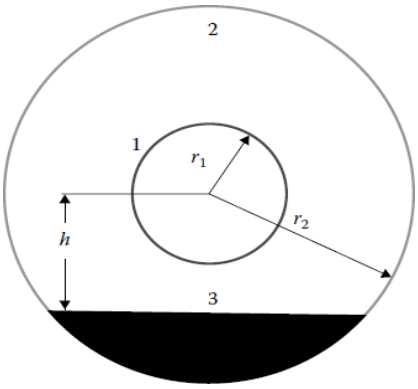

Answer: $F_{1-2} = 1 - F_{1-3} = 1 - \dfrac{\sqrt{r_2^2 - h^2}}{\pi^2 r_1} \tan^{-1}\left(\dfrac{\sqrt{\left(r_2^2 - h^2\right)}}{h}\right)$

$$F_{1-3}=\frac{A_3}{A_1}F_{3-1}=\frac{\sqrt{r_2^2-h^2}}{\pi^2 r_1}\tan^{-1}\left(\frac{\sqrt{\left(r_2^2-h^2\right)}}{h}\right)$$

$$F_{2-2}=1-\frac{\pi r_1}{(\pi-\cos^{-1}(h/r_2))}\left\{1-\frac{\sqrt{r_2^2-h^2}}{\pi^2 r_1}\tan^{-1}\frac{\sqrt{r_2^2-h^2}}{h}\right\}$$

$$-\frac{\sqrt{r_2^2-h^2}}{(\pi-\cos^{-1}(h/r_2))}\left\{1-\frac{1}{\pi}\tan^{-1}\frac{\sqrt{r_2^2-h^2}}{h}\right\}$$

I.5.24 Interpreting the figure in Homework Problem I.5.23 as concentric spheres 1 and 2 with a disk 3 inserted between them, find the factors F_{1-2}, F_{1-3}, and F_{2-2} in algebraic form.

Answer: $R=\frac{b}{h}=\frac{\sqrt{r_2^2-h^2}}{h}$; $F_{1-2}=1-F_{1-3}=1-\frac{1}{2}\left[1-\frac{1}{(1+R^2)^{1/2}}\right]$

$$F_{1-3}=\frac{1}{2}\left[1-\frac{1}{(1+R^2)^{1/2}}\right];$$

$$F_{2-2}=1-\frac{\pi r_1^2}{r_2^2\left[\pi-\cos^{-1}(h/r_2)\right]}\left(1-\frac{1}{2}\left[1-\frac{1}{(1+R^2)^{1/2}}\right]\right)$$

$$-\frac{\pi\left(r_2^2-h^2\right)}{4r_2^2\left[\pi-\cos^{-1}(h/r_2)\right]}\left(1-\frac{2r_1^2}{\left(r_2^2-h^2\right)}\left(1-\frac{1}{(1+R^2)^{1/2}}\right)\right)$$

Chapter 6:

I.6.1 A rectangular carbon steel billet 1 × 0.5 × 0.5 m is initially at 1150 K and is supported in such a manner that it transfers energy by radiation from all of its surfaces to surroundings at T_e = 27°C (assume the surroundings are black). Neglect convective energy transfer and assume the billet radiates like a blackbody. Also, assume for simplicity that the thermal conductivity of the steel is infinite. How long will it take for the billet to cool to 410 K? (For carbon steel, let ρ_{cs} = 7800 kg/m^3 and c_{cs} = 470 J/kg · K.)

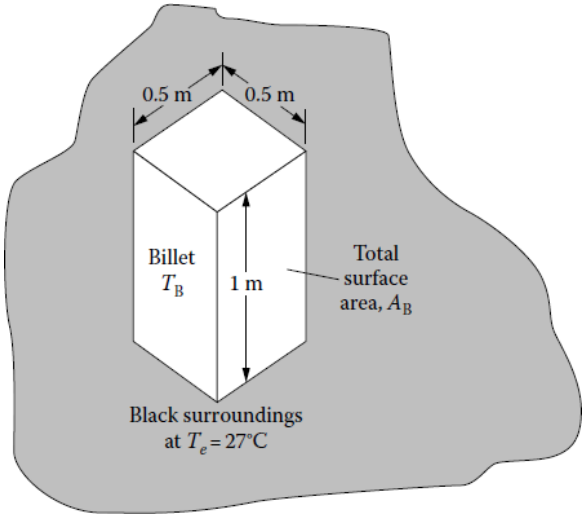

Answer: 9.61 h.

I.6.2 A black circular disk 0.15 m in diameter and well insulated on one side is electrically heated to a uniform temperature. The electrical energy input is 1300 W. The surroundings are black and are at T_e = 500 K. What fraction of the emitted energy is in the wave number region from 0.2 to 1 μm^{-1}?

Answer: 0.680.

I.6.3 A hollow cylindrical heating element is insulated on its outside surface. The element has a 25 cm inside diameter and is 25 cm long. The black internal surface is to be held at 1000 K. The surroundings are in vacuum and are at 400 K. Both ends of the cylinder are open to the surroundings. Estimate the energy that must be supplied to the element (W).

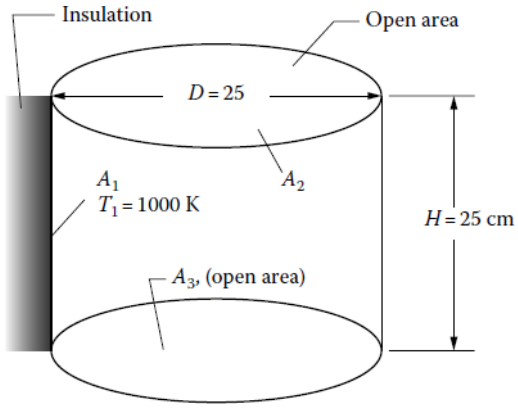

Answer: 4490 W.

I.6.4 The black-surfaced three-sided enclosure shown below has infinitely long parallel sides, with the specified temperatures and energy rate additions. Find Q_1, Q_2, and T_3. (Side 3 is a circular arc).

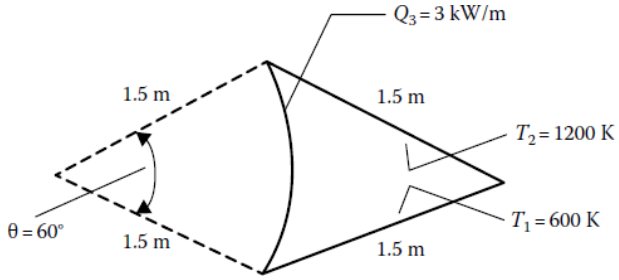

Answers: Q_1 = -123,561 W/m; Q_2 = 120,561 W/m; T_3 = 1032 K.

I.6.5 Two enclosures are identical in shape and size and have black surfaces. For one enclosure, the temperatures of the surfaces are T_1, T_2, T_3,....,T_N. For the second, the surface temperatures are $(T_1^4 + k)^{1/4}$, $(T_2^4 + k)^{1/4}$, $(T_3^4 + k)^{1/4}$, ..., $(T_N^4 + k)^{1/4}$, where k is a constant. Show how the energy transfer rates Q_j at any surface A_j are related for the two enclosures.

I.6.6 An enclosure with black interior surfaces has one side open to an environment at temperature T_e. The sides of the enclosure are maintained at temperatures of T_1, T_2, T_3, ..., T_N. How are the rates of energy input to the sides Q_1, Q_2, Q_3, ..., Q_N influenced by the value of T_e? How can the results for $T_e = 0$ be used to obtain solutions for other T_e?

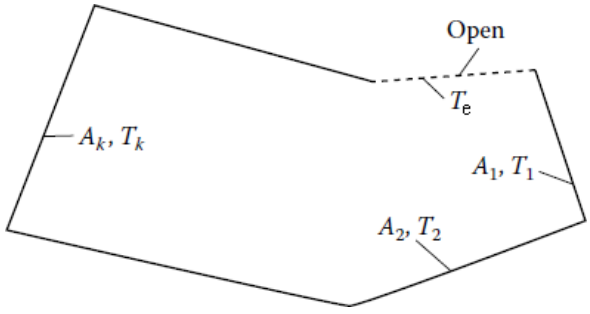

I.6.7 A black 6 cm diameter sphere at a temperature of 1100 K is suspended in the center of a thin 10 cm diameter partial sphere having a black interior surface and an exterior surface with a hemispherical total emissivity of 0.1. The surroundings are at 300 K. A 7.5 cm diameter hole is cut in the outer sphere. What is the temperature of the

outer sphere? What is the Q being supplied to the inner sphere? (For simplicity, do not subdivide the surface areas into smaller zones.)

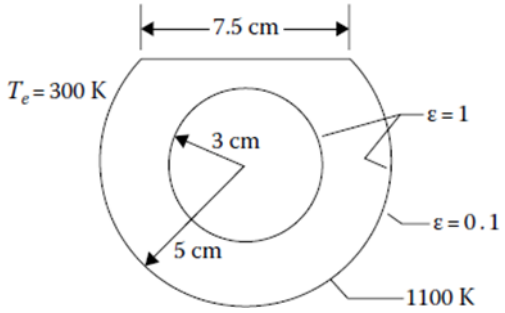

Answer: 988 K; 431 W.

I.6.8 An infinitely long enclosure (normal to the direction shown) is shaped as shown in the following. Assuming that the uniform flux restrictions are met along each surface, find Q_1 and T_2.

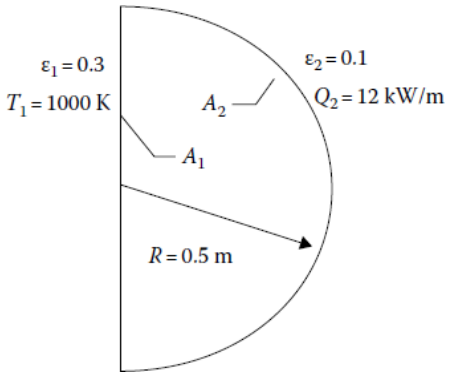

Answers: $Q_1 = -12$ kW/m; $T_2 = 1307$ K.

I.6.9 Two infinitely long diffuse–gray concentric circular cylinders are separated by two concentric thin diffuse–gray radiation shields. The shields have identical emissivities on both sides.

(a) Derive an expression for the energy transferred between the inner and outer cylinders in terms of their temperatures and the necessary radiative and geometric quantities. (Number the surfaces from the inside out; i.e., the inner surface is number 1, the outer surface is number 4.)

(b) Check this result by showing that in the proper limit it reduces to the correct result for four parallel plates with identical emissivities.

(c) Find the percent reduction in energy transfer when the shields are added if the radii for the surfaces are in the ratio 1:2:4:8, and if $\varepsilon_1 = \varepsilon_4 = 0.7$ and $\varepsilon_2 = \varepsilon_3 = 0.1$.

Answer:

(a) $$Q = \frac{A_1\sigma\left(T_1^4 - T_4^4\right)}{G_{12} + \frac{A_1 G_{23}}{A_2} + \frac{A_1 G_{34}}{A_3}} \text{ where } G_{ab} \equiv \frac{1}{\varepsilon_a} + \frac{A_a}{A_b}\left(\frac{1}{\varepsilon_b} - 1\right).$$

(b) $$Q = \frac{A_1\sigma\left(T_1^4 - T_4^4\right)}{3\left(\frac{2}{\varepsilon} - 1\right)}.$$

(c) $Q_{\text{with}}/Q_{\text{without}} = 0.0942$

I.6.10 Consider the gray cylindrical enclosure described in Homework Problem 6.8 of the text with the top in place. A hole 30 cm in diameter is cut in the top. Determine the configuration factors between (a) the base and the hole and (b) the curved wall and the hole. Estimate the radiant energy escaping through the hole. The outside environment is at $T_e \approx 0$ K.

Answer: (a) 0.00238; (b) 0.00238; (c) 2630 W.

I.6.11 A thin gray disk with emissivity 0.9 on both sides is in Earth's orbit. It is exposed to normally incident solar radiation (neglect radiation emitted or reflected from the Earth.) What is the equilibrium temperature of the disk? A single thin radiation shield having emissivity 0.05 on both sides is placed as shown. What is the disk temperature? What is the effect on both of these results of reducing the disk emissivity to 0.5? (Assume the surroundings are at zero absolute temperature and that for simplicity, it is not necessary to subdivide the areas.)

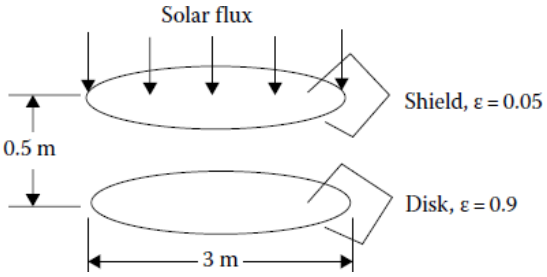

Answer: For unshaded disk, 330.5 K (either value of ε); with shield, 31.1 K ($\varepsilon = 0.05$); 136.1 K (for $\varepsilon = 0.5$).

I.6.12 For the enclosure with four infinitely long parallel walls shown in the following in cross section, calculate the average heat flux on surface 2 (W/m^2). All surfaces are diffuse–gray and are assumed for simplicity to have uniform outgoing flux distributions.

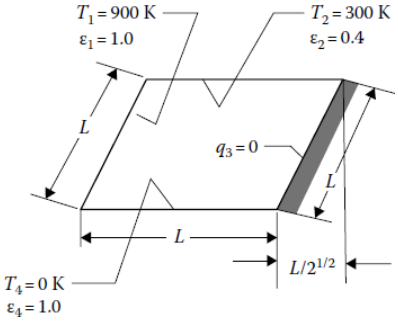

Answer: −4972 W/m^2.

I.6.13 A very long cylinder at temperature T_1 is coaxial with a long square enclosure shown in the following cross section. The conditions on surfaces 1–5 are shown in the table. Find Q_1 and T_2. (For simplicity, do not subdivide the surfaces. Also, note that the configuration factors for this geometry were derived in Homework Problem 5.12 of the text.)

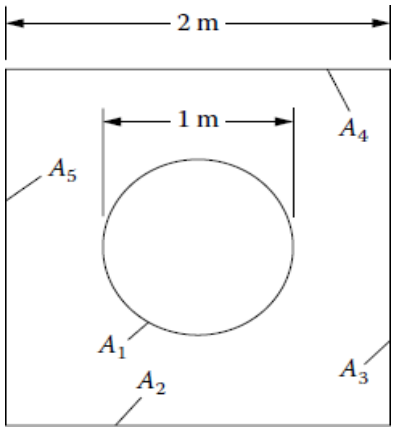

Surface	T(K)	Q (W/m)	ε
1	1100		0.4
2		0	0.5
3	0		1
4	0		1
5	0		1

Answer: $T_2 = 703$ K; $Q_1 = 100$ kW/m.

I.6.14 In a metal-processing operation, a metal sphere at uniform temperature is heated in a vacuum to high temperature by radiative exchange with a circular heating element. The surroundings are cool enough that they do not affect the radiative exchange and may be neglected. The surfaces are diffuse–gray. Derive an expression for the net rate of energy absorption by the sphere. The expression should be given in terms of the quantities shown. For simplicity, do not subdivide the surface areas. Discuss whether this is a reasonable approximation for this geometry for the distribution of reflected energy from the sphere.

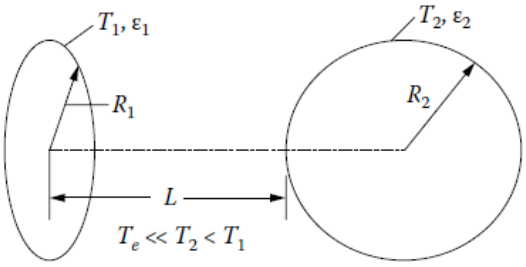

I.6.15 A 10 cm diameter hole extends through the wall of a furnace having an interior temperature of 1350 K. The wall is a 20 cm thick refractory brick. Divide the wall thickness into two zones of equal length and compute the net radiation out of the hole into a room at 300 K. (Neglect energy conduction in the wall.)

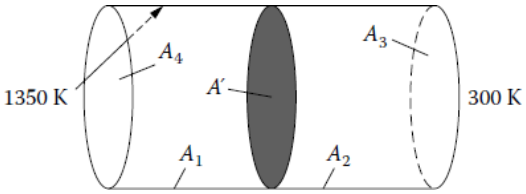

Answer: $T_1 = 1216$ K; $T_2 = 1033$ K; $Q_3 = -560$ W.

I.6.16 A cubical enclosure with edge length of 6 m has a very small sphere placed at its center ($A_{sphere} \ll A_{side}$). The sphere has emissivity $\varepsilon = 0.4$ and is maintained electrically at $T_s = 1300$ K. The interior walls of the cube have the following properties:

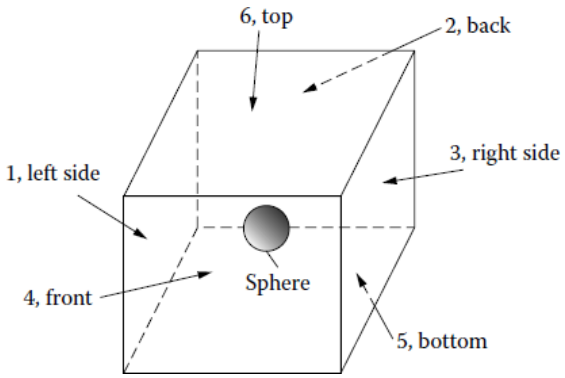

Side	Temperature (K)	Emissivity
1	1100	1.0
2	800	0.5
3	700	0.5
4	400	1.0
5	200	0.2
6	0	1.0

Determine the net q added or removed from each side of the cube and the q added to the sphere. Find the results in kW/m^2. Tabulate all the required configuration factors. (Assume the incident radiation on each surface is uniform.)

Answer: $q_1 = 69.9$ kW/m$_2$; $q_2 = -0.86$ kW/m^2; $q_3 = -6.10$ kW/m^2; $q_4 = -28.0$ kW/m^2; $q_5 = -5.11$ kW/m^2; $q_6 = -29.8$ kW/m^2; $q_s = 54.9$ kW/m^2.

I.6.17 A thin diffuse–gray circular disk with emissivity ε_1 on one side and ε_2 on the other side is being heated in a vacuum by a cylindrical electrical heater with a diameter D. The heater has a diffuse–gray interior surface and is open at both ends.

(a) Derive a formula (which can be in terms of configuration factors) for the net radiative energy rate being gained by the disk while it is being heated. The formula should be in terms of the instantaneous disk temperature and the quantities shown.

For the specific case, $T_h = 1200$ K; $T_e = 300$ K; $D = 0.50$ m; $L = 0.80$ m; $d = 0.30$ m; $l = 0.10$ m; $\varepsilon_1 = 0.70$; $\varepsilon_2 = 0.85$; $\varepsilon_h = 0.80$.

(b) What is the net gain (W) when $T_d = 600$ K?

(c) What is the equilibrium disk temperature long after the heater is turned on?

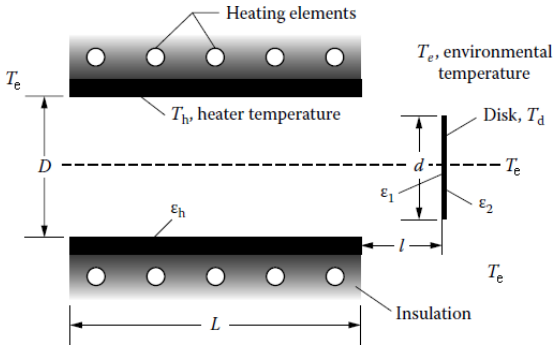

Net gain =

Answer: (a)

$$= \varepsilon_2\sigma\frac{\pi d^2}{4}\left(T_e^4 - T_d^4\right) - \frac{\varepsilon_1\pi d^2}{4}\frac{\left\{\begin{array}{l}\sigma T_d^4\left[1-\left(1-\varepsilon_3\right)\left(F_{3-3}+F_{3-1}F_{1-3}\right)\right]-\varepsilon_3F_{1-3}\sigma T_3^4\\ +\sigma T_4^4\left[-F_{1-4}+\left(1-\varepsilon_3\right)\left(F_{3-3}F_{1-4}-F_{3-4}F_{1-3}\right)\right]\end{array}\right\}}{1-\left(1-\varepsilon_3\right)\left[F_{3-3}+F_{3-1}F_{1-3}\left(1-\varepsilon_1\right)\right]}$$

(b) 4010 W; (c) 902 K.

I.6.18 A hollow satellite in Earth orbit consists of a circular disk and a hemisphere. The disk is facing normal to the direction to the sun. The surroundings are at T_e = 20 K. The satellite walls are thin. All surfaces are diffuse. The properties are $\alpha_{1,\,\text{solar}}$ = 0.95; $\varepsilon_{1,\,\text{infrared}}$ = 0.13; ε_2(gray) = 0.80; ε_3(gray) = 0.50; ε_4(gray) = 0.60. What are the values of T_1 and T_4? (Do not subdivide surfaces. Neglect any emitted or reflected radiation from the Earth.)

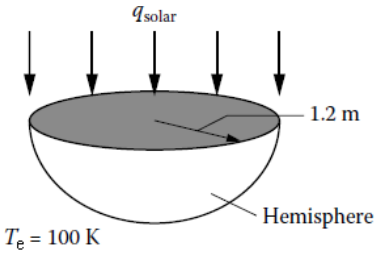

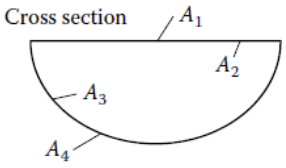

Answer: T_2 = 458 K; T_3 = 345 K.

I.6.19 A space vehicle in orbit around the sun is at the same distance as the Earth. It is a hollow cube with thin walls and is oriented with one side always facing directly toward the sun and the other five sides in the shade. The interior is painted with a coating with ε = 0.60. On the outside, the top is coated with a material with α_{solar} = 0.93 and ε = 0.80, the front and back sides are faced with aluminum foil with ε = 0.04, and the two sides and the bottom have white paint with ε = 0.80. The surroundings are at 0 K. Using as simple a radiation model as is reasonable, obtain the temperatures of the six faces of the cube.

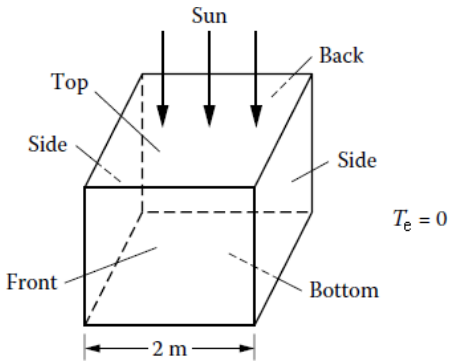

Answer: T_1 (top) = 367 K; T_2 (2 sides, bottom) = 234 K; T_3 (front and back) = 281 K.

I.6.20 Consider two parallel plates of finite extent in one direction. Both plates are perfectly insulated on the outside. Plate 1 is uniformly heated electrically with energy flux q_e. Plate 2 has no external energy input. The environment is at zero absolute temperature.

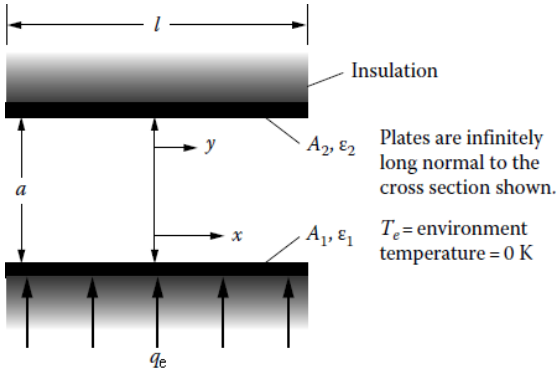

(a) For both plates *black*, show that the integral equations for the surface temperatures are

$$\theta_{b,1}(X) = 1 + \frac{1}{2}\int_{-L/2}^{L/2} \theta_{b,2}(Y) \frac{dY}{\left[(Y-X)^2+1\right]^{3/2}}$$

where $X = x/a$, $Y = y/a$, $\theta = \sigma T^4/q_e$, and $L = l/a$.

$$\theta_{b,2}(Y) = \frac{1}{2}\int_{-L/2}^{L/2} \theta_{b,1}(X) \frac{dX}{\left[(X-Y)^2+1\right]^{3/2}}$$

(b) If both plates are *gray*, show that $\theta_1(X) = \theta_{b,1}(X) + \dfrac{1-\varepsilon_1}{\varepsilon_1}$; $\theta_2(Y) = \theta_{b,2}(Y)$.

I.6.21 A long groove is cut into a metal surface as shown in the following cross section. The groove surface is diffuse–gray and has emissivity ε. The temperature profile along the groove sides, as measured from the apex, is found to be $T(x)$. The environment is at temperature T_e.

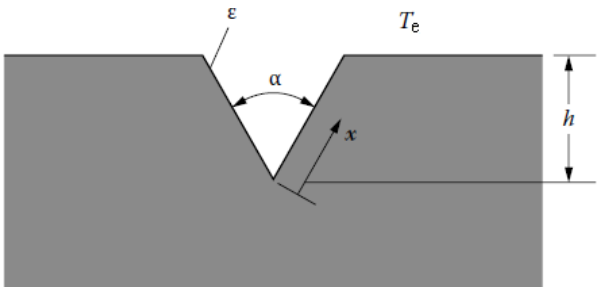

(a) Derive the equations for the energy flux distribution $q(x)$ along the groove surface.

(b) Examine the kernel of the integral equation found in part (a) and show whether it is symmetrical and/or separable.

I.6.22 A hemispherical cavity is in a block of lightly oxidized copper ($\varepsilon_1 = 0.57$) maintained at 800 K in vacuum. The surroundings are at 300 K. Use the integral equation method to compute the outgoing energy flux from the cavity surface.

Answer: 27,140 W/m^2.

I.6.23 A cavity having a gray interior surface S is uniformly heated electrically and achieves a surface temperature distribution $T_{w,0}(S)$ while being exposed to a zero absolute temperature environment, $T_e = 0$. If the environment is raised to T_e and the heating kept the same, what is the surface temperature distribution?

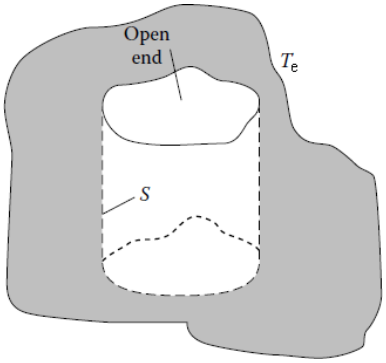

Answer: $T_{w,0}(r) = \left[T_w^4(r) - T_e^4\right]^{1/4}$, where $T_{w,0}(S) = T_w(S, T_e = 0)$.

I.6.24 A gray circular tube insulated on the outside is exposed to an environment at $T_e = 0$ at both ends. The $q(x, T_e = 0)$ has been calculated to maintain the wall temperature at any constant value. Now, let $T_e \approx 0$, and let the wall temperature be uniform at T_w. Show that the $q(x, T_e \neq 0)$ can be obtained as the $q(x, T_e = 0)$ corresponding to the wall temperature $(T_w^4 - T_e^4)^{1/4}$.

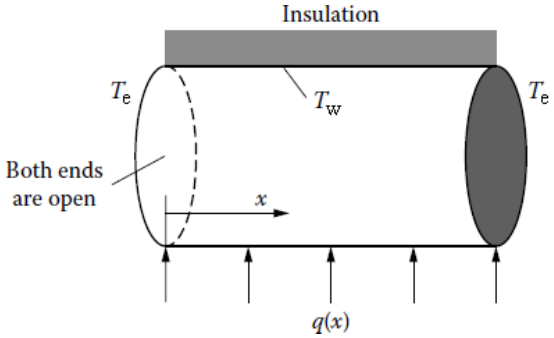

I.6.25 For the geometry and conditions shown in the following, set up the required integral equations for finding $q_1(y)$, $T_2(z)$, and $T_3(x)$. Put the equations in dimensionless form and discuss how you would go about solving the equations. Which method of Chapter 5 appears most useful?

$T_1(y) = T_1$ = constant; $q_2(z) = 0$ (insulated on the outside); $q_3(x) = q_3$ = constant; $\varepsilon_1(y) = 1.0$; $\varepsilon_2(z) = \varepsilon_3(x) = 0.5$

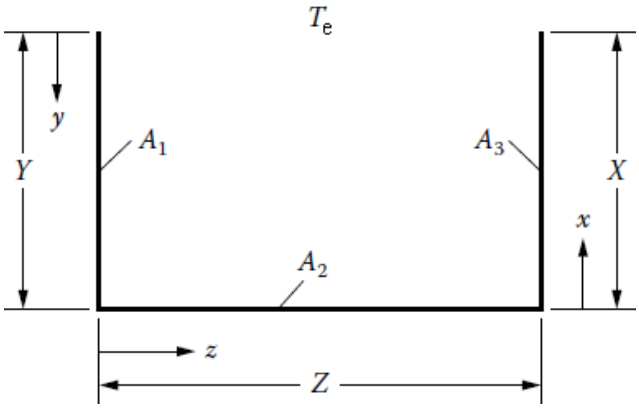

I.6.26 A four-surface enclosure has the properties and temperatures shown in the following. Find the energy flux for each surface and demonstrate that the radiative energy balance is satisfied. Assume that radiosities can be taken as uniform across each surface.

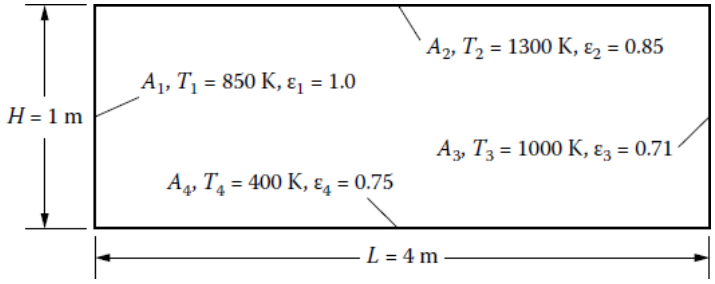

Answer: $q_1 = -54{,}690$ W/m; $q_2 = 108{,}100$ W/m; $q_3 = -16.620$ W/m; $q_1 = -90{,}230$ W/m.

I.6.27 A very long A-frame grain dryer is built with the cross section of an isosceles triangle with the dimensions shown in the following. For solar heating, the right opaque side is exposed to the sun and is black, the left side is insulated. At a particular time, the conditions for the inside surfaces of the dryer are as shown in the table.

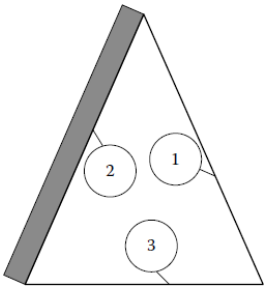

(a) What will be the floor temperature T_3 (K)?

(b) What will be the temperature of the insulated wall T_2?

Surface	L (m)	T (K)	q (W/m²)	ε
1	5	450		1.0
2	5		0	0.537
3	3.5		−600	0.35

Answer: (a) 304 K; (b) 437 K.

I.6.28 A radiator is planned to provide energy rejection from a nuclear power plant that is to provide electrical power for a lunar outpost. The radiator will itself will be horizontal on the lunar surface, and condensing working fluid in the power cycle will maintain the uniform surface temperature of the radiator at 800 K. The radiator is shielded from the nearby lunar outpost by a 1.5 m high vertical insulated plate (see diagram on the next page). The width of the radiator is limited to 2 m. The radiator has a diffuse–gray emissivity of 0.92, while the insulated shield has an emissivity of 0.37. It is expected that the radiator will be quite long. Conduction within the radiator and heat shield can be neglected. For the situation when the radiator is on the night side of the moon,

(a) Set up the equations for finding the energy flux distribution on the radiator, $q_1(x)$, and the temperature distribution on the shield, $T_2(y)$. Note any assumptions.

(b) Solve the equations for $q_1(x)$ and $T_2(y)$. Show that the increment size chosen for solution is small enough that the solutions are grid independent.

(c) If the total energy rejection from the radiator is required to be 1.0 MW, what must be the length of the radiator (m)?

(d) Discuss how the results would change if the influence of incident solar energy on the radiator during daytime is considered.

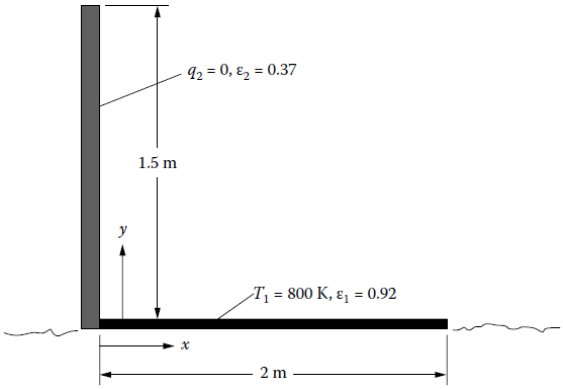

Answers: $T_2(y = 1.5\text{ m}) = 525$ K; $T_2\ (y = 0) = 662$ K; $q_1(x = 0) = 16.5$ kW/m^2; $q_1(x = 2\text{ m}) = 20.8$ kW/m^2; length of radiator = 47.2 m.

Chapter 7:

I.7.1 Two thin vertical posts stand immediately adjacent to a pool of molten material at temperature T_m and are diametrically across the pool from each other. The posts have a square cross-section of area A_x, are of length L, and have thermal conductivity k. The entire surface of the posts has emissivity ε. The pool is of radius r and is assumed to be black. A breeze blows across the posts, and the air has temperature T_a. The air motion produces a energy transfer coefficient h between the post surface and the air.

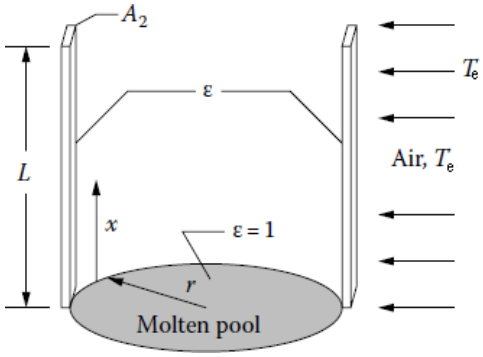

Derive an equation for the temperature distribution T(x) along the posts, including the effect of mutual radiative exchange by the posts. Assume that the temperature at the bottom of the posts is equal to the temperature of the molten pool. Also, assume that the effect of the temperature of the surroundings T_e on radiative transfer can be neglected. Show the necessary boundary conditions for the problem and relations for all of the required configuration factors. (You do not need to substitute the F's into the equation, however.)

I.7.2 How would the analysis in Homework Problem I.7.1 be modified to include the effect of a non-zero environment temperature?

I.7.3. An infinitely long enclosure is shown in cross-section below. It is separated into two compartments by a conducting plate with thermal conductivity k = 45 W/m•K. The properties and conditions on the enclosure surfaces are shown in the table. The vertical ends are at specified temperatures, and the horizontal sides are insulated on the outside.

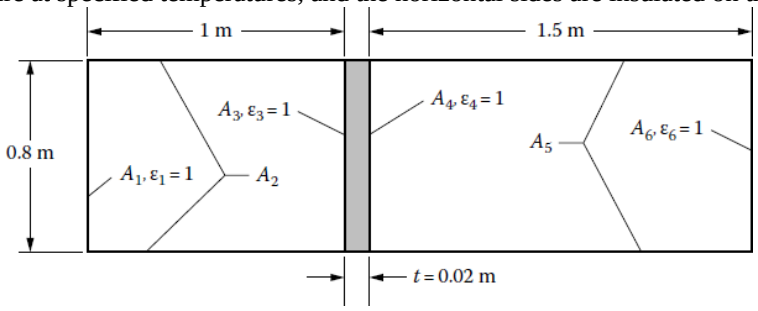

Surface	Emissivity, ϵ	Net energy flux, q (W/m^2)	Temperature, K
1	1.0		1800
2	0.1	0	
3	1.0		
4	1.0		
5	0.3	0	
6	1.0		200

Determine the missing table values of the entries. Assume for simplicity that the surfaces need not be subdivided.

Answer: $q_1 = q_4 = -q_3 = -q_6 = 87{,}667$ W/m^2, $T_2 = 1749$ K, $T_3 = 1693$ K, $T_4 = 1254$ K, and $T_5 = 1055$ K.

I.7.4 Thin wire is extruded at fixed velocity through a die at temperature T_0. The wire then passes through air at T_a until its temperature is reduced to T_L. The energy transfer coefficient to the air is h, and the wire emissivity is ε. It is

desired to obtain the relation between T_L and T_0 as a function of wire velocity V and distance L. Derive a differential equation for wire temperature as a function of distance from the die and state the boundary conditions. (*Hint:* Compute the energy balance for flow in and out of a control volume fixed in space.)

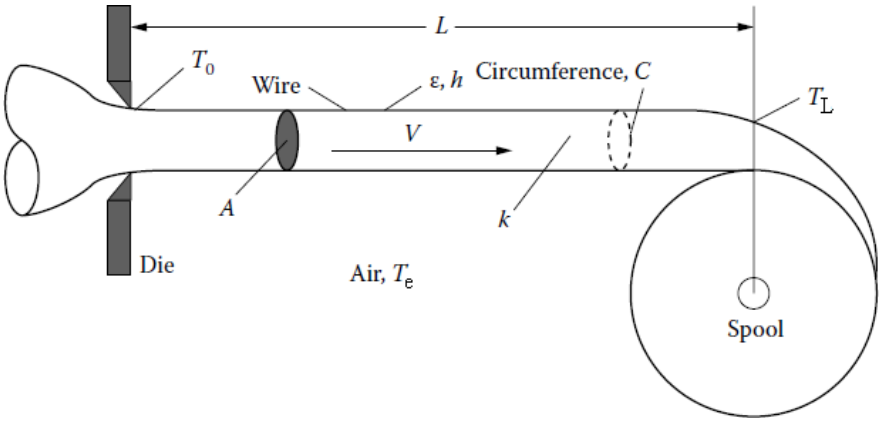

I.7.5 A single circular fin is to dissipate energy from both sides in a vacuum to surroundings at low temperature. The fin is on a tube with 2-cm outer diameter. The tube wall is maintained at 750 K by vapor condensing on the inside of the tube. The fin has 20 cm outer diameter and is 0.30 cm thick. Estimate the rate of energy loss by radiation from the fin if the fin is made from stainless steel [k = 35 W/(m•K)] with a clean surface (ε = 0.15). What is the effect on energy dissipation of increasing the fin thickness to 0.60 cm?

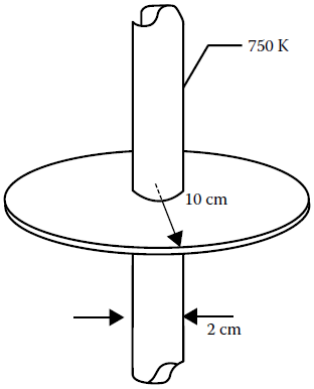

Answer: (c) 65 W; 91.2 W.

I.7.6 The billet in Homework Problem I.I.1 has air at 27°C blowing across it that provides an average convective energy transfer coefficient of $\bar{h}=24\ W/(m^2 \cdot K)$. Estimate the cooling time with both radiation and convection included.

Answer: 4.47 hours.

I.7.7 Opaque liquid at temperature T(0) and mean velocity $\overline{u}$ enters a long tube that is surrounded by a vacuum jacket and a concentric electric heater that is kept at uniform axial temperature T_e. The heater is black, and the tube exterior is diffuse-gray with emissivity ε. The convective energy transfer coefficient between the liquid and the tube wall is h, and the tube wall thermal conductivity is k_w. Derive the relations to determine the mean fluid temperature and the tube wall outer surface temperature as a function of distance x along the tube (assume that the liquid properties are constant).

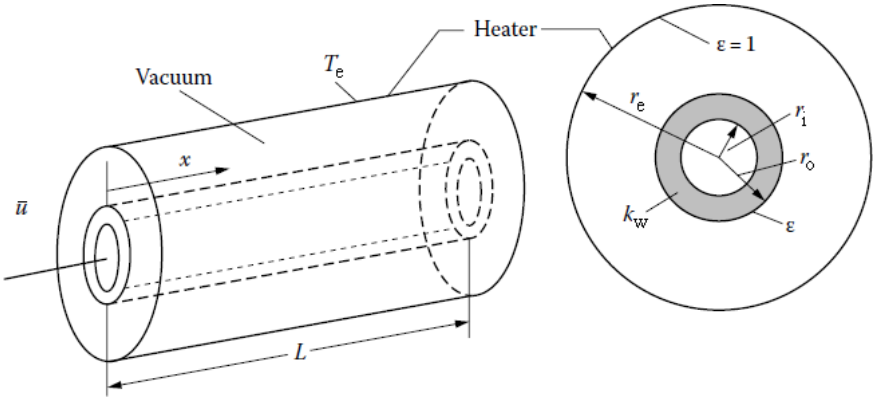

I.7.8 A solar collector is designed to fit onto the horizontal section of a roof as diagrammed below. Flow is from the right to the left in the tubes of the collector. A tilted white diffuse roof section at the left side helps to reflect additional solar flux onto the collector. Set up the equations for determining the local temperature of the tubes for two cases: (a) no flow in the tubes, and (b) flow of water in each tube of 2.00 kg/min. Indicate a possible solution method. Assume that the roof and collector are very long normal to the cross section shown.

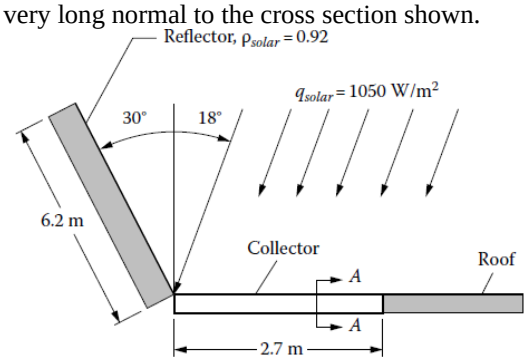

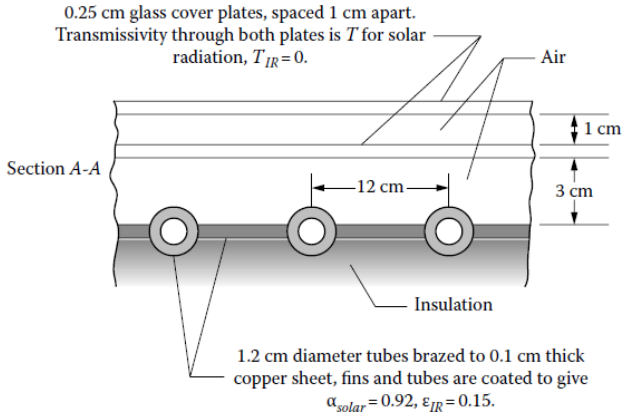

I.7.9 A radio antenna extends normal to a spacecraft surface as shown in the diagram below. The antenna has a circular cross section with diameter D=1 cm. The spacecraft itself is very large, and its surface can be considered to be black with uniform temperature T_b=500K. The environment is at T ≈ 0 K. The antenna material has emissivity =ε(gray, diffuse) and thermal conductivity k = 40W/(m·K).

(a) Derive the differential equation for the temperature distribution in the antenna, T(x). Note any assumptions. Include the effect of radiation exchange between the antenna and the spacecraft.

(b) Place the equation in a convenient nondimensional form, using the nondimensional temperature $\mathcal{G}(X)=T(X)/T_b$, and X = x/L.

(c) Provide a plot of $\mathcal{G}(X)$ vs. X for ε = 0.3, 0.5, and 1.0.

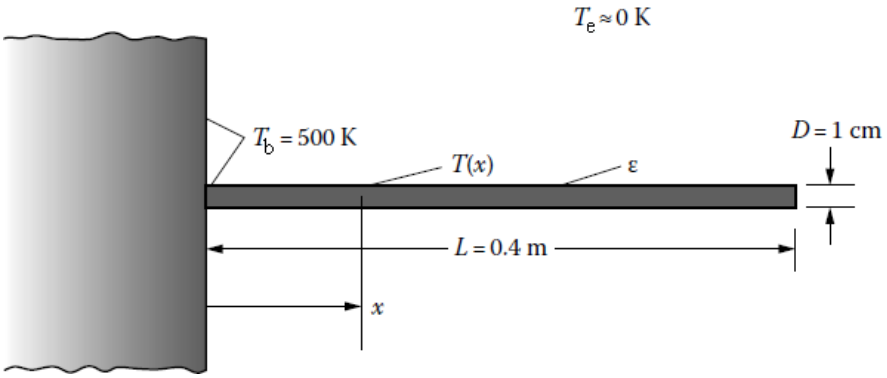

I.7.10 A long gray empty circular tube is in the vacuum of outer space so that the only external energy exchange is by radiation. The metal tube is coated with a material that has a solar absorptivity α_s and an emissivity in the infrared region of ε_{IR}. The solar flux q_s is incident from a direction normal to the tube axis, and the surrounding environment is at a very low temperature T_e that can be neglected in the radiative energy balances. The geometry is as shown in cross-section. The tube is empty so there is internal radiative exchange. Energy is conducted circumferentially within the tube wall. The wall thermal conductivity is k_w.

(a) Set up the energy relations required to obtain the temperature distribution around the tube circumference assuming that radial temperature variations within the tube wall can be neglected.

(b) Place the energy relations in finite difference form and describe how a numerical solution can be obtained.

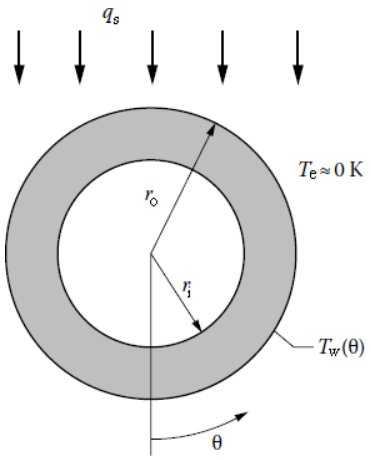

I.7.11 The tube in Homework Problem I.7.10 is shielded from solar radiation by being in the shadow of a space vehicle, so that it cools to a very low temperature. It is then suddenly exposed to the solar flux. Set up the transient energy relations required to calculate the tube circumferential temperature distribution as a function of time using the same conditions and assumptions as in Homework Problem I.7.10. Place the equations in finite difference form and describe how a numerical solution can be obtained.

I.7.12 A thin sheet of copper moves through a radiative-convective oven at a velocity of 0.1 m/s. The sheet and oven are very wide. Air flows at a mass flow rate of 0.2 kg/s per meter of oven width over the sheet in counterflow, and the energy transfer coefficient between the air and sheet surface is constant along the sheet at a value of h = 100 W/(m^2•K). The back of the sheet is insulated. A black radiant heater at T_{Heater} = 1200 K covers the top of the oven as shown. The radiant heater does not interact convectively with the air stream. Louvered curtains at each end of the oven are opaque to radiation but allow air flow. The emissivities of all surfaces are shown.

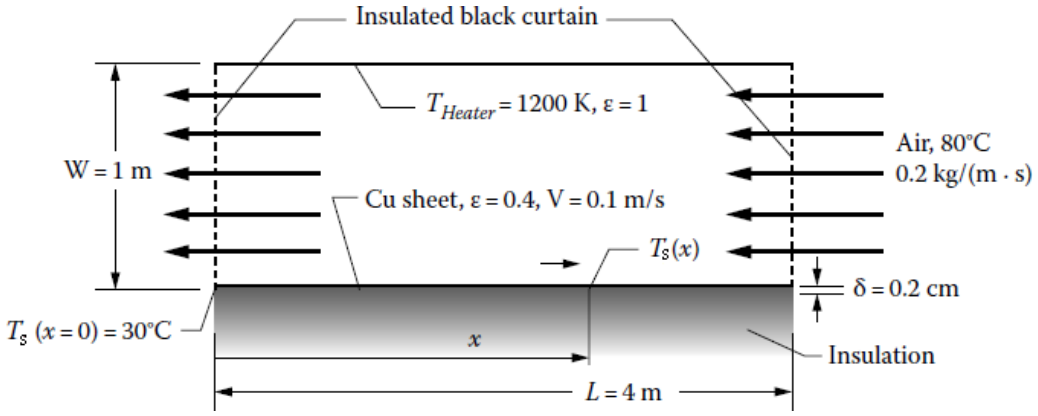

Find the temperature distribution $T_S(x)$ along the copper sheet as a function of position x within the oven and present the result graphically. Discuss all assumptions made in the solution and justify them by numerical argument where possible. Data for copper sheet: $k_s = 400$ W/(m•K); $c_{p,s} = 385$ J/(kg•K); $\rho_s = 9000$ kg/m^3.

I.7.13 For the geometry shown below with one conducting wall:

a) Provide the final governing equations necessary for finding $T_1(x_1)$ and $q_2(x_2)$ in nondimensional form using appropriate nondimensional variables.

b): Find the temperature distribution $T_1(x_1)$ and the energy flux distribution $q_2(x_2)$ and show them on appropriate graphs.

Boundary conditions are $q_1(x_1) = \left[100x_1 - 50x_1^2\right](\text{kW/m}^2)$ where x_1 is in meters, T_2=500 K, and $T_3 = T_4$ = 300K.

Properties for the diffuse surfaces are shown on the figure.

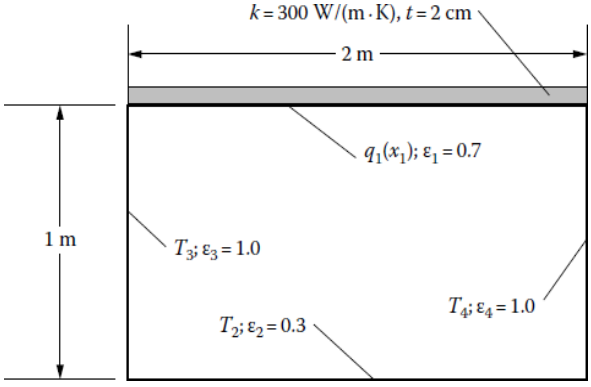

Show that your solution is grid-independent and meets overall energy conservation. Compare your solution to the results for the nonconducting case.

Answer: $T_1(\max) = 1117.7$ K with no conduction, $T_1(\max) = 1102.1$ K with conduction, and $q_2(\max) = \sim -10{,}100$ W/m^2 with no conduction and $q_2(\max) = \sim -9{,}700$ W/m^2 with conduction.

Chapter 9:

I.9.1 A plane layer of semitransparent medium without scattering is at a uniform temperature of T_m = 950 K. The layer is 0.28 m thick. The medium has three absorption bands with constant absorption coefficients $\kappa_{\lambda 1} = 5.5$ m^{-1}, $\kappa_{\lambda 2} = 4.6$ m^{-1}, and $\kappa_{\lambda 3} = 3.8$ m^{-1} in the wavelength bands from 1.3 to 3.1 μm, 3.65 to 5.05 μm, and 5.95 to 8.5 μm. For the remainder of the spectrum, the medium is perfectly transparent. One boundary of the layer is in contact with a black source at T_w = 1030 K. Calculate the intensities leaving the layer at the other boundary in the normal direction, 30° from the normal, and 60° from the normal.

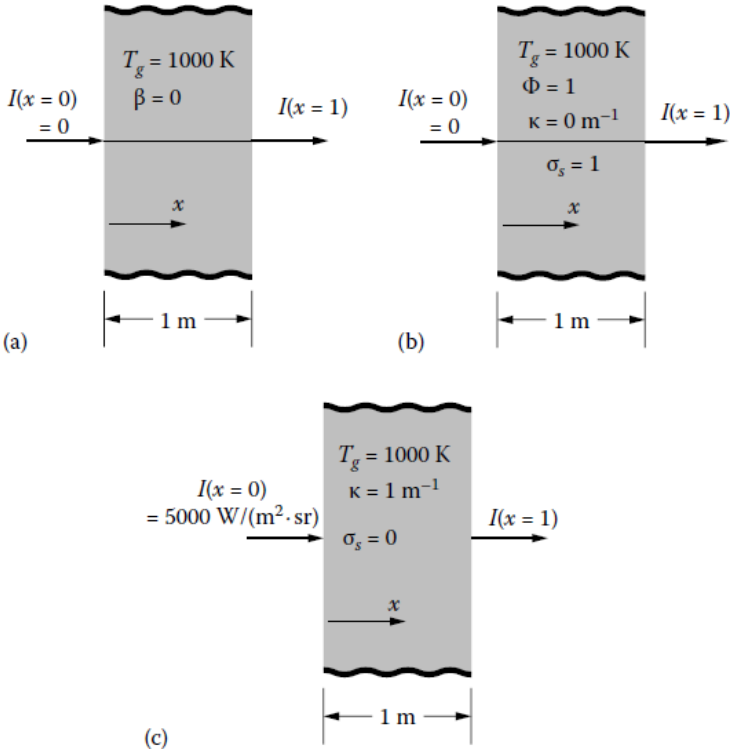

Answer: I(x=0.28 m, θ=0°) = 10458 W/(m²·sr); I(x=0.28 m, θ=30°) = 10262 W/(m²·sr); I(x=0.28 m, θ=60°) = 9699.1 W/(m²·sr).

I.9.2 A large absorbing semitransparent medium without scattering has a single plane boundary. A black plate with constant temperature of T = 1250K is suddenly placed in contact with that boundary. The plate radiates into the medium, which is cool enough that it does not radiate. Determine the radiative energy source $-\nabla \cdot \mathbf{q}_r$ at a location x = 0.82 m into the medium from the plane boundary if the absorption coefficient of the medium is κ = 0.75 m^{-1}.

Answer: 55960 W/m^3.

I.9.3 A semi-infinite medium is absorbing, emitting, and isotropically scattering. It is gray, has n ≈ 1, and has absorption coefficient κ and scattering coefficient σ_s. The medium is initially at uniform temperature T_i. The transparent plane surface of the medium is suddenly subjected to radiative exchange with a large environment at a lower uniform temperature T_e. It is proposed to carry out a numerical solution to obtain the transient temperature distributions in the medium as it cools. Provide the energy and scattering equations in a convenient dimensionless form that are then to be placed in numerical form for solution. Include energy conduction and assume the medium is stationary. The density ρ, specific heat c, and thermal conductivity k of the medium are assumed constant.

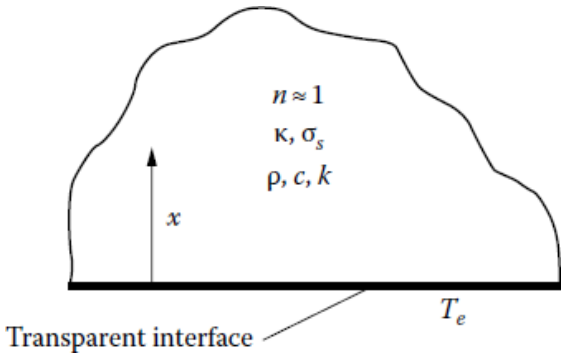

I.9.4 A furnace at atmospheric pressure with interior in the shape of a a cylinder with height equal to two times its diameter is filled with a 50:50 mixture by volume of CO_2 and N_2. The furnace volume is 0.689 m^3. The gas temperature is uniform at 1800 K and the walls are cooled. The interior surfaces are black. At what rate is energy being supplied to the gas (and removed from the walls) to maintain these conditions? For emittance values, use the Alberti et al. (2018) worksheet at *https://doi.org/10.1016/j.jqsrt.2018.08.008.*

Answer: 295 kW.

I.9.5 Pure carbon dioxide at 1 atm and 2500 K is contained between parallel plates 0.3 m apart. What is the radiative flux received at the plates as a result of radiation by the gas? For emittance values, use the Alberti et al. (2018) worksheet at *https://doi.org/10.1016/j.jqsrt.2018.08.008.*

Answer: 163 kW/m^2.

I.9.6 A furnace being designed by a chemical company will be used to burn toxic waste composed of hydrocarbons. Complete elimination of the hydrocarbons with oxygen requires that the temperature of the combustion products in the furnace (60% CO_2, 40% H_2O by volume) be maintained at 1600 K. To prevent leakage of toxic waste or combustion products to the surroundings, the furnace interior is kept at 0.5 atm. The furnace is in the shape of a right circular cylinder of height equal to its diameter of 4 m. What average radiative flux is incident on the interior surface of the furnace? Note any assumptions used in obtaining the result.

Answer: 124 kW/m^2.

I.9.7 Estimate the maximum radiative flux that is incident on any local area on the interior surface of the furnace described in Homework Problem I.9.6.

Answer: 133 kW/m^2.

I.9.8 A thin black plate 1 x 1 cm is at the center of a sphere of CO_2-air mixture at a uniform temperature of 1800 K and 1 atm total pressure. The partial pressure of the CO_2 is 0.8 atm and the sphere diameter is 1 m. How much energy is absorbed by the plate? What will the plate temperature be? (Assume the boundary of the sphere is black and kept cool so that it does not enter into the radiative exchange.)

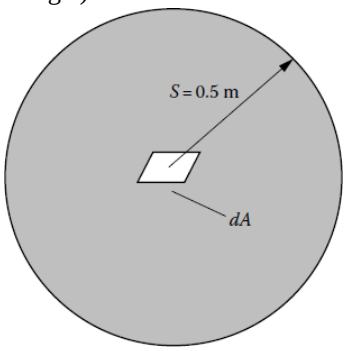

Answer: 13.0 W, 1034 K.

I.9.9 An optically thin gray gas with constant absorption coefficient κ is contained in a long transparent cylinder of diameter D. The surrounding environment is at low temperature that can be considered zero. Initially, the cylinder is at the environment temperature. Then, an electrical discharge is passed through the gas, continuously producing in the gas a uniform energy source $\dot{q}$ per unit volume and time. Derive a relation for the transient gas temperature variation if radiation is assumed to be the only significant mode of energy transfer. What is the maximum temperature T_{max} that the gas will achieve?

Answer: $$\frac{8\kappa\sigma T_{max}^3}{\rho c_v} t = \frac{1}{2}\ln\frac{1+\theta}{1-\theta} + \tan^{-1}\theta;\quad T_{max} = \left(\frac{\dot{q}}{4\kappa\sigma}\right)^{1/4};\theta = \frac{T}{T_{max}}\ .$$

Chapter 10:

I.10.1 Construct a complete flow diagram for the Monte Carlo solution of the problem outlined for gray plates in Homework Problem 6.17.

I.10.2 A large plate of translucent glass is laid upon a sheet of polished aluminum. The aluminum is kept at a temperature of 500 K and has an emissivity of 0.03. The glass is 2 cm thick and has a Rosseland mean absorption coefficient of $\kappa_R = 3.6\ \text{cm}^{-1}$. A transparent liquid flows over the exposed face of the glass and maintains that face at a temperature of 270 K.

(a) What is the energy flux through the glass plate?

(b) What is the temperature distribution in the glass plate?

Neglect energy conduction in your calculations, and for simplicity assume that the refractive indices of the glass and liquid are both one.

ANSWER: $q = 84.8\ \text{W/m}^2$; $T(\tau) = 100\left(133.7 - 11.2\tau\right)^{1/4}\ (\text{K})$.

I.10.3 A long cylinder 12 cm in diameter is surrounded by another cylinder 24 cm in diameter. The surfaces are gray, the inner cylinder is at $T_1 = 910$ K with $e_1 = 0.42$, and the outer cylinder is at $T_2 = 1075$ K with $e_2 = 0.83$. What is the energy transfer from the outer cylinder to the inner cylinder per unit length for vacuum between the cylinders? If the space between the cylinders is filled with a gray medium having absorption and isotropic scattering with extinction coefficient $\beta = \kappa + \sigma_s = 0.41\ \text{cm}^{-1}$, compute the energy transfer using the P_1 method and the diffusion method (energy conduction is neglected).

ANSWER: 5.59 kW/m; 3.94 kW/m; 3.89 kW/m.

I.10.4 Two diffusely emitting and reflecting parallel plates are of finite width and infinite length normal to the cross section shown. The lower plate has uniform temperature $T_1 = 1000$ K, and the upper plate is at $T_2 = 500$ K. The plate emissivities are $\varepsilon_1 = 0.8$ and $\varepsilon_2 = 0.2$. The surroundings have a temperature of 450 K. An absorbing–emitting medium with absorption coefficient $\kappa = 0.5\ \text{m}^{-1}$ is between the plates. The medium is in radiative equilibrium with its surroundings (energy conduction is negligible).

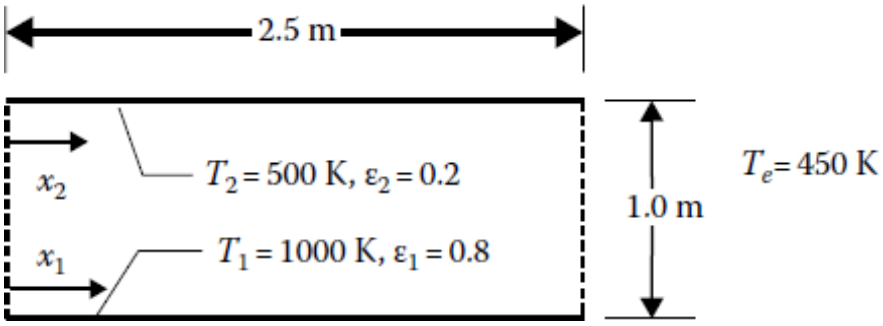

Using the Monte Carlo method, find the distribution of net radiative energy flux on each surface. Show the dependence of the results on the number of samples used in the Monte Carlo solution. Plot the results and compare them with the results of book Homework Problem 6.17.

I.10.5 Use the Monte Carlo method to determine the temperature distribution in the 2D enclosure shown below. The medium in the enclosure is nonscattering and has absorption coefficient $\kappa = 10\ \text{m}^{-1}$.

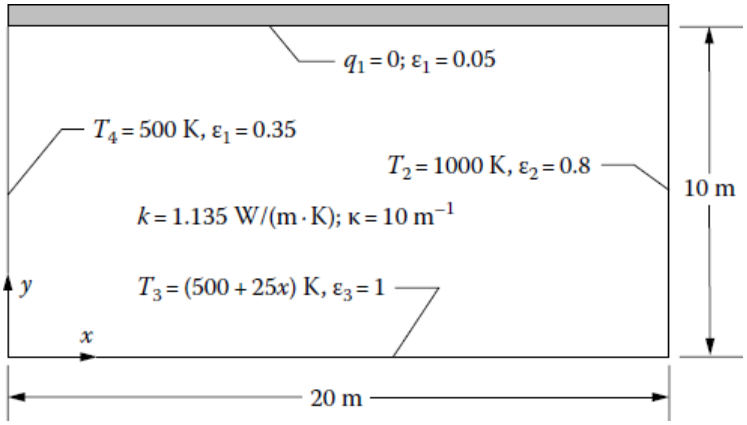

Provide plots of $q_3(x)$ on surface 3, $T_1(x)$ on surface 1, and $T_g(x = 10\text{ m}, y)$ and $T_g(x, y = 5\text{ m})$. Report the number of samples used in the solution.

I.10.6 The gray medium in the enclosure below is nonscattering and has an absorption coefficient of $\kappa = 4$ m^{-1} and a thermal conductivity of $k = 20$ W/m·K.

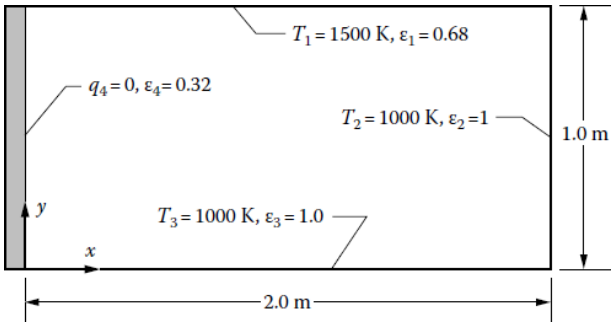

Using the Monte Carlo method for the radiative transfer,

1. Show the governing equation(s) and boundary condition for the problem in specific and dimensionless form. Indicate any simplifying assumptions that are necessary.
2. Provide a plot of $q_3(x)$ on surface 3 and profiles of the medium temperature at $T(x = 0.5, y)$ and $T(x, y = 0.25)$.
3. Show limiting solutions for the cases of $N_{CR} = 0$ and $N_{CR} = \infty$.
4. Show that the solution is grid independent.
5. Show that energy is conserved on the system boundaries.

I.10.7 Use the Monte Carlo method to determine the temperature distribution in the 2D enclosure shown below. The medium in the enclosure is nonscattering and has an absorption coefficient $\kappa = 10$ m^{-1} and thermal conductivity of 1.135 W/m·K.

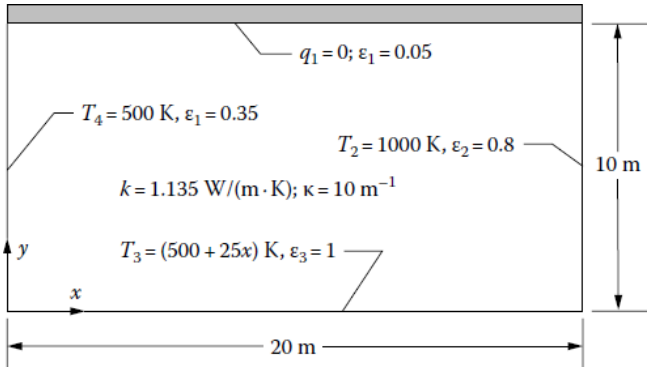

Provide plots of $q_3(x)$ on surface 3, $T_1(x)$ on surface 1, and $T_g(x = 10\text{ m}, y)$ and $T_g(x, y = 5\text{ m})$. Show that your solution is correct in the limit of no radiation and no conduction.

I.10.8 Use the Monte Carlo method to determine the temperature distribution in the 2D enclosure shown below. The medium in the enclosure has isotropic scattering coefficient of $\sigma_s = 5\text{ m}^{-1}$ and absorption coefficient $\kappa = 10\text{ m}^{-1}$ and thermal conductivity of 1.135 W/(m·K).

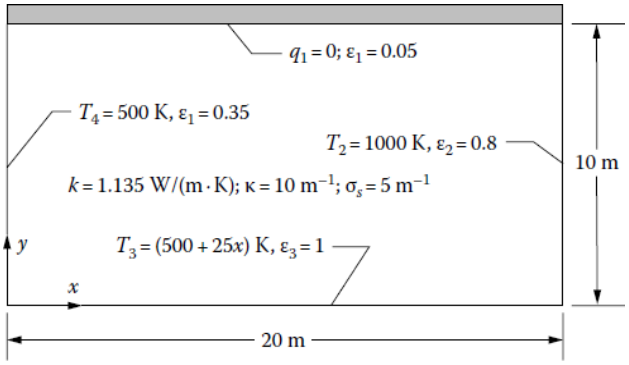

I.10.9 In Homework Problem 10.5, for the situation of a scattering medium between gray plates, it is desired to double the amount of energy being transferred by having the scattering (nonabsorbing) particles suspended in a thermally conducting but nonabsorbing medium. What thermal conductivity of the medium is required to accomplish this?

Answer: 2.04 W/(m•K).

Chapter 11:

I.11.1 As a result of surface treatment, a partially transparent plate has a different reflectivity at each surface. For radiation incident on surface 1 in a single direction, obtain an expression for the overall reflectance and transmittance in terms of ρ_1, ρ_2, and τ.

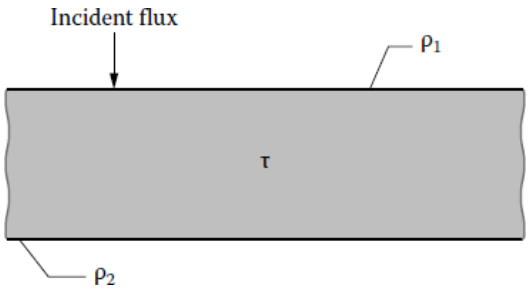

Answer: $R = \dfrac{\rho_1 + \rho_2(1-2\rho_1)\tau^2}{1-\rho_1\rho_2\tau^2}$; $T = \dfrac{(1-\rho_1)(1-\rho_2)\tau}{1-\rho_1\rho_2\tau^2}$

I.11.2 Two parallel, partially transparent plates have different τ values and a different ρ at each surface. Obtain an expression for the overall transmittance of the two-plate system for radiation incident from a single direction.

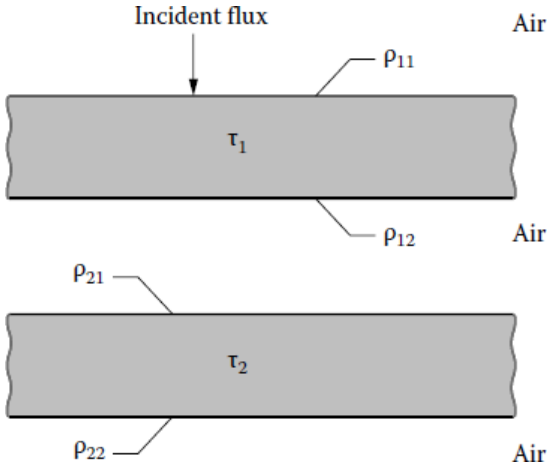

Answer:

$$T = \frac{T_1 T_2}{1 - R_{12} R_{21}}, \quad \text{where } T_n = \frac{(1-\rho_{n1})(1-\rho_{n2})\tau_n}{1-\rho_{n1}\rho_{n2}\tau_n^2}$$

$$\text{and } R_{nm} = \frac{\rho_{nm} + \rho_{nn}(1-2\rho_{nm})\tau_n^2}{1-\rho_{nm}\rho_{nn}\tau_n^2}$$

I.11.3 In a solar still, a thin layer of condensed water is flowing down a glass plate. The plate has a transmittance τ, and the water layer is assumed nonabsorbing. Obtain an expression for the overall transmittance T_L of the system for radiation incident on the glass in a single direction.

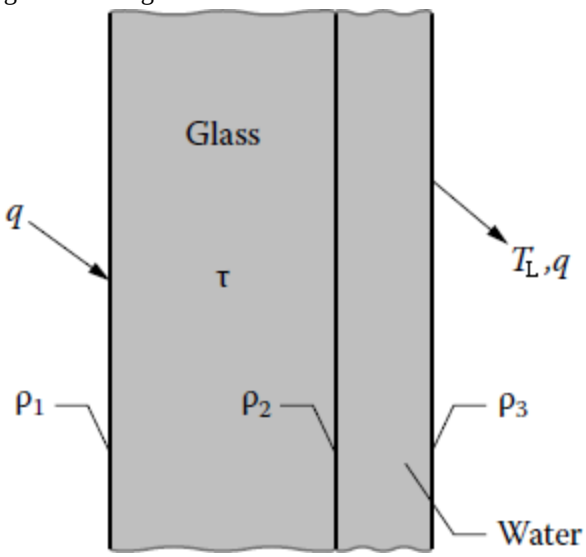

Answer: $$T_L = \frac{(1-\rho_1)(1-\rho_2)(1-\rho_3)\tau}{(1-\rho_2\rho_3)(1-\rho_1\rho_2\tau^2) - \rho_1\rho_3(1-\rho_2)^2\tau^2}$$

I.11.4 Two opaque gray walls have a transparent (nonabsorbing) plate between them. The transparent plate has surface reflectivities ρ. Derive a relation for the energy transfer from wall $w1$ to wall $w2$. Neglect energy conduction in the transparent plate and neglect the fact that ρ depends on the angle of incidence.

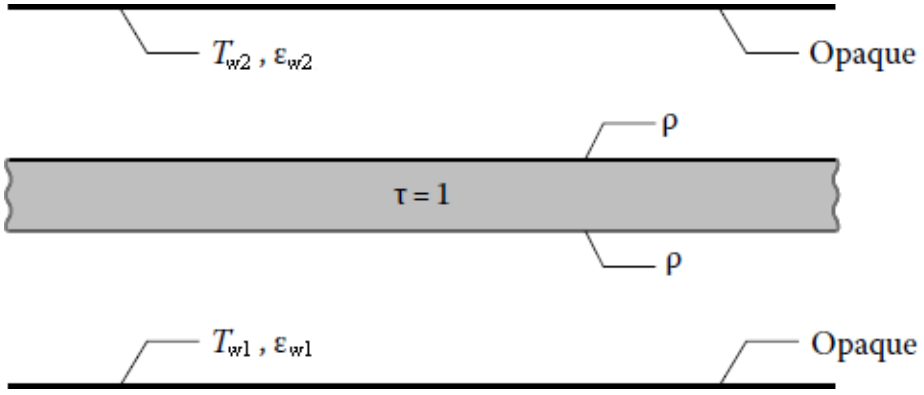

Answer: $q_{w1\to w2} = \dfrac{\sigma\left(T_{w1}^4 - T_{w2}^4\right)}{\dfrac{1}{\varepsilon_{w1}} + \dfrac{1}{\varepsilon_{w2}} - 1 + \dfrac{2\rho}{1-\rho}}$

I.11.5 Water is flowing between two identical glass plates adjacent to an opaque wall. Derive an expression for the fraction of radiation incident from a single direction that is absorbed by the water in terms of the ρ and τ values of the interfaces and layers. (Include only radiative energy transfer.)

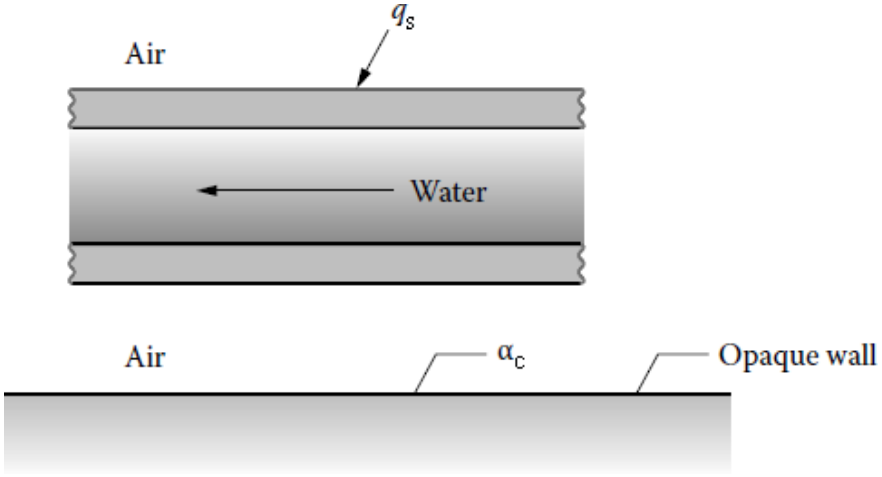

.

I.11.6 A series of three parallel glass plates is being used to absorb incident infrared radiation. The incident radiation is at wavelength $\lambda = 4$ μm. The complex index of refraction of the glass at this wavelength is $n - ik = 1.40 - 5.8 \times 10^{-5}i$. The plates have optically smooth surfaces. The radiation is incident from air in a direction normal to the plates. What fraction of the incident radiation is absorbed by the center plate?

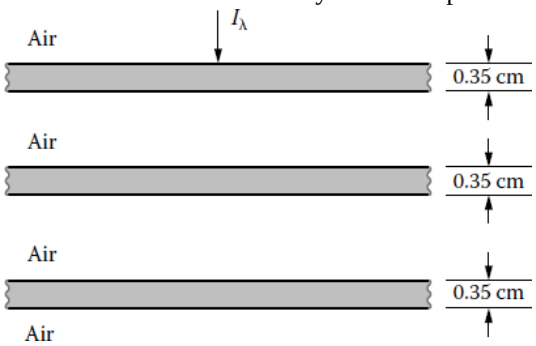

Answer: 0.237.

I.11.7 Two very thick dielectric regions with small absorption coefficients are in perfect contact at an optically smooth interface A_i. Prior to being placed in contact, region 1 was heated to a uniform temperature T_1, while region 2 was kept very cold at $T_2 \ll T_1$. The indices of refraction are such that $n_1 > n_2 > 1$. Derive an expression for the energy flux emitted across A_1 from region 1 into region 2. Evaluate the result for $n_1 = 2.35$, $n_2 = 1.54$, $T_1 = 627$ K, and $T_2 \approx 0$.

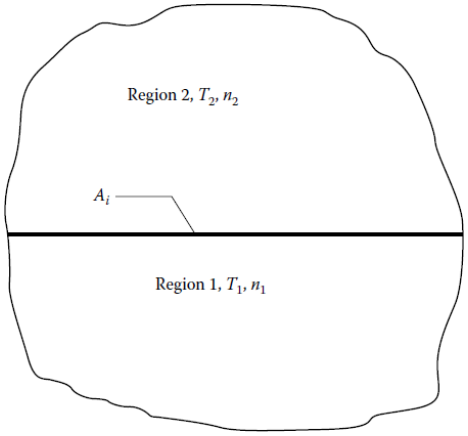

Answer: 18,800 W/m^2.

I.11.8 Two very thick dielectric regions with small absorption coefficients are separated by a plane layer of a third dielectric material that is of thickness $D = 2$ cm. The two interfaces are optically smooth. The plane layer between the two thick regions is perfectly transparent. This plane layer is at low temperature, having been suddenly inserted between the two dielectric regions. For the temperatures shown, calculate the net energy flux being transferred by radiation from medium 1 into medium 2. Include the effects of interface reflections. The effect of energy conduction is neglected. The indices of refraction are given in the figure.

Answer: 13.0 kW/m^2.

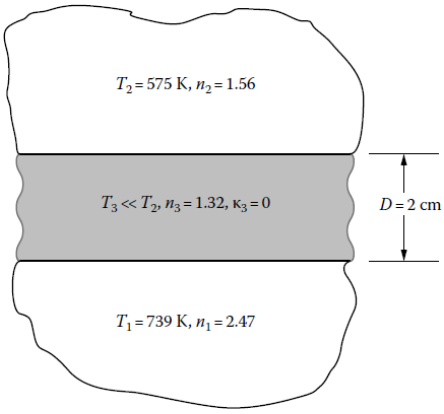

I.11.9 A layer of transmitting glass (silica) is separated from a silicon wafer by a layer of polymer. A laser provides monochromatic energy incident on the assembly of layers. The silicon wafer is opaque at the laser wavelength and has surface absorptivity $\alpha = 0.694$. The silica has a refractive index that gives a surface reflectivity for the laser energy of $\rho_{SiO_2} = 0.04$ and has transmittance for laser energy of $\tau_{SiO_2} = 0.95$ Similarly, the polymer layer has a surface reflectivity for the laser energy of $\rho_{poly} = 0.0452$ and has transmittance for laser energy of $\tau_{poly} = 0.90$. Derive an expression for the reflectance R for the laser energy of the glass/substrate assembly, and also determine the fraction of the incident laser energy that is deposited in the silica and polymer layers.

Answer: 0.302.

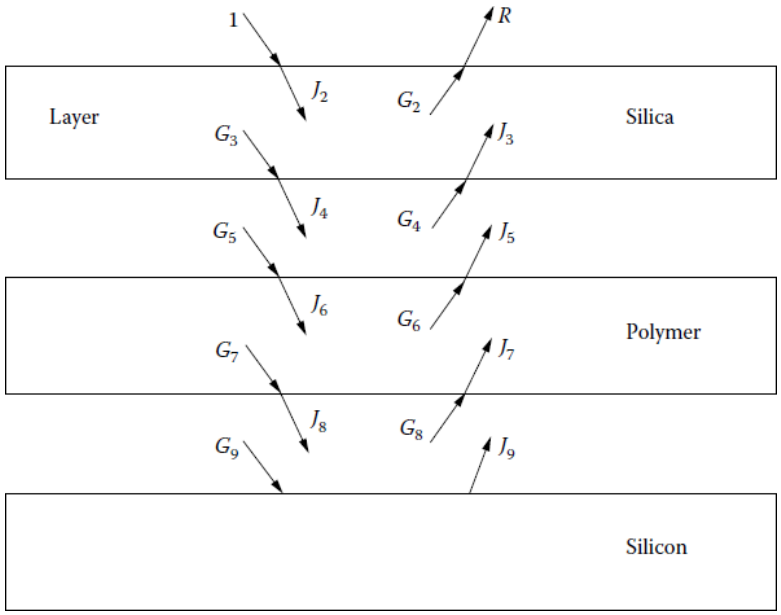
1
R
J2
G2
Layer
Silica
G3
J3
J4
G4
G5
J5
J6
G6
Polymer
G7
J7
J8
G8
G9
J9
Silicon

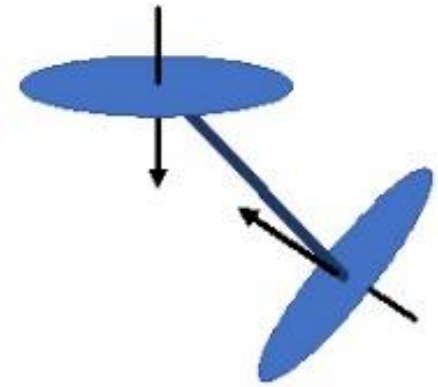

J: PROPOSED ONE-SEMESTER SYLLABUS

Below is a syllabus for a one-semester course in radiation energy transfer. The syllabus is based on a 15-week semester with two 90-minute classes per week, with 27 lecture sessions and three sessions left for examinations, class evaluation, etc. It begins with a general overview of why radiation is an important subject with many applications (Chapter 1). Then come the basics, with the fundamental blackbody properties (Chapter 2), the radiative properties of surfaces (Chapters 3, 4), the definition and use of configuration factors (Chapter 5), energy transfer among gray-diffuse surfaces and in enclosures with gray-diffuse surfaces, and solution techniques for these problems (Chapter 6). The Monte Carlo section for transfer among surfaces is drawn from Section 10.5 and can be introduced at this point. Interactions with conduction and/or convective transfer at enclosure boundaries are then treated (Chapter 7). Chapter 8 introduces the absorption and scattering properties of participating media. the absorption characteristics of participating media. The treatment of transfer through a participating media and a simplified mean-beam-length solution technique is shown (Chapter 9), and a more exact but intuitive method (diffusion solution) is examined as one example of a more general case in Chapter 10 which also introduces some aspects of radiation, conduction and convection in participating media. Chapter 11 deals with radiation in media with non-unity refractive index, such as windows and cover glasses in solar collectors. Finally, Chapter 12 is used to kindle interest in contemporary applications of radiation in nanoscale and inverse problems.

There is considerably more material in the text than can be covered in detail in one semester or quarter. The syllabus described below is suggested for those teaching the course for the first time. Those with experience will of course modify the syllabus to suit their interests and needs,

Chapter 1. Why Study Radiation Energy Transfer **(1-2 sessions of discussion, getting to know students and their interests. Pick whatever chapter content is most interesting at the moment.)**

1.1 Introduction
1.2 Thermal Radiation and the Natural World
1.3 Thermal Radiation in Engineering and Thermodynamics
1.4 Solar Energy
- Solar Energy Conversion
- Radiation Transfer, Architecture, and Visual Comfort
- Astronomy, Astrophysics, and Atmospheric Radiation
- Solar Energy, Global Warming, and Climate Change

1.5 Combustion and Flames
1.6 Porous Media and Packed Beds
1.7 Space Applications
- Spacecraft Thermal Control
- Radiation Energy Transfer in Rocket Nozzles

1.8 Advanced Manufacturing and Materials Processing
1.9 Biomedical Applications
1.10 Conclusions

Chapter 2. The Basics of Thermal Radiation

2.1 Nature of the Governing Equations **(3 class sessions on Sections 2.1 – 2.6)**

2.2 Electromagnetic Waves vs. Photons
2.3 Radiative Energy Exchange and Radiative Intensity
2.4 Solid Angle
2.5 Spectral Intensity
2.6 Characteristics of Blackbody Emission
- Perfect Emitter
- Radiation Isotropy in a Black Enclosure
- Perfect Emitter for Each Direction and Wavelength
- Total Radiation into Vacuum
- Blackbody Intensity and Its Directional Independence
- Blackbody Emissive Power: Cosine-Law Dependence
- Hemispherical Spectral Emissive Power
- Planck's Law: Spectral Distribution of Emissive Power
- Approximations to the Blackbody Spectral Distribution
- Wien's Displacement Law
- Total Blackbody Intensity and Emissive Power
- Blackbody Radiation within a Spectral Band
- Total Blackbody Intensity and Emissive Power
- Summary of Blackbody Properties

2.7 Radiative Energy Along a Line-Of-Sight **(Section 2.7can be downplayed unless plan to place emphasis on Chapters 8-10)**
- Radiative Energy Loss due to Absorption and Scattering
- Mean Penetration Distance
- Optical Thickness
- Radiative Energy Gain due to Emission
- Radiation Pressure
- Radiative Energy Gain due to In-Scattering

2.8 Radiative Transfer Equation (RTE**) (1 session on Sections 2.8, 2.9)**
2.9 Radiative Energy Transfer in Enclosures with Nonparticipating Media
2.10 Probabilistic Interpretation **(This section provides background for Monte Carlo method)**
2.11 Concluding Remarks

Chapter 3. Radiative Properties at Interfaces [2 sessions: Concentrate on meanings of the properties, Kirchhoff's Law and its restrictions (Section 3.3), and relations among the properties. Perhaps dwell on emissivity and its variations with wavelength and direction, and send less time on the other properties except to note that they are there for reference].

3.1 Introduction
3.2 Emissivity
- Directional Spectral Emissivity, $\epsilon_\lambda(\theta,\phi,T)$
- Directional Total Emissivity, $\epsilon(\theta,\phi,T)$
- Hemispherical Spectral Emissivity, $\epsilon_\lambda(T)$
- Hemispherical Total Emissivity, $\epsilon(T)$

3.3 Absorptivity
- Directional Spectral Absorptivity, $\alpha_\lambda(\theta_i,\phi_i,T)$
- Kirchhoff's Law
- Directional Total Absorptivity, $\alpha(\theta_i,\phi_i,T)$

Kirchhoff's Law for Directional Total Properties
Hemispherical Spectral Absorptivity, $\alpha_\lambda(T)$
Hemispherical Total Absorptivity, $\alpha(T)$
Diffuse-Gray Surface

3.4 Reflectivity
Spectral Reflectivities
Total Reflectivities
Summary of Restrictions on Reflectivity Reciprocity Relations

3.5 Transmissivity at an Interface
Spectral Transmissivities
Total Transmissivities
Relations among Reflectivity, Absorptivity, Emissivity, and Transmissivity

Chapter 4. Predicted and Measured Surface Properties
(2 sessions. Concentrate on overview of EM theory and its predictions and comparisons with measured values, solar applications.)

4.1 Prediction of Radiative Properties of Opaque Materials,
4.2 Introduction to Electromagnetic Wave Theory,
4.2.1 Waves Propagating in an Isotropic Dielectric Medium,
4.2.2 Waves Propagating in an Isotropic Conducting Medium,
4.2.3 Polarization,
4.3 Origins of Optical Constants,
4.3.1 Lorentz Model (Non-conductors),
4.3.2 Drude Model (Conductors),
4.4 EM Waves at Interfaces,
4.4.1 Dielectric Materials,
4.4.2 Radiative Properties of Conductors,
4.5 Measurements on Real Surfaces,
4.5.1 Surface Heterogeneity,
4.5.2 Surface Roughness Effects
4.5.3 Surface Temperature,
4.6 Selective Surfaces for Solar Applications,
4.6.1 Characteristics of Solar Radiation,
4.6.2 Modification of Surface Spectral Characteristics,
4.7 Concluding Remarks,

Chapter 5. Configuration Factors for Diffuse Surfaces with Uniform Radiosity (3 sessions, Factors are the basis for most engineering treatments of radiation, so this is an important chapter to cover in some detail.)

5.1 Radiative Transfer Equation for Surfaces Separated by a Transparent Medium
Enclosures with Diffuse Surfaces
Enclosures with Directional (Nondiffuse) and Spectral (Nongray) Surfaces

5.2 Geometric Configuration Factors between Two Surfaces
Configuration Factor for Energy Exchange between Diffuse Differential Areas
Configuration Factor between a Differential Area Element and a Finite Area
Configuration Factor and Reciprocity for Two Finite Areas

5.3Methods for Determining Configuration Factors
Configuration-Factor Algebra
Configuration-Factor Relations in Enclosures
Techniques for Evaluating Configuration Factors
Computer Programs for Evaluation of Configuration
5.4 Constraints on Configuration Factor Accuracy
5.5 Compilation of Known Configuration Factors and their References: Appendix C and Web Catalog

Chapter 6. Radiation Exchange in Enclosures Bounding Transparent Media (4 sessions: This chapter presents the basis for most standard radiative transfer analysis, so a good grasp of the content is important)

6.1 Introduction
6.2 Radiative Transfer for Black Surfaces
Radiation Exchange in a Black Enclosure
6.3 Radiation Among Finite Diffuse-Gray Areas
Net-Radiation Method for Enclosures
Enclosure Analysis in Terms of Energy Absorbed at Surface
Matrix Inversion for Enclosure Equations
6.4 Radiation Analysis Using Infinitesimal Areas
Generalized Net-Radiation Method Using Infinitesimal Areas
Boundary Conditions Specifying Inverse Problems
6.5 Computer Programs for Enclosure Analysis
6.6 Nongray and/or Nondiffuse Surfaces
6.7 Enclosure Theory for Diffuse Nongray Surfaces
Parallel Plates
6.8 Directional-Gray Surfaces
6.9 Radiation Exchange in Enclosures with Specularly Reflecting Surfaces
Cases with Simple Geometries
6.10 Multiple Radiation Shields
6.11 Concluding Remarks

Chapter 7. Radiation Combined with Conduction and Convection at Boundaries (3 sessions; first encounter with nonlinear equations, many important applications.)

7.1 Introduction
7.2 Energy Relations and Boundary Conditions
General Relations
Uncoupled and Coupled Energy Transfer Modes
Control Volume Approach for One- or Two-Dimensional Conduction along Thin Walls
7.3 Radiation Transfer with Conduction Boundary Conditions
Thin Fins with 1D or 2D Conduction
7.4 Radiation with Convection and Conduction

Thin Radiating Fins with Convection
Channel Flows
Natural Convection with Radiation
7.5 Numerical Solution Methods
Numerical Formulations for Combined-Mode Energy Transfer
Verification, Validation and Uncertainty Quantification
7.6 Concluding Remarks

Chapter 8: **Properties of Participating Media (2 sessions; coverage here depends on how deeply will go into participating media. If brief, cover at least highlighted sections.)**

8.1 Introduction
Propagation of Radiation in Absorbing Media
8.2 Spectral Lines and Bands
Physical Mechanisms
Local Thermodynamic Equilibrium (LTE)
Spectral Line Broadening
8.3 Band Models
Probability Density Function-Based Band Correlations
Weighted Sum of Gray Gases
8.4 Gas Total Emittance Correlations
8.5 Mean Absorption Coefficients
8.6 Translucent Liquids and Solids
8.7 Absorption and Scattering: Definitions
Absorption and Scattering Coefficients, Cross Sections, Efficiencies
Scattering Phase Function
8.7 Scattering by Spherical Particles
Large Specularly Reflecting Sphere
Large Diffuse Sphere
Large Ideal Dielectric Sphere with $n \approx 1$
Diffraction by a Large Sphere
Geometric Optics Approximation
8.8 Scattering by Small Particles
Rayleigh Scattering by Small Spheres
Scattering Cross Section for Rayleigh Scattering
Phase Function for Rayleigh Scattering
8.9 Lorenz-Mie Theory for Spherical and Cylindrical Particles
8.10 Approximate Anisotropic Scattering Phase Functions
Forward-Scattering Phase Function
Linear-Anisotropic Phase Function
Delta-Eddington Phase Function
Henyey–Greenstein Phase Function

8.11 Dependent Absorption and Scattering
8.12 Remarks

Chapter 9. Radiative Transfer Relations in Media (2 sessions; brief coverage might include highlighted sections)

9.1 Introduction
9.2 Energy Equation and Boundary Conditions
9.3 Radiative Transfer in Absorbing, Emitting, and Scattering Medium
- Radiative Transfer Equation
- Source Function
- Gray Medium

9.4 Mean Beam-Length Approximation
- Mean Beam Length for a Medium between Parallel Plates
- Radiation from Entire Medium Volume to its Entire Boundary for Optically Thin Media
- Correction to Mean Beam Length when Medium is not Optically Thin

9.5 Exchange of Total Radiation in an Enclosure by use of Mean Beam Length
- Total Radiation from Entire Medium Volume to All or Part of its Boundary
- Exchange between Entire Medium Volume and an Emitting Boundary

9.6 Radiative Transfer in Plane Layers with Participating Media
- Radiative Transfer Equation and Radiative Intensity
- Local Radiative Flux in a Plane Layer
- Divergence of the Radiative Flux: Radiative Energy Source
- Source Function in a Plane Layer
- Relations for Isotropic Scattering

9.7 Gray Plane Layer in Radiative Equilibrium
- Energy Equation
- Results for Gray Medium with $dq_r/dx = 0$ between Diffuse-Gray Boundaries at Specified Temperatures

10. Numerical Solution of Radiative Transfer in Participating Media (1 Session; Can skim the methods, describe how each works in physical terms.)

10.1 Introduction
10.2 Series Expansion and Moment Methods
- Optically Thick Media: Radiative Diffusion
- Moment-Based Methods

10.3 Discrete Ordinates (S_N) Method
10.4 Zonal Method
- Exchange Area Relations
- Zonal Formulation for Radiative Equilibrium

10.5 The Monte Carlo Method

Basis of the Monte Carlo Method
Application to Thermal Radiative Transfer in Enclosures
Model of the Radiative Exchange Process
Monte Carlo for Participating Media
10.6 Conjugate Energy Transfer in Participating Media
Radiation Combined with Conduction
Combined Convection, Conduction, and Radiation
Verification, Validation, and Uncertainty Quantification

Chapter 11. Radiative Effects in Solids, Windows, and Coatings (1 session; pick an area of interest for concentration, perhaps flat plate solar collector design.)

11.1 Introduction
11.2 Transmission, Absorption, and Reflection for Windows
Single Partially Transmitting Layer with Thickness $D >> \lambda$
Multiple Parallel Windows
Transmission through Multiple Parallel Glass Plates
Flat Plate Solar Collectors
Thin Film with Interference Effects
11.4 Light Pipes and Fiber Optics
11.5 Final Remarks

Chapter 12: Emerging Areas (1 session; this chapter is chiefly discussion of areas where radiative transfer is becoming increasingly important.)

12.1 Introduction
12.2 Nanoscale Radiation Energy Transfer
12.3 Radiation Transfer for Inverse Applications
12.4 Radiation Transfer in Emerging Manufacturing Processes
12.5 Radiation Transfer for Diagnostics
12.6 Radiation and Climate Effects
12.7 Conclusions

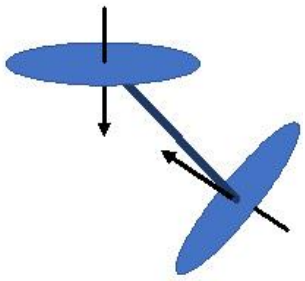

K: RADIATIVE PROPERTIES

Tables K.1 and K.2 of normal total emissivities and normal total absorptivities for incident solar radiation, respectively, are provided here for convenience in working problems and to give the reader an indication of the magnitudes to be expected. As discussed in Chapter 4, many factors such as roughness and oxidation can strongly affect the radiative properties. No attempt is made here to describe in detail the condition of the material sample; hence, the values given here are only reasonable approximations in some instances. For detailed information on radiative properties including sample descriptions and results from many sources, the reader is referred to the collections in Gubareff et al. (1960), Wood et al. (1964), Touloukian and Ho (1970, 1972a,b), and Palik (1998). The list of properties given by Touloukian and Ho in three volumes is very extensive. Additional information is in Svet (1965). Henninger (1984) has information on spacecraft materials and absorption for the solar spectrum. Additional properties are available on the web, with varying degrees of credibility. As will be seen from the references cited, for the same material, there can be considerable differences in the property values measured by different investigators.

REFERENCES

Gubareff, G. G., Janssen, J. E., and Torborg, R. H.: *Thermal Radiation Properties Survey*, 2nd edn., Honeywell Research Center, Minneapolis-Honeywell Regulator Co., Minneapolis, MN, 1960.

Henninger, J. H.: *Solar Absorptance and Thermal Emittance of Some Common Spacecraft Thermal-Control Coatings*, NASA Reference Publication 1121, Washington, DC, 1984.

Palik, E. D. (ed.): *Handbook of Optical Constants of Solids*, vols. I–IV, Elsevier, New York, 1998.

Svet, D. I.: *Thermal Radiation; Metals, Semiconductors, Ceramics, Partly Transparent Bodies, and Films*, Consultants Bureau, Plenum Publishing, New York, 1965.

Touloukian, Y. S. and Ho, C. Y. (eds.): Thermophysical properties of matter, TRPC data services, in Y. S. Touloukian and D. P. DeWitt (eds.), *Thermal Radiative Properties: Metallic Elements and Alloys*, vol. 7, 1970; Y. S. Touloukian, and D. P. DeWitt (eds.), *Thermal Radiative Properties: Nonmetallic Solids*, vol. 8, 1972a; Y. S. Touloukian, and D. P. DeWitt (eds.), Y. S. Touloukian, D. P. DeWitt, and R. S. Hernicz (eds.), *Thermal Radiative Properties: Coatings*, vol. 9, 1972b, Plenum Press, New York.

Wood, W. D., Deem, H. W., and Lucks, C. F.: *Thermal Radiative Properties*, Plenum Press, New York, 1964.

TABLE K.1
Normal Total Emissivity

Metal	Surface Temperature,[a] °F (K)	ε_n
Aluminum:		
Highly polished plate	400–1100 (480–870)	0.038–0.06
Bright foil	70 (295)	0.04
Polished plate	212 (373)	0.095
Heavily oxidized	200–1000 (370–810)	0.20–0.33
Antimony, polished	100–500 (310–530)	0.28–0.31
Bismuth, bright	176 (350)	0.34
Brass:		
Highly polished	500–700 (530–640)	0.028–0.031
Polished	200 (370)	0.09
Dull	120–660 (320–620)	0.22
Oxidized	400–1000 (480–810)	0.60
Cadmium	77 (298)	0.02
Chromium, polished	100–2000 (310–1370)	0.08–0.40
Copper:		
Highly polished	100 (310)	0.02
Polished	100–500 (310–530)	0.04–0.05
Scraped, shiny	100 (310)	0.07
Slightly polished	100 (310)	0.15
Black oxidized	100 (310)	0.78
Dow metal	0–600 (255–590)	0.15
Gold:		
Highly polished	200–1100 (370–870)	0.018–0.035
Polished	266 (400)	0.018
Haynes alloy X, oxidized	600–2000 (590–1370)	0.85–0.88
Iron:		
Highly polished, electrolytic	100–500(310–530)	0.05–0.07
Polished	800–900 (700–760)	0.14–0.38
Freshly rubbed with emery	100 (310)	0.24
Wrought iron, polished	100–500 (310–530)	0.28
Cast iron, freshly turned	100 (310)	0.44
Iron plate, pickled, then rusted red	68 (293)	0.61
Cast iron, oxidized at 1100°F	400–1100(480–870)	0.64–0.78
Cast iron, rough, strongly oxidized	100–500 (310–530)	0.95
Lead:		
Polished	100–500 (310–530)	0.06–0.08
Rough unoxidized	100 (310)	0.43
Oxidized at 1100°F	100 (310)	0.63
Magnesium, polished	100–500 (310–530)	0.07–0.13
Mercury, unoxidized	40–200 (280–370)	0.09–0.12
Molybdenum:		
Polished	100–500 (310–530)	0.05–0.08
Polished	1000–2500 (810–1640)	0.10–0.18
Polished	5000 (3030)	0.29
Monel:		
Polished	100 (310)	0.17
Oxidized at 1100°F	1000 (810)	0.45

(continued)

TABLE K.1 (*Continued*)
Normal Total Emissivity

Metal	Surface Temperature,[a] °F (K)	ε_n
Nickel:		
Electrolytic	100–500 (310–530)	0.04–0.06
Technically pure, polished	440–710 (500–650)	0.07–0.087
Electroplated on iron, not polished	68 (293)	0.11
Plate oxidized at 1100°F	390–1110 (470–870)	0.37–0.48
Nickel oxide	1200–2300 (920–1530)	0.59–0.86
Platinum:		
Electrolytic	500–1000 (530–810)	0.06–0.10
Polished plate	440–1160 (500–900)	0.054–0.104
Silver, polished	100–1000 (310–810)	0.01–0.03
Stainless steel:		
Type 304 foil (1 mil)	80 (300)	0.05
Inconel X foil (1 mil)	80 (300)	0.10
Inconel X, polished	−300 to 900 (90–760)	0.19–0.20
Inconel B, polished	−300 to 900 (90–760)	0.19–0.22
Type 301, polished	75 (297)	0.16
Type 310, smooth	1500 (1090)	0.39
Type 316, polished	400–1900 (480–1310)	0.24–0.31
Steel:		
Polished sheet	−300 to 0 (90–273)	0.07–0.08
Polished sheet	0–300 (273–420)	0.08–0.14
Mild steel, polished	500–1200 (530–920)	0.27–0.31
Sheet with skin due to rolling	70 (295)	0.66
Sheet with rough oxide layer	70 (295)	0.81
Tantalum	2500–5000 (1640–3030)	0.2–0.3
Foil	80 (300)	0.05
Tin:		
Polished sheet	93 (310)	0.05
Bright tinned iron	76 (298)	0.043–0.064
Tungsten:		
Polished	80 (300)	0.03
Clean	100–1000 (310–810)	0.03–0.08
Filament	80 (300)	0.032
Filament	6000 (3590)	0.39
Zinc:		
Polished	100–1000 (310–810)	0.02–0.05
Galvanized sheet, fairly bright	100 (310)	0.23
Gray oxidized	70 (295)	0.23–0.28
Dielectric	**Surface Temperature,[a] °F (K)**	ε_n
Alumina on inconel	1000–2000 (810–1370)	0.65–0.45
Asbestos:		
Cloth	199 (365)	0.90
Paper	100 (310)	0.93
Board	100 (310)	0.96
Asphalt pavement	100 (310)	0.93

(continued)

TABLE K.1 (*Continued*)
Normal Total Emissivity

Dielectric	Surface Temperature,[a] °F (K)	ε_n
Brick:		
White refractory	2000 (1370)	0.29
Fireclay	1800 (1260)	0.75
Rough red	100 (310)	0.93
Carbon, lampsoot	100 (310)	0.95
Ceramic, glazed earthenware	70 (295)	0.90
Clay, fired	158 (340)	0.91
Concrete, rough	100 (310)	0.94
Corundum, emery rough	200 (370)	0.86
Cotton cloth	68 (293)	0.77
Granite	70 (295)	0.45
Ice:		
Smooth	32 (273)	0.966
Rough crystals	32 (273)	0.985
Magnesium oxide, refractory	300–900 (420–760)	0.69–0.55
Marble, white	100 (310)	0.95
Mica	100 (310)	0.75
Paint:		
Oil, all colors	212 (373)	0.92–0.96
Red lead	200 (370)	0.93
Lacquer, flat black	100–200 (310–370)	0.96–0.98
Silicone, flat black	−149 to 212 (173–273)	0.90
Velostat black plastic	27 (300)	0.85
Paper:		
Roofing	100 (310)	0.91
White	100 (310)	0.95
Plaster	100 (310)	0.91
Porcelain, glazed	70 (295)	0.92
Rokide A on molybdenum	600–1500 (590–1090)	0.79–0.60
Rubber, hard	68 (293)	0.92
Sand	68 (293)	0.76
Sandstone	100–500 (310–530)	0.83–0.90
Silicon carbide	300–1200 (420–920)	0.83–0.96
Silk cloth	68 (293)	0.78
Slate	100 (310)	0.67–0.80
Snow	20 (270)	0.82
Soil:		
Black loam	68 (293)	0.66
Plowed field	68 (293)	0.38
Soot, candle	200–500 (370–530)	0.95
Water, deep	32–212 (273–373)	0.96
Wood:		
Sawdust	100 (310)	0.75
Oak, planed	70 (295)	0.90
Beech	158 (340)	0.94

[a] When temperatures and emissivities both have ranges, linear interpolation can be used over these values.

TABLE K.2
Normal Total Absorptivity for Incident Solar Radiation (Receiving Material at 300 K)

Metal	ε_n
Aluminum:	
Highly polished	0.10
Polished	0.20
Chromium, electroplated	0.40
Copper:	
Highly polished	0.18
Clean	0.25
Tarnished	0.64
Oxidized	0.70
Galvanized iron	0.38
Gold, bright foil	0.29
Iron:	
Ground with fine grit	0.36
Blued	0.55
Sandblasted	0.75
Magnesium, polished	0.19
Nickel:	
Highly polished	0.15
Polished	0.36
Electrolytic	0.40
Platinum, bright	0.31
Silver:	
Highly polished	0.07
Polished	0.13
Commercial sheet	0.30
Stainless steel #301, polished	0.37
Tungsten, highly polished	0.37
Dielectric	ε_n
Aluminum oxide (Al_2O_3)	0.06–0.23
Asphalt pavement, dust-free	0.93
Brick, red	0.75
Clay	0.39
Concrete roofing tile:	
Uncolored	0.73
Brown	0.91
Black	0.91
Earth, plowed field	0.75
Felt, black	0.82
Graphite	0.88
Grass	0.75–0.80
Gravel	0.29
Leaves, green	0.71–0.79
Magnesium oxide (MgO)	0.15
Marble, white	0.46

(continued)

TABLE K.2 (*Continued*)
Normal Total Absorptivity for Incident Solar Radiation (Receiving Material at 300 K)

Dielectric	ε_n
Paint:	
Aluminum	0.55
Oil, zinc white	0.30
Oil, light green	0.50
Oil, light gray	0.75
Oil, black on galvanized iron	0.90
Silicone, flat black	0.95–0.97
Velostat black plastic	0.96
Paper, white	0.28
Slate, blue gray	0.88
Snow, clean	0.2–0.35
Soot, coal	0.95
Titanium dioxide (TiO_2)	0.12
Zinc oxide	0.15
Zinc sulfide (ZnS)	0.21
Coating	ε_n
Black coatings:	
Anodize black	0.88
Carbon black paint NS-7	0.96
Ebonol C black	0.97
Martin black velvet paint	0.91
3M black velvet paint	0.97
Tedlar black plastic	0.94
Velostat black plastic	0.96
White coatings:	
Barium sulfate with polyvinyl alcohol	0.06
Catalac white paint	0.23
Dow Corning white paint DC-007	0.19
Magnesium oxide white paint	0.09
Potassium fluorotitanate white paint	0.15
Tedlar white plastic	0.39
Titanium oxide white paint with methyl silicone	0.20
Zinc oxide with sodium silicate	0.15
Conversion coatings (values can vary significantly with coating thickness):	
Alzac A-2	0.16
Black chrome	0.96
Black copper	0.98
Black iridite	0.62
Black nickel	0.91
Vapor-deposited coatings on glass substrates:	
Aluminum	0.08
Chromium	0.56
Gold	0.19
Nickel	0.38
Silver	0.04

(continued)

TABLE K.2 (*Continued*)
Normal Total Absorptivity for Incident Solar Radiation (Receiving Material at 300 K)

Coating	ε_n
Titanium	0.52
Tungsten	0.60
Plastic films with metal backing:	
Mylar film, 3 mil aluminum backing	0.17
Tedlar film, 1 mil gold backing	0.26
Teflon film, 2 mil aluminum backing	0.08
Teflon film, 1 mil gold backing	0.22
Teflon film, 2 mil silver backing	0.08

[a] Receiving material at 300 K.

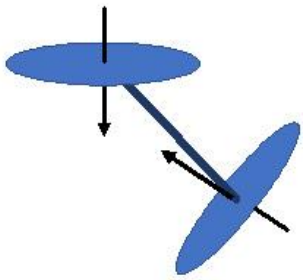

L: CATALOG OF SELECTED CONFIGURATION FACTORS*

1

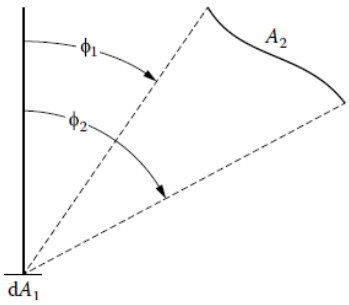

Area dA_1 of differential width and any length, to infinitely long strip dA_2 of differential width and with parallel generating line to dA_1

$$dF_{d1-d2} = \frac{\cos\phi}{2} d\phi = \frac{1}{2} d(\sin\phi)$$

2

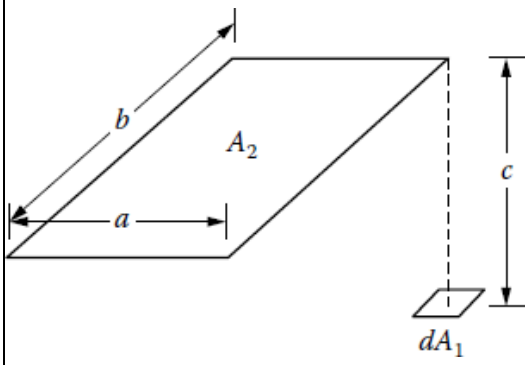

Plane element dA_1 to plane parallel rectangle; normal to element passes through the corner of a rectangle

$$X = \frac{a}{c}; \quad Y = \frac{b}{c}$$

$$F_{d1-d2} = \frac{1}{2\pi}\left(\frac{X}{\sqrt{1+X^2}} \tan^{-1} \frac{Y}{\sqrt{1+X^2}} + \frac{Y}{\sqrt{1+Y^2}} \tan^{-1} \frac{X}{\sqrt{1+Y^2}} \right)$$

3

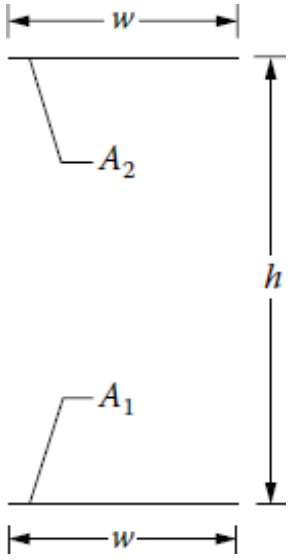

Two infinitely long, directly opposed parallel plates of the same finite width

$$H = \frac{h}{w}$$

$$F_{1-2} = F_{2-1} = \sqrt{1+H^2} - H$$

4

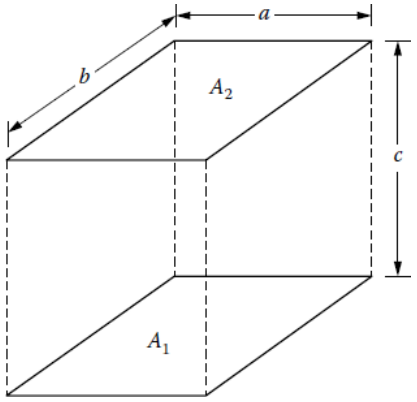

Identical, parallel, directly opposed rectangles

$$X = \frac{a}{c}; \quad Y = \frac{b}{c}$$

$$F_{1-2} = \frac{2}{\pi XY}\left\{\begin{array}{l} \ln\left[\dfrac{(1+X^2)(1+Y^2)}{1+X^2+Y^2}\right]^{1/2} \\ +X\sqrt{1+Y^2}\,\tan^{-1}\dfrac{X}{\sqrt{1+Y^2}} \\ +Y\sqrt{1+X^2}\,\tan^{-1}\dfrac{Y}{\sqrt{1+X^2}} \\ -X\tan^{-1}X - Y\tan^{-1}Y \end{array}\right\}$$

5

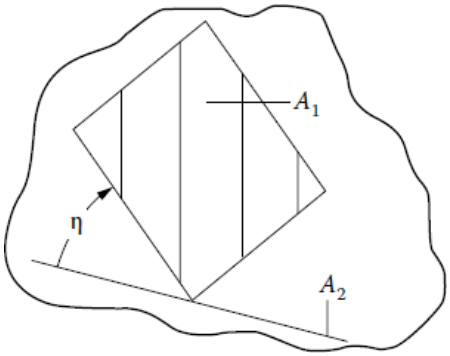

Finite rectangle A_1 of any size, tilted at angle η relative to an infinite plane A_2

$$F_{1-2} = \frac{1}{2}(1-\cos\eta)$$

6

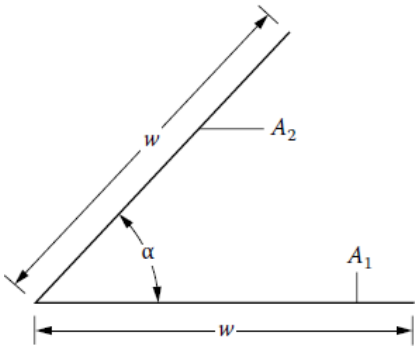

Two infinitely long plates of equal finite width *w*, having one common edge and having an included angle α to each other

$$F_{1-2} = F_{2-1} = 1 - \sin\frac{\alpha}{2}$$

7

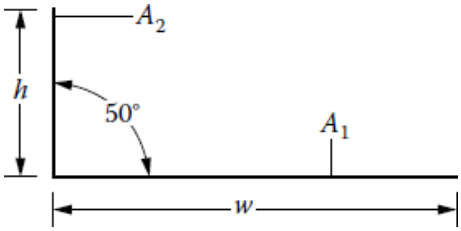

Two infinitely long plates of unequal widths *h* and *w*, having one common edge and having an angle of 90° to each other.

$$H = \frac{h}{w}$$

$$F_{1-2} = \frac{1}{2}(1+H-\sqrt{1+H^2})$$

8

Two finite rectangles of the same length, having one common edge and having an angle of 90° to each other

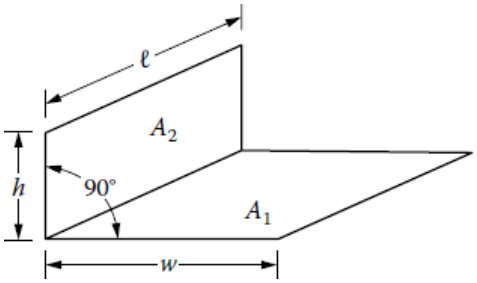

$$H = \frac{h}{l}; \quad W = \frac{w}{l}$$

$$F_{1-2} = \frac{1}{\pi W}\left(\begin{array}{l} W\tan^{-1}\frac{1}{W} + H\tan^{-1}\frac{1}{H} \\ \quad -\sqrt{H^2+W^2}\tan^{-1}\frac{1}{\sqrt{H^2+W^2}} \\ \quad +\frac{1}{4}\ln\left\{\begin{array}{l} \frac{(1+W^2)(1+H^2)}{1+W^2+H^2} \\ \quad \times\left[\frac{W^2(1+W^2+H^2)}{(1+W^2)(W^2+H^2)}\right]^{W^2} \\ \quad \times\left[\frac{H^2(1+H^2+W^2)}{(1+H^2)(H^2+W^2)}\right]^{H^2} \end{array}\right. \end{array}\right)$$

9

Plane element dA_1 to circular disk in plane parallel to element; normal to element passes through the center of a disk

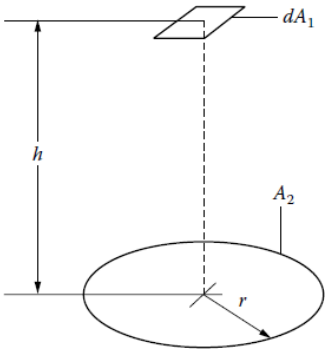

$$F_{d1-2} = \frac{r^2}{h^2+r^2}$$

10

Parallel circular disks with centers along the same normal

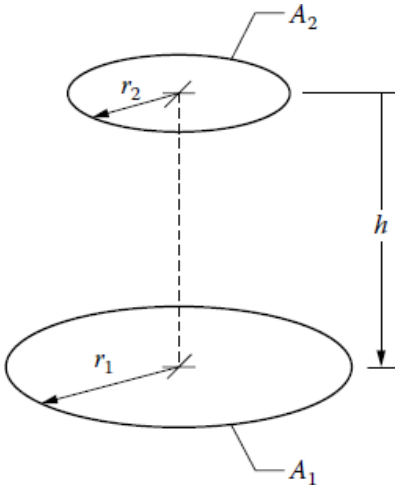

$$R_1 = \frac{r_1}{h}; \quad R_2 = \frac{r_2}{h}$$

$$X = 1 + \frac{1+R_2^2}{R_1^2}$$

$$F_{1-2} = \frac{1}{2}\left[X - \sqrt{X^2 - 4\left(\frac{R_2}{R_1}\right)^2}\right]$$

11

Infinitely long plane of finite width to parallel infinitely long cylinder

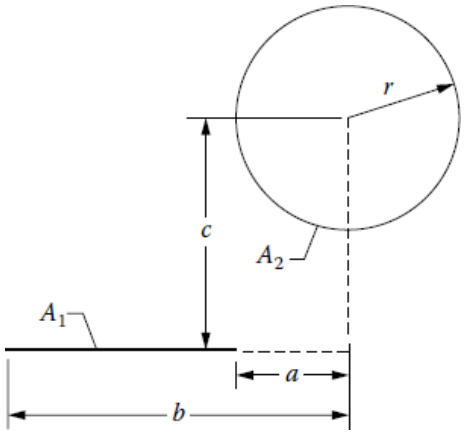

$$F_{1-2} = \frac{r}{b-a}\left(\tan^{-1}\frac{b}{c} - \tan^{-1}\frac{a}{c}\right)$$

12 Infinitely long parallel cylinders of the same diameter

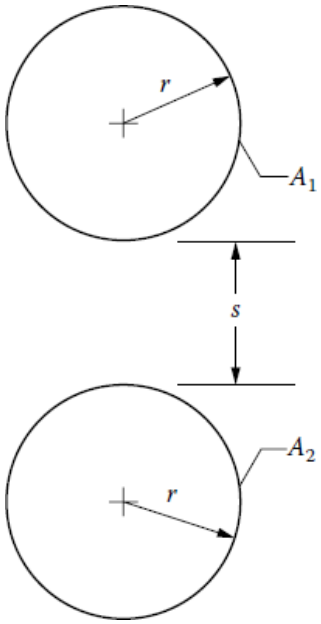

$$X = 1 + \frac{s}{2r}$$

$$F_{1-2} = F_{2-1} = \frac{1}{\pi}\left(\sqrt{X^2 - 1} + \sin^{-1}\frac{1}{X} - X\right)$$

13 Concentric cylinders of infinite length

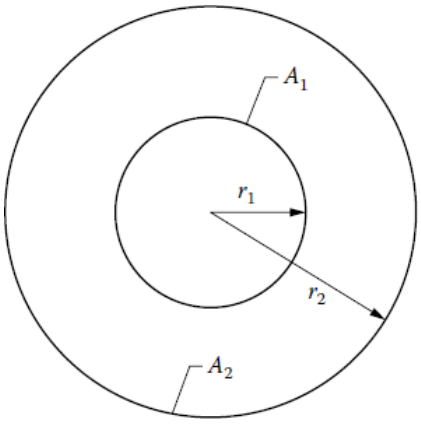

$$F_{1-2} = 1$$

$$F_{2-1} = \frac{r_1}{r_2}$$

$$F_{2-2} = 1 - \frac{r_1}{r_2}$$

14

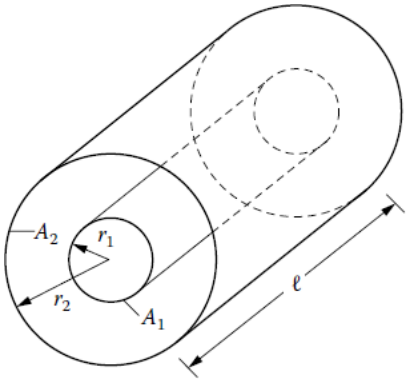

Two concentric cylinders of the same finite length

$$R = \frac{r_2}{r_1}; \quad L = \frac{l}{r_1}$$

$$A = L^2 + R^2 - 1$$

$$B = L^2 - R^2 + 1$$

$$F_{2-1} = \frac{1}{R} - \frac{1}{\pi R}\left\{\cos^{-1}\frac{B}{A} - \frac{1}{2L}\times\left[\begin{array}{l}\sqrt{(A+2)^2-(2R)^2}\cos^{-1}\dfrac{B}{RA} \\ \\ +B\sin^{-1}\dfrac{1}{R} - \dfrac{\pi A}{2}\end{array}\right]\right\}$$

$$F_{2-2} = 1 - \frac{1}{R} + \frac{2}{\pi R}\tan^{-1}\frac{2\sqrt{R^2-1}}{L} - \frac{L}{2\pi R}$$

$$\times\left[\begin{array}{l}\dfrac{\sqrt{4R^2+L^2}}{L}\sin^{-1}\dfrac{4(R^2-1)+(L^2/R^2)(R^2-2)}{L^2+4(R^2-1)} \\ \\ -\sin^{-1}\dfrac{R^2-2}{R^2} + \dfrac{\pi}{2}\left(\dfrac{\sqrt{4R^2+L^2}}{L} - 1\right)\end{array}\right]$$

where for any argument ξ

$$-\frac{\pi}{2} \le \sin^{-1}\xi \le \frac{\pi}{2}$$

$$0 \le \cos^{-1}\xi \le \pi$$

15

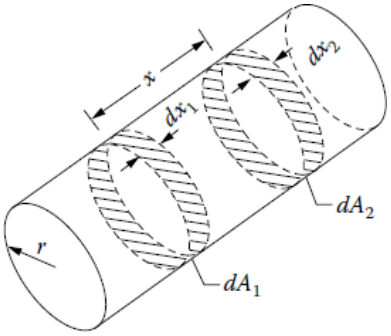

Two ring elements on the interior of a right circular cylinder

$$X = \frac{x}{2r}$$

$$dF_{d1-d2} = \left[1 - \frac{2X^3 + 3X}{2(X^2+1)^{3/2}}\right]dX_2$$

16

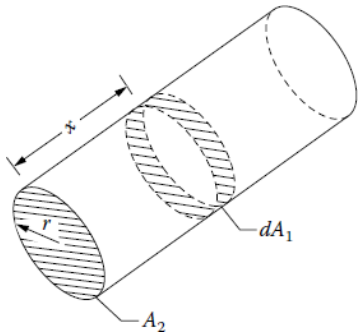

Ring element dA_1 on interior of right circular cylinder to circular disk A_2 at the end of a cylinder

$$X = \frac{x}{2r}$$

$$F_{d1-2} = \frac{X^2 + (1/2)}{\sqrt{X^2+1}} - X$$

17 Sphere of radius r_1 to disk of radius r_2; normal to center of disk passes through the center of a sphere

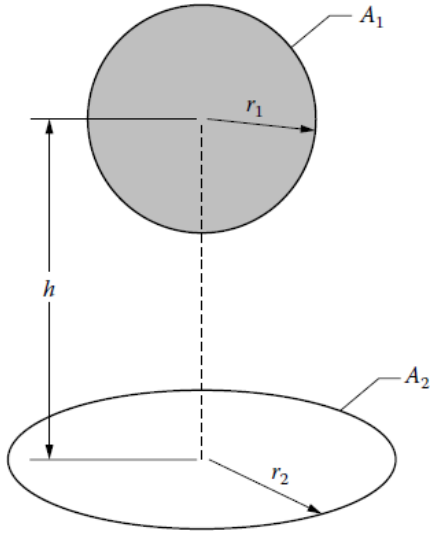

$$R_2 = \frac{r_2}{h}$$

$$F_{1-2} = \frac{1}{2}\left(1 - \frac{1}{\sqrt{1+R_2^2}}\right)$$

18 Concentric spheres

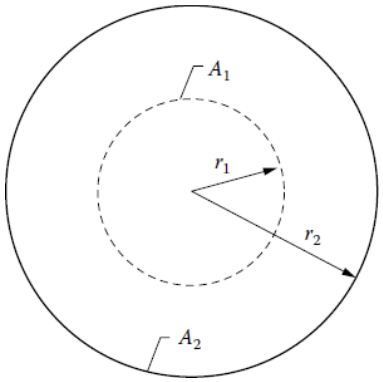

$$F_{1-2} = 1$$

$$F_{2-1} = \left(\frac{r_1}{r_2}\right)^2$$

$$F_{2-2} = 1 - \left(\frac{r_1}{r_2}\right)^2$$

19 Differential or finite areas on the inside of a spherical cavity

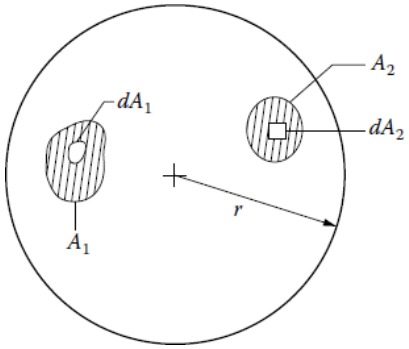

$$dF_{d1-d2} = dF_{1-d2} = \frac{dA_2}{4\pi r^2}$$

$$F_{d1-2} = F_{1-2} = \frac{A_2}{4\pi r^2}$$

* A catalog of over 320 factors is available at *http:www.thermalradiation.net/IndexCat.html.*

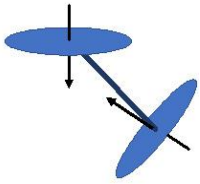

M: EXPONENTIAL INTEGRAL RELATIONS AND TWO-DIMENSIONAL RADIATION FUNCTIONS

M.1 EXPONENTIAL INTEGRAL RELATIONS

A summary of some useful exponential integral relations is presented here. Additional relations are in Chandrasekhar (1960), Kourganoff (1963), and Abramowitz and Stegun (1965, available on-line at various sites, since not copyrighted by the original publisher, US Department of Commerce.).

For positive real arguments, the *n*th exponential integral is defined as

$$E_n(x) \equiv \int_0^1 \mu^{n-2} \exp\left(\frac{-x}{\mu}\right) d\mu \tag{M.1}$$

and only positive integral values of *n* will be considered here. An alternative form is

$$E_n(x) = \int_1^\infty \frac{1}{t^n} \exp(-xt)\, dt \tag{M.2}$$

By differentiating Equation M.1 under the integral sign, the recurrence relation is obtained:

$$\begin{aligned} \frac{d}{dx} E_n(x) &= -E_{n-1}(x) \quad x \geq 2 \\ \frac{d}{dx} E_1(x) &= -\frac{1}{x} \exp(-x) \end{aligned} \tag{M.3}$$

Another recurrence relation obtained by integration is

$$nE_{n+1}(x) = \exp(-x) - xE_n(x) = \exp(-x) + x\frac{d}{dx} E_{n+1}(x) \quad n \geq 1 \tag{M.4}$$

Also, integration results in

$$\int E_n(x)\, dx = -E_{n+1}(x) \tag{M.5}$$

By use of Equation M.4, all exponential integrals can be reduced to the first exponential integral given by

$$E_1(x) = \int_0^1 \mu^{-1} \exp\left(\frac{-x}{\mu}\right) d\mu \tag{M.6}$$

Alternative forms of $E_1(x)$ are

$$E_1(x) = \int_1^\infty t^{-1} \exp(-xt)\, dt = \int_x^\infty t^{-1} \exp(-t)\, dt \tag{M.7}$$

For $x = 0$, the exponential integrals are equal to

$$\begin{aligned} E_n(0) &= \frac{1}{n-1} \quad n \geq 2 \\ E_1(0) &= +\infty \end{aligned} \tag{M.8}$$

For large values of *x* there is the asymptotic expansion

$$E_n(x) = \frac{\exp(-x)}{x}\left[1 - \frac{n}{x} + \frac{n(n+1)}{x^2} - \frac{n(n+1)(n+2)}{x^3} + \cdots\right] \tag{M.9}$$

Therefore, as $x \longrightarrow \infty$, $E_n(x) \longrightarrow \exp(-x)/x \longrightarrow 0$.

Series expansions are of the form

$$\begin{aligned} E_1(x) &= -\gamma - \ln x + x - \frac{x^2}{2\times 2!} + \frac{x^3}{3\times 3!} - \cdots \\ &= -\gamma - \ln x - \sum_{n=1}^{\infty} (-1)^n \frac{x^n}{x \times n!} \\ E_2(x) &= 1 + (\gamma - 1 + \ln x)x - \frac{x^2}{1\times 2!} + \frac{x^3}{2\times 3!} - \cdots \\ E_3(x) &= \frac{1}{2} - x + \frac{1}{2}\left(-\gamma + \frac{3}{2} - \ln x\right)x^2 + \frac{x^3}{1\times 3!} - \cdots \end{aligned} \tag{M.10}$$

where $\gamma = 0.577216$ is Euler's constant. The general series expansion given by Abramowitz and Stegun (1965) is

$$E_n(x) = \frac{(-x)^{n-1}}{(n-1)!}[-\ln x + \psi(n)] - \sum_{\substack{m=0 \\ (m\neq n-1)}}^{\infty} \frac{(-x)^m}{(m-n+1)m!} \tag{M.11}$$

where $\Psi(1) = -\gamma$ and $\psi(n) = -\gamma + \sum_{m=1}^{n-1} \frac{1}{m} \quad n \geq 2$.

Some approximations are:

Using Equation (M.3) gives $E_2(x) \approx 0.9\exp(-1.8x)$

In Cess and Tiwari (1972), the following approximations are used:

$$E_2(x) \approx \frac{3}{4}\exp\left(-\frac{3}{2}x\right)$$

$$E_3(x) \approx \frac{1}{2}\exp\left(-\frac{3}{2}x\right)$$

Tabulations of $E_n(x)$ are in Kourganoff (1963) and Abramowitz and Stegun (1965, available on-line). Breig and Crosbie (1974) present forms of a generalized exponential integral function that are convenient for numerical computation. The generalized forms include, as a special case, the $E_n(x)$ discussed here.

M.2 TWO-DIMENSIONAL RADIATION FUNCTIONS

For two-dimensional (2D) problems, the exponential integral functions are replaced by another set of integral functions. These are the S_n functions and can be defined in a number of equivalent ways. An expression that is easily evaluated by numerical integration is

$$S_n(x) = \frac{2}{\pi}\int_0^{\pi/2} \exp\left(-\frac{x}{\cos\theta}\right)\cos^{n-1}\theta d\theta \tag{M.12}$$

An alternative form is

$$S_n(x) = \frac{2}{\pi}\int_1^{\infty} \frac{\exp(-xt)}{t^n(t^2-1)^{1/2}}\,dt \quad x \geq 0,\ n = 0,1,2,\ldots \tag{M.13}$$

TABLE M.1
Values of Exponential Integrals $E_n(x)$

x	$E_1(X)$	$E_2(x)$	$E_3(x)$	$E_4(x)$	$E_5(x)$
0	∞	1.00000	0.50000	0.33333	0.25000
0.01	4.03793	0.94967	0.49028	0.32838	0.24669
0.02	3.35471	0.91311	0.48097	0.32353	0.24343
0.03	2.95912	0.88167	0.47200	0.31876	0.24022
0.04	2.68126	0.85354	0.46332	0.31409	0.23706
0.05	2.46790	0.82784	0.45492	0.30949	0.23394
0.06	2.29531	0.80405	0.44676	0.30499	0.23087
0.07	2.15084	0.78184	0.43883	0.30056	0.22784
0.08	2.02694	0.76096	0.43112	0.29621	0.22486
0.09	1.91874	0.74124	0.42361	0.29194	0.22191
0.10	1.82292	0.72255	0.41629	0.28774	0.21902
0.15	1.46446	0.64104	0.38228	0.26779	0.20514
0.20	1.22265	0.57420	0.35195	0.24945	0.19221
0.25	1.04428	0.51773	0.32468	0.23254	0.18017
0.30	0.90568	0.46912	0.30004	0.21694	0.16893
0.35	0.79422	0.42671	0.27767	0.20250	0.15845
0.40	0.70238	0.38937	0.25729	0.18914	0.14867
0.50	0.55977	0.32664	0.22160	0.16524	0.13098
0.60	0.45438	0.27618	0.19155	0.14463	0.11551
0.70	0.37377	0.23495	0.16606	0.12678	0.10196
0.80	0.31060	0.20085	0.14432	0.11129	0.09007
0.90	0.26018	0.17240	0.12570	0.09781	0.07963
1.00	0.21938	0.14850	0.10969	0.08606	0.07045
1.20	0.15841	0.11110	0.08393	0.06682	0.05525
1.40	0.11622	0.08389	0.06458	0.05206	0.04343
1.60	0.08631	0.06380	0.04991	0.04068	0.03420
1.80	0.06471	0.04882	0.03872	0.03187	0.02698
2.00	0.04890	0.03753	0.03013	0.02502	0.02132
2.25	0.03476	0.02718	0.02212	0.01855	0.01592
2.50	0.02491	0.01980	0.01630	0.01378	0.01191
2.75	0.01798	0.01449	0.01205	0.01027	0.00892
3.00	0.01305	0.01064	0.00893	0.00767	0.00670
3.25	0.00952	0.00785	0.00664	0.00573	0.00504
3.50	0.00697	0.00580	0.00495	0.00430	0.00379

Source: Kourganoff, V., *Basic Methods in Transfer Problems*, Dover, New York, 1963.

Another form is

$$S_n(a\tau) = \frac{\tau^n}{\pi}\int_{-\infty}^{\infty} \frac{\exp\left[-a(x^2+\tau^2)^{1/2}\right]}{(x^2+\tau^2)(n+1)/2}\,dx, \quad a \geq 0,\ \tau \geq 0,\ n = 0,1,2,\ldots \tag{M.14}$$

From the definition of $S_n(x)$, the values at $x = 0$ can be found from ($n > 0$):

$$S_n(0) = \frac{1}{\pi^{1/2}}\frac{\Gamma(n/2)}{\Gamma[(n+1)/2]} \tag{M.15}$$

TABLE M.2
Values of the Two-Dimensional Radiation Function $S_n(x)$

x	$S_0(x)$	$S_1(x)$	$S_2(x)$	$S_3(x)$	$S_4(x)$
0	∞	1.00000	0.63662	0.50000	0.42441
0.002	4.03015	0.99067	0.63463	0.49873	0.42341
0.005	3.44684	0.97958	0.63167	0.49683	0.42192
0.02	2.56460	0.93598	0.61732	0.48746	0.41454
0.04	2.12411	0.88960	0.59908	0.47530	0.40491
0.07	1.76969	0.83169	0.57329	0.45772	0.39092
0.10	1.54512	0.78217	0.54910	0.44089	0.37744
0.15	1.29236	0.71168	0.51180	0.41438	0.35607
0.20	1.11581	0.65169	0.47776	0.38965	0.33597
0.25	0.98135	0.59940	0.44651	0.36656	0.31708
0.30	0.87374	0.55312	0.41772	0.34496	0.29929
0.35	0.78477	0.51172	0.39111	0.32475	0.28256
0.40	0.70953	0.47441	0.36648	0.30582	0.26680
0.45	0.64484	0.44059	0.34362	0.28807	0.25195
0.5	0.58850	0.40979	0.32237	0.27143	0.23797
0.6	0.49499	0.35580	0.28417	0.24115	0.21237
0.7	0.42050	0.31016	0.25093	0.21443	0.18962
0.8	0.35991	0.27124	0.22191	0.19082	0.16939
0.9	0.30986	0.23783	0.19650	0.16993	0.15137
1.0	0.26803	0.20899	0.17419	0.15142	0.13532
1.2	0.20277	0.16227	0.13728	0.12042	0.10826
1.5	0.13611	0.11218	0.09661	0.08571	0.07764
2.0	0.07251	0.06183	0.05442	0.04900	0.04484
3.0	0.02212	0.01964	0.01778	0.01633	0.01516
4.0	0.00710	0.00646	0.00595	0.00554	0.00520
5.0	0.00235	0.00217	0.00202	0.00190	0.00180

This yields $S_1(0) = 1$, $S_2(0) = 2/\pi$, $S_3(0) = 1/2$, and $S_4(0) = 4/(3\pi)$. The $S_0(x)$ is related to the modified Bessel function by

$$S_0(x) = \frac{2}{\pi} K_0(x) \tag{M.16}$$

The derivative of $S_n(x)$ is given by

$$\frac{dS_n(x)}{dx} = -S_{n-1}(x), \quad n \geq 1 \tag{M.17}$$

Hence, the integral of S_n is

$$\int S_n(x)dx = -S_{n+1}(x), \quad n \geq 0 \tag{M.18}$$

Additional information is in Yuen and Wong (1983).

REFERENCES

Abramowitz, M. and Stegun, I. A.: *Handbook of Mathematical Functions*, Dover, New York, 1965.

Breig, W. F. and Crosbie, A. L.: Numerical computation of a generalized exponential integral function, *Math. Comput*., 28(126), 575–579, 1974.

Cess, R. D., and Tiwari, S. N.: Infrared Radiative Energy Transfer in Gases, in T. F. Irvine, Jr., and J. P. Hartnett (eds.), *Advances in Heat Transfer*, vol. 8, pp. 229–283, Academic Press, New York, 1972

Chandrasekhar, S.: *Radiative Transfer*, Dover, New York, 1960.

Kourganoff, V.: *Basic Methods in Transfer Problems*, Dover, New York, 1963.

Yuen, W. W. and Wong, L. W.: Numerical computation of an important integral function in two-dimensional radiative transfer, *JQSRT*, 29(2), 145–149, 1983.